

TA7
.C6
CER-85-86-12
COPY 2

WIND-TUNNEL STUDY OF WIND LOADS
ON LAJET SOLAR COLLECTOR MODULE

by

S. T. Thoroddsen¹
J. A. Peterka² and J. E. Cermak³



**FLUID MECHANICS AND
WIND ENGINEERING PROGRAM**

COLLEGE OF ENGINEERING

COLORADO STATE UNIVERSITY
FORT COLLINS, COLORADO

CER85-86STT-JAP-JEC/2

WIND-TUNNEL STUDY OF WIND LOADS
ON LAJET SOLAR COLLECTOR MODULE

by

S. T. Thoroddsen¹
J. A. Peterka² and J. E. Cermak³

for

LaJet Energy Company
3130 Antilley Road
P.O. Box 3599
Abilene, Texas 79604

Fluid Mechanics and Wind Engineering Program
Fluid Dynamics and Diffusion Laboratory
Department of Civil Engineering
Colorado State University
Fort Collins, Colorado 80523

CSU Project 2-96350

November 1985

¹Graduate Research Assistant, CSU

²Professor, Fluid Mechanics and Wind
Engineering Program, CSU

³Professor and Senior Counsel, Fluid
Mechanics and Wind Engineering Program, CSU

TABLE OF CONTENTS

<u>Chapter</u>		<u>Page</u>
	LIST OF FIGURES	ii
	LIST OF TABLES	iii
	LIST OF SYMBOLS	iv
1	INTRODUCTION	1
	1.1 General	1
	1.2 Modeling	1
	1.3 Measurement Strategy	3
2	TEST EQUIPMENT AND INSTRUMENTATION	4
	2.1 Wind Tunnel	4
	2.2 Force Balance	5
	2.3 Signal Processing	7
	2.4 The Solar Collector Model	7
	2.5 Frequency Response	8
3	TEST RESULTS	10
	3.1 Presentation of Data	10
	3.1.1 Load Coefficients	10
	3.1.2 Force and Moment Transformations	11
	3.2 Mean Loading	16
	3.2.1 Stowed Positions	17
	3.2.2 Loading in the "Primed System"	17
	3.3 Load Spectra	17
	3.4 Modifications of Solar Collector Model	19
	3.5 Effects of Porosity	20
	3.6 Accuracy of Data	20
4	DISCUSSION	22
	REFERENCES	23
	FIGURES	24
	TABLES	41
	APPENDIX A - Mean Loading	A-1
	APPENDIX B - Mean Loading in "Primed System"	B-1
	APPENDIX C - Load Spectra	C-1
	APPENDIX D - Modal Analysis and Random Vibration	D-1

LIST OF FIGURES

<u>Figure</u>		<u>Page</u>
1	Fluid Dynamics and Diffusion Laboratory at Colorado State University	25
2	The Fluid Dynamics and Diffusion Laboratory, Industrial Aerodynamics Wind Tunnel	26
3	Mean Velocity and Turbulence Intensity Profiles Approaching the Model	27
4	Mean Velocity Profiles in Front of and Behind the Collector Model	28
5	Turbulence Intensity Profiles in Front of and Behind the Collector Model	29
6	Longitudinal Velocity Spectra in Front of and Behind the Collector Model at 10 in. from the Floor	30
7	Longitudinal Velocity Spectra in Front of and Behind the Collector Model at 10 in. from the Floor	31
8	The Force Balance and Coordinate System	32
9	The Signal Processing System	33
10	The Solar Collector Model in the Wind Tunnel	34
11	Schematic of the Model Support System	35
12	Horizontal Velocity Profile Adjacent to the Model	37
13	Force Balance Coordinates and Model Set-up	38
14	Model Coordinate Systems	39
15	Spectra of Normal Force vs. Porosity	40
A.1	M_x vs. Wind Direction for 30, 40, 50, 60, 75 Deg. Declination	A-2
A.2	M_y vs. Wind Direction for 30, 40, 50, 60, 75 Deg. Declination	A-3
A.3	F_x vs. Wind Direction for 30, 40, 50, 60, 75 Deg. Declination	A-4
A.4	F_y vs. Wind Direction for 30, 40, 50, 60, 75 Deg. Declination	A-5

<u>Figure</u>		<u>Page</u>
A.5	F_z vs. Wind Direction for 30, 40, 50, 60, 75 Deg. Declination	A-6
A.6	M_x vs. Wind Direction for 20, 10, 0, -10, -20 Deg. Declination	A-7
A.7	M_y vs. Wind Direction for 20, 10, 0, -10, -20 Deg. Declination	A-8
A.8	F_x vs. Wind Direction for 20, 10, 0, -10, -20 Deg. Declination	A-9
A.9	F_y vs. Wind Direction for 20, 10, 0, -10, -20 Deg. Declination	A-10
A.10	F_z vs. Wind Direction for 20, 10, 0, -10, -20 Deg. Declination	A-11
A.11	Wind Loading for 90, 75, 60, 45, 30, 15 Deg. Hour Angles	A-12
A.12	Wind Loading for 90, 75, 60, 45, 30, 15 Deg. Hour Angles	A-13
A.13	Wind Loading for 90, 75, 60, 45, 30, 15 Deg. Hour Angles	A-14
A.14	Wind Loading for 90, 75, 60, 45, 30, 15 Deg. Hour Angles	A-15
A.15	Wind Loading for 90, 75, 60, 45, 30, 15 Deg. Hour Angles	A-16
A.16	Umbrella-Like Stowed Position (Force Coefficients for F_x , F_y , and F_z)	A-17
A.17	Umbrella-Like Stowed Position (Mean Moment Coefficient)	A-18
C.1a-h	Load Spectra for Declination Angle 0°, Hour Angle 90°.	C-2
C.2a-h	Load Spectra for Declination Angle 0°, Hour Angle 75°.	C-10
C.3a-e	Load Spectra for Declination Angle 0°, Hour Angle 60°.	C-18
C.4a-e	Load Spectra for Declination Angle 0°, Hour Angle 45°.	C-23
C.5a-h	Load Spectra for Declination Angle 0°, Hour Angle 30°.	C-28
C.6a-e	Load Spectra for Declination Angle 0°, Hour Angle 15°.	C-36

<u>Figure</u>		<u>Page</u>
C.7a-h	Load Spectra for Declination Angle 0° , Hour Angle 0° . .	C-41
C.8a-c	Load Spectra for Declination Angle -20° , Hour Angle 0° .	C-49
C.9a-e	Load Spectra for Declination Angle 20° , Hour Angle 0° . .	C-52
C.10a-e	Load Spectra for Declination Angle 40° , Hour Angle 0° . .	C-57
C.11a-e	Load Spectra for Declination Angle 50° , Hour Angle 0° . .	C-62
C.12a-j	Load Spectra for Declination Angle 60° , Hour Angle 0° . .	C-67
C.13a-k	Load Spectra for Declination Angle 75° , Hour Angle 0° . .	C-77
C.14a-h	Load Spectra for Umbrella Stowed Position, Declination Angle 0° , Hour Angle 0°	C-88

LIST OF TABLES

<u>Table</u>		<u>Page</u>
1	Reference Quantities	42
2	Dimensions used in Transformations	43
3a	Transformation Code for Non-zero Declination	44
3b	Transformation Code for Non-zero Hour Angle	45
4	Effects of Modified Solar Collector Model	46
B.1	Mean Loading in "Primed" System	B-2
C.1	Run Matrix for Spectral Measurements	C-1a

LIST OF SYMBOLS

<u>Symbol</u>	<u>Description</u>
α	Power law exponent
A	Reference area
C_F, C_M	Force and moment coefficients
D	Reference dimension
f	Frequency Hz
f_r	Reduced frequency
f_o	Natural frequency Hz
F_x, F_y, F_z	Resultant forces of wind loads in x, y, z directions
$H(f)^2$	Mechanical admittance (transfer function)
L	Reference length
M_x, M_y, M_z	Resultant moment of applied wind load about x, y, z-axes
n	Frequency Hz
q	Reference dynamic pressure, $\rho U_\infty^2/2$
$S_{()}(f)$	Power spectral density of ()
$S_F^*(n), S_M^*(n)$	Reduced force and moment spectrum
U	Local mean velocity
U_∞	Reference mean velocity outside the boundary layer
U_{rms}	Root-mean-square of fluctuating velocity
σ	Standard deviation
ζ	Critical damping ratio
z	Height above tunnel floor
z_∞	Height for reference velocity

1. INTRODUCTION

1.1 General

The study reported herein was aimed at determining mean and dynamic wind loading for the design of a large 95-mirror LaJet Energy Company solar collector module. A two-axis drive system is used to track the diurnal and seasonal movements of the sun. Wind forces on the collector module are transferred to the supporting frame through this drive system which supports the module. The drive system has to be designed structurally to withstand extreme wind speeds in a stowed position, but also has to be sturdy enough to keep the reflected sunlight focused at the right spot for moderate wind conditions.

To determine the fluctuating wind-load on the solar collector a six-component force balance was used. Measuring six components allows the transformation of forces and moments to the desired location in the drive mechanism.

1.2 Modeling

The development of boundary-layer wind tunnels has provided a method for determination of wind loads on buildings and structures. A boundary-layer wind tunnel differs from other types of wind tunnels in that a thick turbulent boundary layer is developed along the floor of a long test section whose characteristics produce an accurate scaled model of the atmospheric boundary layer.

The criteria to be satisfied for accurate modeling of the atmospheric boundary layer and wind loads on a structure have been documented in the literature [1,2,3]. In general, the requirements are that the model and prototype be geometrically similar, that the approach mean velocity at the building site have a vertical profile shape similar

to the full-scale flow, that the turbulence characteristics of the flows be similar, and that the Reynolds number for the model and prototype be equal. These criteria are satisfied by constructing a scale model of the structure and its surroundings and performing the wind tests in a wind tunnel specifically designed to model atmospheric boundary-layer flows. The wind-tunnel simulation produces both the vertical profile shape in mean velocity and the properly scaled turbulence characteristics.

Reynolds number similarity requires that the quantity UD/ν be equal for model and prototype. Since ν , the kinematic viscosity of air, is identical for both, Reynolds numbers cannot be made equal with reasonable wind velocities. To accomplish this the air velocity in the wind tunnel would have to be as large as the model scale factor times the prototype wind velocity, a velocity which would introduce unacceptable compressibility effects. However, for sufficiently high Reynolds numbers ($>2 \times 10^4$) the pressure coefficient at any location on the structure will be essentially constant for a large range of Reynolds numbers. Typical values encountered are 10^7 - 10^8 for the full-scale and 10^5 - 10^6 for the wind-tunnel model. In this range acceptable flow and wind load similarity is achieved without Reynolds number equality.

Wind-tunnel boundary layers can be adjusted somewhat to account for different model scales. For models which are about 1:200 or smaller, the wind-tunnel boundary layers can relatively easily be adjusted to fit the model scale. For models at a scale of 1:100 or larger, the physical size of the wind-tunnel facility required to completely scale the boundary layer becomes prohibitive. Definitive studies to show quantitatively how the wind loads on a structure are distorted by small

mismatches in the modeled boundary layer have not been performed, particularly for dynamic loadings. However, the authors' experience with measuring loads on models of similar shape but differing scale, in addition to data available in the literature, suggests that the scale used for this study (1:40) should not cause significant distortions in the measured data.

1.3 Measurement Strategy

The measurement method applied here is that a rigid model of the structure is mounted on a force balance in such a way that the resulting natural frequency of the balance/model is higher than the scaled first mode frequencies of the structure. A balance of this type can have up to six degrees of freedom for measurement of three forces and three moments. The measurements give directly the fluctuating wind loads, usually in spectral form, without inclusion of structure inertial loads. The loading data can then be combined analytically with structural properties to obtain the mean and dynamic root-mean-square (rms) structural response. The peak response is estimated by adding the mean value to a statistically chosen factor times the rms value. If structural properties change, the analysis can be repeated without having to retest the model.

An existing force balance was modified for this study to measure six loading components, five moments and a horizontal force (which are resolved into three forces and three moments at the drive rotation point).

2. TEST EQUIPMENT AND INSTRUMENTATION

2.1 Wind Tunnel

Three large wind tunnels are available in the Fluid Dynamics and Diffusion Laboratory at Colorado State University for wind engineering investigations (see Figure 1). The wind tunnel used for this study was the Industrial Aerodynamics tunnel shown in Figure 2. It has a 62-ft long test section with a 6 x 6 ft cross section. Velocity is continuously variable from 0 to 75 fps using a 75 hp variable pitch fan.

The boundary layer used for this study was obtained using a flow trip--spires and a 7-in. barrier wall--at the test section entrance, followed by pegboards for floor roughness. This roughness in combination with the spires and barrier gave mean velocity profile at the model site given by

$$\frac{U}{U_{\infty}} = \left(\frac{z}{z_{\infty}} \right)^{\alpha} \quad (1)$$

where U is the mean velocity at height z , U_{∞} is a reference velocity at height z_{∞} , and α is a power law exponent which varies with floor roughness. The value of α used in this test was 0.14 ($\sim 1/7$) corresponding to open country. The mean velocity and longitudinal turbulence intensity are shown in Figure 3. Shown in Figures 4 and 5 are the mean and turbulence intensity profiles measured in front of and behind the collector model. The drop in mean velocity and increased turbulence caused by the model is evident. Longitudinal velocity spectra were also measured at two heights in front and behind the model. Both of those spectra are shown in Figures 6 and 7.

2.2 Force Balance

The force balance used in this project is shown in Figure 8. Basically, it is a strain-sensing apparatus consisting of three main parts: a heavy steel reaction or inertial ring, a steel sprung plate supported by steel cross-beams and a stem of aluminum tubing. The reaction ring is bolted to the wind-tunnel turntable below the floor level. The entire balance rotates along with the model on the turntable, and thus defines a body-centered coordinate system. The right-handed coordinate system of the balance itself (Figure 8) is oriented with the z-axis coinciding with the stem and force balance vertical axis, and the x and y axes in the horizontal plane. The height of this plane is at two different levels, defined by an upper and lower set of strain gages, one attached to the sprung portion of the balance and the other to the stem. Each level has two complete strain gage bridge networks which sense the total bending moment about the x and y axes at that level, the bending moments being the result of wind forces on the entire solar collector model. Two other sets of strain gages sense the torsional moments about the z-axis (M_z) and a lift force along z (F_z). These gages are located at the lower level. Figure 8 shows schematically the means by which the moments about the y-axis at level 1 (My_1) and level 2 (My_2) are sensed.

The strain gages at level 1 are attached to necked-down segments of the steel cross-members which connect the sprung portion of the balance to the reaction base. The upper gages are attached to the stem, and are shown in Figure 8. Temperature-compensating resistors within some of the gage bridge networks are installed within the base of the force balance. All strain gages are p-type silicon semiconductor electrical

resistance gages, having a nominal gage factor of about 140. The lower gages are type SPB3-20-35 by BLH, and the upper gages are type BG-1-500 by Micro-Engineering II. The gages sensing F_z are from Micron Instruments. Gage excitation and amplification were provided by Accudata Model 218 gage control/amplifiers, manufactured by Honeywell.

The collector model was built and mounted in such a way that all loads are transmitted to the stem above level 2. This results in two important characteristics: 1) constant shear force in the stem between levels 1 and 2, proportional to the difference in moment at the two levels, and 2) a moment in the stem which varies linearly between the two levels. These characteristics are used in transforming forces and moments to the desired level.

The balance was designed to have a high natural frequency of vibration to permit the measurement of dynamic loading without excessive resonant amplification. This requirement was set by the need to measure loads up to a certain reduced frequency nD/U . For a given velocity in the tunnel and model dimension, we can calculate the required frequency of the loading that is needed to obtain the response of the prototype. The limitations and implications of the natural frequency of vibration of the balance and the model itself are discussed in Section 2.5.

Calibration of the entire force balance system was performed in the wind tunnel using the same electronics and data-acquisition system used during testing. A fishing string was tied to the tallest stem which supports the model and weights were used to pull on the string at the expected height of the wind loading.

Calibration results indicated that all six channels (M_{x_1} , M_{x_2} , M_{y_1} , M_{y_2} , M_z , F_z) have a nonlinearity of less than 1 percent (typically

0.25 percent) of full scale. Interaction between channels was small except that F_2 reacted to M_x . This interaction was calibrated as being of the order of 10 percent and was compensated for in the software of the digital signal processing.

2.3 Signal Processing

The signal processing system is shown in Figure 9. It consists of the strain gages of the force balance, gage amplifiers to boost the strain signals to approximately ± 10 VFS, anti-aliasing filters and a pressure measurement system. The filters were Wavetek Model 852 8-pole (48 dB/octave) Butterworth low-pass filters. They were primarily used to compensate for force balance resonance. These filters were set at a cut-off frequency (-3dB) of 30 Hz. The analog signals passing through this system are digitized using a 16-channel Preston Scientific analog/digital converter. Mean and rms for each channel are calculated on-line, but the digital time-series are then stored on magnetic tapes. These time-series can then be retrieved later for moment transformation and spectral calculations.

2.4 The Solar Collector Model

The model used in this study was built by the sponsor (LaJet Solar Energy Company). This model is shown in Figure 10. The model is built to a scale of 1:40. The main disc frame had six elements made of brass tubing. These frame elements were later replaced by solid steel bars silver-soldered together, to make the model stiffer. These bars are 0.20 in. in diameter. Between those main elements is another finer structure made of aluminum wire 0.05 in. in diameter. The 95 mirrors were 1.5 in. in diameter and tied to this smaller frame, using thread. The disc formed by the 95 mirrors was approximately 19 in. in diameter. A pie-shaped piece of 1/6 the disc area was open--see Figure 10.

The large disc was then supported on a stem which was screwed to the force balance. The force balance was located under the tunnel floor as shown in Figure 8.

Three different stem lengths were used, to account for the different height from ground of the solar collector, for different declination and hour angles. These stems are referred to as small middle and large, see Table 2. The discrepancy of height from ground between model and prototype arises because the model is supported below the disc, but the prototype is supported from above, as shown in Figure 11.

Blockage effects caused by the model were estimated as less than 3 percent. The results were not corrected for this blockage, the effects of which should be very small. The variations of mean, peak and rms velocity by the side of the collector are shown in Figure 12. The velocity characteristics shown are due to local disturbances created by the collector and do not indicate blockage problems.

A Reynolds number check was performed to see if the small bars on the back of the disk were small enough to show Reynolds number dependence. The test was run for velocities from 10 to 50 fps (at 10 m prototype height) for 90 degree wind direction, that is when the wind glances by the back side of the collector blowing through the fine truss-structure. The drag coefficient was constant over the range tested, indicating Reynolds number effects were not significant.

2.5 Frequency Response

One of the biggest concerns from the start of planning the study was designing the collector model to have a natural frequency of vibration which would be high enough to enable measurements of dynamic wind

loading without excessive resonant amplification by the force balance-model system. Strict design criteria for the mass and moment of inertia of the model were decided on by assuming that the model itself would behave like a rigid mass. On receiving the model it was evident that the model itself had some very predominant internal modes of vibration at low frequencies. The model was then modified. The main brass-members were replaced by silver-soldered steel. Rods were also connected from the support stem to the outer edges of the mirror disc. These modifications were considered adequate to obtain dynamic loading with reasonable accuracy.

It should be pointed out that the internal vibrations of the model do not change the measured mean loading.

The low-pass filter cut-off frequency was set at 30 Hz for all channels, to rid the signal of some of the high frequency vibrations.

The frequency response of a mechanical system is defined as:

$$|H(f)| = \frac{1}{\sqrt{[1-(f/f_0)^2]^2 + (2\zeta f/f_0)^2}} \quad (2)$$

Where f_0 is the natural frequency and ζ is the critical damping ratio. This could be subtracted from the load-spectra if we knew f_0 and ζ but because of the complexity of the vibrations it is considered infeasible. Many different modes are observed and the changes in declination, hour angle and stem length change the natural frequency of each mode making corrections for mechanical amplification infeasible. A more plausible approach is to assume the spectral values to be correct up to a certain frequency below internal mode frequencies and then extrapolate over that boundary if necessary.

3. TEST RESULTS

3.1 Presentation of Data

3.1.1 Load Coefficients

All data is presented in nondimensional form so that results are applicable to either the model or prototype. This is done by reducing the measured values of force F , moment M , frequency n , and power spectral density $S(n)$ by dividing them by a combination of reference quantities having the same dimension. Forces are presented in the form of force coefficient, defined as

$$C_F = \frac{F}{qA} \quad (3)$$

and moments are in the form of moment coefficient, defined as

$$C_M = \frac{M}{qAL} \quad (4)$$

where q , A , and L are wind dynamic pressure, area and length reference quantities. All reference quantities are defined for both model and prototype in Table 1. The reference velocity U was always measured at 10 meters height for prototype.

The description of power spectral density of any process, say force $S_F(n)$, involves the tabulation of S_F vs. frequency n . If this function is to be applicable at any scale, both S_F and n must be nondimensional. The frequency n has the dimension of 1/time, so that the nondimensional version, called the reduced frequency, is defined as

$$f_r = \frac{nD}{U} \quad (5)$$

As an example of the significance of reduced frequency, bodies of cylindrical shape tend to shed vortices at a particular value of f_r known as the Strouhal number. The constant Strouhal number forces the relationships between n , D and U (setting any two also sets the

third) over a wide range of cylinder sizes and velocities. For further discussion on the reduced frequency, see reference [4], page 321. The spectral value S_F has the dimension of force²/(unit frequency), and must therefore be multiplied by a reference frequency and divided by the square of a reference force. The obvious reference force is qA , as was used in the force coefficient. There is no natural reference frequency, and the actual frequency n is used instead.* The resulting reduced force spectrum is defined as

$$S_F^*(n) = \frac{nS_F(n)}{(qA)^2} \quad (6)$$

Similarly, the reduced moment spectrum is defined as

$$S_M^*(n) = \frac{nS_M(n)}{(qAL)^2} \quad (7)$$

Note that although the notation indicates these to be a function of frequency n , they can be tabulated or plotted against any function of n , of which the reduced frequency nD/U is usually selected.

3.1.2 Force and Moment Transformations

As explained in Section 2.2 and shown schematically in Figure 8, five moments and one force were measured with the force balance. But since the most vulnerable part of the structure is the drive system, moments and forces have to be transformed to the location of the drive system. This location moves around in model-space when we vary the declination or hour angles. Declination angle of the solar collector is varied to account for seasonal changes in the solar height and different

*There are definite advantages to this convention. For example, the spectrum may be integrated with respect to $\ln n$, instead of n , to yield the mean square value (since $d(\ln n) = dn/n$). In other words, when plotted on a logarithmic frequency axis, areas under the reduced spectrum curve in various frequency bands may be geometrically compared for the distribution of energy. Also, the quantity $nS(n)$ is, directly, the amount of energy which would be transmitted to a mechanical resonator at frequency n (see Appendix D, "white noise/resonator approximation").

latitudes of the sites. The hour angle varies to track the nocturnal sweep of the sun. Looking at the probable boundaries on latitudinal location it was considered adequate to measure wind loading for declination angles between -23.5 to 72.5 degrees (zero degrees is with the collector z-axis pointing straight up, positive angles point to the south--see Figure 11). The hour angle varies between -90 to 90 degrees but because of symmetry it is sufficient to study 0- to 90-degree hour angles (zero degrees is with the collector z-axis pointing straight up, positive values point the collector west--see Figure 11). For each combination of an hour angle and declination angle, loading has to be measured for many different wind directions, to get a complete picture of the loading. Because of the overwhelming number of combinations (about 3000 taking 10-degree steps), it was decided to vary the two angles independently. That is, vary the declination from -20 to 75 degrees keeping the hour angle equal to zero. Keeping the hour angle zero retains the symmetry of the collector with respect to the wind so it is sufficient to vary the wind direction only from 0 to 180 degrees. On the other hand, the hour angle is varied from 0 to 90 keeping the declination zero. For this case there is no symmetry about a vertical plane, so the wind direction has to be varied in steps over the whole 360 degrees.

The moments and force measured by the force balance are denoted M_{x_1} , M_{y_1} , M_z , M_{x_2} , M_{y_2} , F_z . Figure 13 shows the relationship between force-balance coordinates and model set-up. This figure also shows the definition of wind directions. The force balance x-axis always points straight into a zero degree wind.

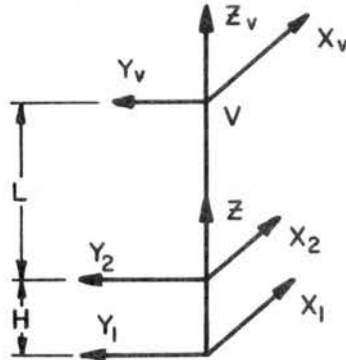
To make things easier to visualize, the moments and forces are transformed to the drive system (support point) in three stages. First,

forces and moments are transformed up to the ball point around which the wind-tunnel model turns. It is called V, see Figure 13. The height L varies depending on what support stem is used. L is the distance from the upper set of strain gages to the ball point V. The upper set of strain gages is located 1.5 in. below the tunnel floor. Using the declination angle (α) or hour angle (θ), the loads are then transferred to the x',y',z' coordinate system in the support point. The support point or drive system is located 225 in. in prototype scale (5.625 in. in model scale) from the mirror plane. For the model the mirror surface is 2 in. from the ball point V. R is the distance from V to the support point (= 7.625 in. model scale). After this the "prime" coordinate system is rotated to the x'',y'',z'' ("double prime") system, which z-axis is perpendicular to the mirror plane. For nonzero declination angles this rotation is about the y' -axis; for nonzero hour angles the rotation is about the x' -axis. Figures 14a and 14b show the various coordinate systems. Table 2 gives the values of the dimensions used for different declination and hour angles.

The transformation formulas and corresponding computer codes are presented in the following.

Transformation to the ball point V is achieved by the following equations

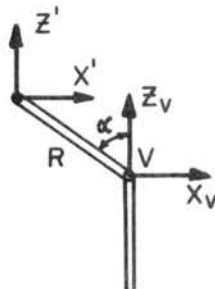
$$\begin{aligned}
 Fx_v &= F_x = (My_1 - My_2)/H \\
 Fy_v &= F_y - (Mx_1 - Mx_2)/H \\
 Fz_v &= F_z = \text{measured} \\
 Mx_v &= Mx_1 + F_y (H + L) \\
 My_v &= My_1 - F_x (H + L) \\
 Mz_v &= M_z = \text{measured}
 \end{aligned}
 \tag{8}$$



Now to get to the "primed" system from V , we separately treat the case when declination is zero and when hour angle is zero.

A. Hour Angle = 0

Transformation to the "primed" system is achieved by using the declination angle α . Forces stay the same, but moments are changed.



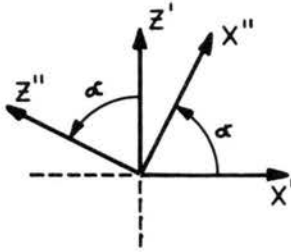
$$F_{x'} = F_{x_v} ; F_{y'} = F_{y_v} ; F_{z'} = F_{z_v}$$

$$M_{x'} = M_{x_v} + F_y \cdot R \cdot \cos\alpha \quad (9)$$

$$M_{y'} = M_{y_v} - F_z \cdot R \cdot \sin\alpha - F_x \cdot R \cdot \cos\alpha$$

$$M_{z'} = M_{z_v} + F_y \cdot R \cdot \sin\alpha .$$

Rotation around the y-axis gives us the "double-prime" system;



$$F_{y''} = F_{y'} ; M_{y''} = M_{y'}$$

$$F_{x''} = F_{x'} \cdot \cos\alpha + F_{z'} \cdot \sin\alpha$$

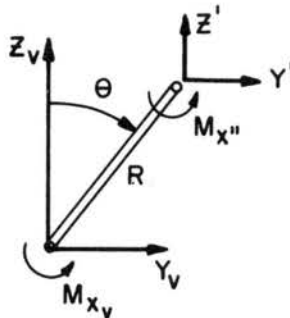
$$M_{x''} = M_{x'} \cdot \cos\alpha + M_{z'} \cdot \sin\alpha \quad (10)$$

$$F_{z''} = F_{z'} \cdot \cos\alpha - F_{x'} \cdot \sin\alpha$$

$$M_{z''} = M_{z'} \cdot \cos\alpha - M_{x'} \cdot \sin\alpha$$

B. Declination = 0

Transformation to the "primed" system is achieved by using the hour angle θ . Forces stay the same.



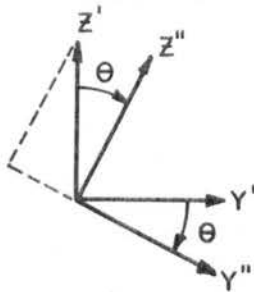
$$F_{x'} = F_x, F_{y'} = F_y, F_{z'} = F_z$$

$$M_{x'} = M_{x_v} + F_y \cdot R \cdot \cos\theta - F_z \cdot R \sin\theta$$

$$M_{y'} = M_{y_v} - F_x \cdot R \cos\theta \quad (11)$$

$$M_{z'} = M_{z_v} + F_x \cdot R \sin\theta$$

Rotation around the x-axis gives us the "double-prime" system;



$$M_{x''} = M_{x'}, \quad F_{x''} = F_{x'}$$

$$Q_{z''} = Q_{z'} \cdot \cos\theta + Q_{y'} \cdot \sin\theta \quad (12)$$

$$Q_{y''} = Q_{y'} \cdot \cos\theta - Q_{z'} \cdot \sin\theta$$

where Q stands for forces and moments.

The computer codes corresponding to cases A and B are shown in Tables 3a and 3b.

3.2 Mean Loading

For each wind-tunnel run, time-series of force balance load-components were taken and stored on magnetic tape. These time-series consist of four segments of 2048 points each. Sampled at 92 samples per second this represents 89 seconds of data-taking. These time-series were then transformed to the support point according to the previous equations. The mean forces and moments in the "double primed" coordinate system of Figure 14 are plotted up and listed in Appendix A. Figures A.1 to A.10 show mean loading for declination angles of 75, 60, 50, 40, 30, 20, 10, 0, -10, -20, holding the hour angle zero. Figures A.11 to A.15 show the mean loading for 90, 75, 60, 45, 30 and

15 degree hour angle, holding declination equal zero. The moment turning the disc in its own plane, M_z , was so small that it was not plotted. Corresponding numerical values are listed in Table A.2.

3.2.1 Stowed Positions

The various positions listed above are typically realized when the solar collector is tracking the sun, but for very high wind conditions there is danger of structural damage. The operation would then be halted and the collector put in a stowed position. Two stowed positions have been suggested. One is keeping the collector close to the ground with zero declination and hour angle. This case was reported with the different declination angles in Appendix A. The other one is realized by swinging the collector up into the air so that it looks like an umbrella. This umbrella-like stowed position has been suggested to prevent snow from settling on the mirror surfaces. Mean loading for this stowed position is shown in Figures A.16 and A.17.

3.2.2 Loading in the "Primed System"

To simplify the application of the data to design the drive mechanism, mean loading has also been calculated for the "primed" coordinate system of Figure 14. In this system the x' and y' -axes lie in a plane parallel to the ground. For zero hour angle F_y and M_y are identical in the "primed" and "double primed" systems. The same is true for F_x and M_x when the declination is zero. A listing of the results are presented in Appendix B.

3.3 Load Spectra

Load spectra were measured for numerous combinations of declination, hour angles and wind directions. Wind directions were selected with respect to large mean loading. The plots of the spectra

are shown in Appendix C, along with a listing of wind directions and velocities. The information on top of the plots applies only to the first curve. As explained earlier in Section 2.5, the spectral results are limited in frequency by the internal vibrations of the solar collector model. To eliminate as many as possible of these internal vibrations from the load-signal the low-pass filters were set at a cut-off frequency of 30 Hz. Because of the roll-off, any load-components of frequency higher than 25 Hz are affected by this cutoff. What reduced frequency this corresponds to has to be calculated each time, but for most of the spectral runs the wind velocity is about 25 fps. This means that reduced frequencies of more than 1.0 do not give valid results. Abrupt peaks in the spectra should also be ignored as they are most likely associated with internal mode mechanical vibrations. Appendix D shows how the load spectral results can be used to estimate the response of the structure. Because of the spectral noise caused by the vibrations of the model the white-noise approximation is recommended rather than integrating the spectra. This makes it easy to estimate the rms-response according to Eq. (D.10) as:

$$\sigma_M = \sqrt{\frac{\pi}{4\zeta}} f_{r_o} S(f_{r_o}) \quad (13)$$

by calculating the reduced natural frequency f_{r_o} for the prototype ($D = 40$ ft, U is the wind speed in ft/sec at 32.8 ft height and f_o is the natural prototype frequency of the particular vibration), then reading $f_{r_o} S(f_{r_o})$ from the spectral plots and substituting that value into Eq. (13) which will then give the rms moment or force coefficient.

The most critical parameter in estimating the response is the critical damping ratio ζ . For tall buildings this ratio is estimated

in the range 0.5-2.0 percent, depending on the material of the frame. For the type of structure considered here, the critical damping ratio is probably not more than 1 percent unless aerodynamic damping is high. On-site testing of the mechanical damping of the structure would give valuable information. The installation of some kind of mechanisms to increase the damping will undoubtedly prove beneficial to decrease dynamic response.

3.4 Modifications of Solar Collector Model

To minimize the high mean moment around y' -axis observed for 75-degree declination, some modifications of the solar collector were proposed. For the 75-degree declination (0-degree hour angle) two factors contribute to the high mean y' -moment. One is obviously the gap and the other is the increased wind velocity with height. By partially filling the gap and/or removing the four top mirrors the moments can be lowered considerably. These modifications also affect the normal force F_z . Table 4 shows schematically the modifications and the corresponding changes in mean y' -moment and normal force.

Setup I is the original unmodified solar collector, used as a reference. For Setup II a 15 sq in. plate, which the sponsor provided, was placed in a vertical position in the middle of the gap. For Setup III another plate was made with approximately the same area, but placed at the lower edge of the gap, to provide a larger moment arm. This plate was also vertical. Setup IV represents the four highest mirrors having been removed. With the mirrors still removed the lower plate was added in setup V. For Setup VI the gap was practically filled up with cardboard, lying in the plane of the mirror surface. The loading for each setup was measured for 0- and 180-degree wind directions.

Negative percentages denote lower magnitude of forces or moments. The results of the five modifications show a consistent pattern: 1) filling the gap increases the force and decreases the moment with the moment arm of the added area acting as an important influence, and 2) decreasing mirror area at the top of the collector decreases both force and moment. Setup V is an attractive option which provides 30 to 40 percent reduction in moment with a very small increase in normal force.

3.5 Effects of Porosity

To see the effect of the porosity of the collector model the disc area was covered with a sheet of stiff plastic. For 90-degree hour angle and 270 degree wind, the normal force was measured with and without the plastic sheet. The effective drag coefficient decreases slightly as the disk is covered. Using the area of the mirror-surfaces only (plus stem) we get a drag-coefficient of 1.7 compared to C_f of 1.6 for the total area of the plastic disc. But on the other hand, the dynamic loading increases drastically when the disc is not porous as shown in Figure 15, for the normal force.

3.6 Accuracy of Data

The accuracy of the data presented in this report is hard to estimate. In the following a few factors will be mentioned which could cause errors in the experiments.

The size of the wind tunnel and the large scale of the model (1:40) put limitations on the wind-spectra hitting the model, which manifests itself in that some of the large-scale fluctuations are missing. This is a known discrepancy and could be estimated theoretically.

The model and its support system are not an exact replica. This will probably cause small errors because the main loading is on the mirrors.

The strain gages of the force balance are subject to temperature drift as the air in the wind tunnel heats up during test runs. This is not considered to be a large factor because the duration of each wind-tunnel run is only about 89 seconds.

The moment transformations magnify any errors because the distance between the two levels of strain gages is only 5 inches. The farther the moments have to be transferred, the larger the amplification of the errors. So set-ups requiring the larger support stems would be expected to be less accurate than the ones using the small support stem.

Using magnitude analysis it is evident that the forces are more accurate than the moments, from a percentage error standpoint.

By looking at the data and doing simple calculations the accuracy of the moments is estimated of the order 0.05 coefficient, which is about 10 percent of maximum.

4. DISCUSSION

Mean and dynamic wind loading were measured for many different combinations of declination, hour angle and wind direction. Highest loading cases were experienced for large declination or hour angles as expected. No predominant vortex shedding phenomena were observed.

The critical damping ratio of the vibrational modes in the prototype has pronounced effects on the dynamic response. Accurate estimation of the damping ratio by full-scale experiments would therefore be extremely useful for the response calculations.

The porosity of the collector disc is definitely beneficial because of reduction in dynamic loading with relatively small increase in mean drag coefficient.

REFERENCES

1. Cermak, J. E., "Laboratory Simulation of the Atmospheric Boundary Layer," AIAA Jl., Vol. 9, September 1981.
2. Cermak, J. E., "Applications of Fluid Mechanics to Wind Engineering," A Freeman Scholar Lecture, ASME Jl. of Fluids Engineering, Vol. 97, No. 1, March 1975.
3. Cermak, J. E., "Aerodynamics of Buildings," Annual Review of Fluid Mechanics, Vol. 8, 1976, pp. 75-106.
4. Simiu, E. and R. H. Scanlan, Wind Effects on Structures: An Introduction to Wind Engineering, John Wiley & Sons, New York, 1978.

FIGURES

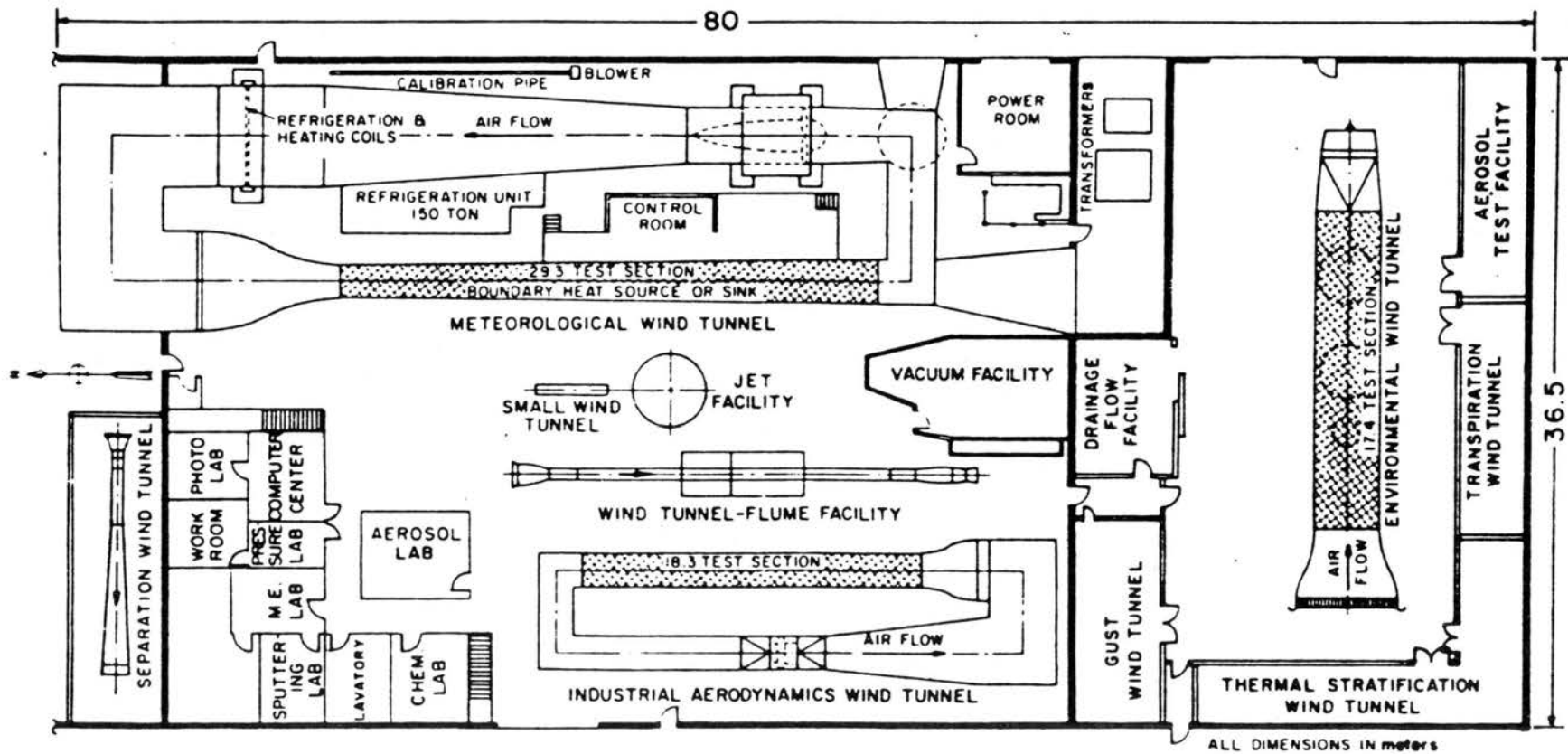


Figure 1. Fluid Dynamics and Diffusion Laboratory, Colorado State University

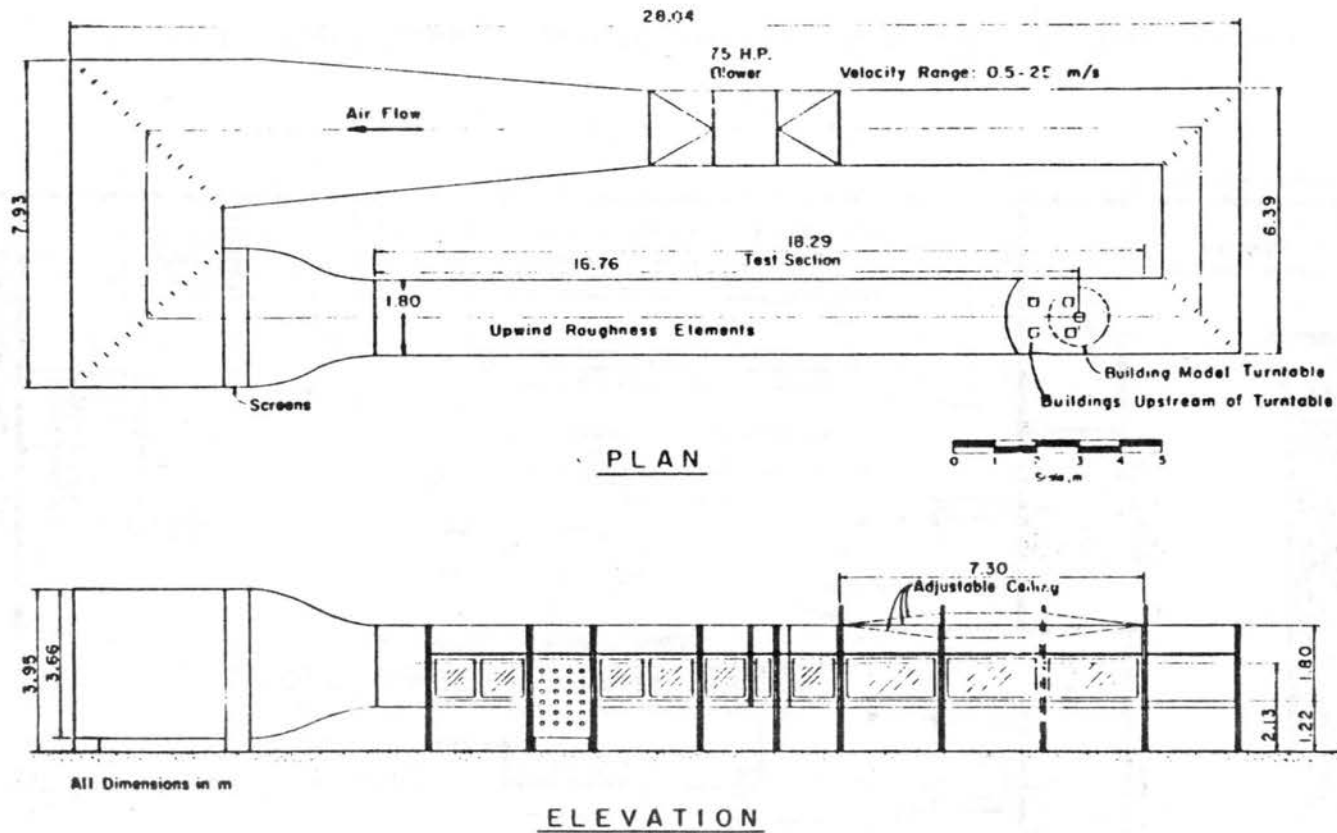


Figure 2. The Fluid Dynamics and Diffusion Laboratory Industrial Aerodynamics Wind Tunnel

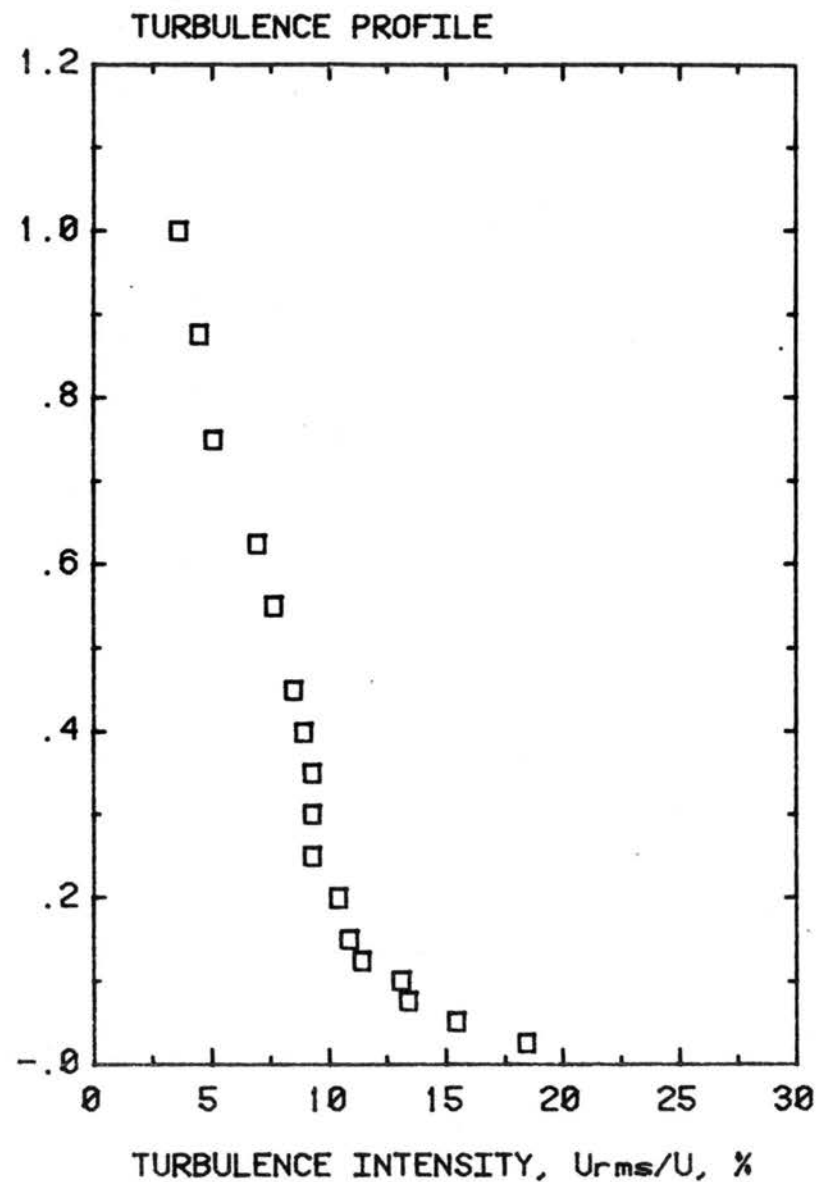
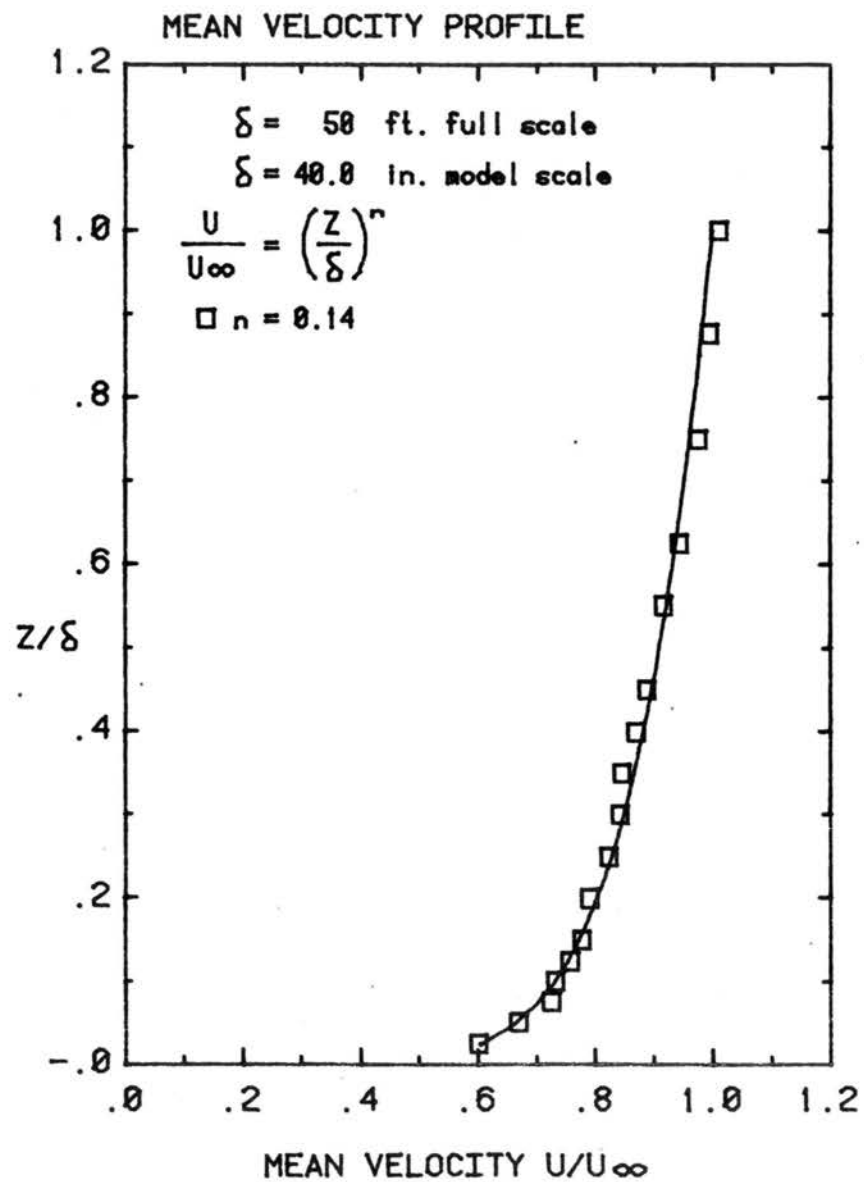
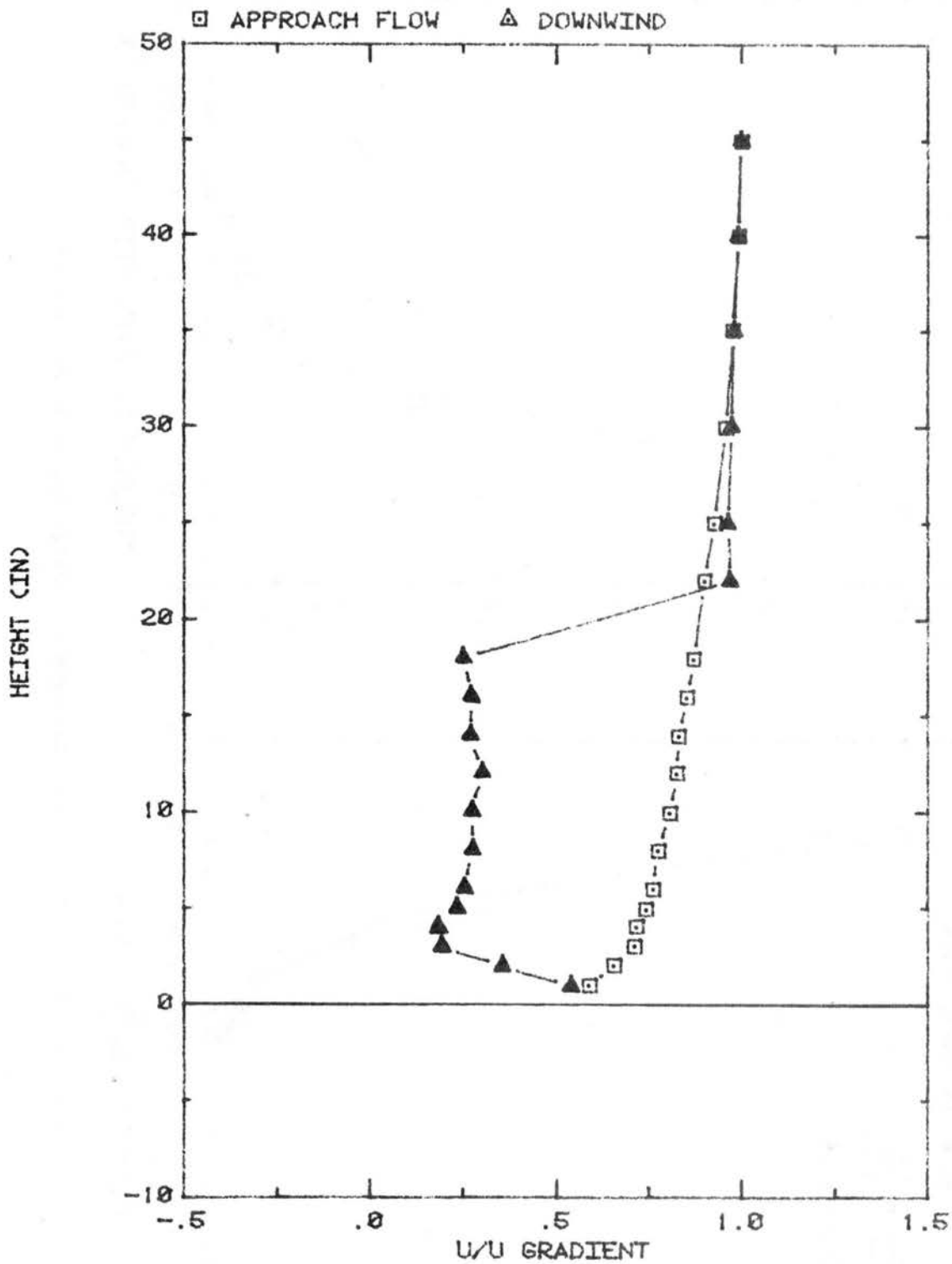
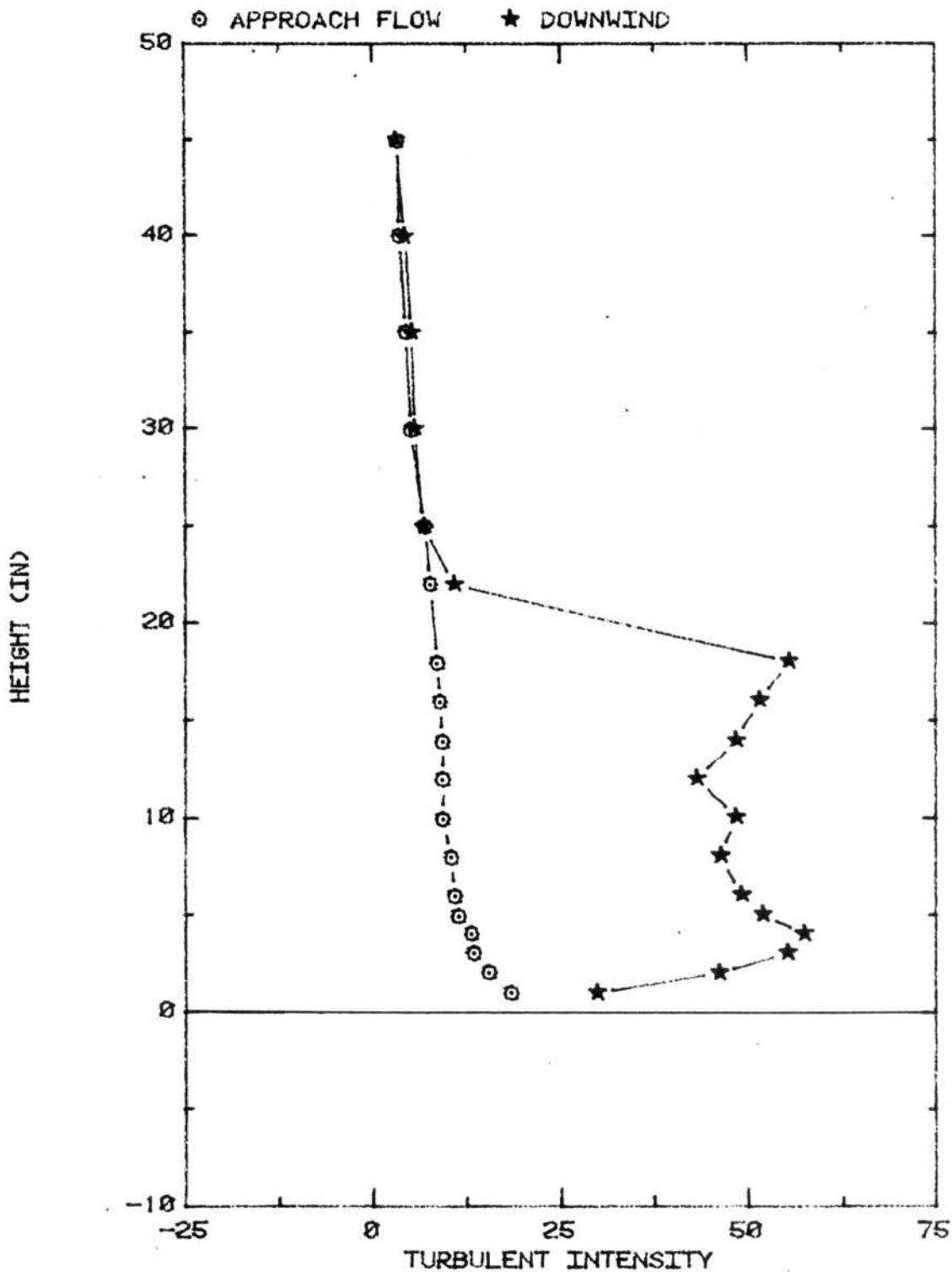


Figure 3. Mean Velocity and Turbulence Profiles Approaching the Model



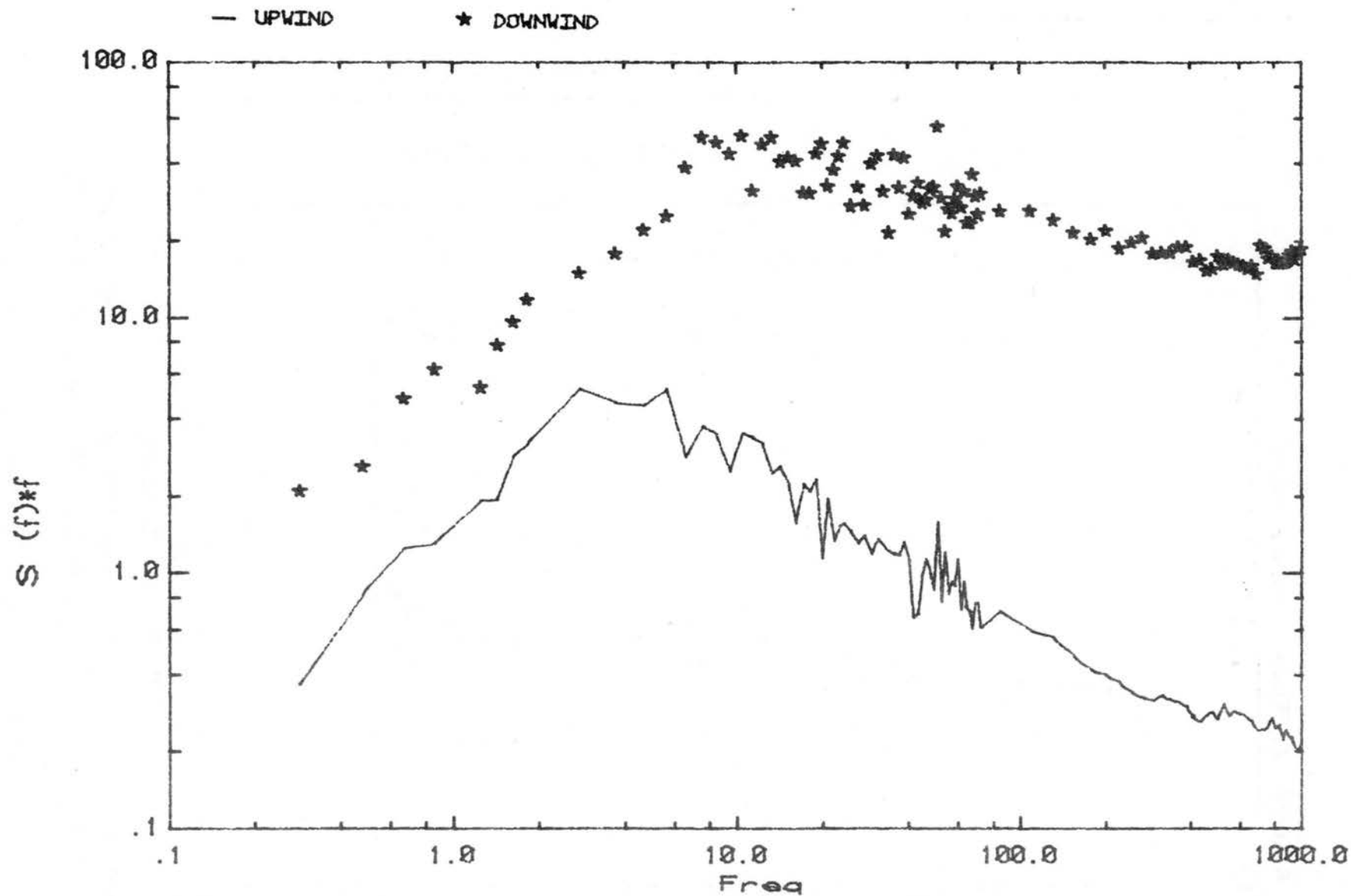
VELOCITY PROFILES APPROACHING AND BEHIND THE COLLECTOR
COLLECTOR RAISED 60 DEG, PROFILE 10 INCHES BEHIND SUPPORT

Figure 4. Mean Velocity Profiles in Front of and Behind the Collector Model



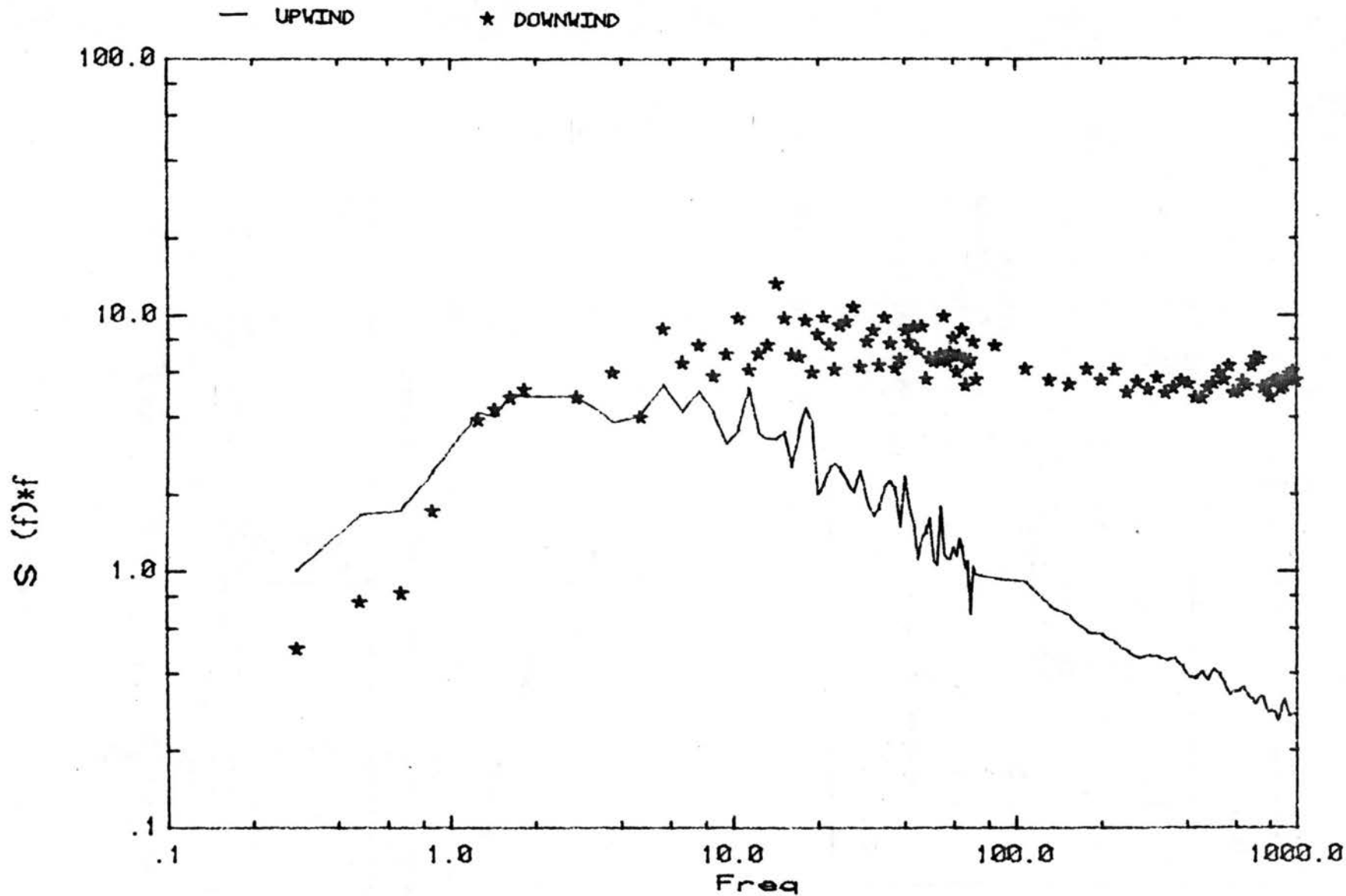
TURBULENCE INTENSITY PROFILES APPROACHING AND BEHIND COLLECTOR
COLLECTOR RAISED 60 DEG. PROFILE 10 INCHES BEHIND SUPPORT

Figure 5. Turbulence Intensity Profiles in Front of and Behind the Collector Model



LONGITUDINAL VELOCITY SPECTRA AT 20 IN MODEL SCALE

Figure 6. Longitudinal Velocity Spectra in Front of and Behind the Collector Model
at 10 in. from the Floor



LONGITUDINAL VELOCITY SPECTRA AT 9.8 INCHES (10 M FULL SCALE)

Figure 7. Longitudinal Velocity Spectra in Front of and Behind the Collector Model at 10 in. from the Floor

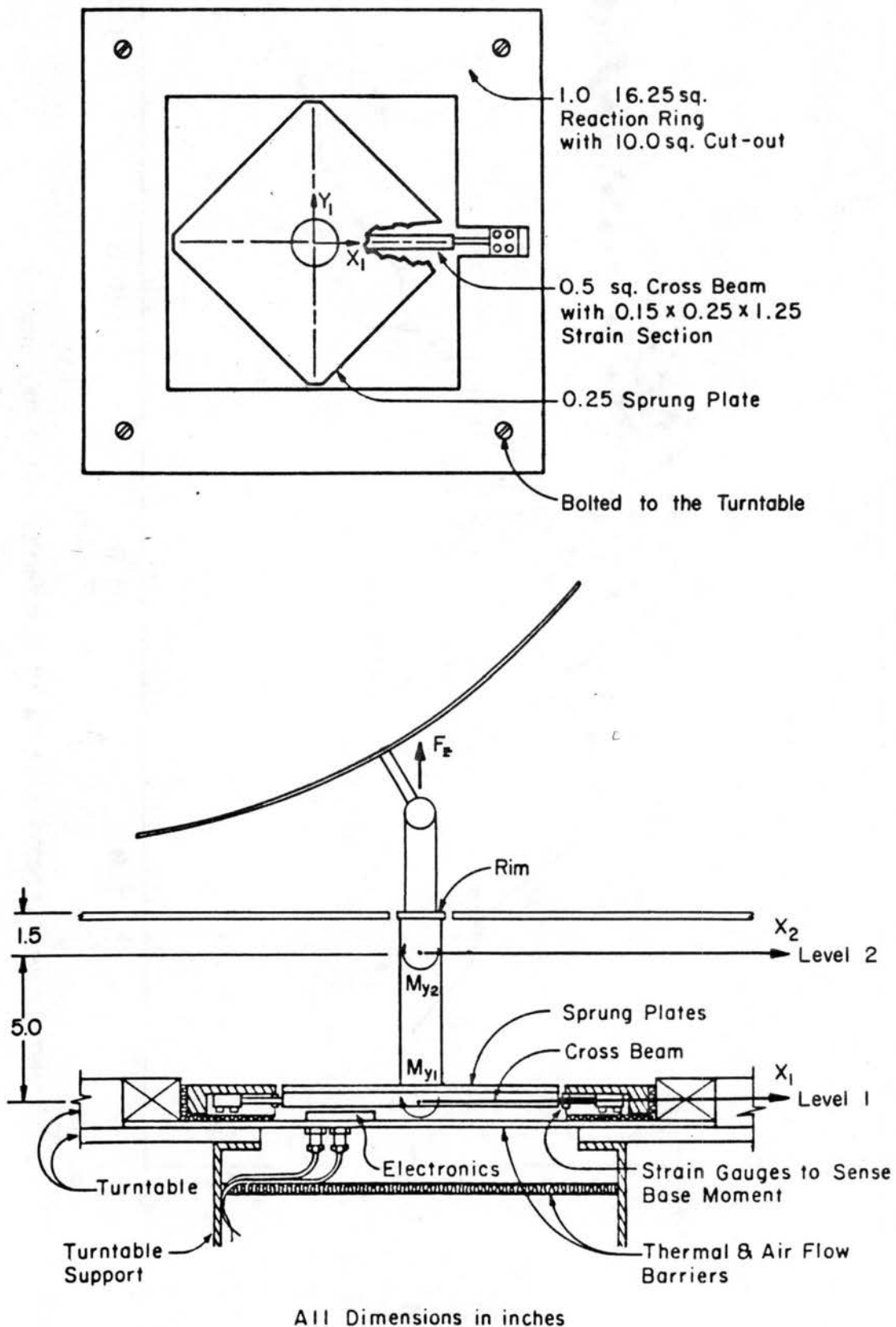


Figure 8. The Force Balance and Coordinate System

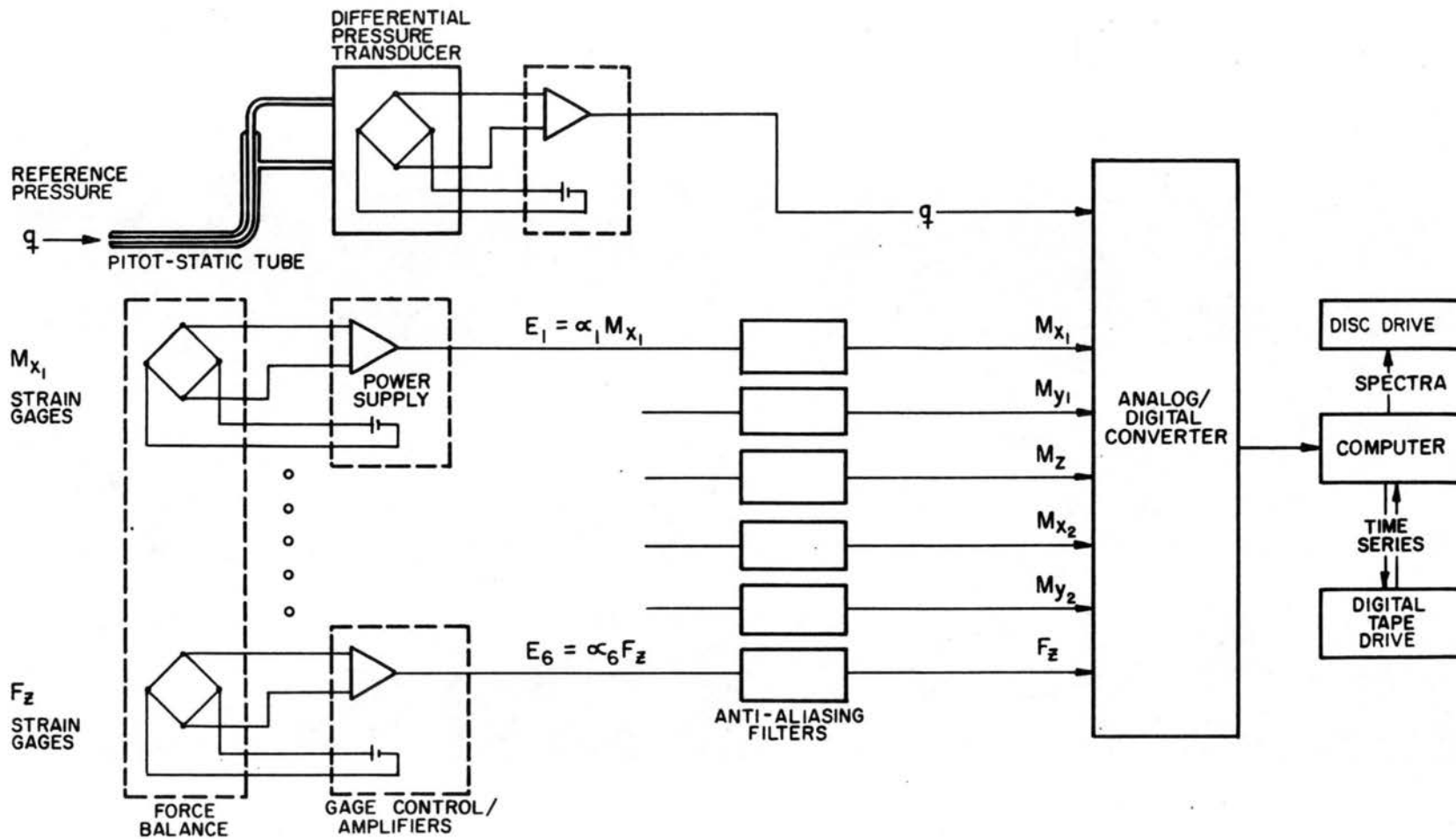


Figure 9. The Signal Processing System

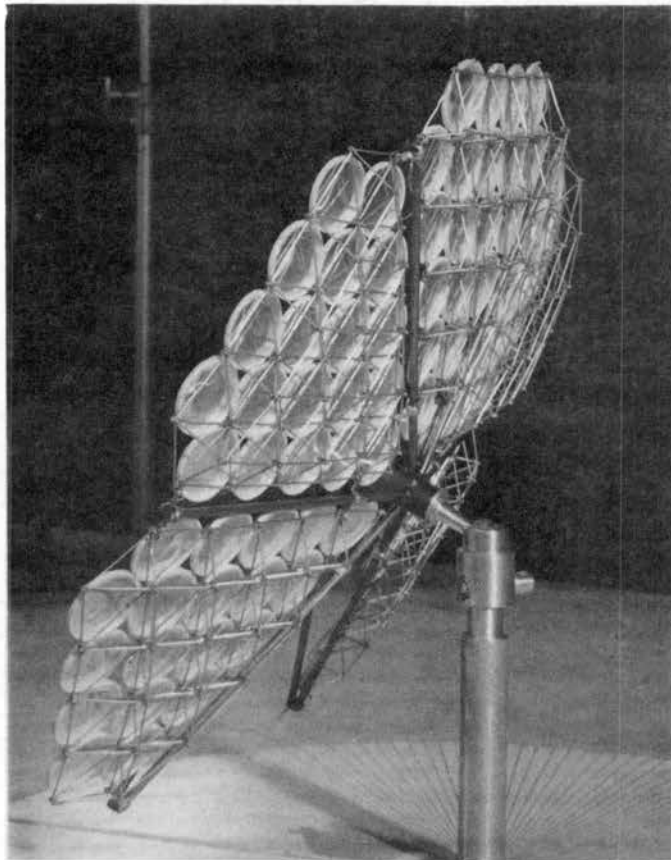
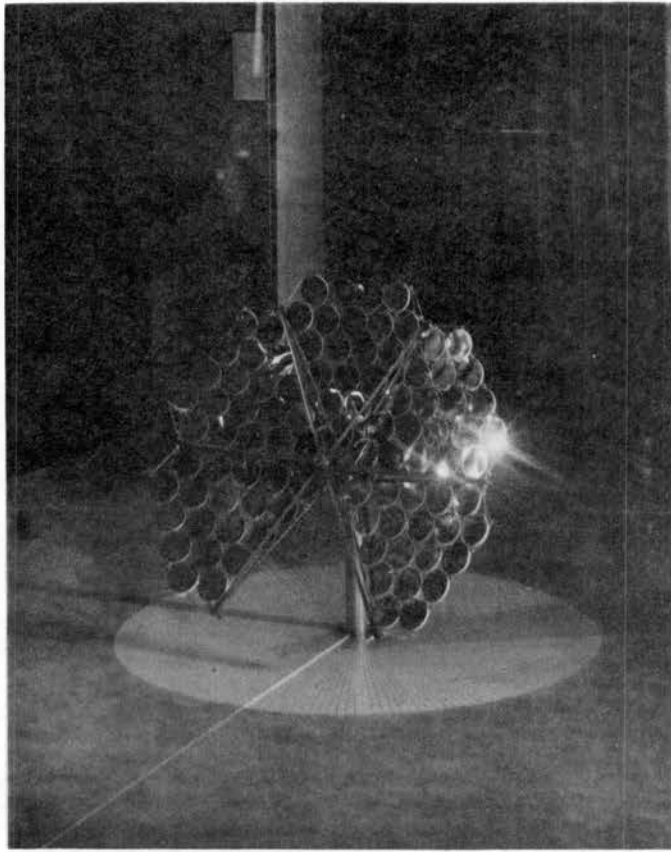
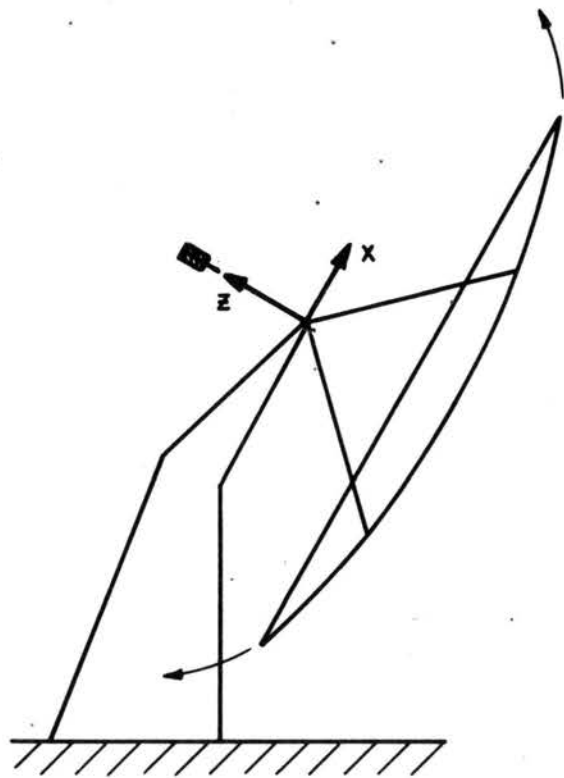
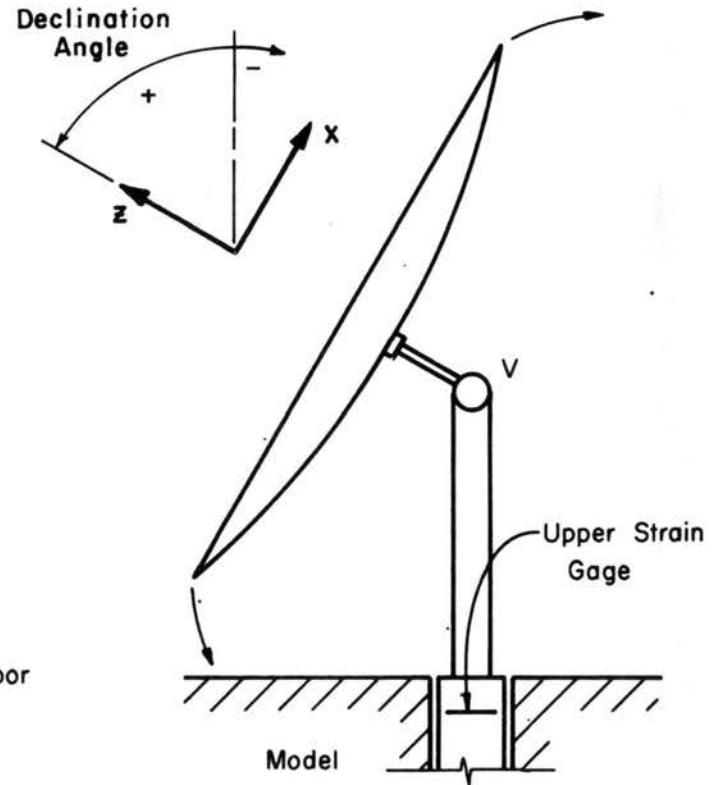


Figure 10. The Solar Collector Model in the Wind Tunnel



Prototype Collector

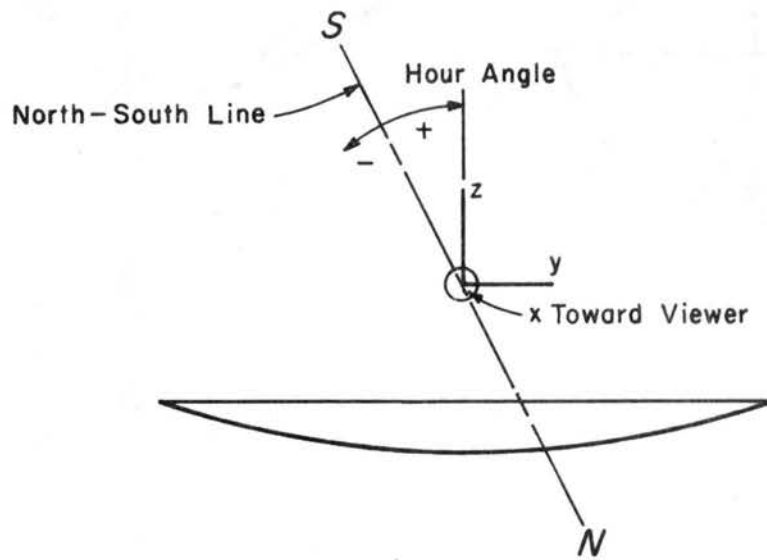
Ground = Tunnel Floor



Model

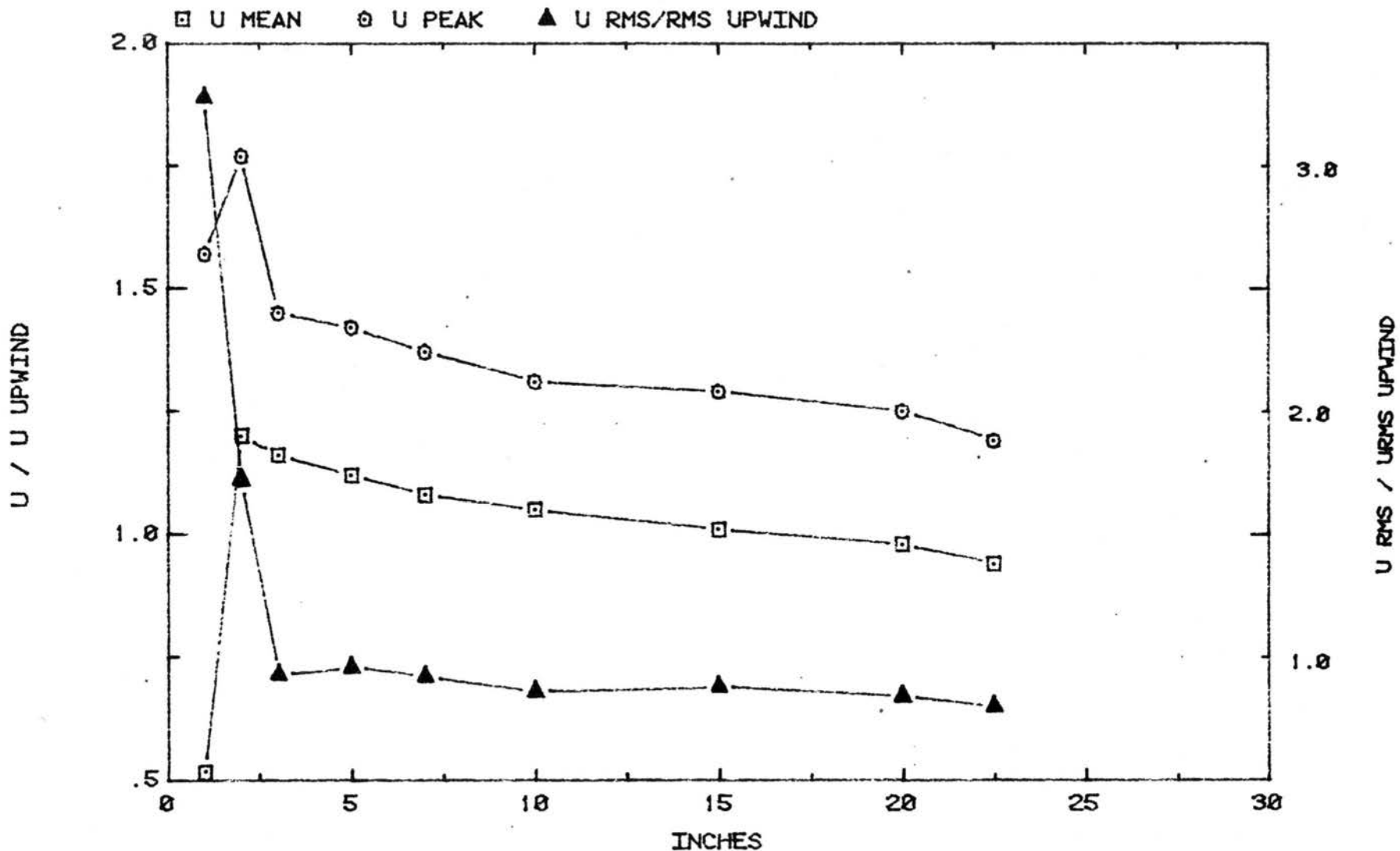
Upper Strain Gage

Figure 11a. Schematic of the Model Support System



View Along x Axis Fixed at Pivot

Figure 11b. Schematic of the Model Support System



VELOCITY VARIATIONS BY THE SIDE OF THE MODEL TO THE WALL
 AT 9.8 INCHES HEIGHT (10 M FULL SCALE)

Figure 12. Horizontal Velocity Profile Adjacent to the Model

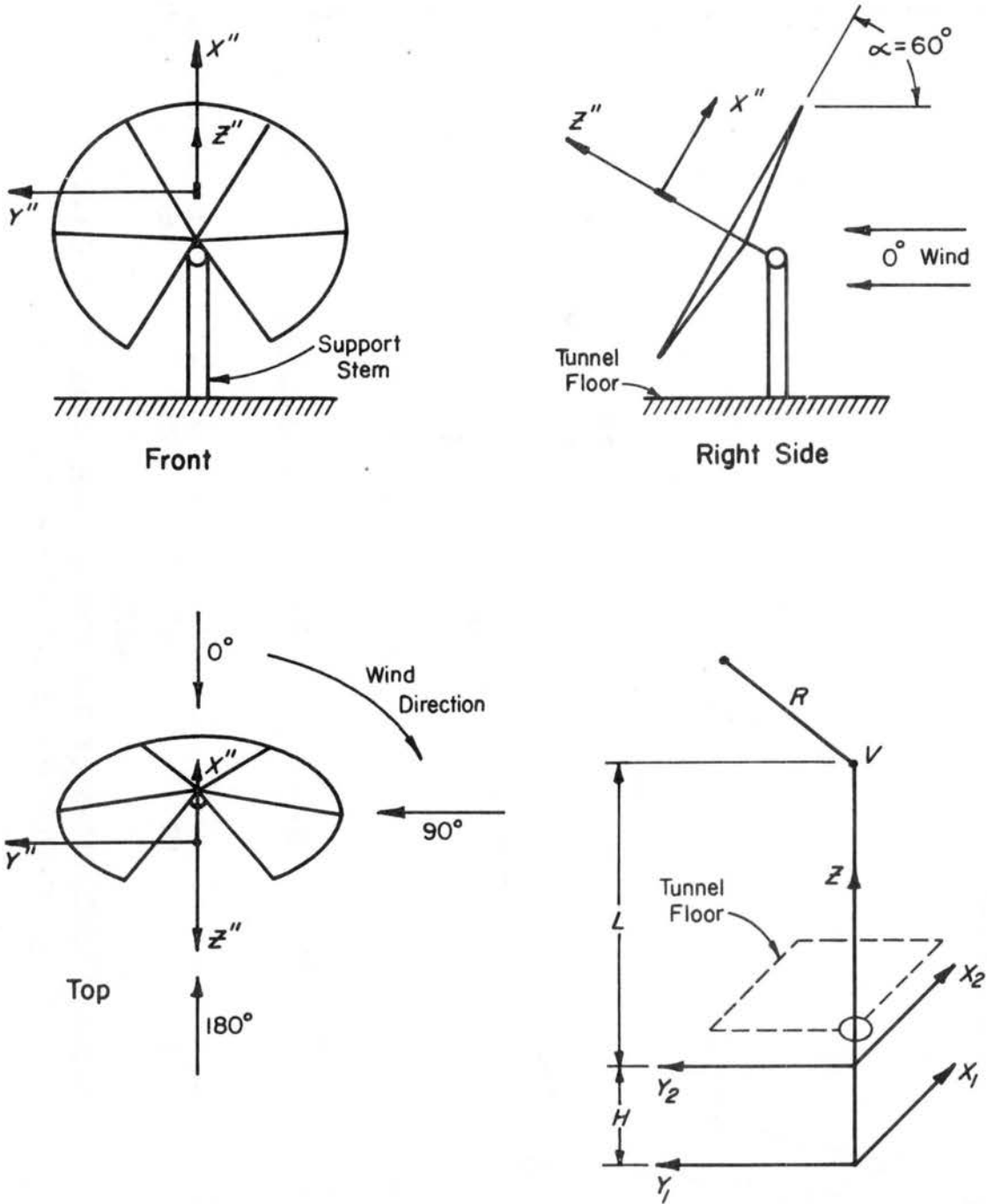
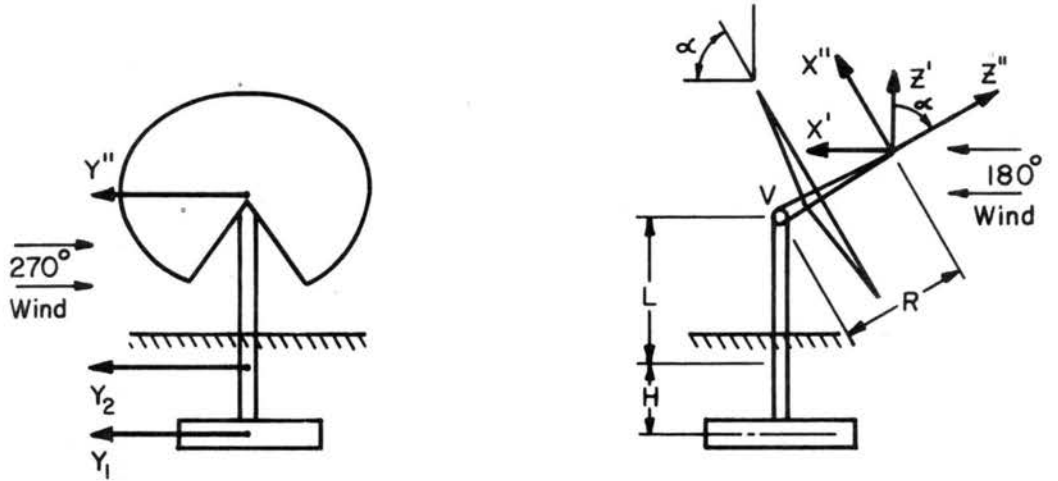
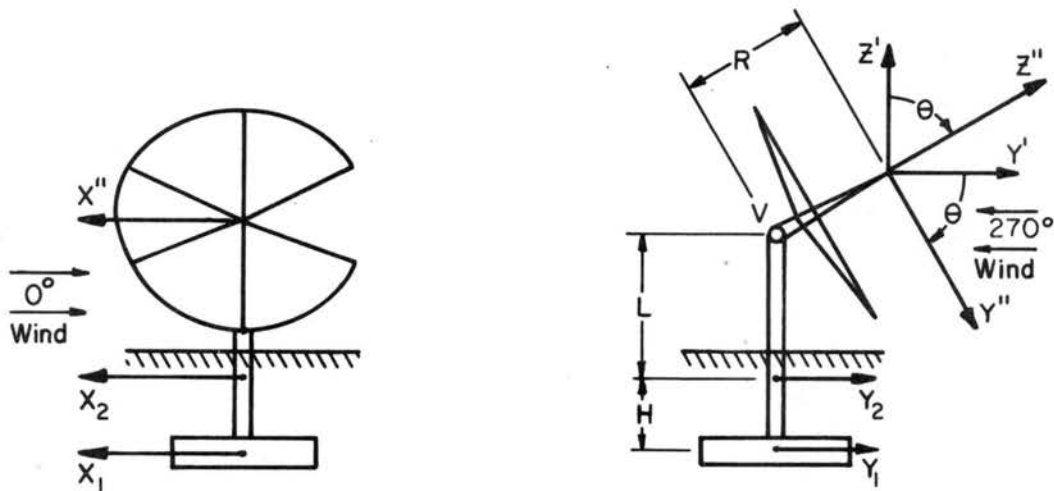


Figure 13. Force Balance Coordinates and Model Set-up



a. Non-zero declination



b. Non-zero hour angle

Figure 14. Model Coordinate Systems

RUN NO.530 WIND DIRECTION 270 Deg. VEL. U = 22.5 fps

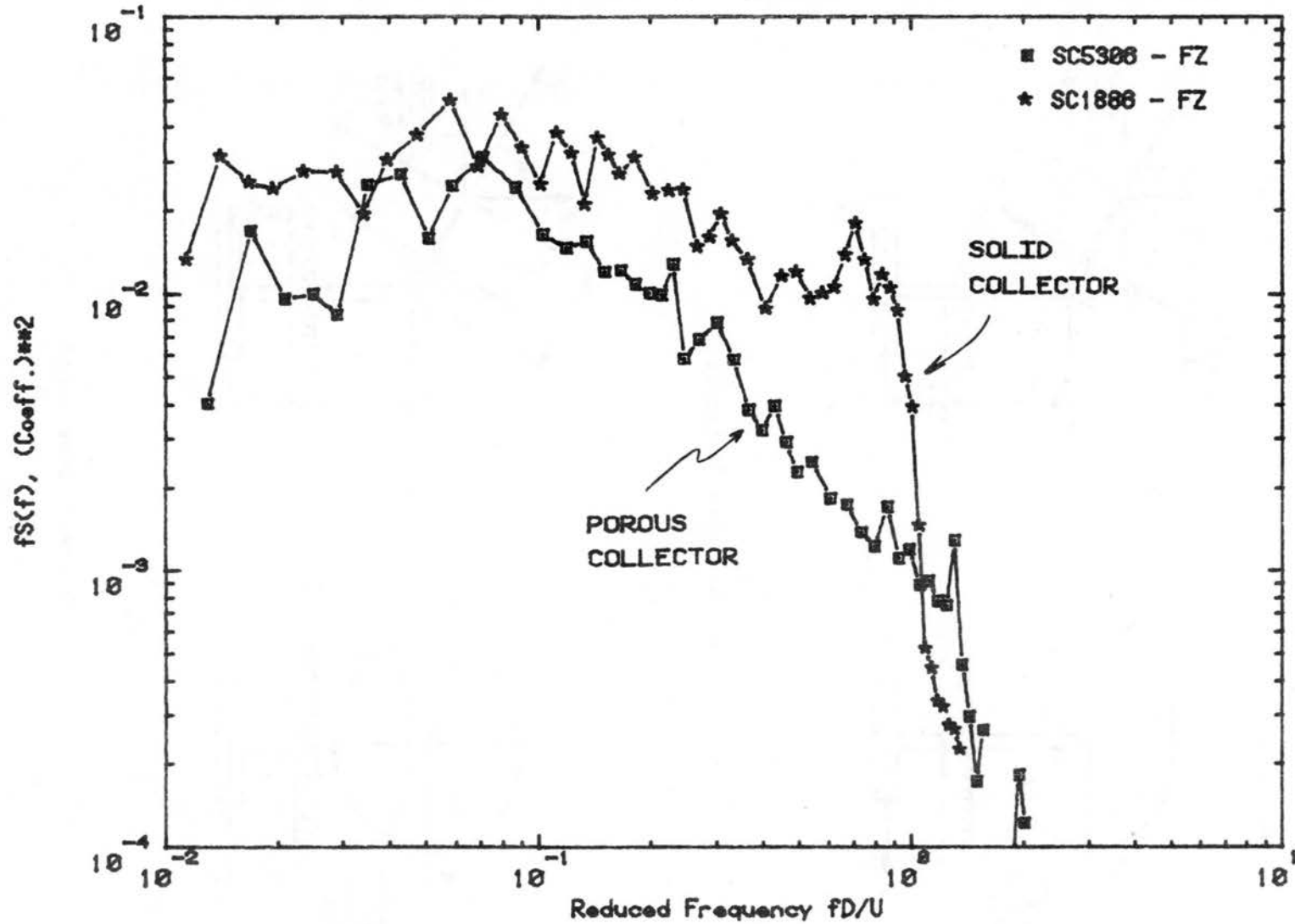


Figure 15. Spectra of Normal Force vs. Porosity

TABLES

Table 1. Reference Quantities

	H	L	D	A = H · D	AL
Model	1.0 ft	1.0 ft	1.0 ft	1.0 ft ²	1.0 ft ³
Prototype	40 ft	40 ft	40 ft	1600 ft ²	64000 ft ³

$$q = 1/2 \rho U^2 = \text{dynamic pressure}$$

where $\rho =$ air density at site in lb/ft³
 $= 0.00238$ slugs/ft³ at sea level

Alternatively

$$1/2 \rho U^2 = 0.00256 U^2 \text{ with } U \text{ in mph.}$$

$U =$ wind velocity in ft/sec at 10 m (32.8 ft) prototype height
or 9.84 in. in model scale

From the above we obtain formulas for calculating prototype forces and moments:

$$F_i = C_{F_i} \cdot q \cdot 1600 \text{ [lb]}$$

$$M_i = C_{M_i} \cdot q \cdot 64000 \text{ [lb-ft]}$$

Table 2. Dimensions Used in Transformations

Declination Angle	Hour Angle	Stem Length
75	0	middle
60	0	middle
40	0	small
30	0	small
20	0	small
10	0	small
0	0	small
-10	0	small
-20	0	small
0	0	small
0	15	small
0	30	small
0	45	middle
0	60	middle
0	75	large
0	90	large
0 (u m b r e l l a s t o w e d)	0	large

stem lengths: small - 2.25 inches
 middle - 5.0 inches
 large - 8.0 inches

To calculate the length L , from upper strain gages to V we add 3.5 inches to the stem lengths (1.5 because gages are below floor level and 2 inches accounting for the height of the connection piece).

Table 3a. Transformation Code for Non-zero Declination

```

C*****
SUBROUTINE TRSNF(IBUF,SL,SINHR,COSHR,SINDC,COSDC,JDUP)
COMMON /FIL/ IDCB(144,7),NFILE,LU
DIMENSION IBUF(128,7),SL(7)
REAL MXV,MYV,L,MX1,MX2,MY1,MZ1,MZ2,MZV,MY11
C
H=5.0/12.
L = 11.5/12.
R = (2.+5.625) 12.
C
DO 10 I=1,128
  FMX1 = FLOAT(IBUF(I,1)) * SL(1)
  FMY1 = FLOAT(IBUF(I,2)) * SL(2)
  FX = (FMY1-FLOAT(IBUF(I,5))*SL(5))/H
  FY = -(FMX1-FLOAT(IBUF(I,4))*SL(4))/H
  FZ = FLOAT(IBUF(I,3))*SL(3)
C
C      INTERACTION CORRECTION BETWEEN FZ AND MX
C
  FZ = FZ - .136 * FMX1
C
  MXV = FY*(L/H) + FMX1
  MYV = -FX*(L/H) + FMY1
  MZV = FLOAT(IBUF(I,3))*SL(3)
C
  MX1 = MXV+FY*R*COSDC
  MY1 = MYV-FX*R * COSDC - FZ*R*SINDC
  MZ1 = MZV + FY*R * SINDC
C
  MX2 = MX1 * COSDC + MZ1 * SINDC
  MZ2 = MZ1 * COSDC - MX1 * SINDC
  FX2 = FX * COSDC + FZ * SINDC
  FZ2 = FZ * COSDC - FX * SINDC
C
  IBUF(I,1) = IFIX(MX2/SL(1))
  IBUF(I,2) = IFIX(MY1/SL(2))
  IBUF(I,3) = IFIX(MZ2/SL(3))
  IBUF(I,4) = IFIX(FX2/SL(4))
  IBUF(I,5) = IFIX(FY/SL(5))
  IBUF(I,6) = IFIX(FZ2/SL(6))
10 CONTINUE
C
C      NOW THAT CALCULATION IS DONE WRITE IT BACK TO THE FILE.
C
DO 20 I=1,NFILE
  CALL POSNT(IDCB(1,I),IERR, 1)
  CALL WRITF(IDCB(1,I),IERR,IBUF(1,I),128)
20 CONTINUE
RETURN
END
*
```



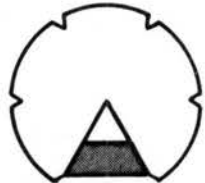
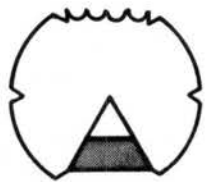



Table 3b. Transformation Code for Non-zero Hour Angle

```

C*****
SUBROUTINE TRSNF(IBUF,SL,SINHR,COCHR,SINDC,COSDC,IBUF)
COMMON /FIL/ IDCB(144,7),NFILE,LU
DIMENSION IBUF(120,7),SL(7)
REAL MXV,MYV,L,MX1,MX2,MY1,MZ1,MZ2,MZV,MY11
C
H=5.0/12.
L = 11.5/12.
R = (2.+5.625) 12.
C
DO 10 I=1,120
  FMX1 = FLOAT(IBUF(I,1)) * SL(1)
  FMY1 = FLOAT(IBUF(I,2)) * SL(2)
  FX = (FMY1-FLOAT(IBUF(I,5))*SL(5))/H
  FY = -(FMX1-FLOAT(IBUF(I,4))*SL(4))/H
  FZ = FLOAT(IBUF(I,6))*SL(6)
C
C      INTERACTION CORRECTION BETWEEN FZ AND MX
C
  FZ = FZ - .136 * FMX1
C
  MXV = FY*(L+H) + FMX1
  MYV = -FX*(L+H) + FMY1
  MZV = FLOAT(IBUF(I,3))*SL(3)
C
  MX1 = MXV + FY*R*COSHR - FZ*R*SINHR
  MY11 = MYV - FX*R*COSHR
  MZ1 = MZV + FX*R*SINHR
  MX2 = MX1
  FX2 = FX
  MY1 = MY11*COSHR - MZ1*SINHR
  MZ2 = MZ1*COSHR + MY11*SINHR
  FZ2 = FZ*COSHR + FY*SINHR
  FY = FY*COSHR - FZ*SINHR
C
  IBUF(I,1) = IFIX(MX2/SL(1))
  IBUF(I,2) = IFIX(MY1/SL(2))
  IBUF(I,3) = IFIX(MZ2/SL(3))
  IBUF(I,4) = IFIX(FX2/SL(4))
  IBUF(I,5) = IFIX(FY/SL(5))
  IBUF(I,6) = IFIX(FZ2/SL(6))
10 CONTINUE
C
C NOW THAT CALCULATION IS DONE WRITE IT BACK TO THE FILE.
C
DO 20 I=1,NFILE
  CALL POSNT(IDCB(1,I),IERR,-1)
  CALL WRITF(IDCB(1,I),IERR,IBUF(1,I),120)
20 CONTINUE
RETURN
END
$

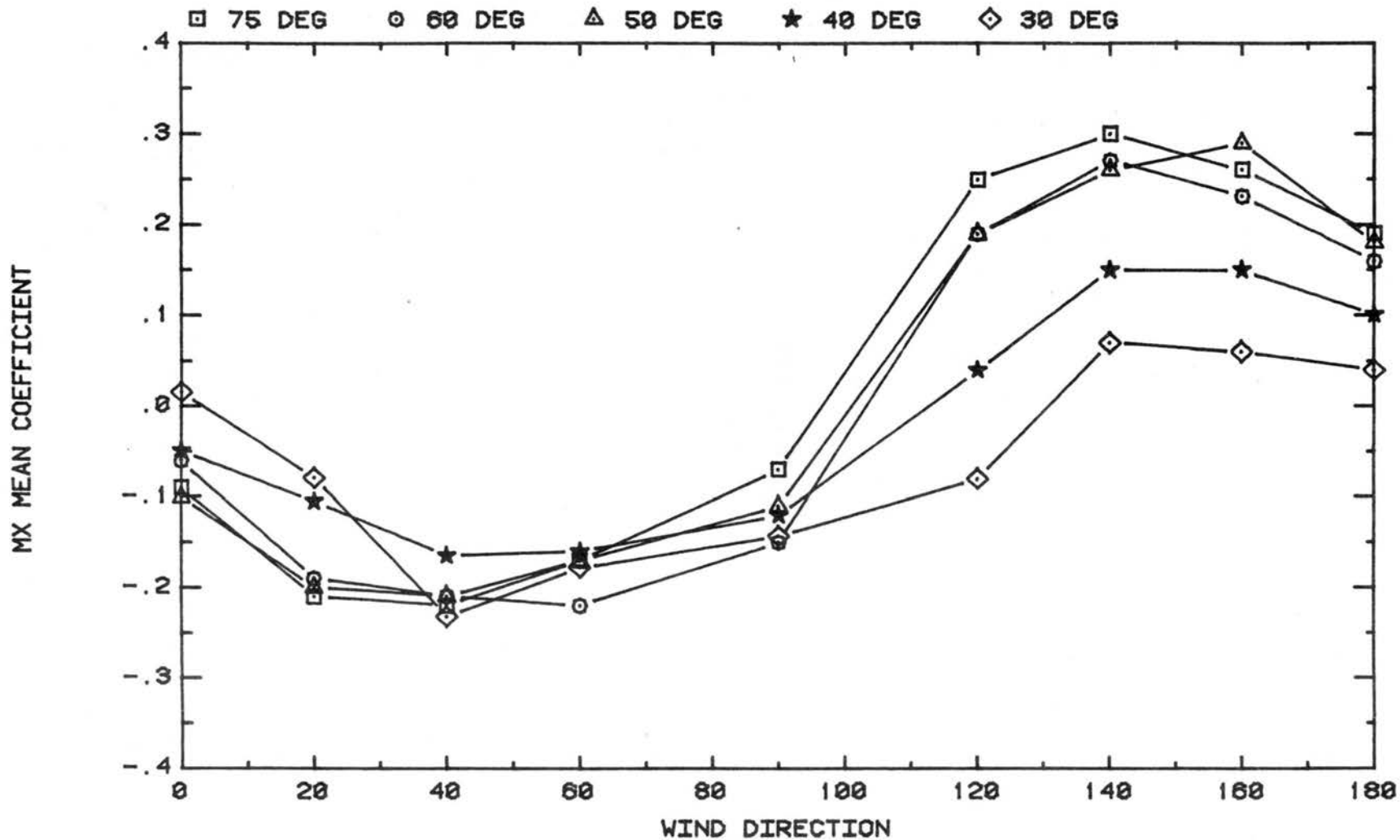
```

Table 4. Effects of Modified Solar Collector Model

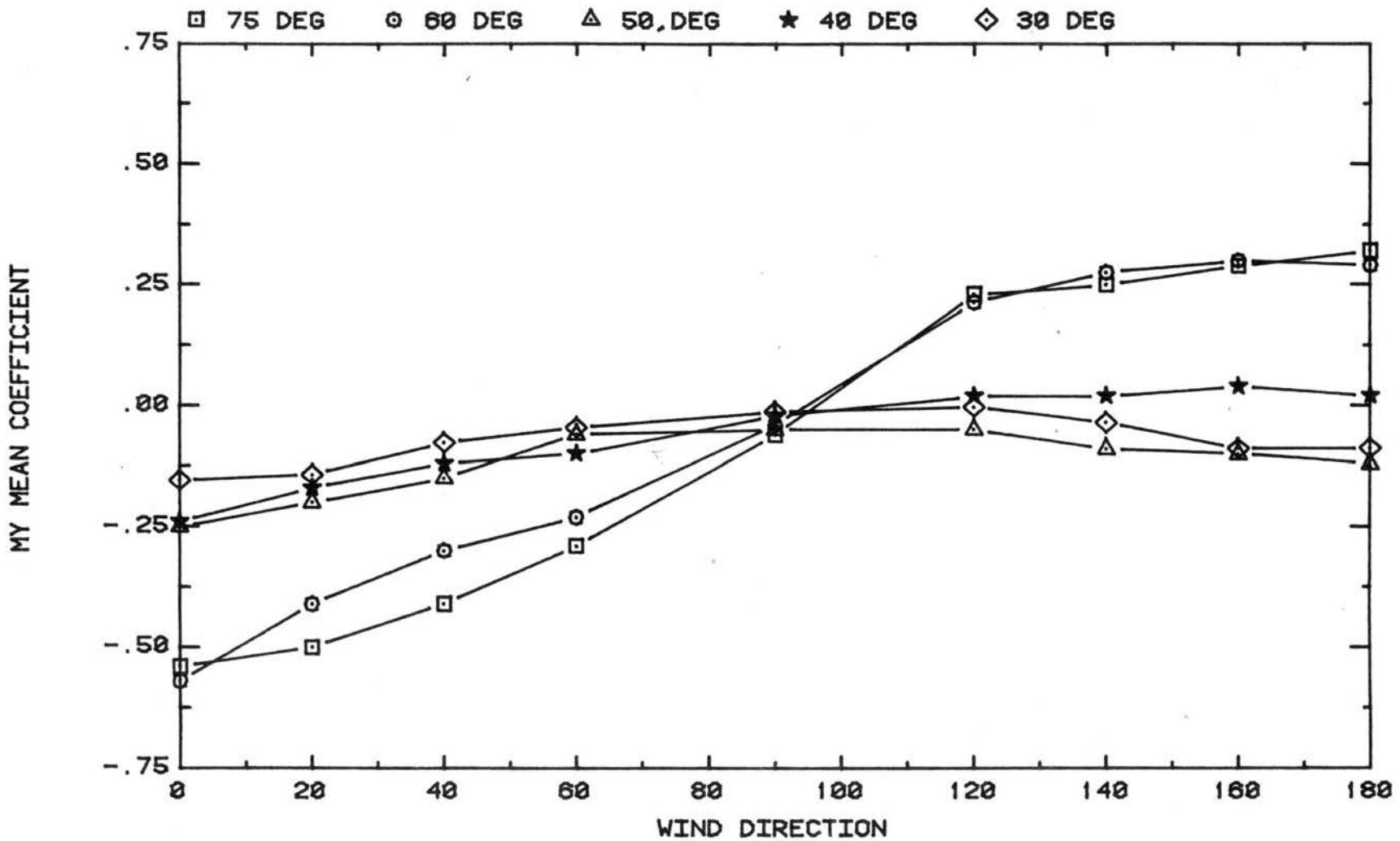
Set-up	0°		180°	
	M_y	F_z	M_y	F_z
I 	100%	100%	100%	100%
II 	-21%	-8%	-21%	-4%
III 	-24%	+9%	-19%	+8%
IV 	-32%	+4%	-40%	+2%
V 	-30%	+21%	-26%	+12%
VI 	-12%	+11%	-30%	+9%

APPENDIX A

MEAN LOADING

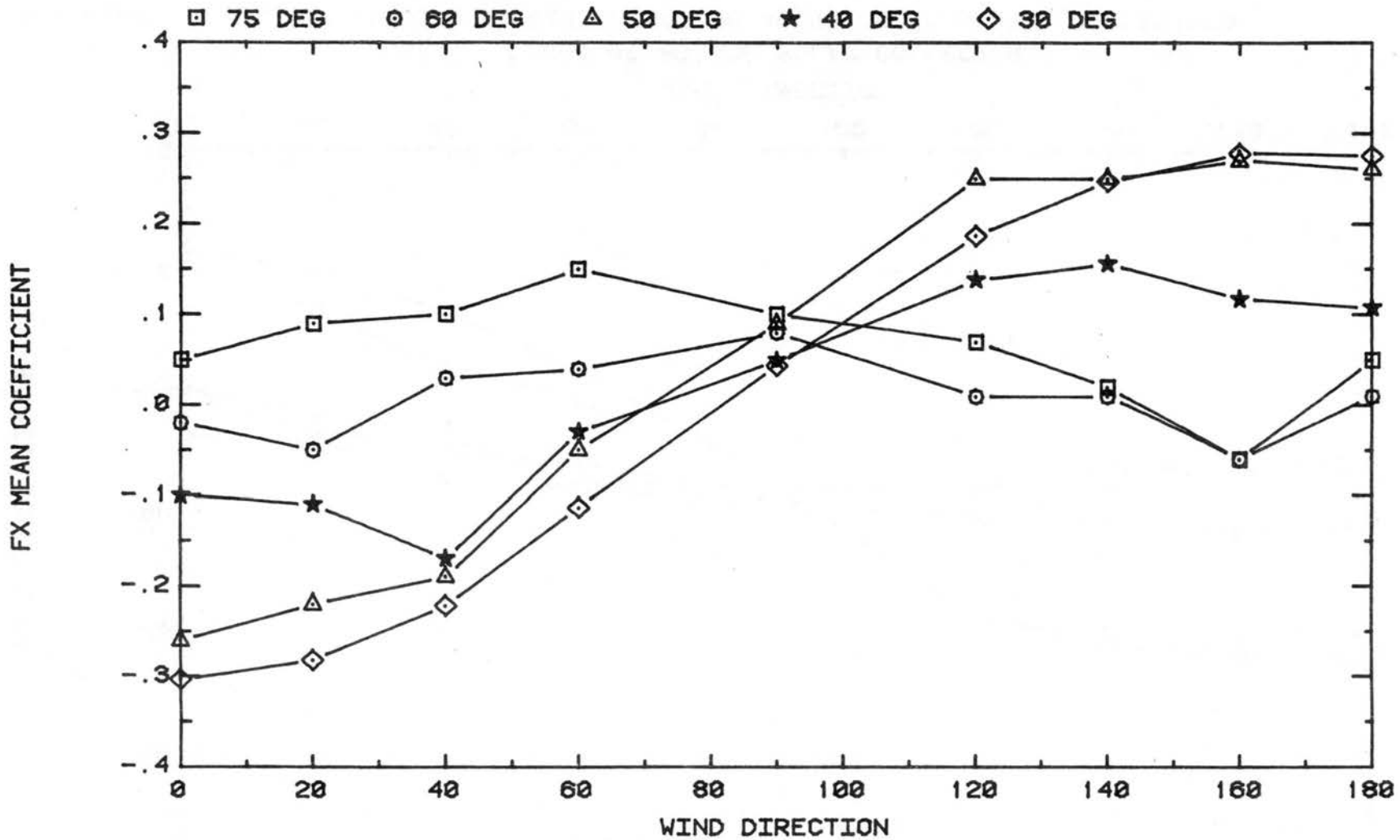


LAJET 95-MIRROR SOLAR COLLECTOR
 FIGURE A.1. MX VS WIND DIRECTION FOR 30,40,50,60,75 DEG DECLINATION



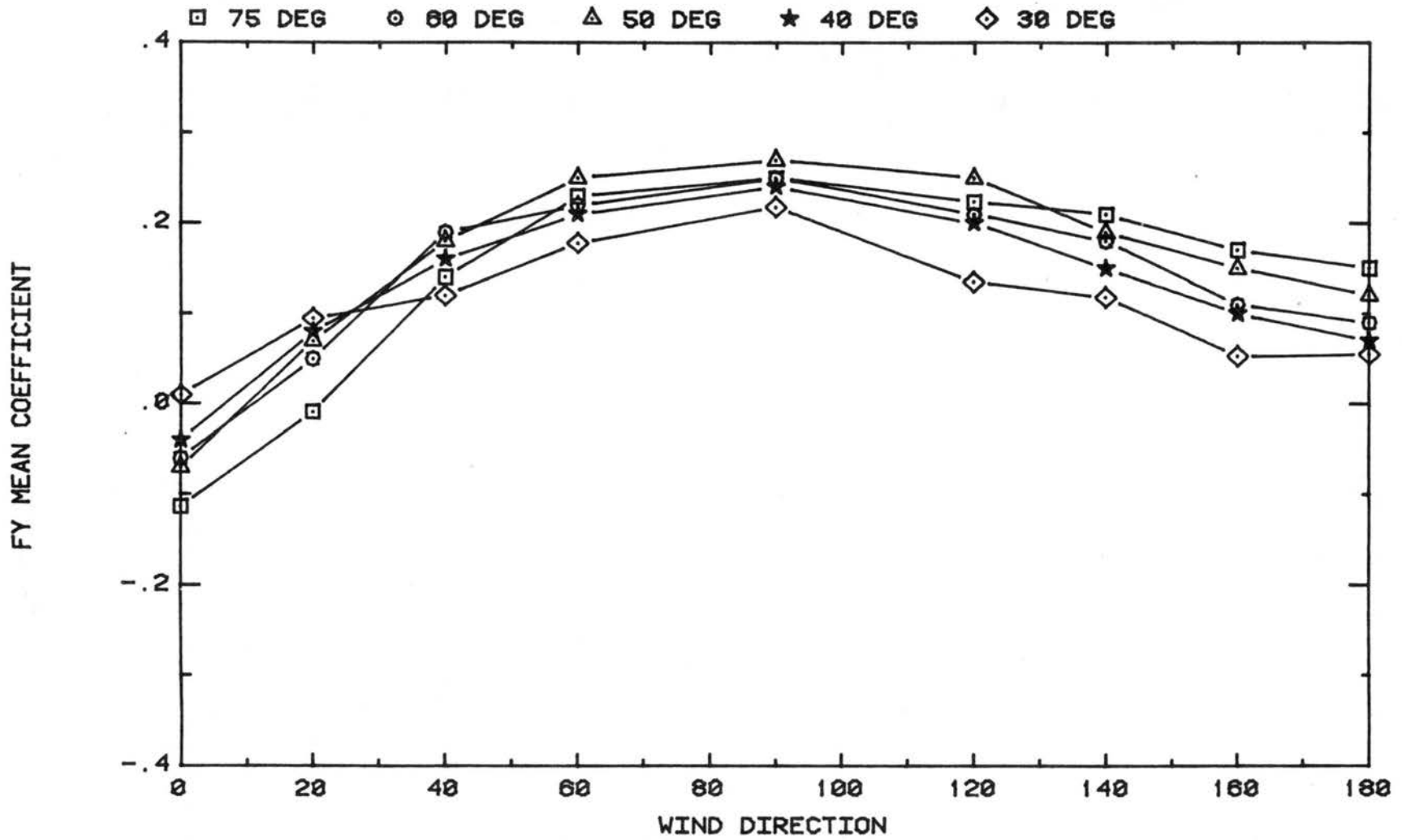
LAJET 95-MIRROR SOLAR COLLECTOR

FIGURE A.2. MY VS WIND DIRECTION FOR 30, 40, 50, 60, 75 DEGREE DECLINATION



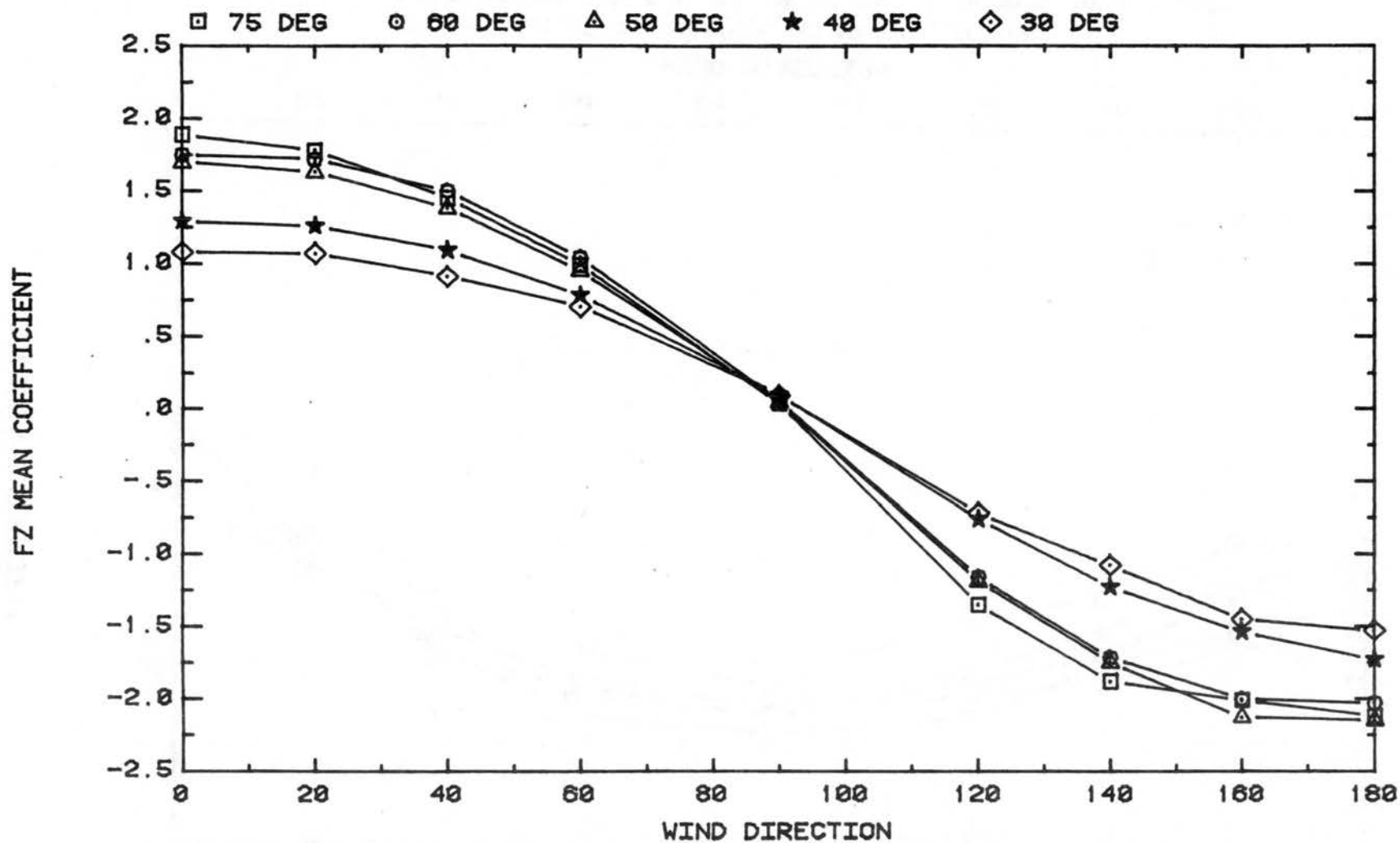
LAJET 95-MIRROR SOLAR COLLECTOR

FIGURE A.3. FX VS WIND DIRECTION FOR 30, 40, 50, 60, 75 DEG DECLINATION

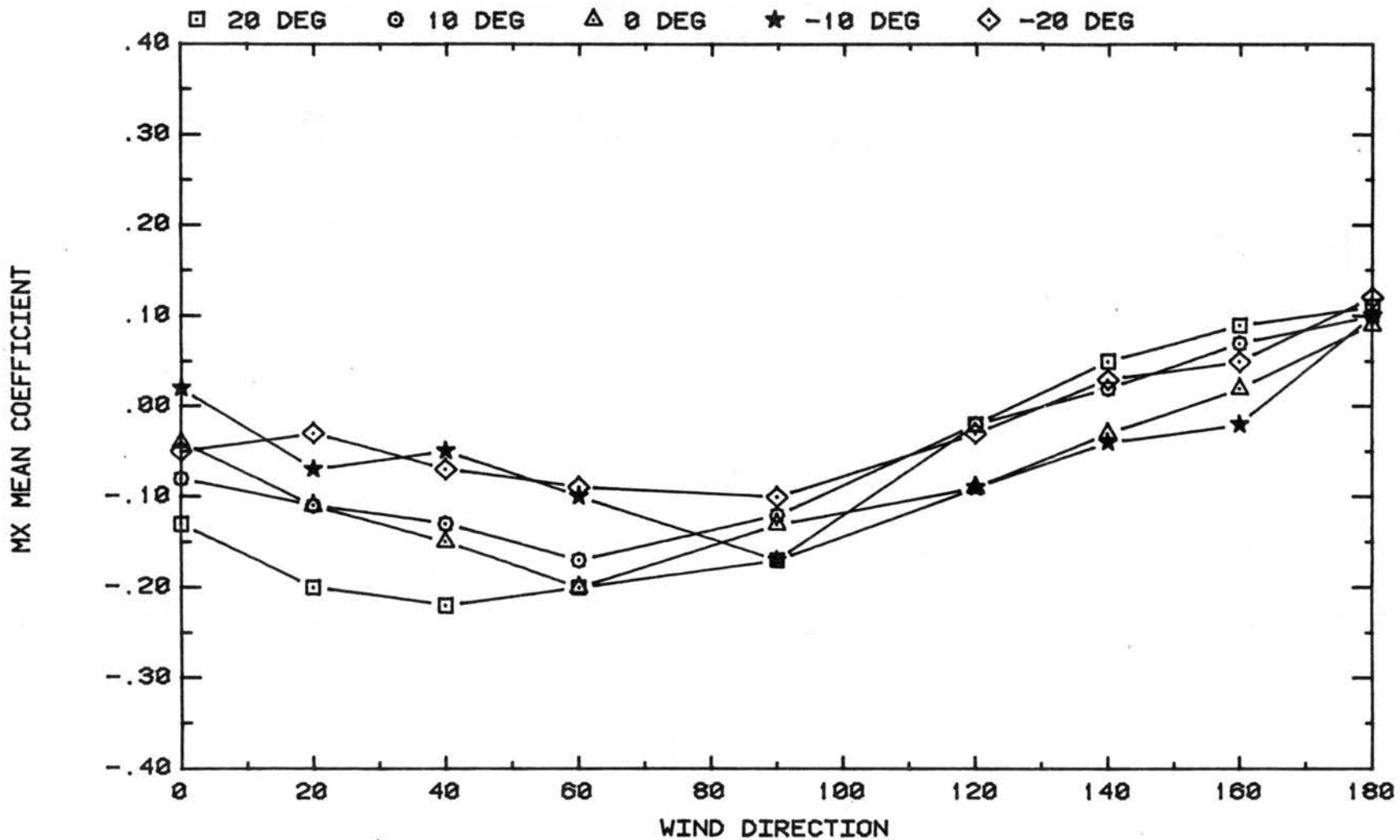


LAJET 95-MIRROR SOLAR COLLECTOR

FIGURE A.4. FY VS WIND DIRECTION FOR 30, 40, 50, 60, 75 DEGREE DECLINATION

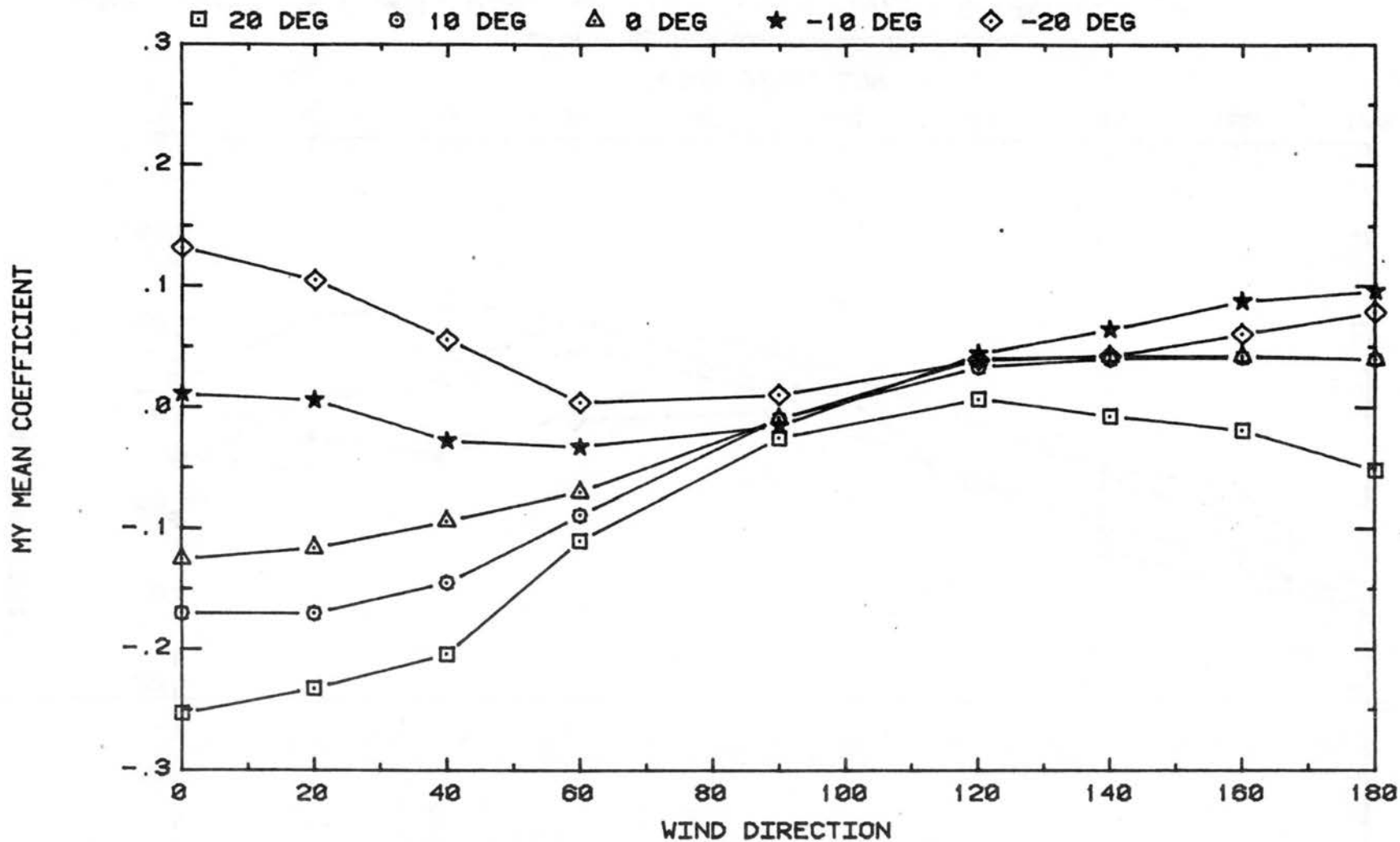


LAJET 95-MIRROR SOLAR COLLECTOR
 FIGURE A.5. FZ VS WIND DIRECTION FOR 30, 40, 50, 60, 75 DEGREE DECLINATION

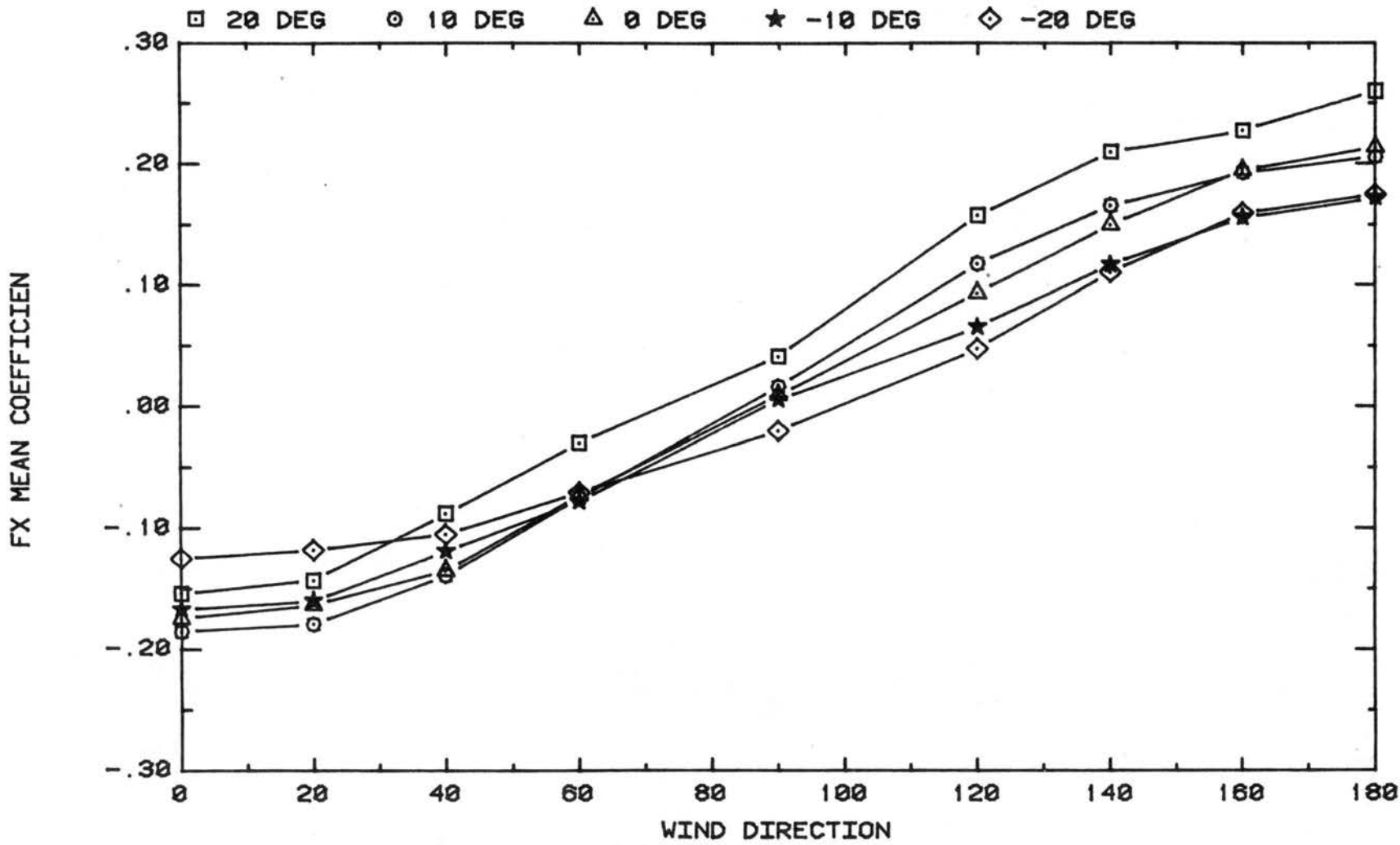


LAJET 95-MIRROR SOLAR COLLECTOR

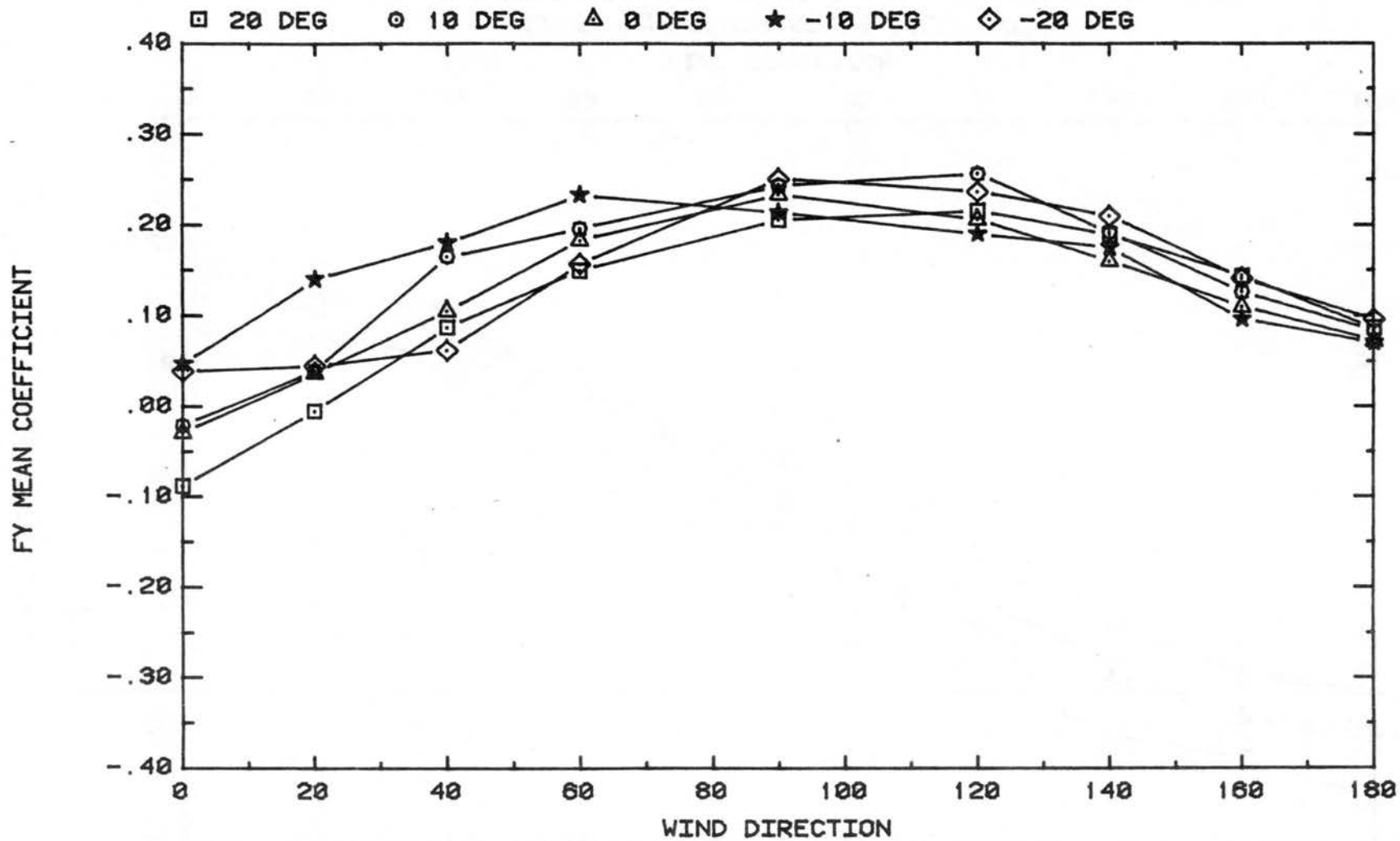
FIGURE A.6. MX VS WIND DIRECTION FOR 20,10,0,-10,-20 DEGREE DECLINATION



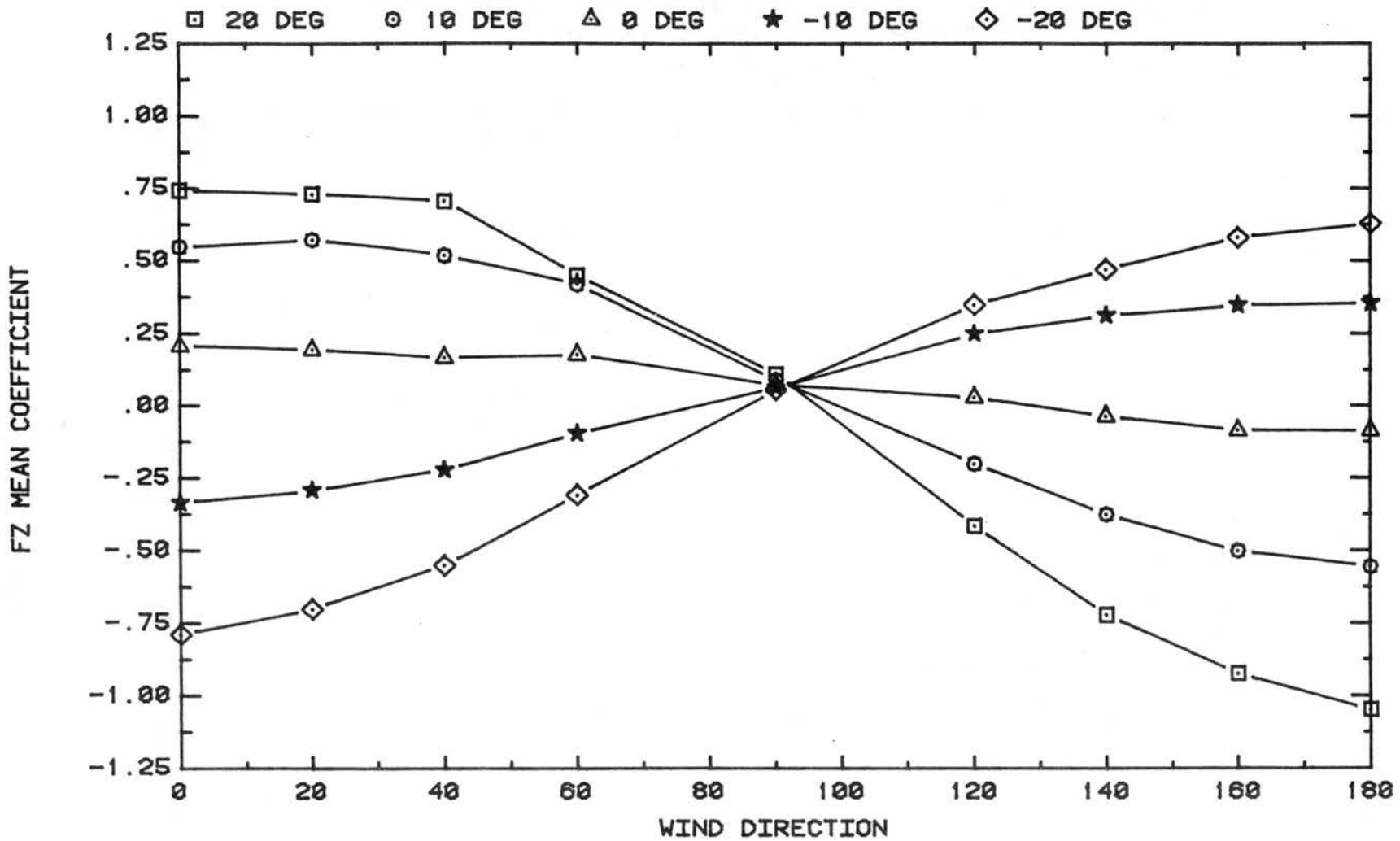
LAJET 95-MIRROR SOLAR COLLECTOR
 FIGURE A.7. MY VS WIND DIRECTION FOR 20,10,0,-10,-20 DEGREE DECLINATION



LAJET 95-MIRROR SOLAR COLLECTOR
 FIGURE A.8. FX VS WIND DIRECTION FOR 20,10,0,-10,-20 DEG DECLINATION

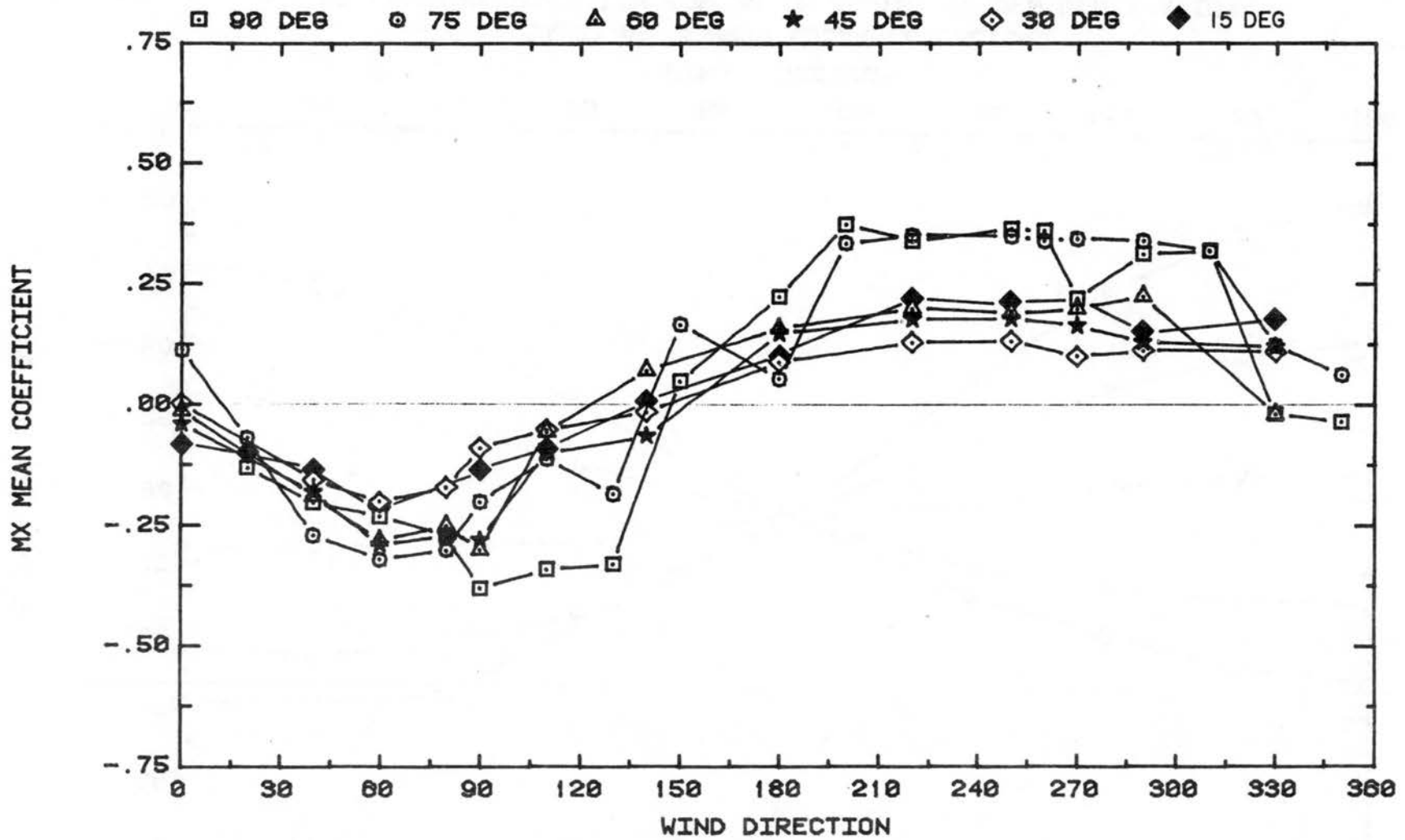


LAJET 95-MIRROR SOLAR COLLECTOR
 FIGURE A.9. FY VS WIND DIRECTION FOR 20, 10, 0, -10, -20 DEGREE DECLINATION

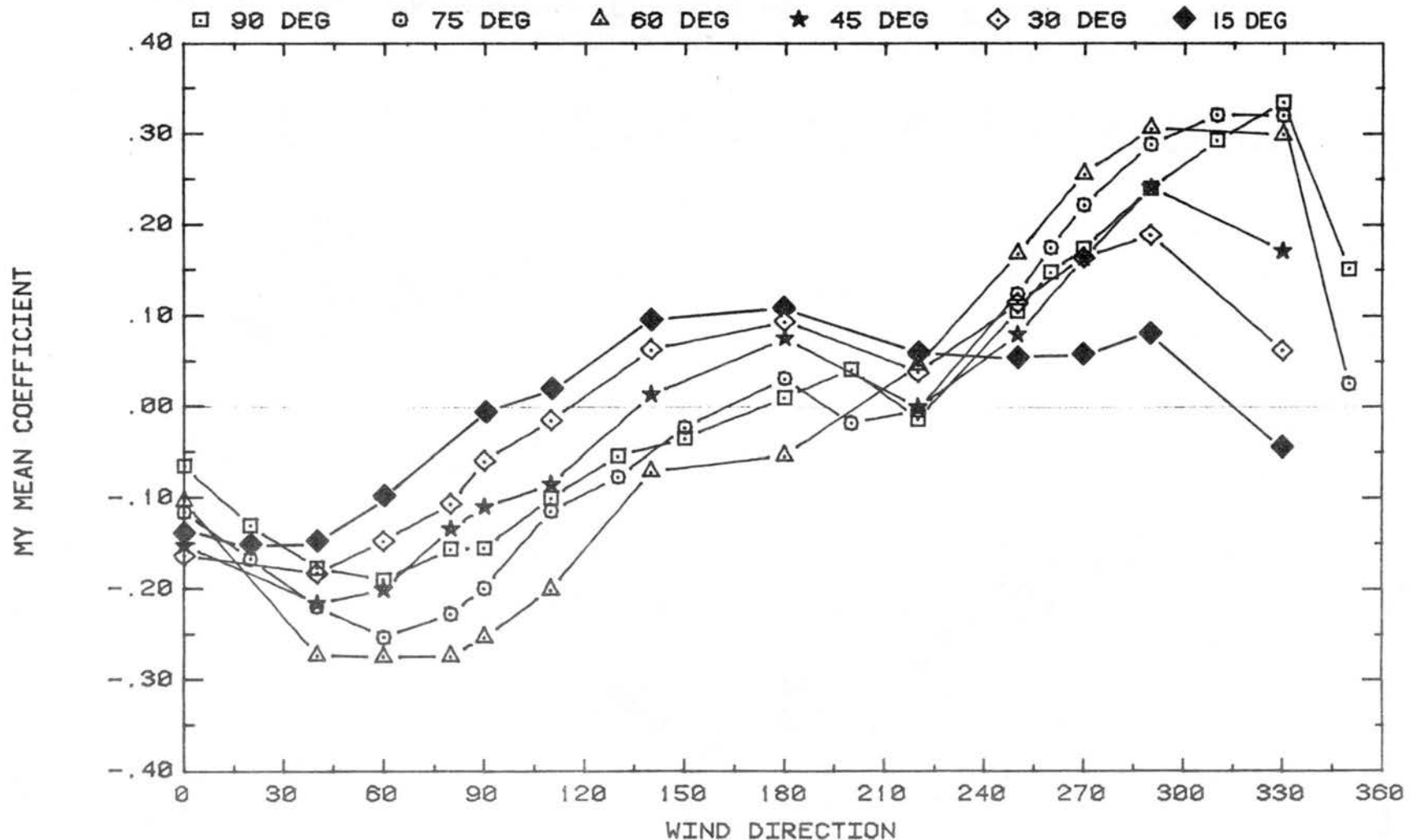


LAJET 95-MIRROR SOLAR COLLECTOR

FIGURE A.10. FZ VS WIND DIRECTION FOR 20,10,0,-10,-20 DEG DECLINATION

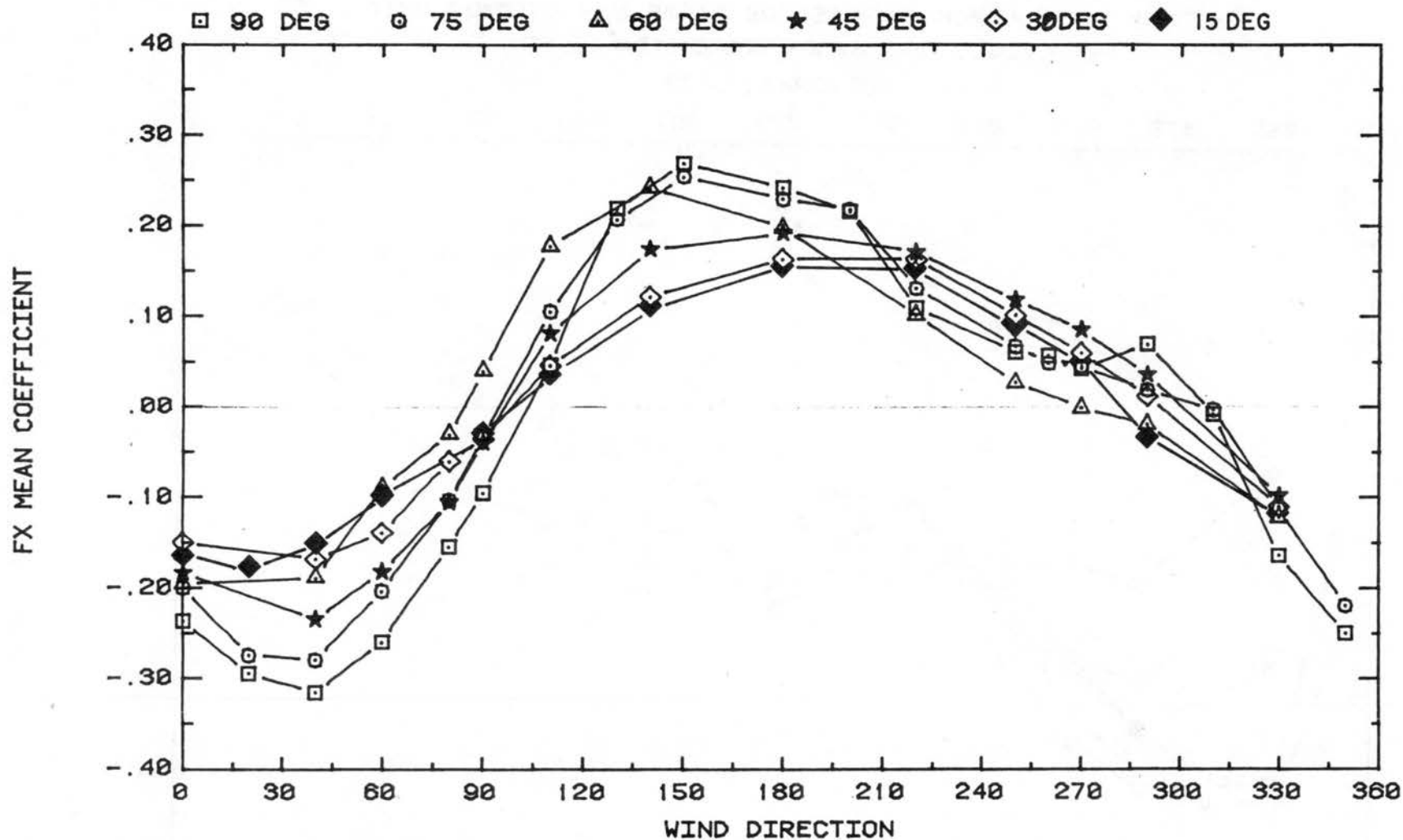


LAJET 95-MIRROR SOLAR COLLECTOR
 FIGURE A.11. WIND LOADING FOR 90,75,60,45,30,15 DEGREE HOUR ANGLES

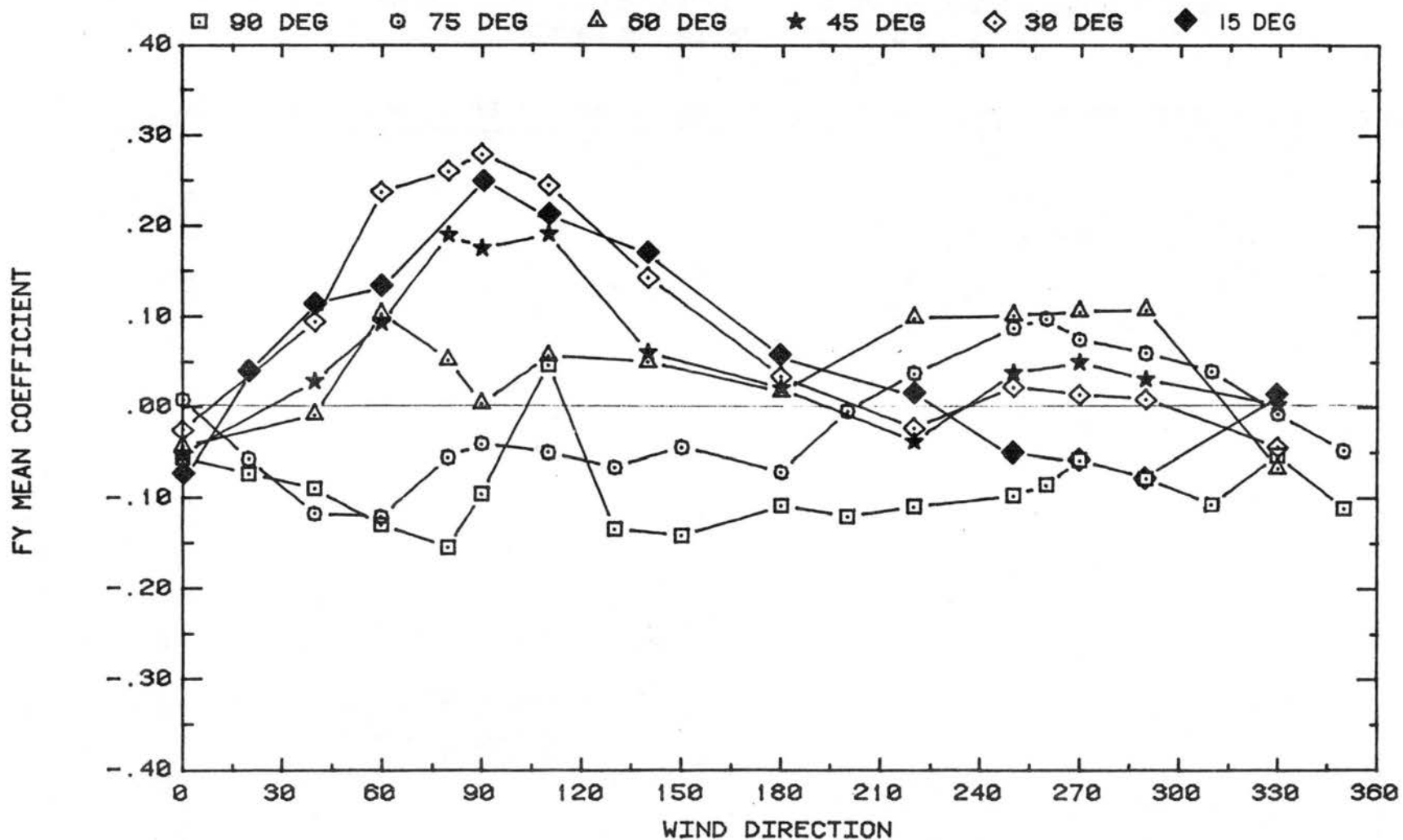


LAJET 95-MIRROR SOLAR COLLECTOR

FIGURE A.12. WIND LOADING FOR 90,75,60,45,30,15 DEGREE HOUR ANGLES

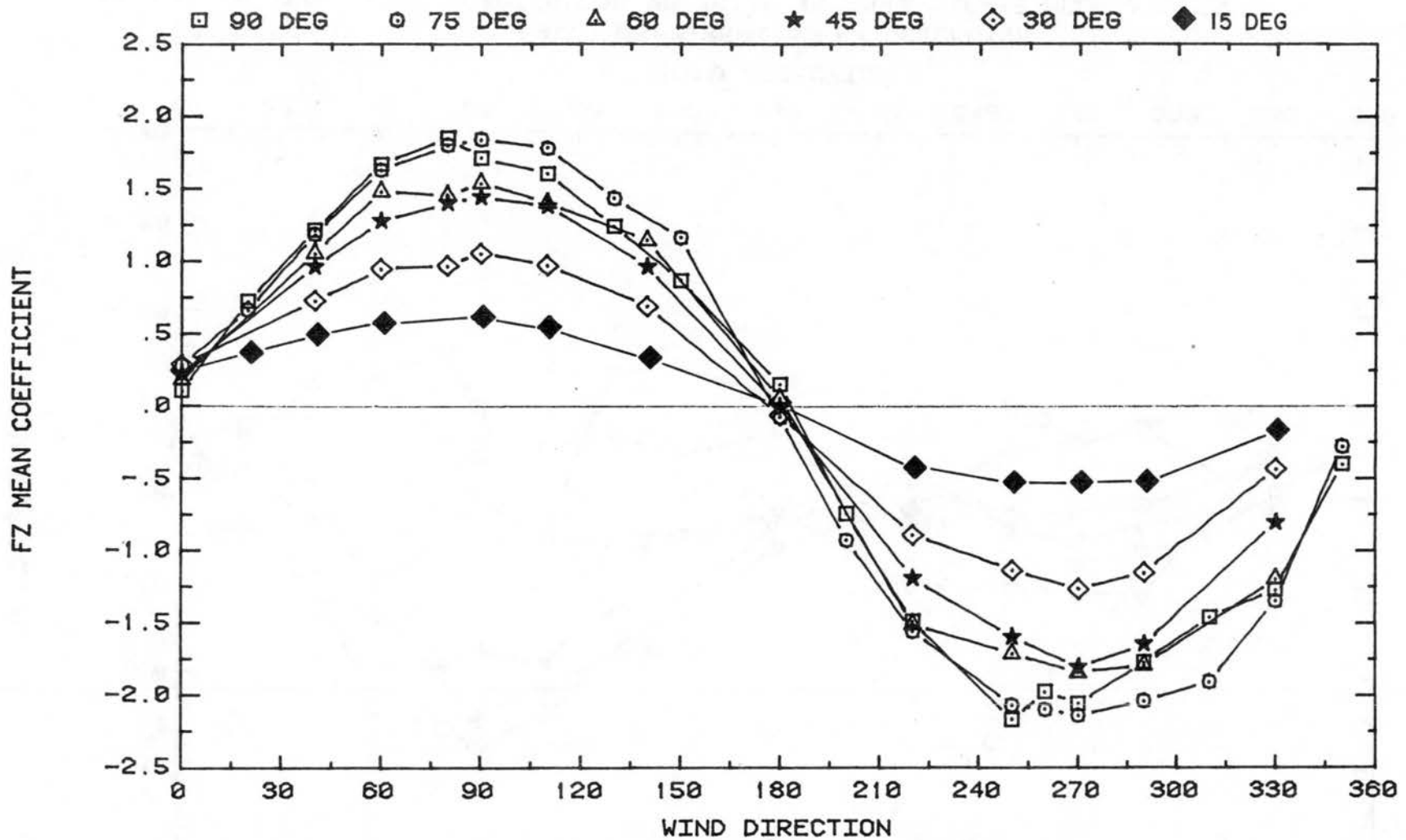


LAJET 95-MIRROR SOLAR COLLECTOR
 FIGURE A.13. WIND LOADING FOR 90,75,60,45,30,15 DEGREE HOUR ANGLES



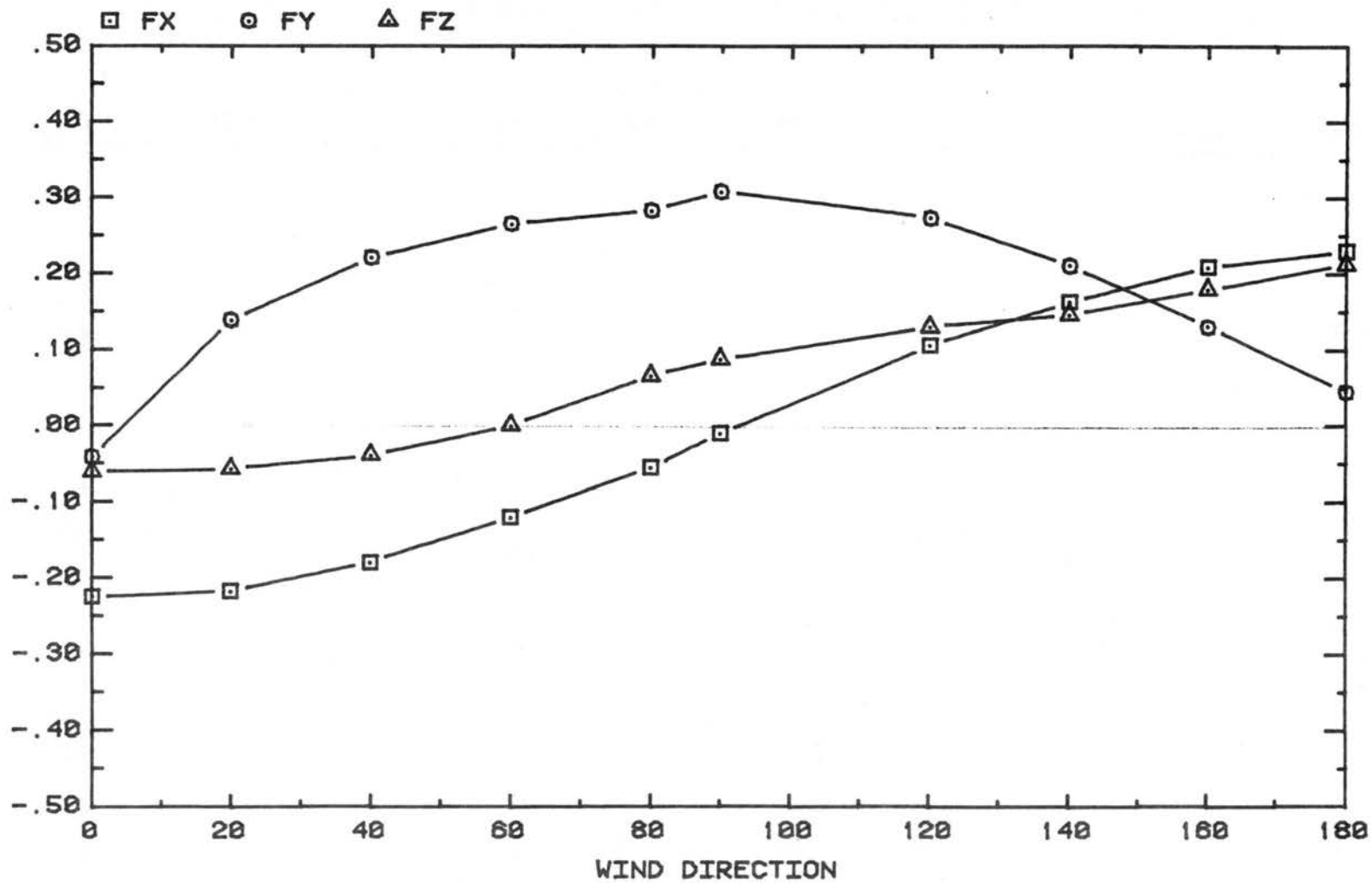
LAJET 95-MIRROR SOLAR COLLECTOR

FIGURE A.14. WIND LOADING FOR 90,75,60,45,30,15 DEGREE HOUR ANGLES

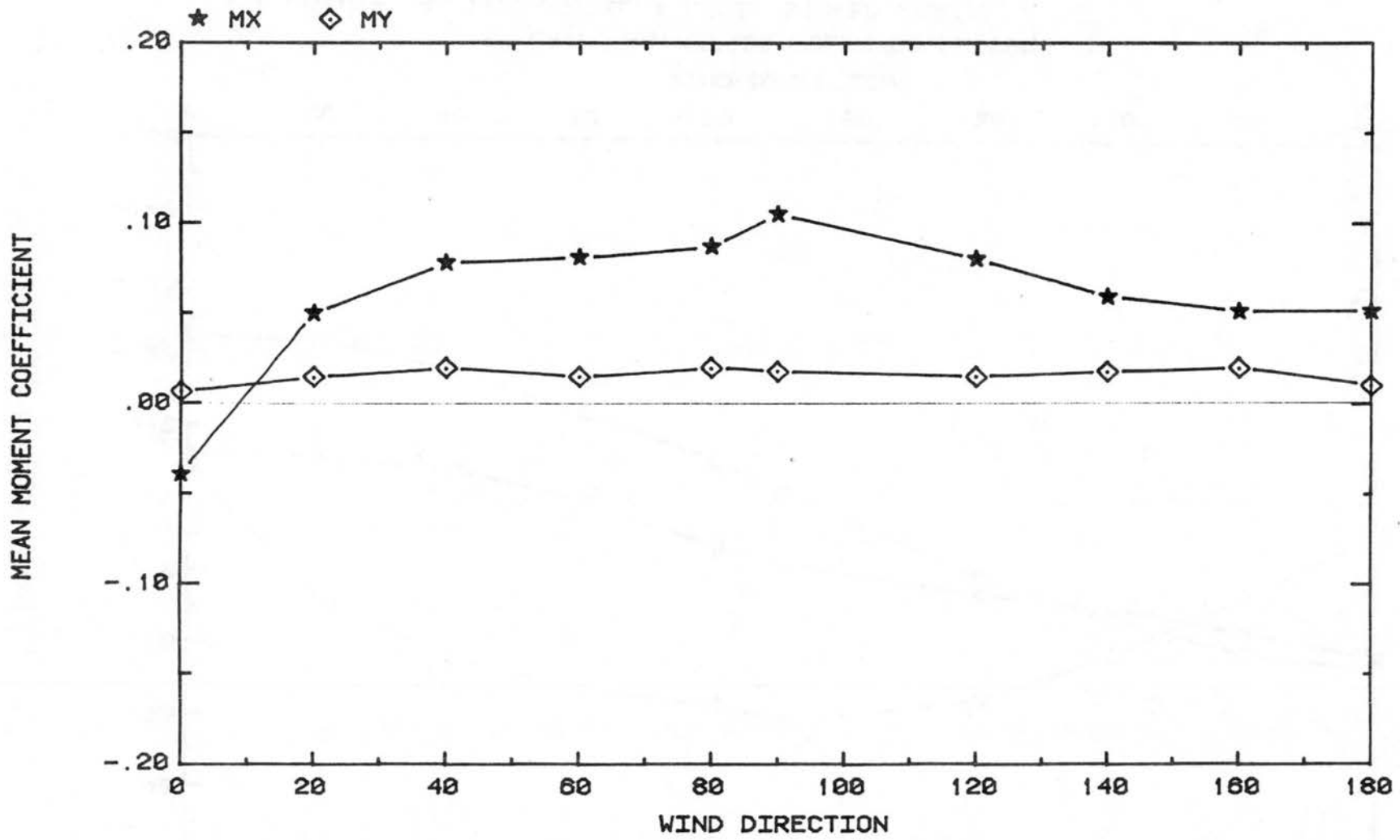


LAJET 95 -MIRROR SOLAR COLLECTOR
 FIGURE A.15. WIND LOADING FOR 90,75,60,45,30,15 DEGREE HOUR ANGLES

FORCE COEFFICIENTS FOR FX, FY, FZ



LAJET 95-MIRROR SOLAR COLLECTOR
FIGURE A.16. UMBRELLA LIKE STOWED POSITION



LAJET 95-MIRROR SOLAR COLLECTOR

FIGURE A.17. UMBRELLA LIKE STOWED POSITION

Table A.1. Mean Loading for Declination Angles

Decl.	Hour	WD	$M_{x''}$	$M_{y''}$	$F_{x''}$	$F_{y''}$	$F_{z''}$
75	0	0	-0.09	-0.54	0.05	-0.11	1.89
		20	-0.21	-0.50	0.09	-0.01	1.78
		40	-0.22	-0.41	0.10	0.14	1.45
		60	-0.17	-0.29	0.15	0.23	0.99
		90	-0.07	-0.06	0.10	0.25	0.04
		120	0.25	0.23	0.07	0.22	-1.35
		140	0.30	0.25	0.02	0.21	-1.88
		160	0.26	0.29	-0.06	0.17	-2.01
		180	0.19	0.32	0.05	0.15	-2.12
60	0	0	-0.06	-0.57	-0.02	-0.06	1.75
		20	-0.19	-0.41	-0.05	0.05	1.72
		40	-0.21	-0.30	0.03	0.19	1.50
		60	-0.22	-0.23	0.04	0.22	1.04
		90	-0.15	-0.04	0.08	0.25	0.06
		120	0.19	0.21	0.01	0.21	-1.16
		140	0.27	0.28	0.01	0.18	-1.72
		160	0.23	0.30	-0.06	0.11	-2.00
		180	0.16	0.29	0.01	0.09	-2.03
50	0	0	-0.10	-0.25	-0.26	-0.07	1.70
		20	-0.20	-0.20	-0.22	0.07	1.63
		40	-0.21	-0.15	-0.19	0.18	1.38
		60	-0.17	-0.06	-0.05	0.25	0.95
		90	-0.11	-0.05	0.09	0.27	0.05
		120	0.19	-0.05	0.25	0.25	-1.19
		140	0.26	-0.09	0.25	0.19	-1.75
		160	0.29	-0.10	0.27	0.15	-2.13
		180	0.18	-0.12	0.26	0.12	-2.15
40	0	0	-0.05	-0.24	-0.10	-0.04	1.29
		20	-0.11	-0.17	-0.11	0.08	1.26
		40	-0.17	-0.12	-0.17	0.16	1.09
		60	-0.16	-0.10	-0.03	0.21	0.78
		90	-0.12	-0.02	0.05	0.24	0.10
		120	0.04	0.02	0.14	0.20	-0.76
		140	0.15	0.02	0.16	0.15	-1.23
		160	0.15	0.04	0.12	0.01	-1.54
		180	0.10	0.02	0.11	0.07	-1.73
30	0	0	0.02	-0.15	-0.30	0.01	1.08
		20	-0.08	-0.14	-0.28	0.10	1.07
		40	-0.23	-0.08	-0.22	0.12	0.91
		60	-0.18	-0.05	-0.11	0.18	0.70
		90	-0.14	-0.01	0.04	0.22	0.10
		120	0.08	0.00	0.19	0.14	-0.72
		140	0.07	-0.04	0.25	0.12	-1.08
		160	0.06	-0.09	0.28	0.05	-1.45
		180	0.04	-0.09	0.28	0.06	-1.53

Table A.1. Mean Loading for Declination Angles (continued)

Decl.	Hour	WD	M_x''	M_y''	F_x''	F_y''	F_z''
20	0	0	-0.13	-0.25	0.15	-0.09	0.74
		20	-0.20	-0.23	-0.14	-0.01	0.73
		40	-0.22	-0.20	0.09	0.09	0.71
		60	-0.20	-0.11	-0.03	0.15	0.45
		90	-0.17	-0.03	0.04	0.21	0.11
		120	0.02	0.01	0.16	0.22	-0.41
		140	0.05	0.01	0.21	0.19	-0.72
		160	0.09	0.02	0.23	0.14	-0.92
		180	0.11	-0.05	0.26	0.09	-1.05
10	0	0	-0.08	-0.17	-0.19	-0.02	0.55
		20	-0.11	-0.17	-0.18	0.04	0.57
		40	-0.13	-0.15	-0.14	0.17	0.52
		60	-0.17	-0.09	-0.08	0.20	0.42
		90	-0.12	-0.01	0.02	0.24	0.09
		120	-0.02	0.03	0.12	0.26	-0.20
		140	0.02	0.04	0.17	0.19	-0.38
		160	0.07	0.04	0.19	0.13	-0.50
		180	0.10	0.04	0.21	0.08	-0.56
-10	0	0	0.02	0.01	-0.17	0.05	-0.33
		20	-0.07	-0.01	-0.16	0.14	0.29
		40	-0.05	-0.03	-0.12	0.18	0.22
		60	-0.10	-0.03	-0.08	0.23	-0.10
		90	-0.17	-0.02	0.01	0.21	0.06
		120	-0.09	0.05	0.07	0.19	0.25
		140	-0.04	0.07	0.12	0.18	0.31
		160	-0.02	0.09	0.16	0.10	0.35
		180	0.10	0.10	0.17	0.07	0.35
-20	0	0	-0.05	0.13	-0.13	0.04	-0.79
		20	-0.03	0.11	-0.12	0.05	-0.70
		40	-0.07	0.06	-0.11	0.06	-0.55
		60	-0.09	0.04	-0.07	0.16	-0.31
		90	-0.10	0.01	-0.02	0.25	0.06
		120	-0.03	0.04	0.05	0.24	0.35
		140	0.03	0.04	0.11	0.21	0.47
		160	0.05	0.06	0.16	0.14	0.58
		180	0.12	0.08	0.18	0.10	0.63

Table A.2. Mean Loading for Hour Angles

Decl.	Hour	WD	$M_{x''}$	$M_{y''}$	$F_{x''}$	$F_{y''}$	$F_{z''}$
0	90	0	0.10	-0.06	-0.24	-0.06	0.11
		20	-0.13	-0.13	-0.29	-0.07	0.72
		40	-0.20	-0.18	-0.32	-0.09	1.21
		60	-0.23	-0.19	-0.26	-0.13	1.67
		80	-0.27	-0.16	-0.15	-0.15	1.85
		90	-0.38	-0.16	-0.10	-0.10	1.71
		110	-0.34	-0.10	0.05	0.05	1.60
		130	-0.33	-0.05	0.22	-0.13	1.24
		150	0.05	-0.04	0.27	-0.14	0.87
		180	0.22	0.01	0.24	-0.11	0.15
		200	0.37	0.04	0.22	-0.12	-0.75
		220	0.34	-0.01	0.11	-0.11	-1.49
		250	0.37	0.11	0.06	-0.10	-2.17
		260	0.36	0.15	0.06	-0.09	-1.98
		270	0.22	0.17	0.04	-0.06	-2.06
		290	0.31	0.24	0.07	-0.08	-1.77
310	0.32	0.29	-0.01	-0.11	-1.46		
330	-0.02	0.34	-0.16	-0.05	-1.27		
350	-0.04	0.15	-0.25	-0.11	-0.40		
0	75	0	0.12	-0.12	-0.20	-0.01	0.29
		20	-0.07	-0.17	-0.27	-0.06	0.67
		40	-0.27	-0.22	-0.28	-0.12	1.19
		60	-0.32	-0.25	-0.20	-0.12	1.63
		80	-0.30	-0.23	-0.10	-0.06	1.80
		90	-0.20	-0.20	-0.03	-0.04	1.84
		110	-0.11	-0.11	-0.11	-0.05	1.78
		130	-0.18	-0.08	0.21	-0.07	1.43
		150	0.17	-0.02	0.25	-0.04	1.16
		180	0.05	0.03	0.23	-0.07	-0.93
		200	0.34	-0.02	0.22	-0.00	-1.56
		220	0.35	-0.00	0.13	0.04	-2.07
		250	0.35	0.12	0.07	0.09	-2.10
		260	0.34	0.18	0.05	0.10	-2.14
		270	0.35	0.22	0.05	0.08	-2.04
		290	0.34	0.29	0.02	0.06	-1.91
310	0.32	0.32	-0.01	0.04	-1.35		
330	0.12	0.32	-0.11	-0.01	-0.28		
350	0.06	0.03	-0.22	-0.05	-0.10		
0	60	0	-0.01	-0.10	-0.20	-0.04	0.19
		40	-0.19	-0.27	-0.19	-0.01	1.06
		60	-0.28	-0.28	-0.09	0.10	1.48
		80	-0.25	-0.27	-0.03	0.05	1.45
		90	-0.30	-0.25	0.04	0.00	1.54
		110	-0.06	-0.20	0.18	0.06	1.40
		140	0.07	-0.07	0.24	0.05	1.14
		180	0.16	-0.05	0.20	0.02	0.05
		220	0.20	0.05	0.10	0.10	-1.51
250	0.19	0.17	0.03	0.10	-1.72		

Table A.2. Mean Loading for Hour Angles (continued)

Decl.	Hour	WD	M_x''	M_y''	F_x''	F_y''	F_z''
0	60	270	0.20	0.26	-0.00	0.11	-1.84
		290	0.23	0.31	-0.02	0.11	-1.79
		330	-0.02	0.30	-0.12	-0.07	-1.20
0	45	0	-0.04	-0.15	-0.18	-0.05	0.23
		40	-0.18	-0.22	-0.23	0.03	0.96
		60	-0.29	-0.20	-0.18	0.09	1.28
		80	-0.27	-0.13	-0.11	0.19	1.40
		90	-0.28	-0.11	-0.04	-0.18	1.44
		110	-0.10	-0.09	0.08	0.19	1.38
		140	-0.07	0.01	0.17	0.06	0.96
		180	0.15	0.08	0.19	0.02	-0.01
		220	0.18	-0.00	0.17	-0.04	-1.19
		250	0.18	0.08	0.12	0.04	-1.60
		270	0.16	0.16	0.09	0.05	-1.81
		290	0.13	0.24	0.04	0.03	-1.65
		330	0.12	0.17	-0.10	0.00	-0.81
0	30	0	0.01	-0.16	-0.15	-0.03	0.29
		40	-0.16	-0.18	-0.17	0.10	0.73
		60	-0.20	-0.15	-0.14	0.24	0.95
		80	-0.17	-0.11	-0.06	0.26	0.97
		90	-0.09	-0.06	-0.04	-0.28	1.05
		110	-0.15	-0.15	0.05	0.25	0.97
		140	-0.01	0.06	0.12	0.14	0.69
		180	0.09	0.09	0.16	0.03	-0.06
		220	0.13	0.04	0.16	-0.02	-0.89
		250	0.13	0.11	0.10	0.02	-1.14
		270	0.10	0.16	0.06	0.01	-1.27
		290	0.11	0.19	0.01	0.01	-1.15
		330	0.11	0.06	-0.11	-0.04	-0.43
0	15	0	-0.08	-0.14	-0.16	-0.07	0.19
		20	-0.10	-0.15	-0.18	0.04	0.37
		40	-0.14	-0.15	-0.15	0.11	0.50
		60	-0.21	-0.10	-0.10	0.13	0.58
		90	-0.13	-0.01	-0.03	0.25	0.61
		110	-0.09	-0.02	0.04	0.21	0.54
		140	0.01	0.09	0.11	0.17	0.33
		180	0.10	0.11	0.16	0.06	-0.05
		220	0.22	0.06	0.15	0.02	-0.44
		250	0.21	0.05	0.10	-0.05	-0.54
		270	0.20	0.06	0.05	-0.06	-0.54
		290	0.15	0.08	-0.03	-0.08	-0.54
		330	0.17	-0.05	-0.12	-0.02	-0.18

Table A.3. Mean Loading for Umbrella-Like Stowed Position

WD	$M_{x''}$	$M_{y''}$	$F_{x''}$	$F_{y''}$	$F_{z''}$
0	-0.04	0.01	-0.22	-0.04	-0.06
20	0.05	0.02	-0.22	0.14	-0.06
40	0.08	0.02	-0.18	0.22	-0.04
60	0.08	0.02	-0.12	0.27	0.00
80	0.09	0.02	-0.05	0.28	0.07
90	0.11	0.02	-0.01	0.31	0.09
120	0.08	0.02	0.11	0.27	0.13
140	0.06	0.02	0.16	0.21	0.15
160	0.05	0.02	0.21	0.13	0.18
180	0.05	0.01	0.23	0.05	0.21

Table A.4. Mean $M_{z''}$

Declination Angle

WD	75°	60°	50°	40°	30°	20°	10°	0°	-10°	-20°
0	0.06	0.07	0.07	0.04	0.01	0.04	0.02	0.01	0.02	-0.01
20	0.12	0.11	0.10	0.06	0.02	0.05	0.02	0.01	-0.01	-0.01
40	0.12	0.10	0.07	0.07	0.05	0.05	0.02	0.01	-0.02	-0.02
60	0.10	0.13	0.07	0.06	0.04	0.09	0.02	0.01	-0.01	-0.02
90	-0.06	0.05	0.04	0.06	0.03	0.03	0.01	0.01	-0.01	0.01
120	-0.06	0.03	-0.03	0.04	0.04	0.01	0.00	0.01	0.01	0.01
140	-0.11	-0.09	-0.07	-0.02	0.01	0.00	0.00	0.00	0.01	0.01
160	-0.12	-0.08	-0.09	-0.03	0.01	-0.01	-0.00	0.00	0.00	0.02
180	-0.11	-0.11	-0.08	-0.03	-0.05	-0.02	-0.01	-0.00	0.01	0.02

Hour Angles

WD	90°	75°	60°	45°	30°	15°
0	-0.05	-0.10	-0.05	-0.04	-0.02	-0.01
20	-0.05	-0.09	--	--	--	--
40	-0.04	-0.10	-0.11	-0.03	-0.01	-0.00
60	-0.03	-0.11	-0.09	-0.02	-0.01	0.00
80	0.00	-0.07	-0.07	0.01	0.00	0.01
90	0.02	-0.05	-0.08	0.01	0.01	0.01
110	0.03	0.04	-0.11	0.01	0.03	0.02
130	-0.04	-0.03	--	--	--	--
140	-0.02	0.04	0.03	0.02	--	--
150	-0.01	-0.01	--	--	--	--
180	0.03	0.04	0.05	0.05	0.03	0.02
200	0.02	0.02	--	--	--	--
220	0.02	0.05	0.05	0.01	0.01	0.01
250	0.03	0.06	0.06	0.00	0.00	0.01
260	0.03	0.08	--	--	--	--
270	0.02	0.07	0.06	-0.01	-0.01	0.00
290	0.03	0.07	0.06	-0.00	-0.01	-0.02
310	0.02	0.05	--	--	--	--
330	0.13	0.06	0.03	-0.02	-0.01	-0.01
350	0.12	-0.04	0.03	--	--	--

APPENDIX B

MEAN LOADING IN "PRIMED" SYSTEM

Table B.1. Mean Loading in "Primed" System

Decl.	Hour	WD	$M_{x'}$	$M_{z'}$	$F_{x'}$	$F_{z'}$
75	0	0	-0.08	-0.07	-1.81	0.54
		20	-0.18	-0.21	-1.70	0.55
		40	-0.17	-0.18	-1.38	0.47
		60	-0.14	-0.14	-0.92	0.40
		90	0.04	-0.08	-0.01	0.11
		120	0.12	0.23	1.32	-0.28
		140	0.18	0.26	1.82	-0.47
		160	0.18	0.22	1.93	-0.58
		180	0.13	0.11	2.06	-0.50
60	0	0	-0.09	-0.02	-1.53	0.86
		20	-0.19	-0.11	-1.52	0.82
		40	-0.19	-0.13	-1.28	0.78
		60	-0.22	-0.13	-0.88	0.56
		90	-0.12	-0.11	-0.01	0.10
		120	0.07	0.18	1.01	-0.57
		140	0.21	0.19	1.50	-0.85
		160	0.19	0.16	1.70	-1.05
		180	0.11	0.08	1.76	-1.01
50	0	0	-0.12	-0.03	-1.47	0.89
		20	-0.21	-0.09	-1.39	0.88
		40	-0.19	-0.12	-1.18	0.74
		60	-0.16	-0.09	-0.76	0.57
		90	-0.10	-0.06	0.02	0.10
		120	0.15	0.13	1.07	-0.57
		140	0.22	0.15	1.50	0.93
		160	0.26	0.16	1.81	-1.16
		180	0.11	0.09	1.81	-1.18
40	0	0	-0.06	-0.00	-0.91	0.92
		20	-0.12	-0.02	-0.89	0.90
		40	-0.17	-0.05	-0.83	0.73
		60	-0.16	-0.06	-0.52	0.58
		90	-0.13	-0.03	-0.03	0.11
		120	0.01	0.06	0.59	-0.49
		140	0.13	0.08	0.91	-0.84
		160	0.13	0.07	1.08	-1.11
		180	0.10	0.04	1.19	-1.26
30	0	0	0.01	0.02	-0.80	0.78
		20	-0.08	-0.02	-0.78	0.79
		40	-0.23	-0.07	-0.65	0.68
		60	-0.17	-0.05	-0.45	0.55
		90	-0.14	-0.05	-0.09	0.07
		120	-0.09	-0.01	0.52	-0.53
		140	0.06	0.04	0.75	-0.81
		160	0.05	0.04	0.97	-0.12
		180	0.06	-0.02	1.00	-1.19

Table B.1. Mean Loading in "Primed" System (continued)

Decl.	Hour	WD	$M_{x'}$	$M_{z'}$	$F_{x'}$	$F_{z'}$
20	0	0	-0.13	-0.01	-0.40	0.64
		20	-0.21	-0.02	-0.38	0.64
		40	-0.22	-0.03	-0.32	0.63
		60	-0.22	0.02	-0.18	0.41
		90	-0.17	-0.03	-0.08	-0.09
		120	-0.02	0.00	0.29	-0.34
		140	0.05	0.02	0.36	-0.64
		160	0.09	0.02	0.53	-0.79
180	0.11	0.02	0.60	-0.90		
10	0	0	-0.08	0.01	-0.28	0.51
		20	-0.11	-0.00	-0.28	0.53
		40	-0.13	-0.00	-0.23	0.49
		60	-0.17	-0.01	-0.15	0.40
		90	-0.12	-0.01	0.00	0.09
		120	-0.02	-0.00	0.15	-0.18
		140	0.02	0.00	0.23	-0.34
		160	0.07	0.01	0.28	-0.46
180	0.10	0.01	0.30	-0.51		
-10	0	0	-0.02	0.02	-0.22	-0.30
		20	-0.07	0.02	-0.21	-0.26
		40	-0.05	0.03	-0.16	-0.20
		60	-0.10	0.02	-0.09	-0.08
		90	-0.17	0.03	0.02	0.06
		120	-0.09	0.03	0.11	0.24
		140	-0.04	0.01	0.17	0.29
		160	-0.02	-0.01	0.21	0.32
180	0.10	-0.04	0.39	0.32		
-20	0	0	-0.04	0.03	-0.39	-0.70
		20	-0.03	0.02	-0.35	-0.62
		40	-0.06	0.03	-0.29	-0.48
		60	-0.08	0.04	-0.17	-0.27
		90	-0.09	0.04	0.00	0.06
		120	-0.03	0.01	0.17	0.31
		140	0.03	-0.01	0.27	0.40
		160	0.04	-0.03	0.35	0.49
180	0.10	-0.05	0.38	0.53		

Table B.1. Mean Loading in "Primed" System (continued)

Decl.	Hour	WD	M_y'	M_z'	F_y'	F_z'
0	90	0	-0.05	0.06	0.11	0.06
		20	-0.05	0.13	0.72	0.07
		40	-0.04	0.18	1.21	0.09
		60	-0.03	0.19	1.67	0.13
		80	0.00	0.16	1.85	0.15
		90	0.02	0.16	1.71	0.10
		110	0.03	0.10	1.60	-0.05
		130	-0.04	0.05	1.24	0.13
		150	-0.01	0.04	0.87	0.14
		180	0.03	-0.01	0.15	0.11
		200	0.02	-0.04	-0.75	0.12
		220	0.02	0.14	-1.49	0.11
		250	0.03	-0.11	-2.17	0.10
		260	0.03	-0.15	-0.20	0.09
		270	0.02	-0.17	-2.06	0.06
		290	0.03	-0.24	-1.77	0.08
		310	0.02	-0.29	-1.46	0.11
330	0.13	-0.34	-1.27	0.05		
350	0.12	-0.15	-0.40	0.11		
0	75	0	-0.12	0.09	0.28	0.07
		20	-0.13	0.14	0.63	0.23
		40	-0.15	0.19	1.12	0.42
		60	-0.17	0.22	1.54	0.54
		80	-0.13	0.20	1.72	0.52
		90	-0.10	0.18	1.77	0.52
		110	-0.07	0.10	1.71	0.51
		130	-0.05	0.07	1.36	0.43
		150	-0.04	0.01	1.11	0.34
		180	0.04	-0.02	-0.92	-0.17
		200	0.03	0.03	-1.51	-0.40
		220	0.05	0.02	-1.99	-0.57
		250	0.09	-0.10	-2.01	-0.63
		260	0.12	-0.15	-2.04	-0.65
		270	0.13	-0.20	-1.95	-0.60
		290	0.14	-0.26	-1.83	-0.55
		310	0.13	-0.30	-1.29	-0.39
330	0.14	-0.29	-0.27	-0.07		
350	-0.03	-0.03	-0.11	0.02		
0	60	0	-0.10	0.06	0.14	0.13
		40	-0.23	0.18	0.91	0.54
		60	-0.21	0.20	1.33	0.65
		80	-0.20	0.20	1.28	0.68
		90	-0.19	0.18	1.34	0.77
		110	-0.19	0.12	1.24	0.65
		140	-0.05	0.05	1.01	0.53
		180	0.02	0.07	0.05	0.01
		220	0.07	-0.01	-1.26	-0.84
250	0.14	-0.11	-1.44	0.95		

Table B.1. Mean Loading in "Primed" System (continued)

Decl.	Hour	WD	$M_{y'}$	$M_{z'}$	$F_{y'}$	$F_{z'}$
0	60	270	0.18	-0.19	-1.54	-1.01
		290	0.20	-0.24	-1.50	-0.99
		330	0.18	-0.24	-1.07	0.54
0	45	0	-0.14	0.08	0.12	0.20
		40	-0.18	0.13	0.70	0.66
		60	-0.16	0.13	0.97	0.84
		80	-0.09	0.10	1.12	0.86
		90	-0.07	0.08	1.14	0.89
		110	-0.05	0.07	1.11	0.84
		140	0.03	0.02	0.72	0.64
		180	0.09	-0.02	-0.01	-0.02
		220	0.01	0.01	-0.87	-0.82
		250	0.06	-0.06	-1.11	-1.16
		270	0.11	-0.12	-1.25	-1.32
		290	0.17	-0.17	-1.15	-1.19
		330	0.11	-0.14	-0.57	-0.57
		350	-0.03	-0.03	-0.11	0.02
0	30	0	-0.15	0.07	0.12	0.27
		40	-0.16	0.08	0.45	0.58
		60	-0.13	0.07	0.68	0.70
		80	-0.09	0.06	0.71	0.71
		90	-0.04	0.04	0.77	0.77
		110	-0.12	0.10	0.70	0.72
		140	0.07	-0.00	0.47	0.52
		180	0.10	-0.02	-0.00	-0.07
		220	0.04	-0.01	-0.47	-0.76
		250	0.10	-0.06	-0.55	-0.10
		270	0.14	-0.09	-0.62	-1.11
		290	0.16	-0.10	-0.57	-1.00
		330	0.05	-0.04	-0.25	-0.35
		0	15	0	-0.14	0.03
20	-0.15			0.03	0.14	0.35
40	-0.14			0.04	0.24	0.45
60	-0.10			0.03	0.27	0.52
90	-0.01			0.01	0.40	0.53
110	0.02			0.02	0.34	0.47
140	0.10			-0.00	0.25	0.28
180	0.11			-0.00	0.04	-0.06
220	0.06			0.00	-0.10	-0.43
250	0.05			-0.01	-0.19	-0.50
270	0.05			-0.04	-0.20	-0.51
290	0.07			-0.05	-0.22	-0.50
330	0.05			-0.01	-0.22	-0.50
350	-0.03			-0.03	-0.11	0.02

APPENDIX C

LOAD SPECTRA

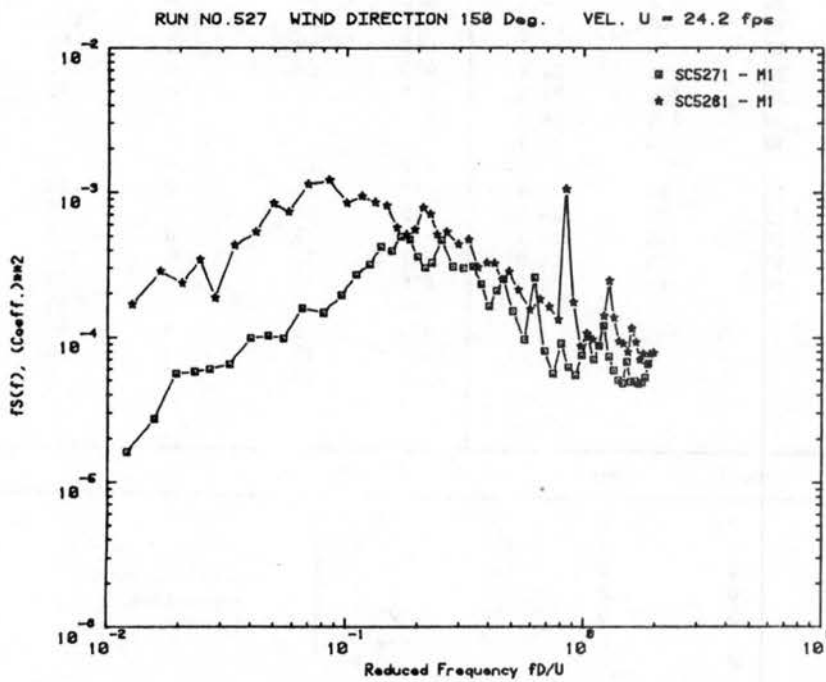
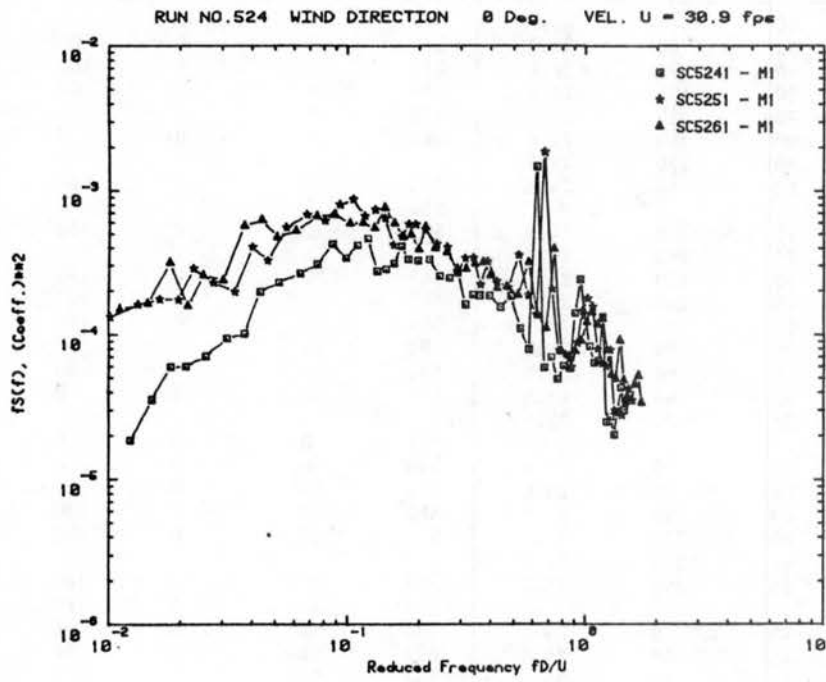
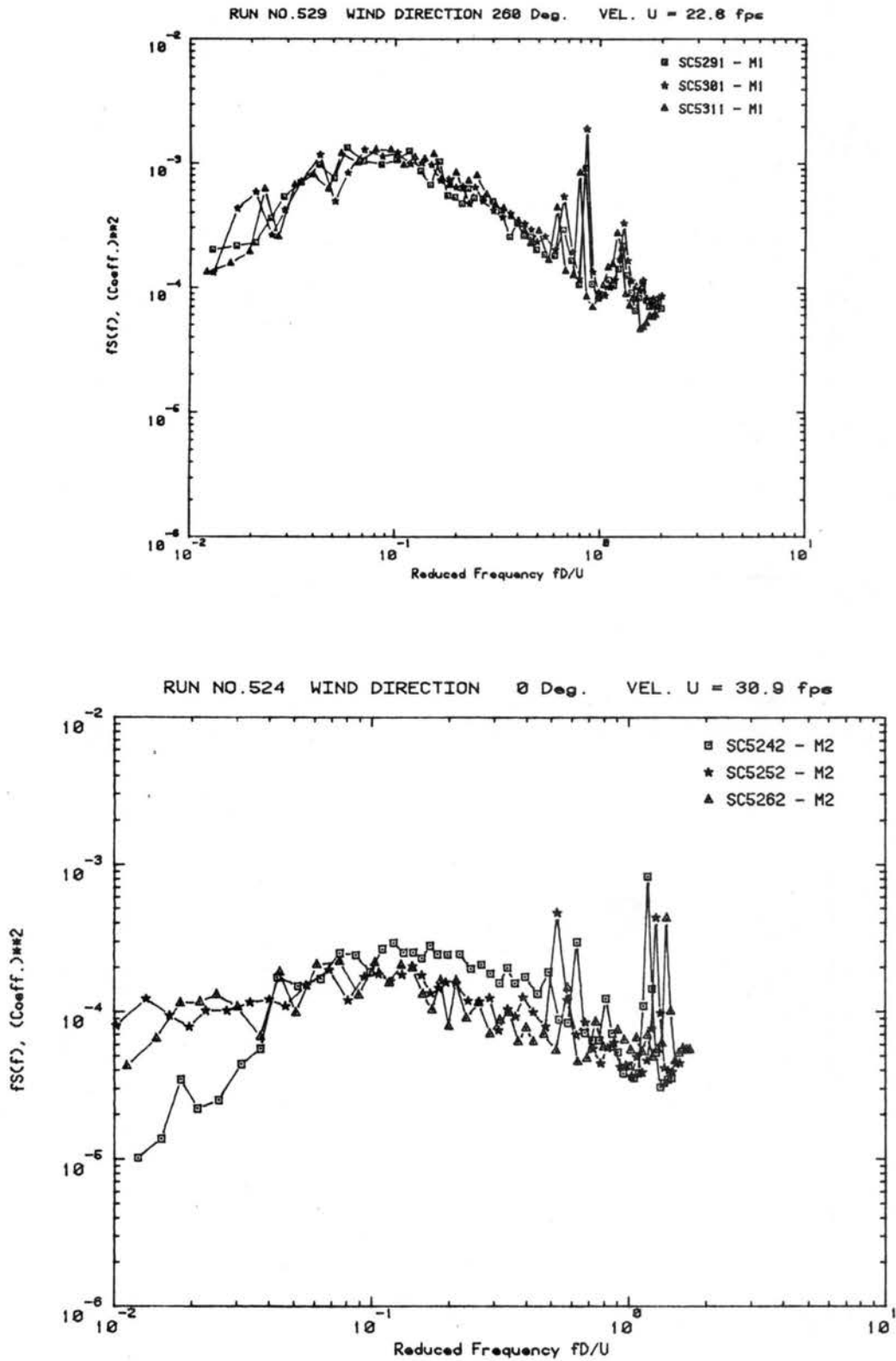


Figure C.1a. Load Spectra for Declination Angle 0° , Hour Angle 90°



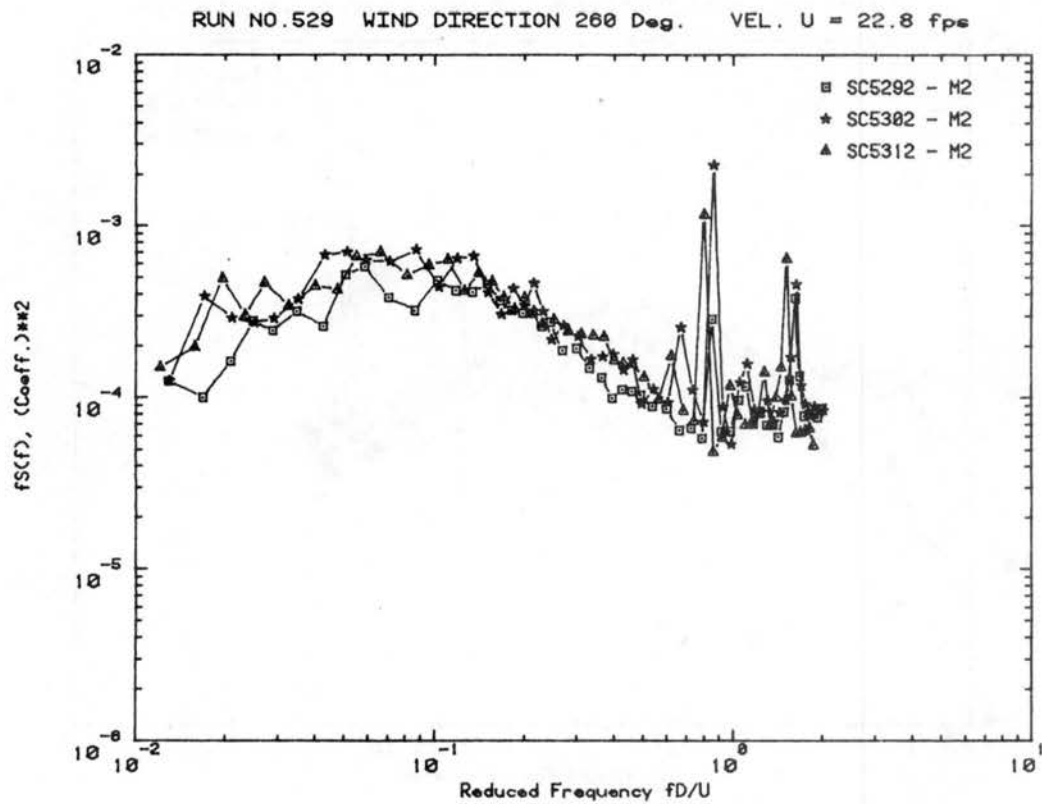
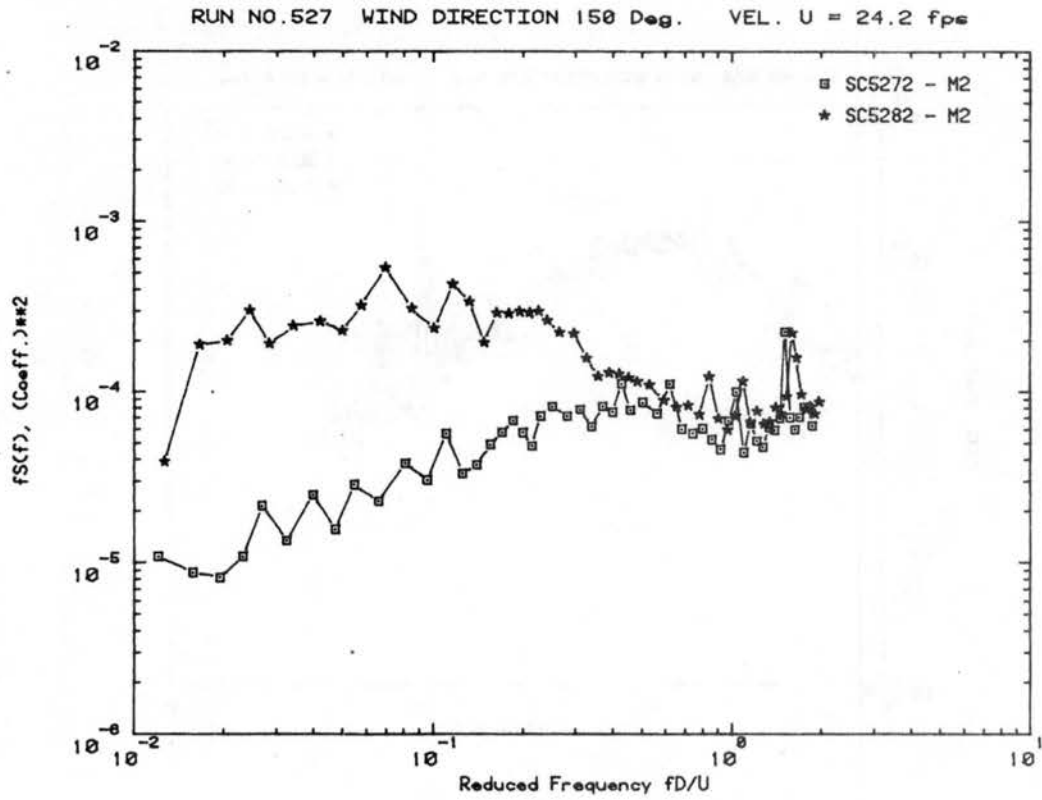


Figure C.1c. Load Spectra for Declination Angle 0° , Hour Angle 90°

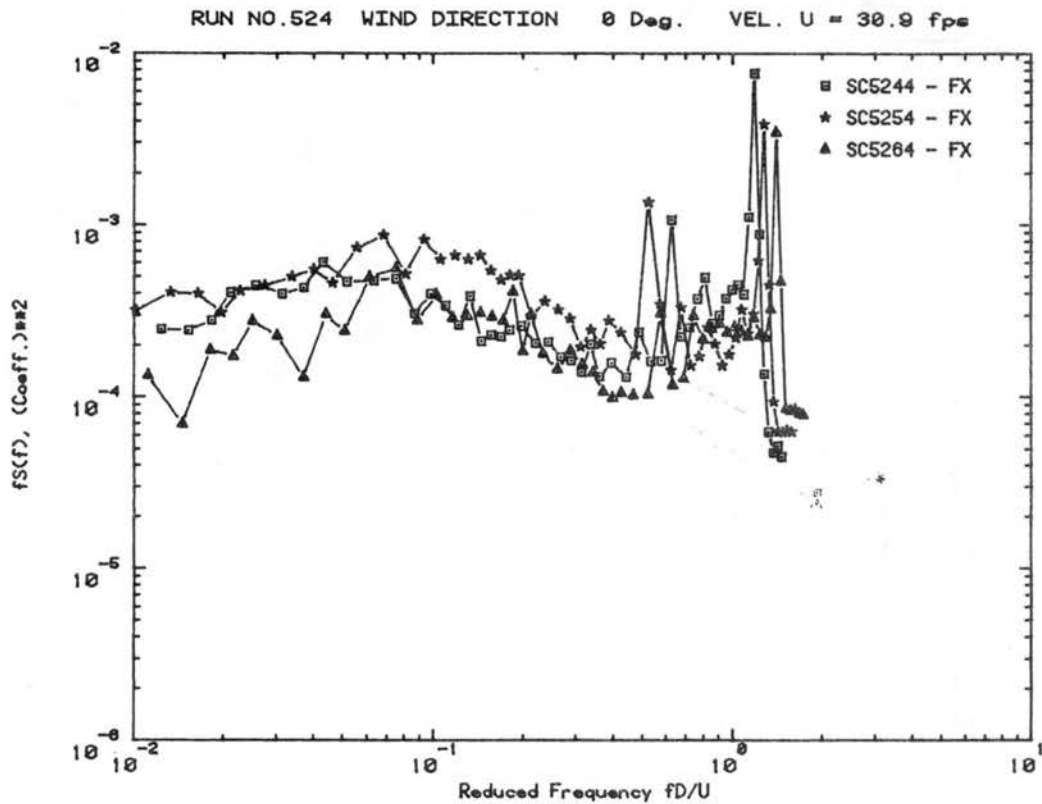
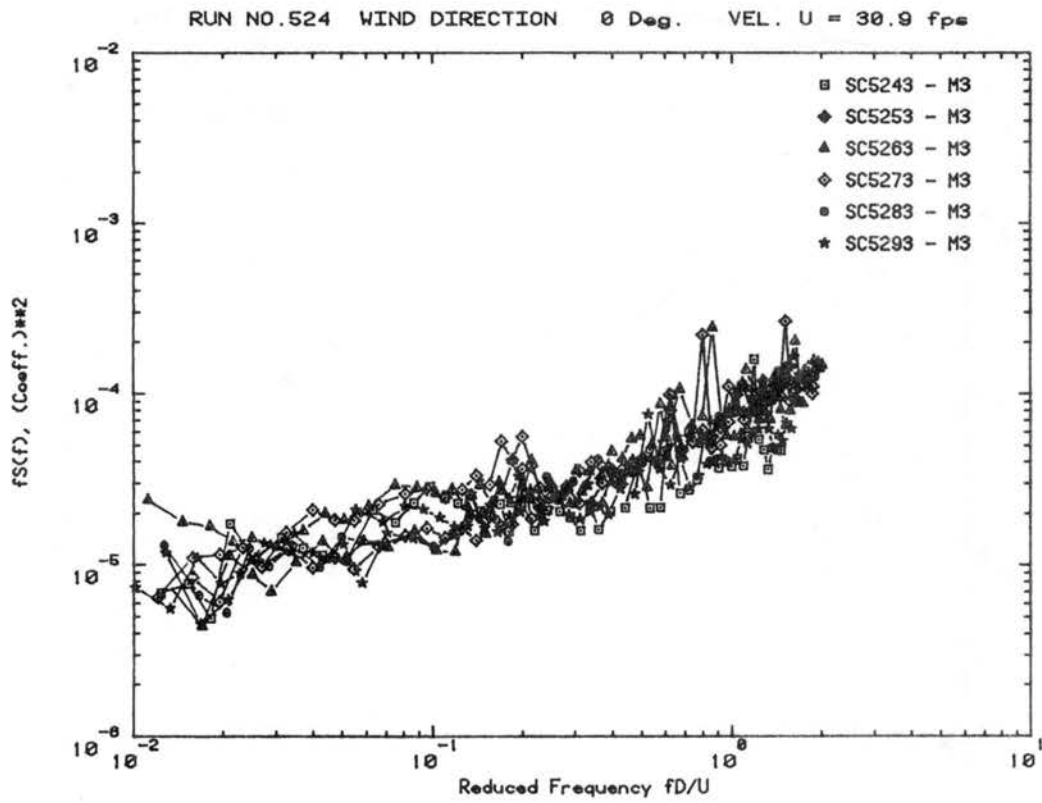


Figure C.1d. Load Spectra for Declination Angle 0° , Hour Angle 90°

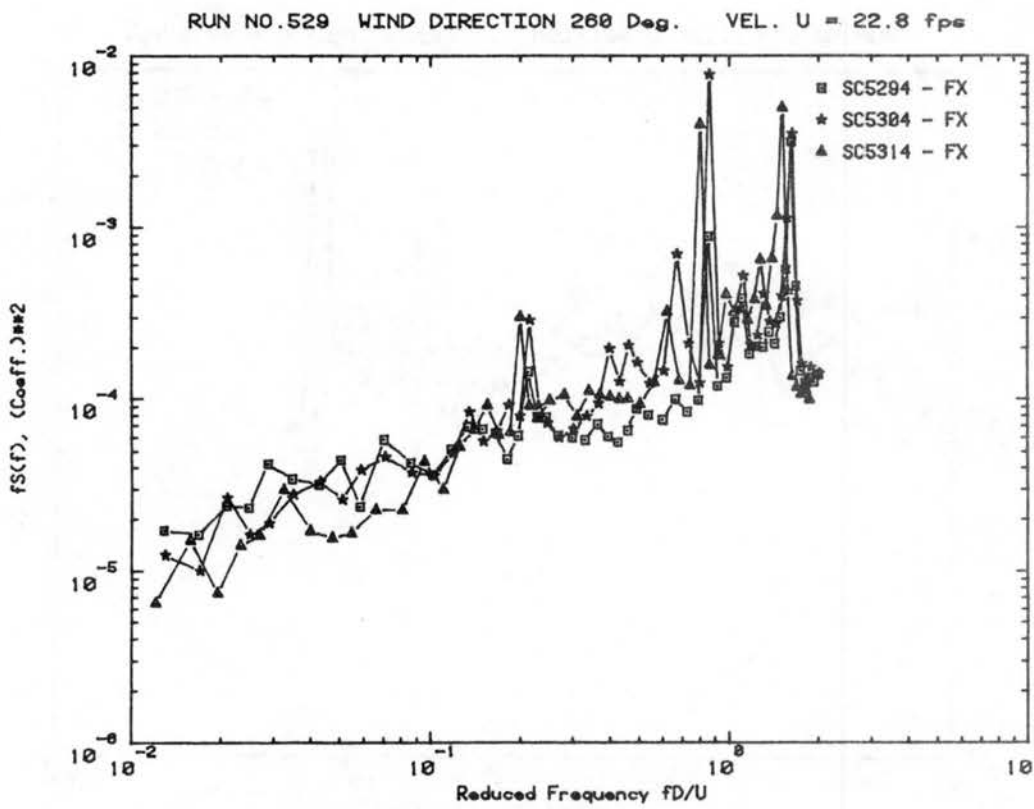
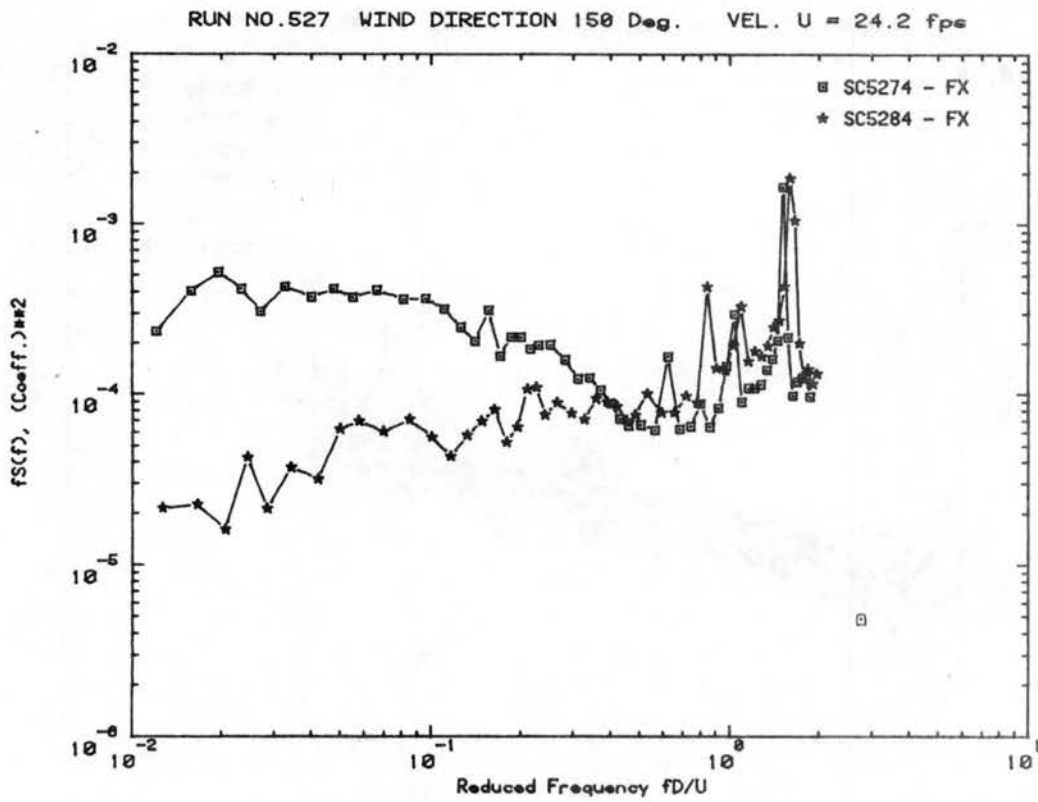


Figure C.1e. Load Spectra for Declination Angle 0° , Hour Angle 90°

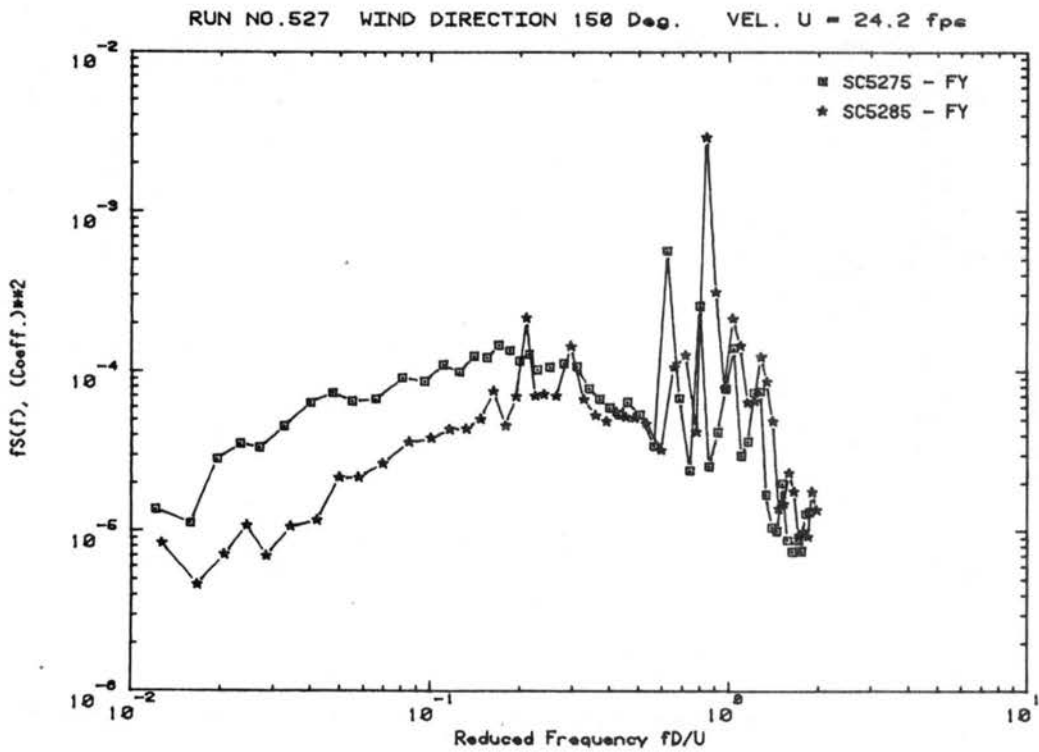
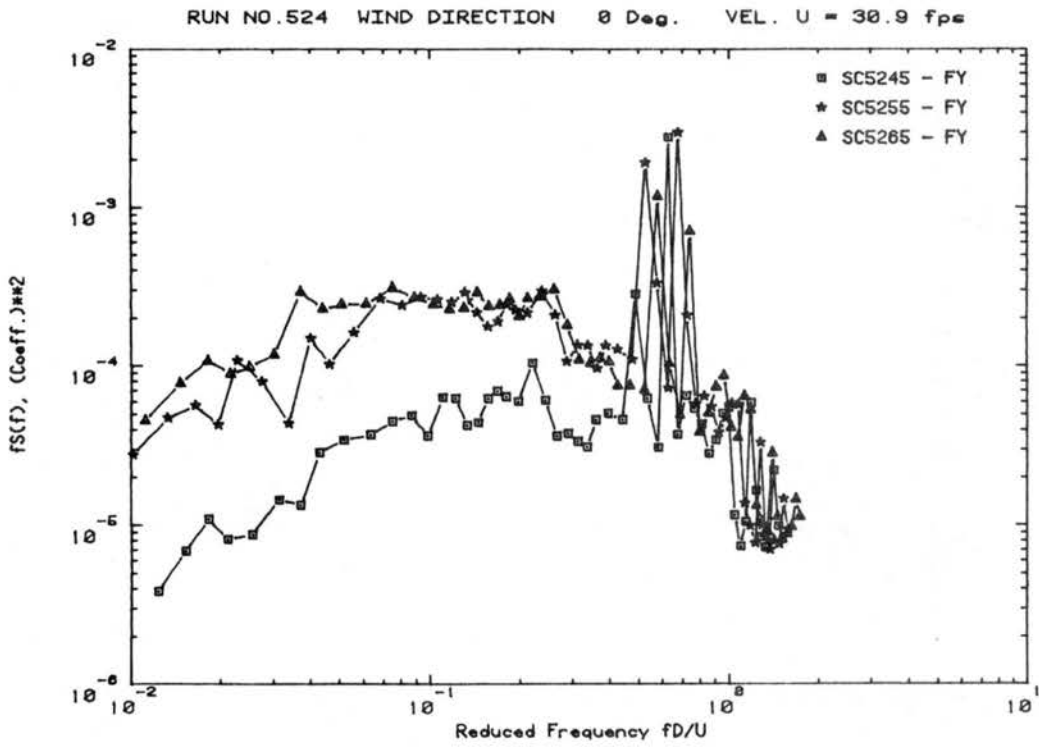


Figure C.1f. Load Spectra for Declination Angle 0°, Hour Angle 90°

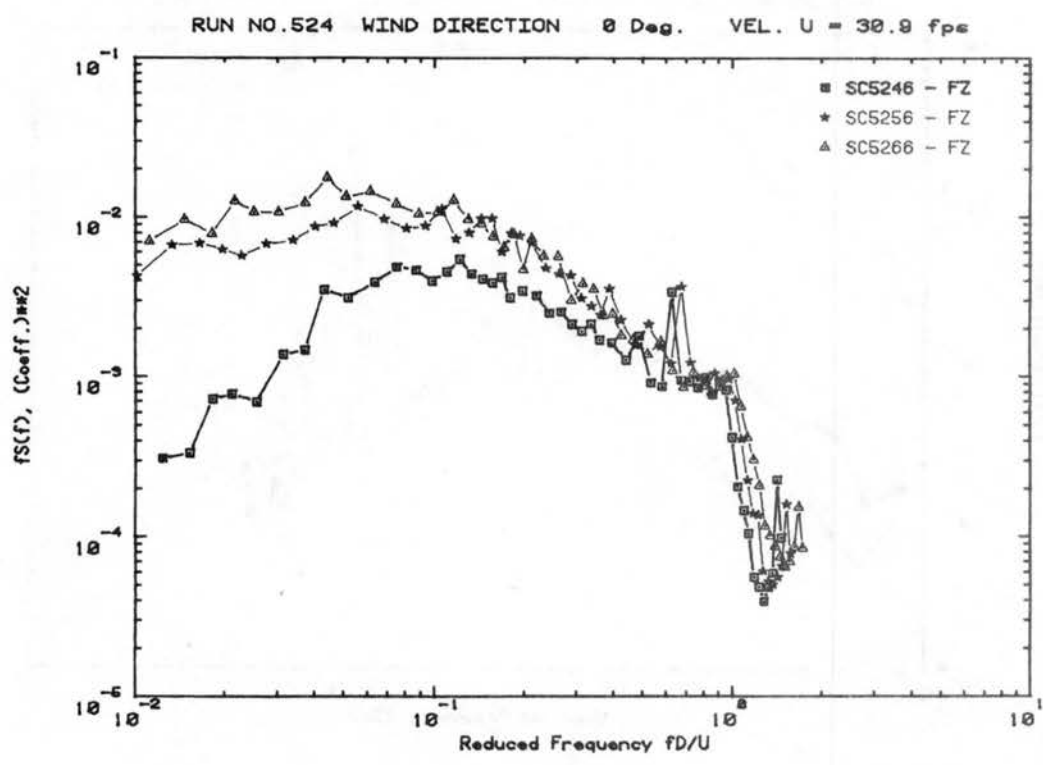
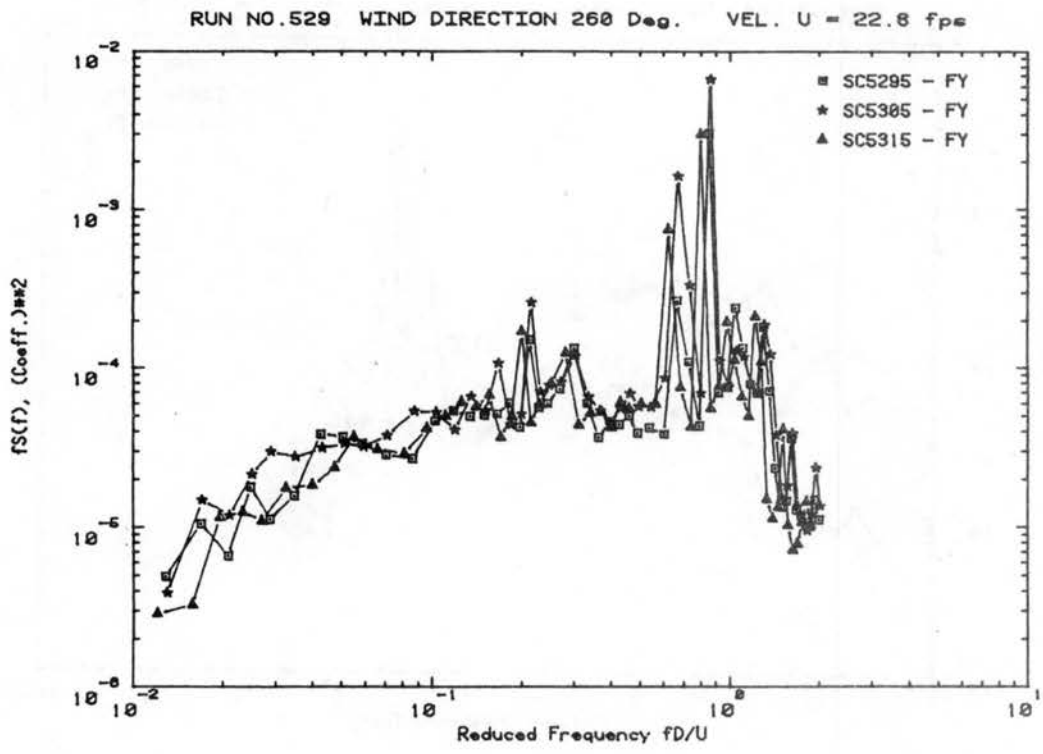


Figure C.1g. Load Spectra for Declination Angle 0° , Hour Angle 90°

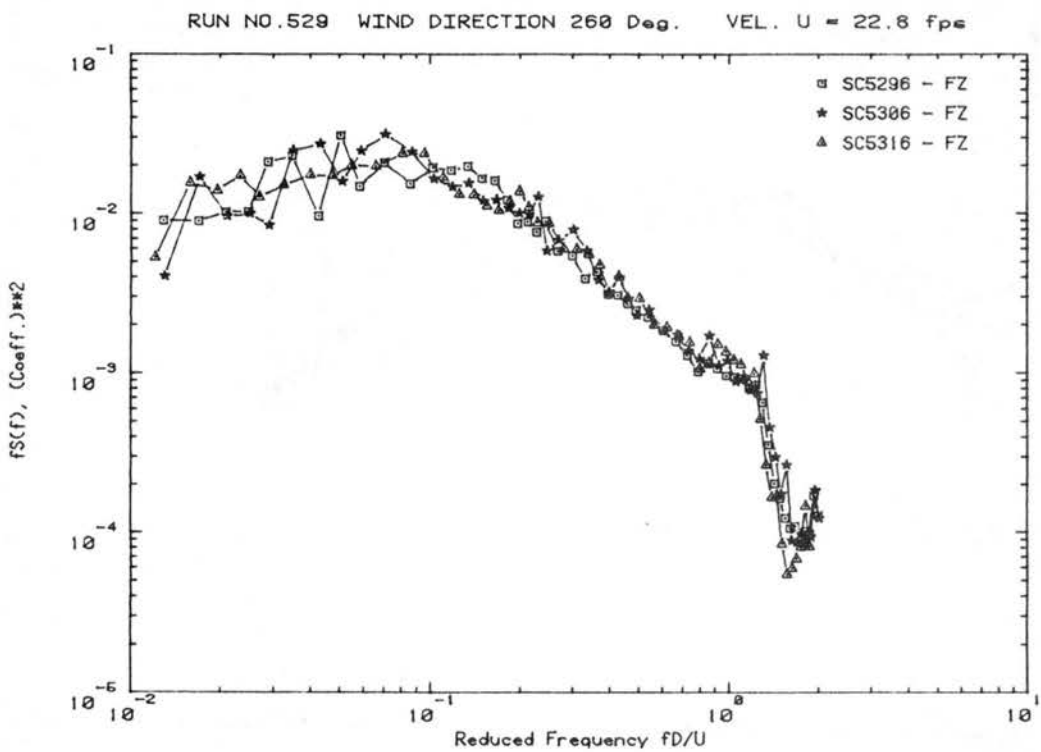
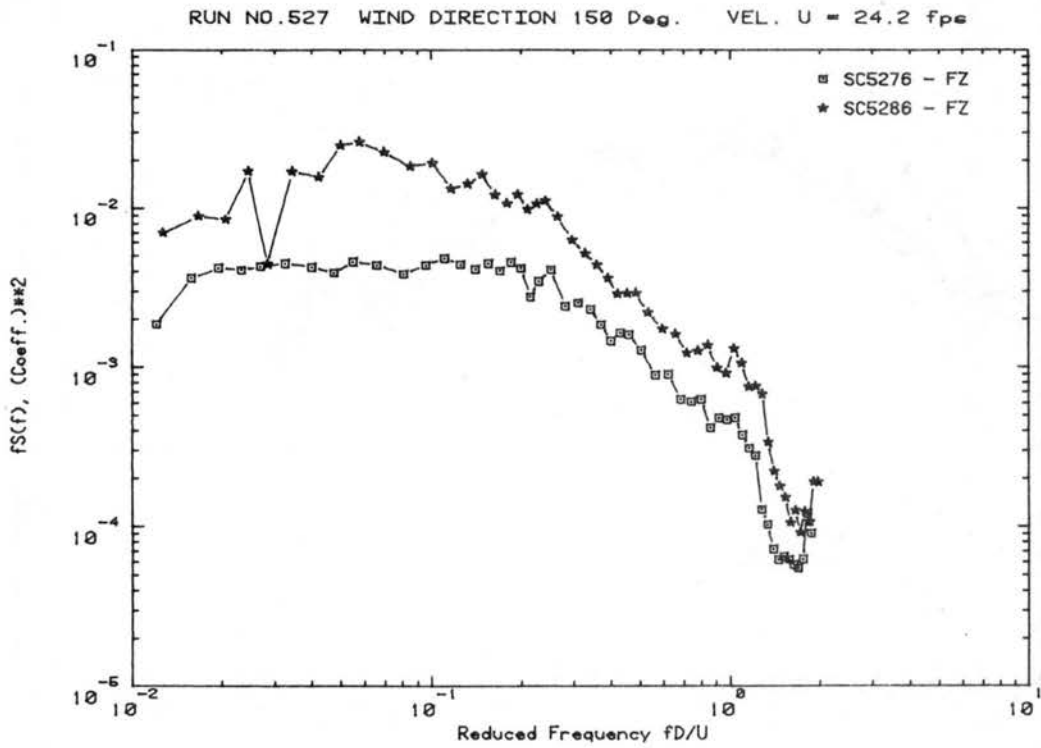
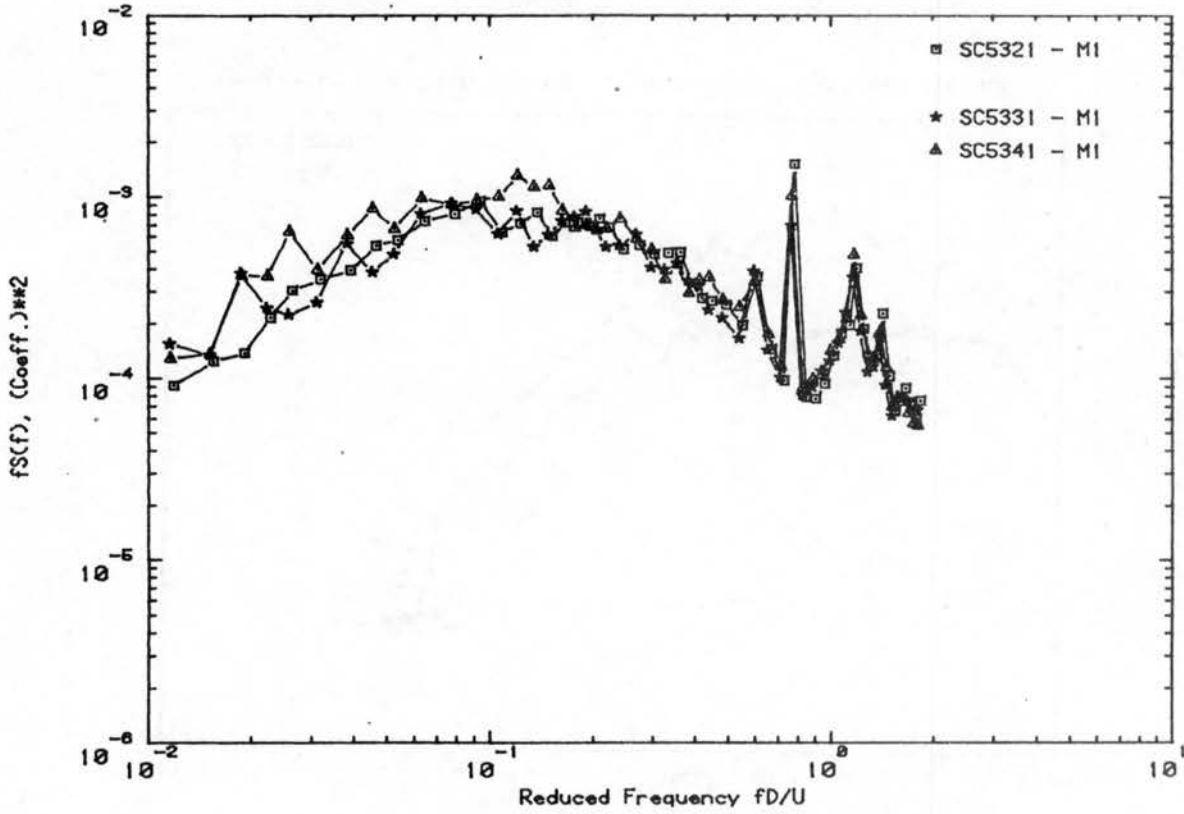


Figure C.1h. Load Spectra for Declination Angle 0° , Hour Angle 90°

RUN NO.532 WIND DIRECTION 310 Deg. VEL. U = 24.6 fps



RUN NO.535 WIND DIRECTION 250 Deg. VEL. U = 25.1 fps

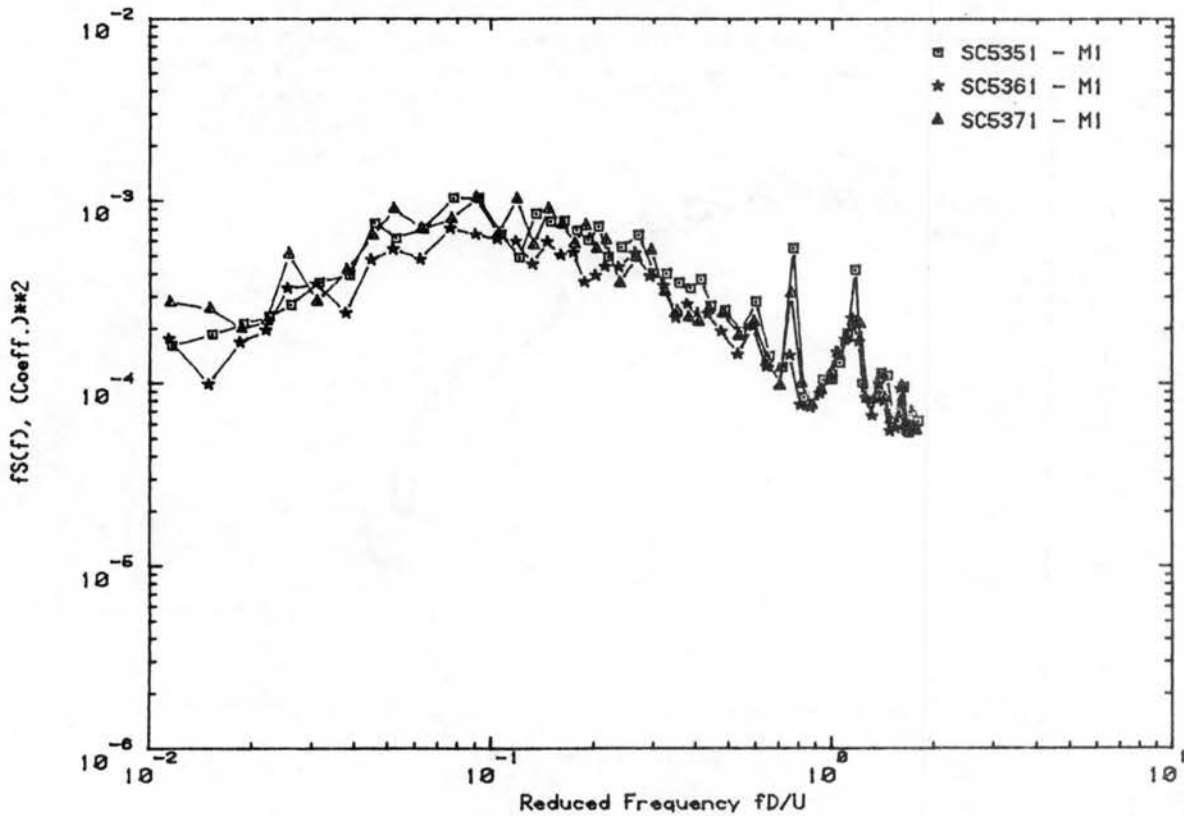
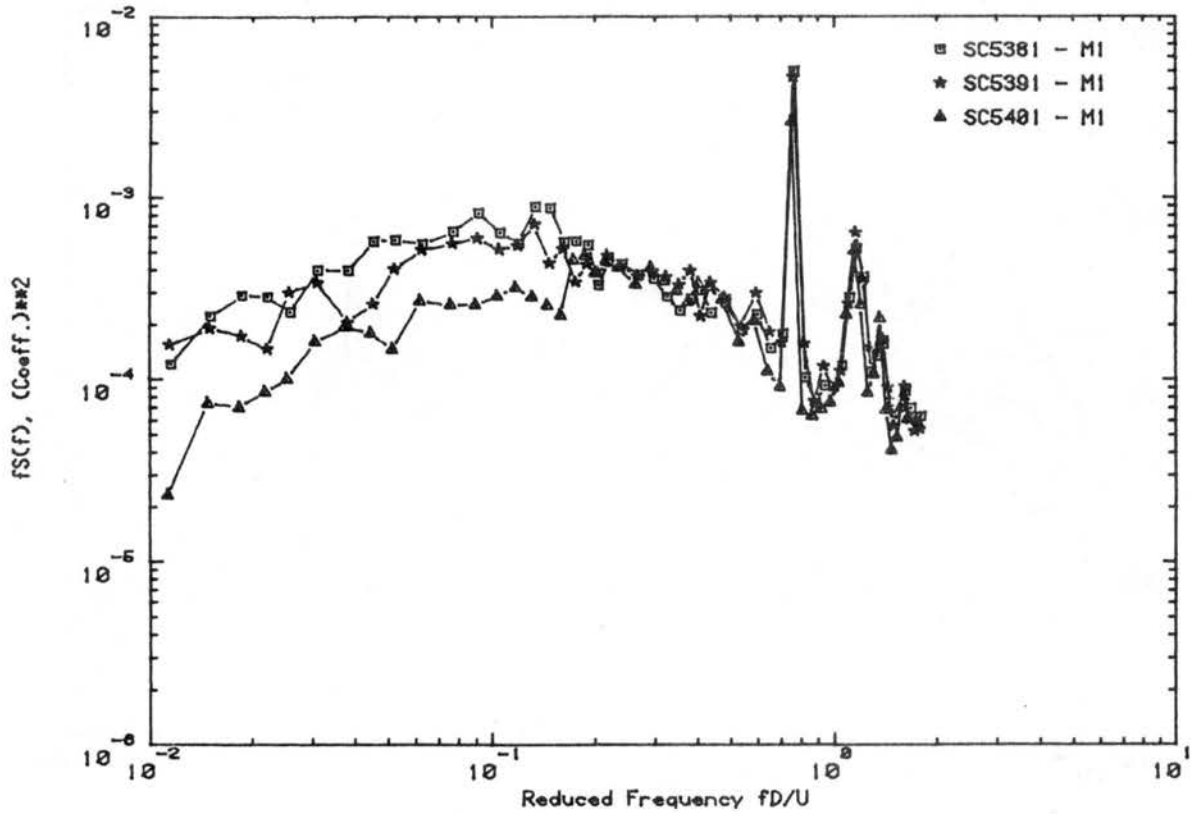


Figure C.2a. Load Spectra for Declination Angle 0°, Hour Angle 75°

RUN NO.538 WIND DIRECTION 60 Deg. VEL. U = 25.3 fps



RUN NO.532 WIND DIRECTION 310 Deg. VEL. U = 24.6 fps

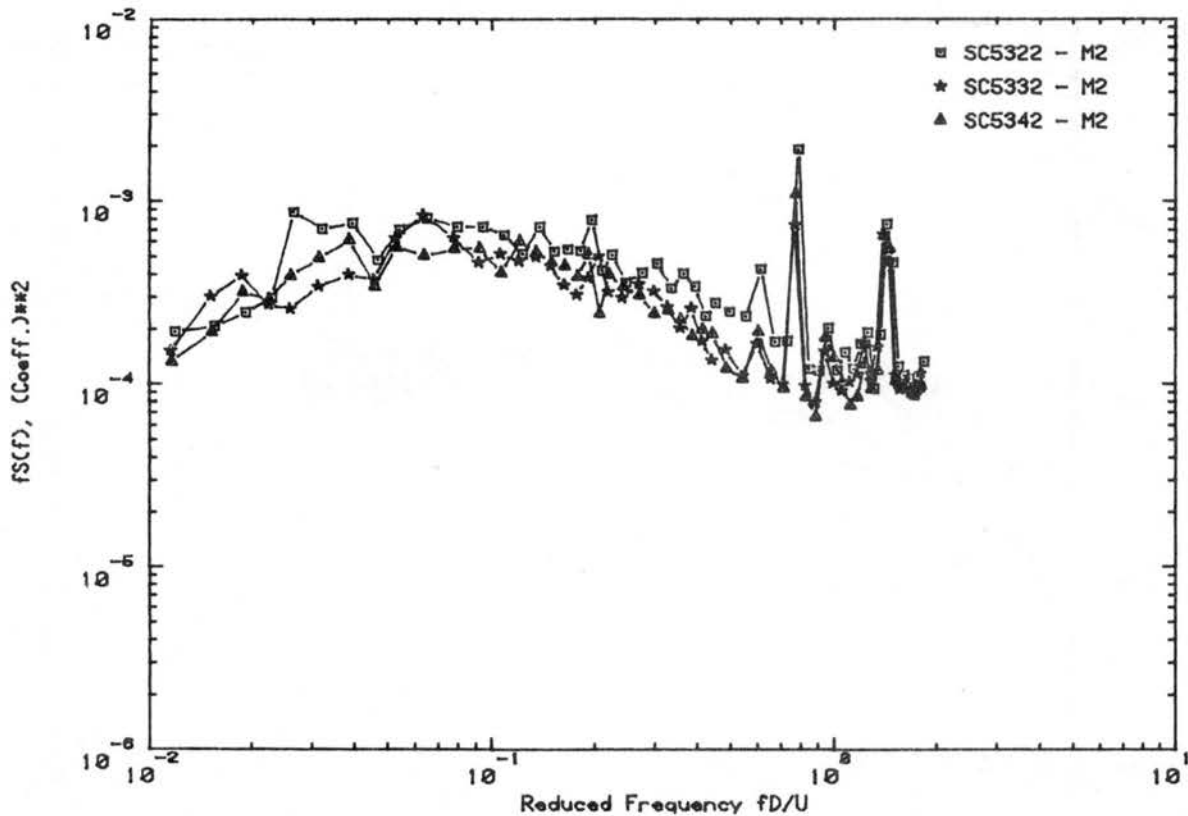
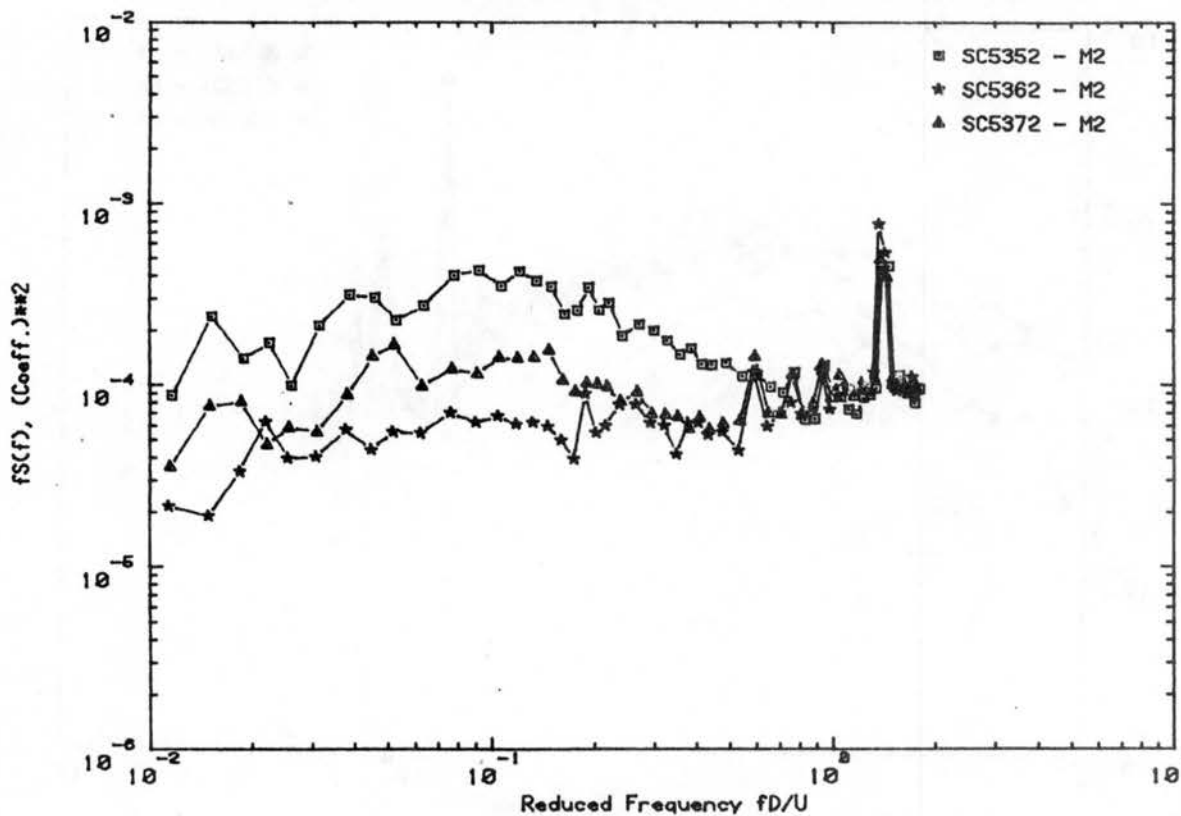


Figure C.2b. Load Spectra for Declination Angle 0°, Hour Angle 75°

RUN NO.535 WIND DIRECTION 250 Deg. VEL. U = 25.1 fps



RUN NO.538 WIND DIRECTION 60 Deg. VEL. U = 25.3 fps

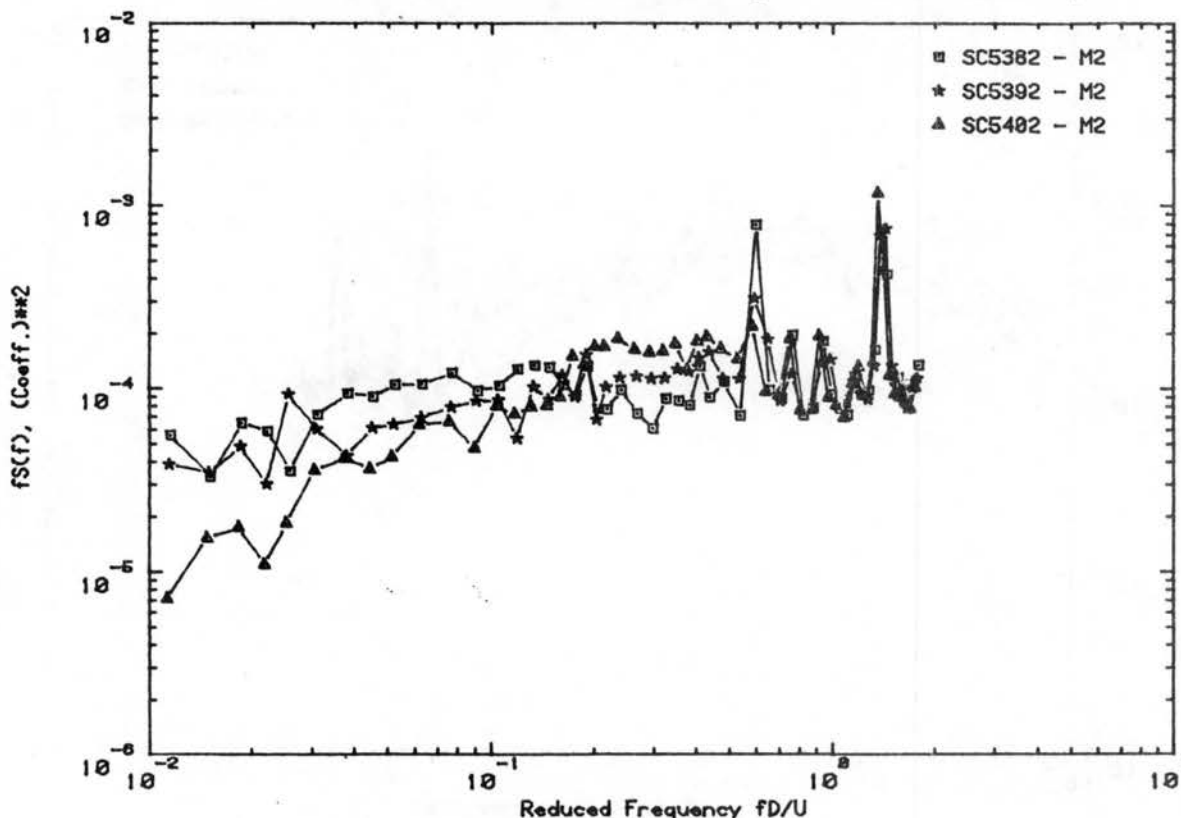
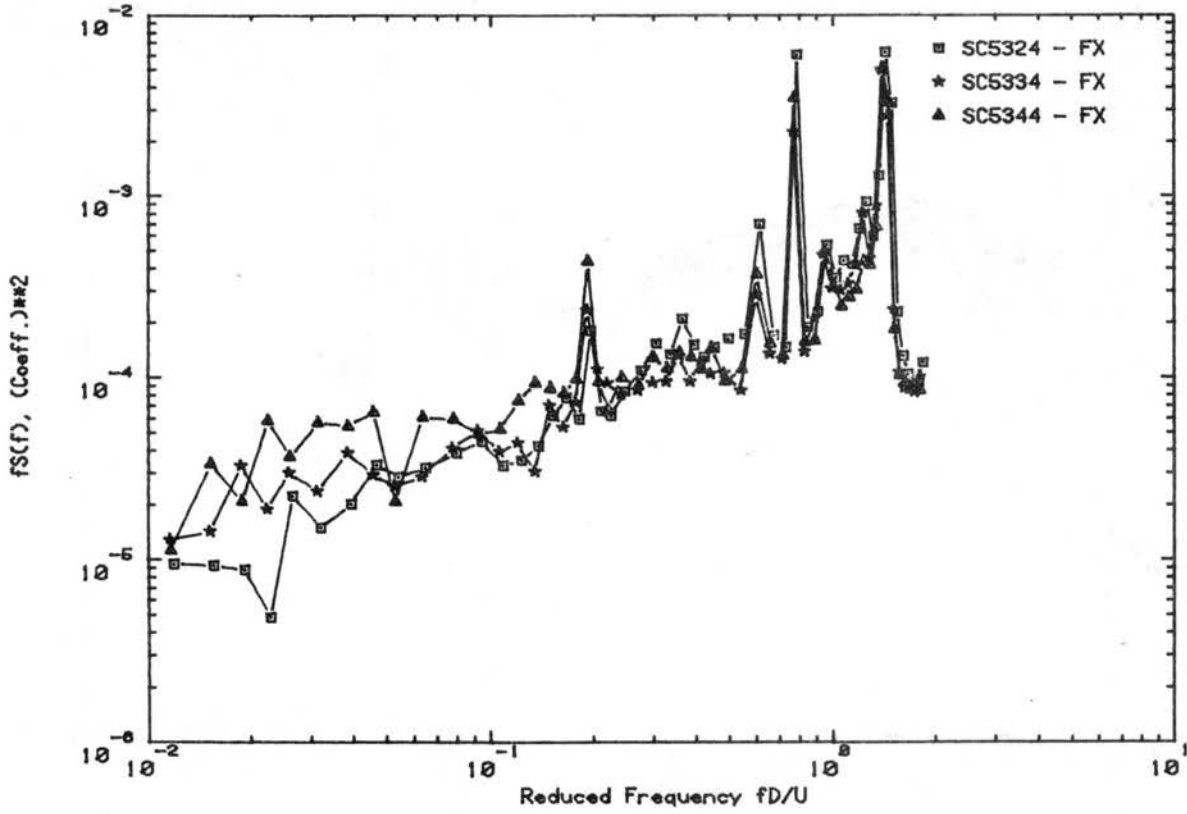


Figure C.2c. Load Spectra for Declination Angle 0°, Hour Angle 75°

RUN NO.532 WIND DIRECTION 310 Deg. VEL. U = 24.6 fps



RUN NO.535 WIND DIRECTION 250 Deg. VEL. U = 25.1 fps

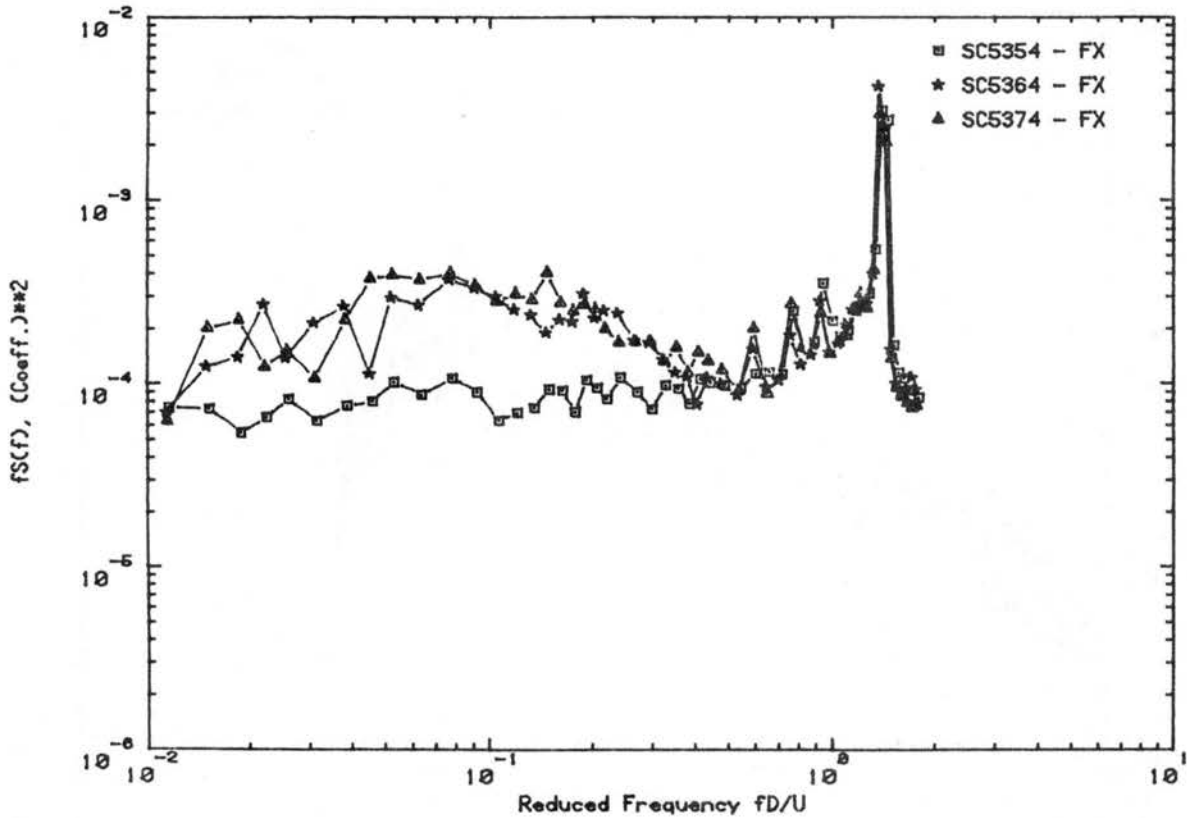
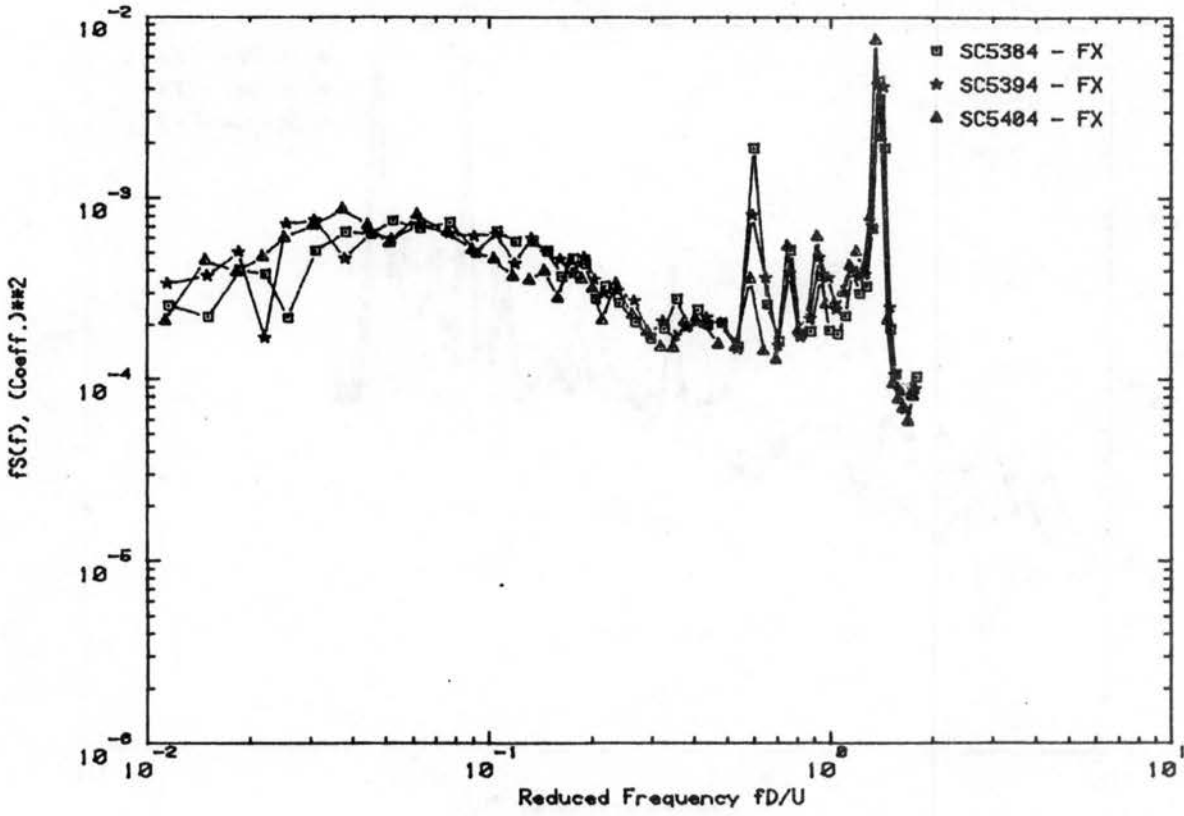


Figure C.2d. Load Spectra for Declination Angle 0°, Hour Angle 75°

RUN NO.538 WIND DIRECTION 60 Deg. VEL. U = 25.3 fps



RUN NO.532 WIND DIRECTION 310 Deg. VEL. U = 24.6 fps

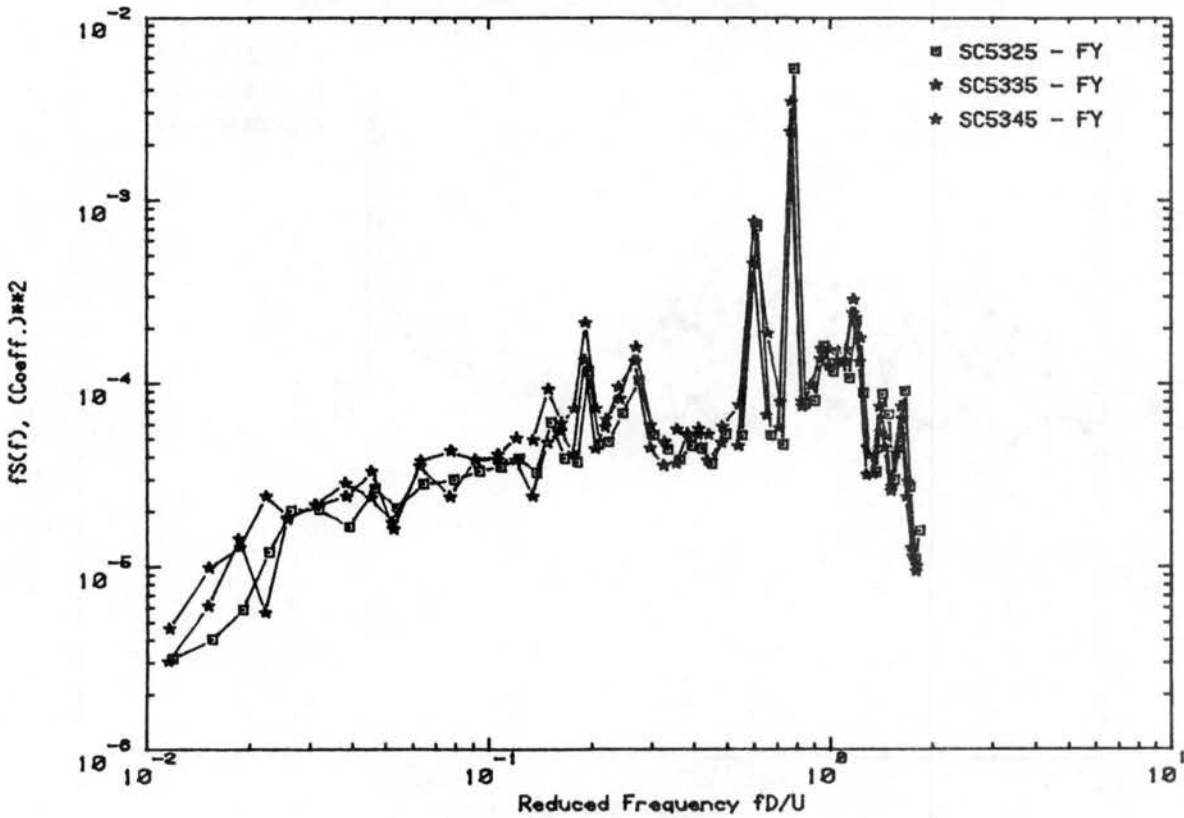
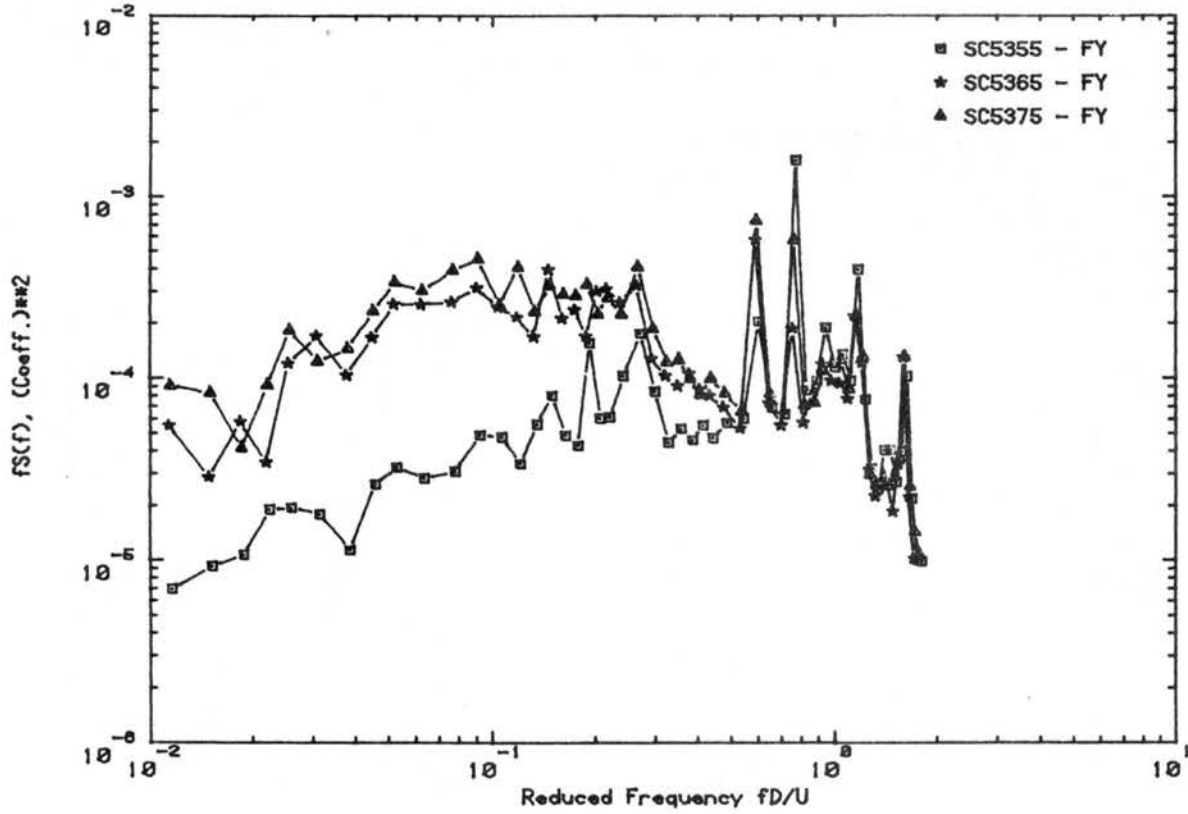
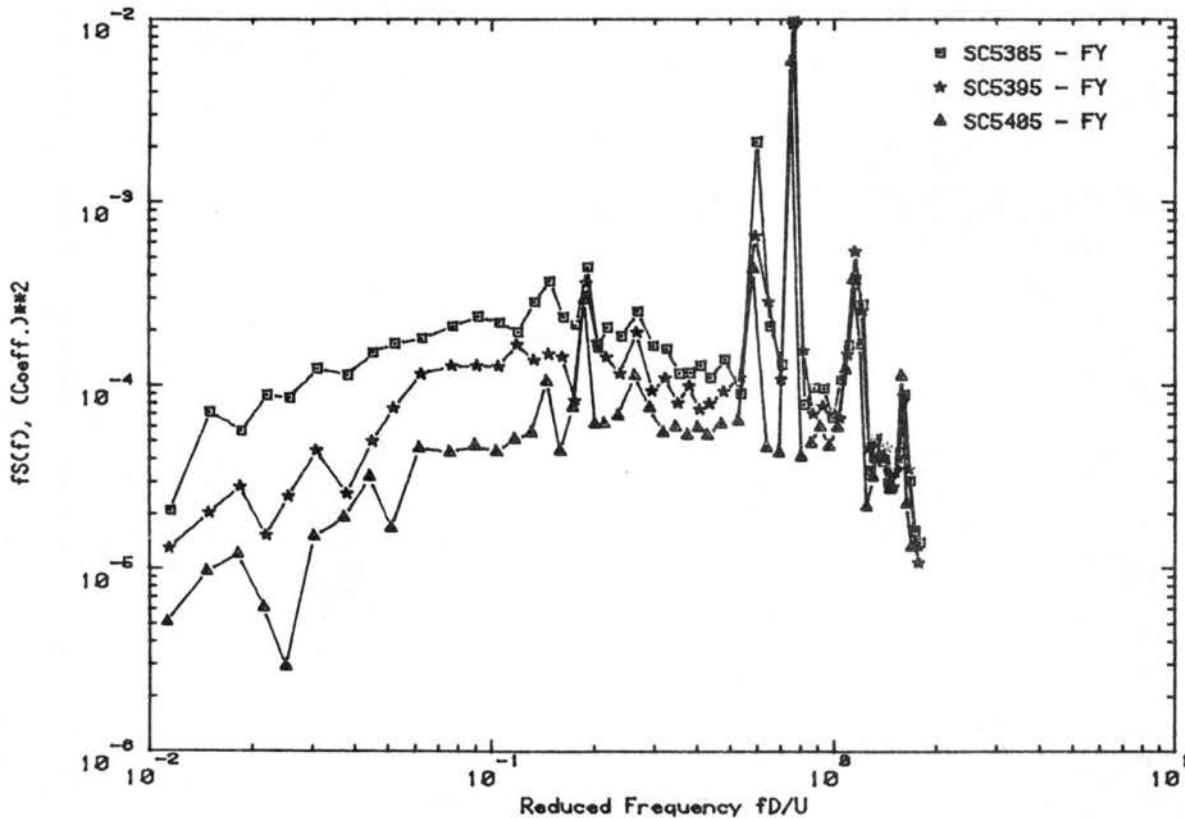


Figure C.2e. Load Spectra for Declination Angle 0°, Hour Angle 75°

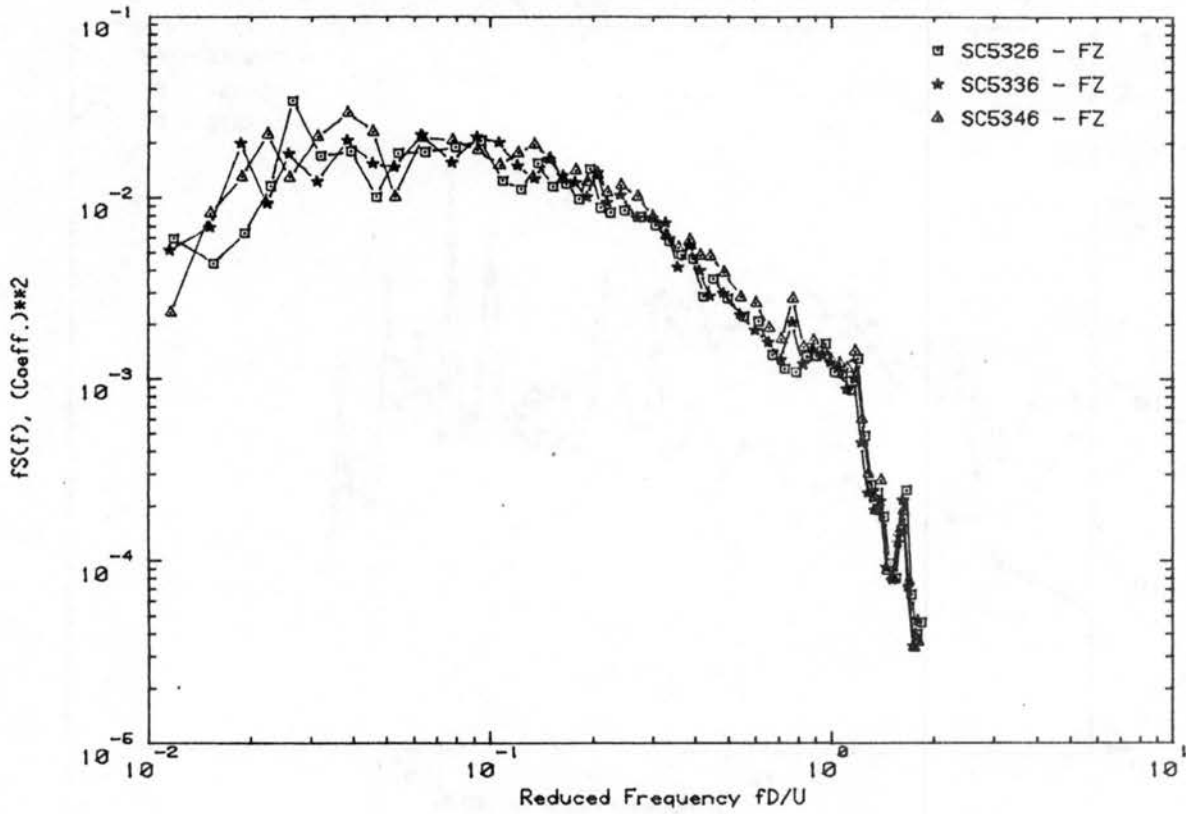
RUN NO.535 WIND DIRECTION 250 Deg. VEL. U = 25.1 fps



RUN NO.536 WIND DIRECTION 60 Deg. VEL. U = 25.3 fps

Figure C.2f. Load Spectra for Declination Angle 0° , Hour Angle 75°

RUN NO.532 WIND DIRECTION 310 Deg. VEL. U = 24.6 fps



RUN NO.537 WIND DIRECTION 90 Deg. VEL. U = 25.5 fps

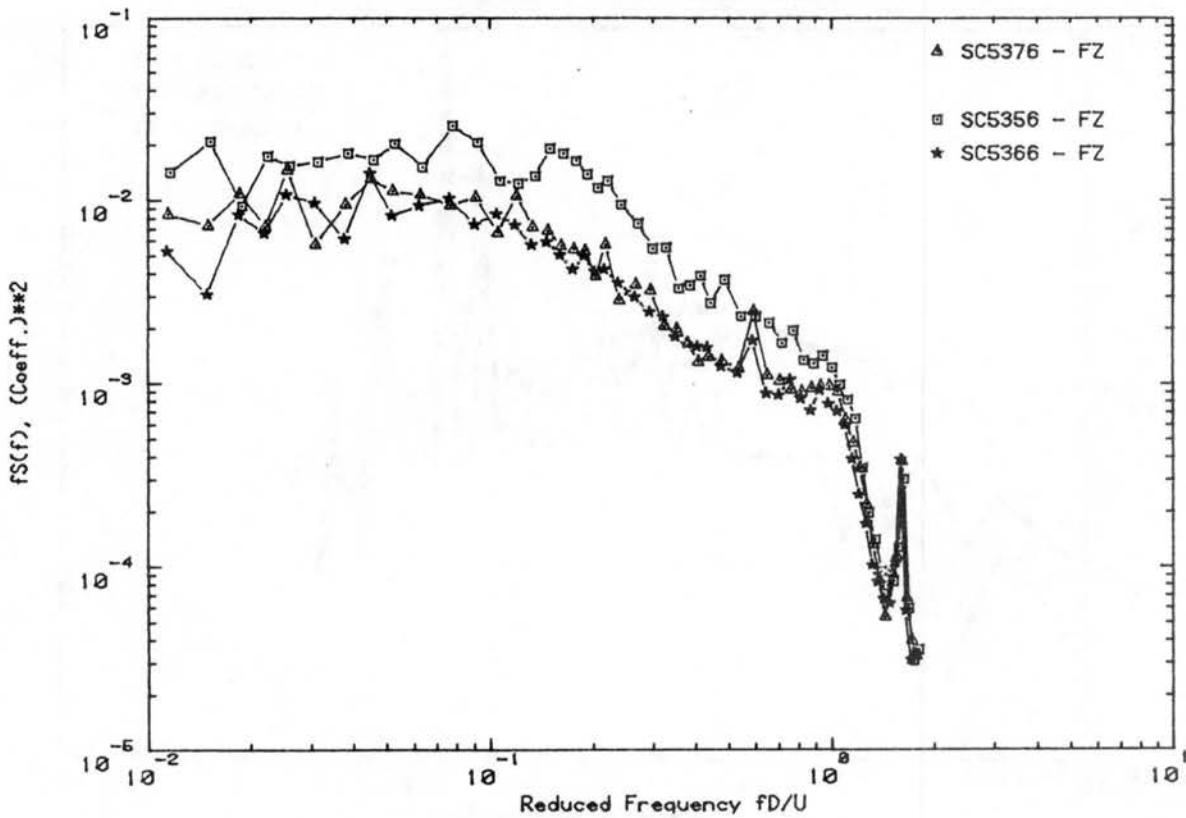


Figure C.2g. Load Spectra for Declination Angle 0°, Hour Angle 75°

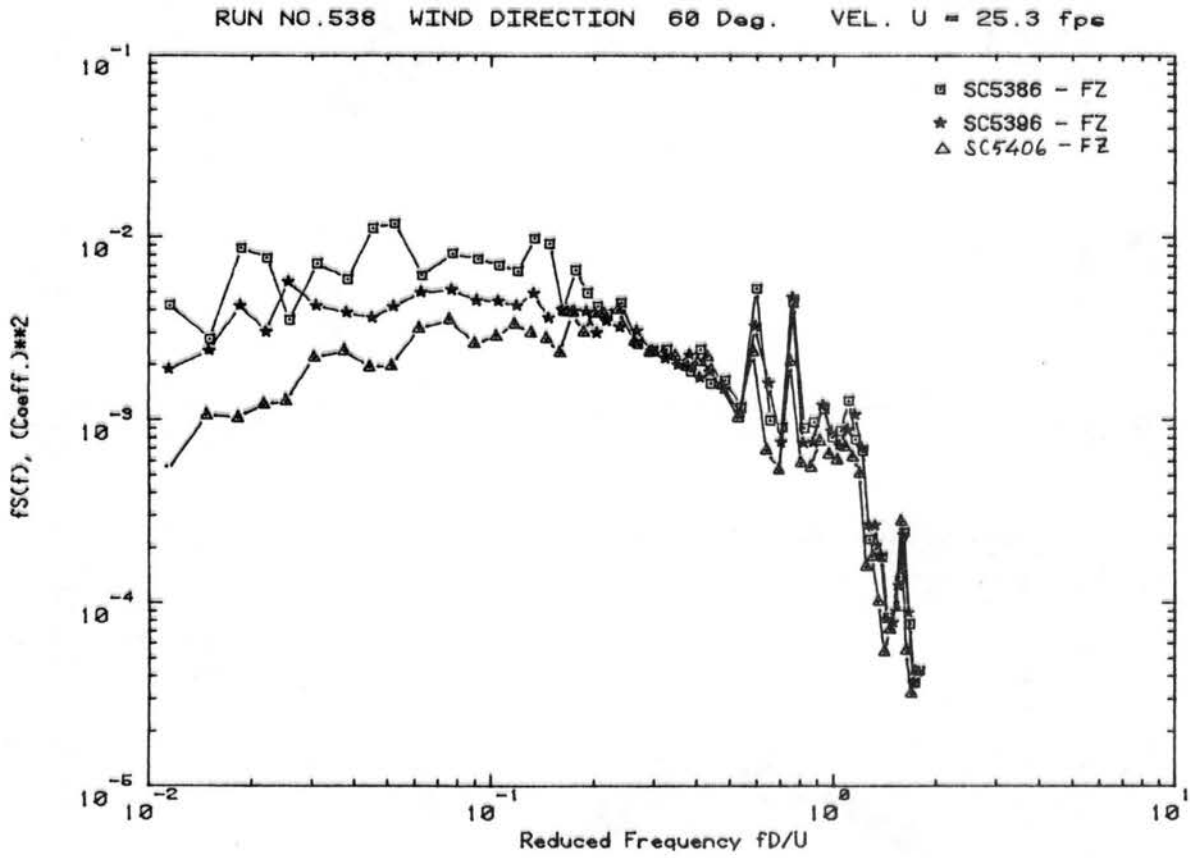
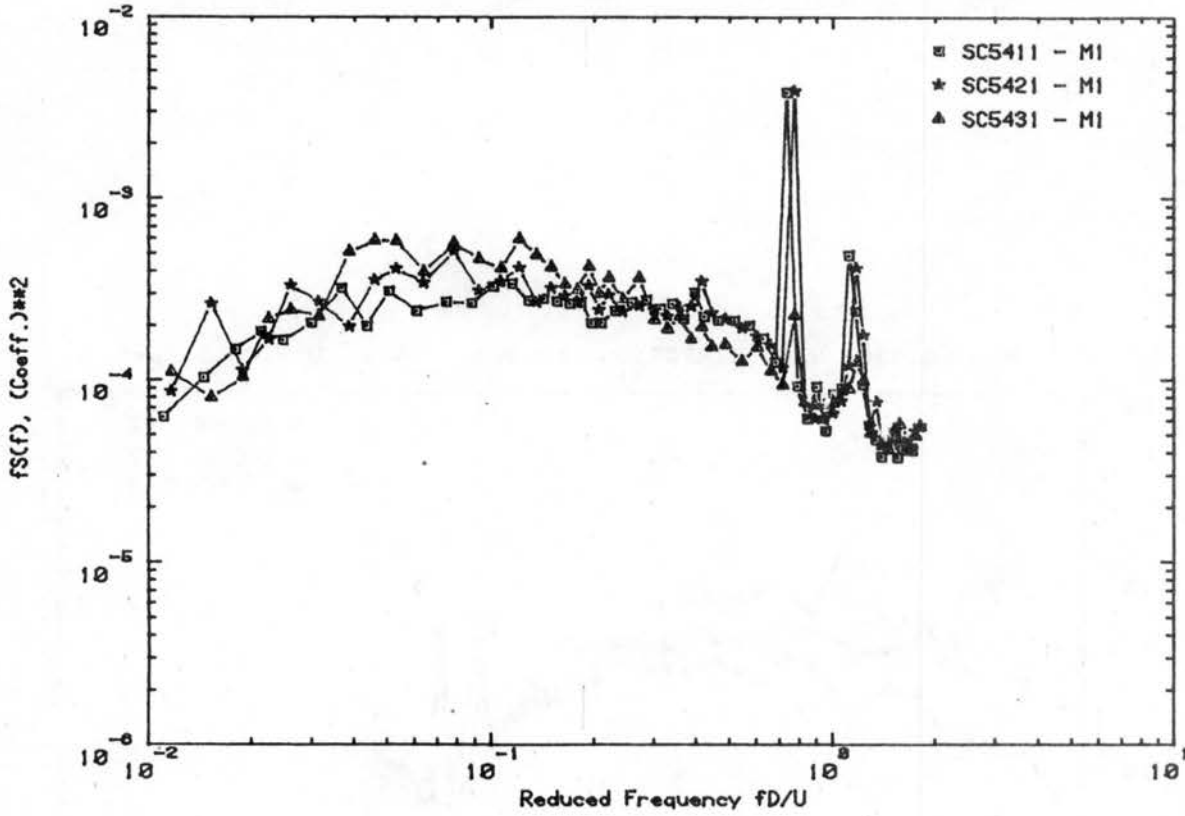


Figure C.2h. Load Spectra for Declination Angle 0° , Hour Angle 75°

RUN NO.541 WIND DIRECTION 60 Deg. VEL. U = 26.3 fps



RUN NO.544 WIND DIRECTION 220 Deg. VEL. U = 24.7 fps

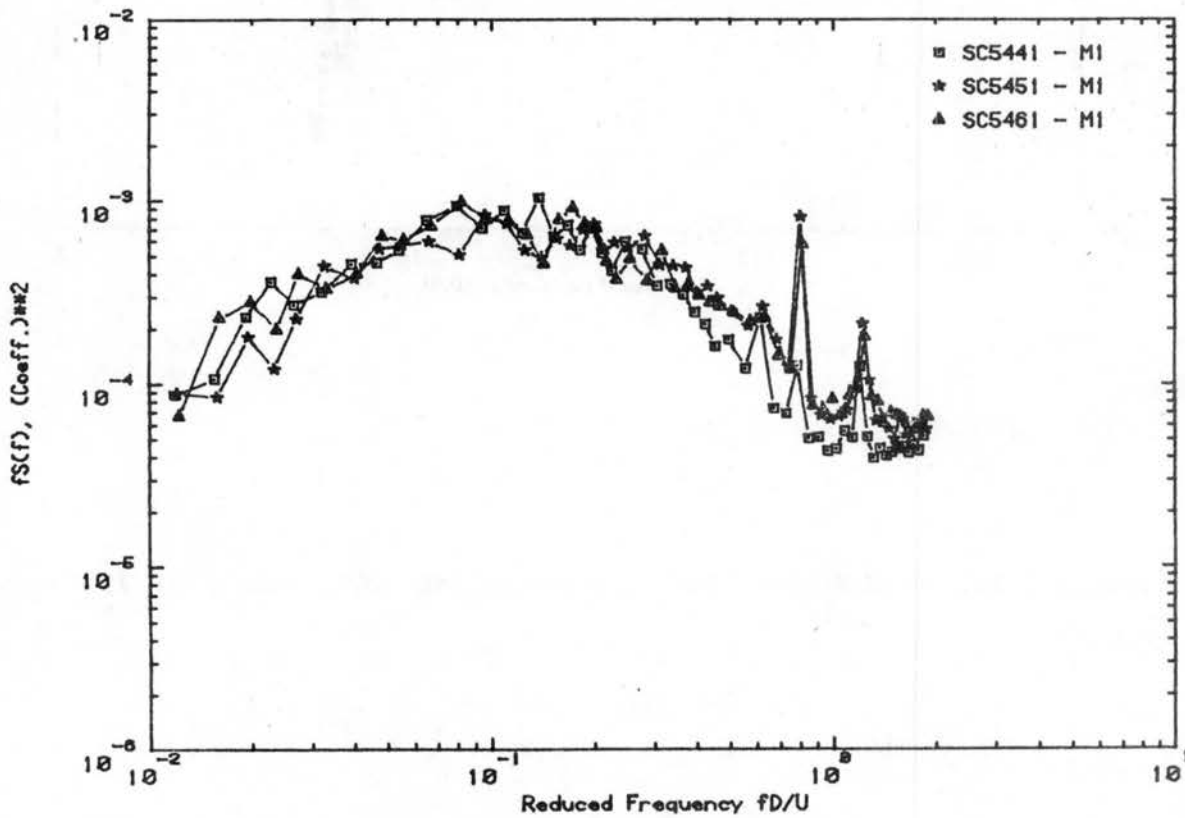
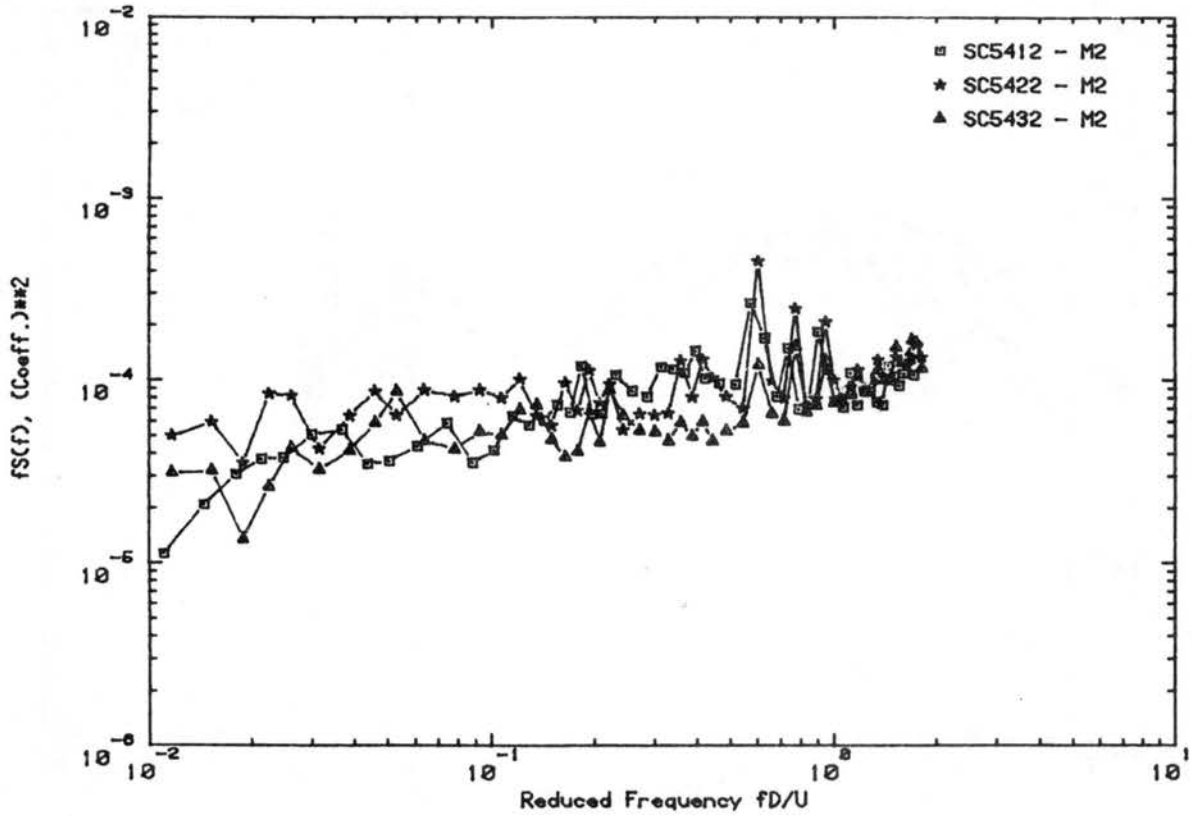


Figure C.3a. Load Spectra for Declination Angle 0°, Hour Angle 60°

RUN NO.541 WIND DIRECTION 60 Deg. VEL. U = 26.3 fps



RUN NO.544 WIND DIRECTION 220 Deg. VEL. U = 24.7 fps

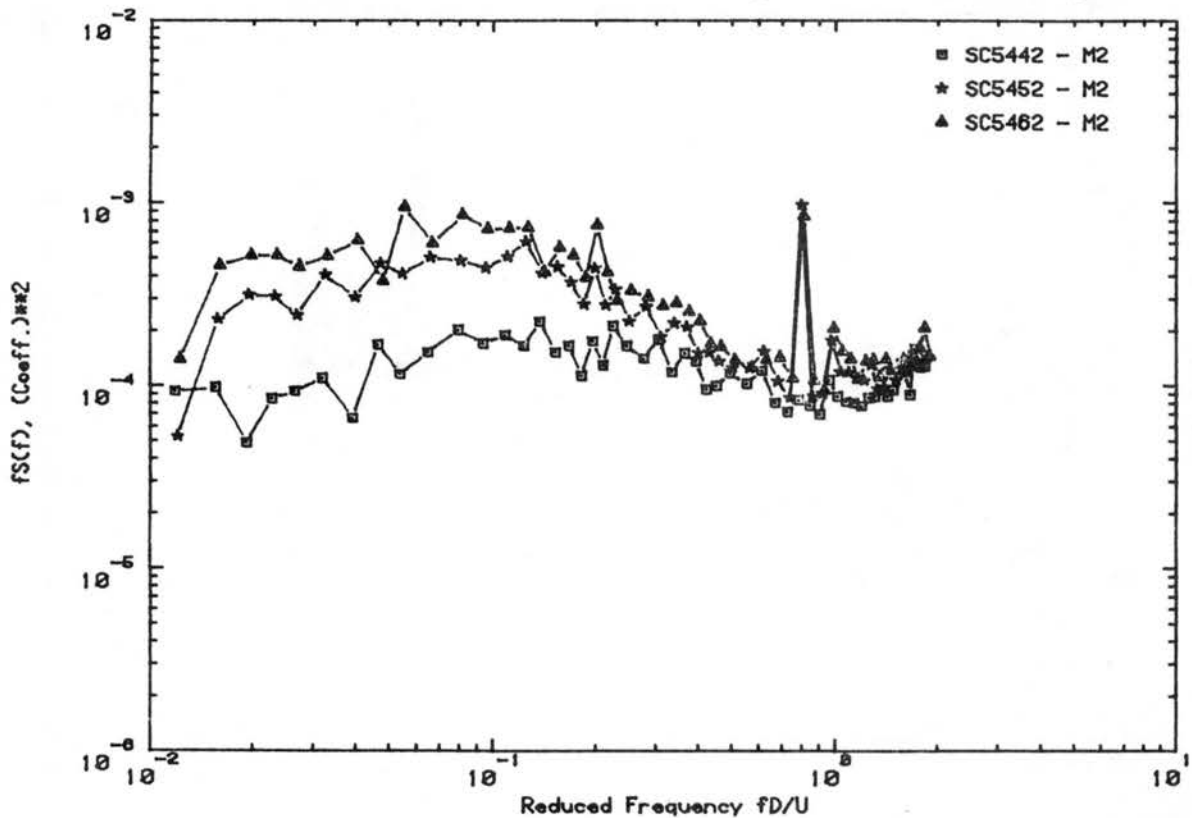
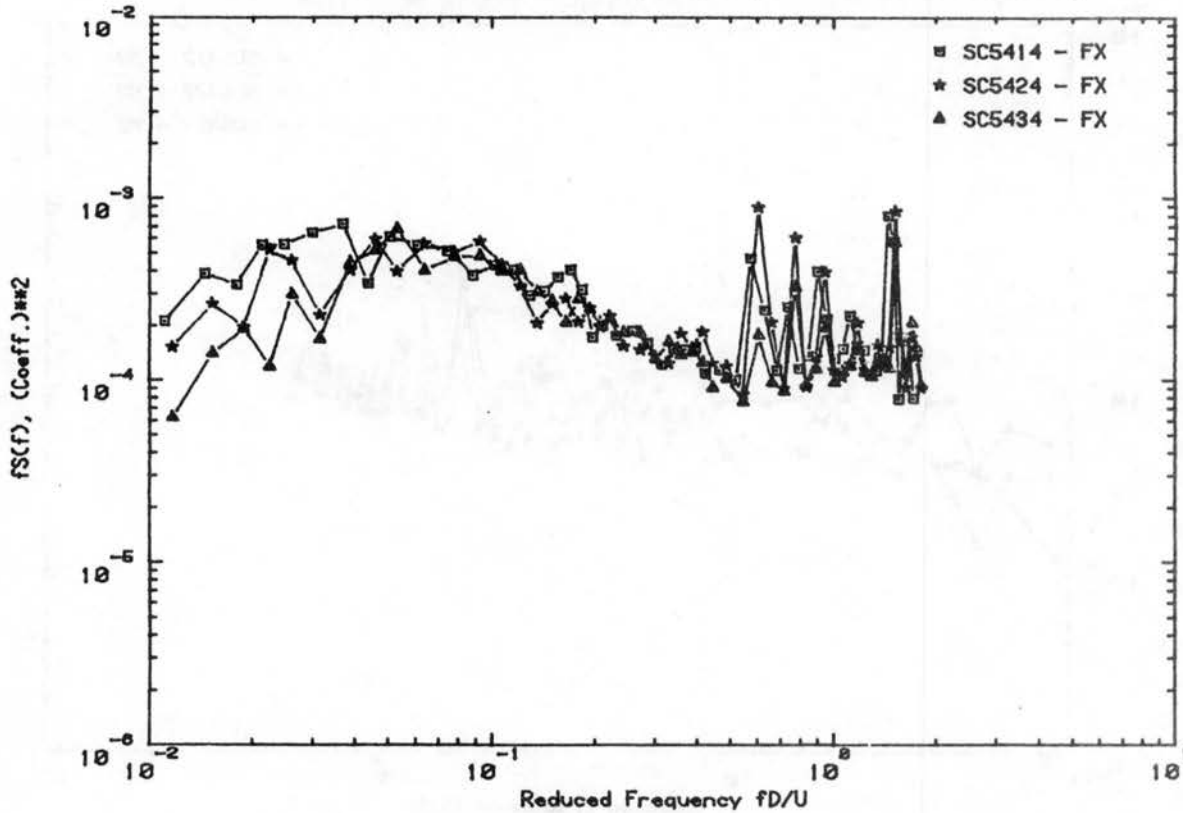


Figure C.3b. Load Spectra for Declination Angle 0°, Hour Angle 60°

RUN NO.541 WIND DIRECTION 60 Deg. VEL. U = 26.3 fps



RUN NO.544 WIND DIRECTION 220 Deg. VEL. U = 24.7 fps

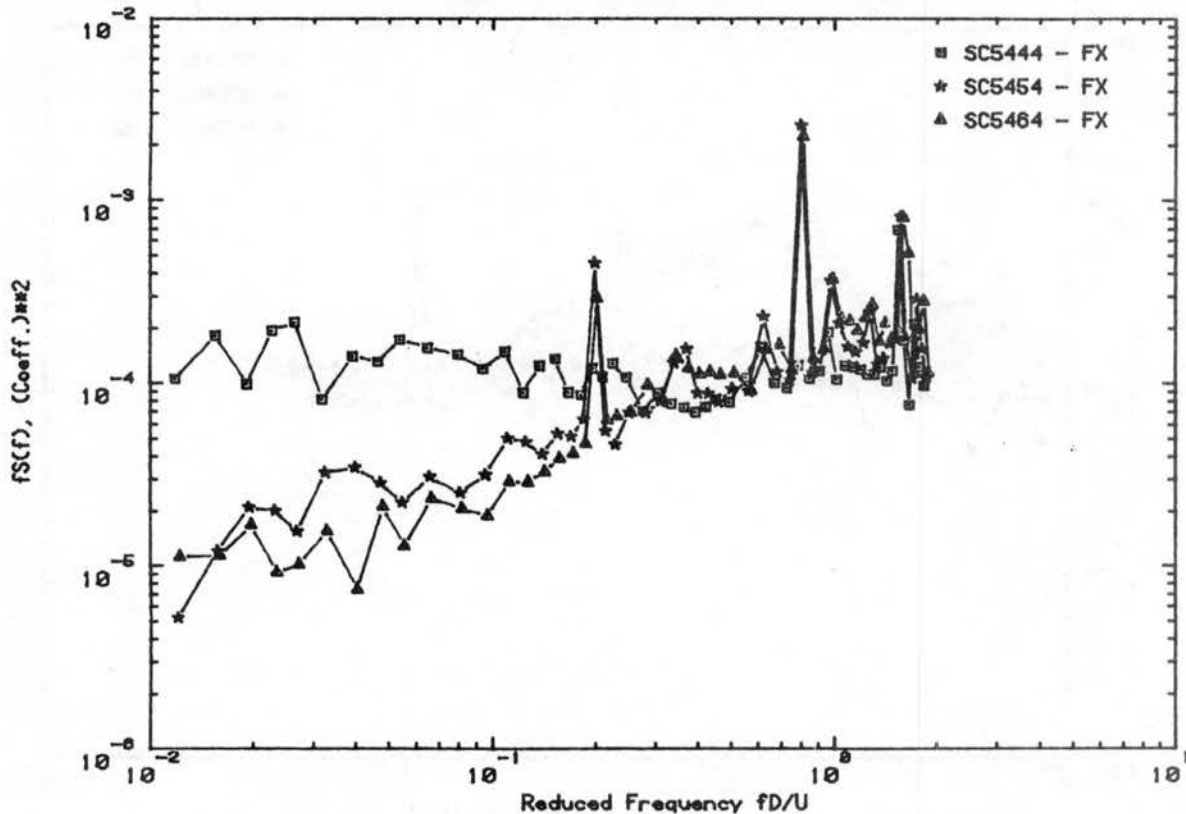
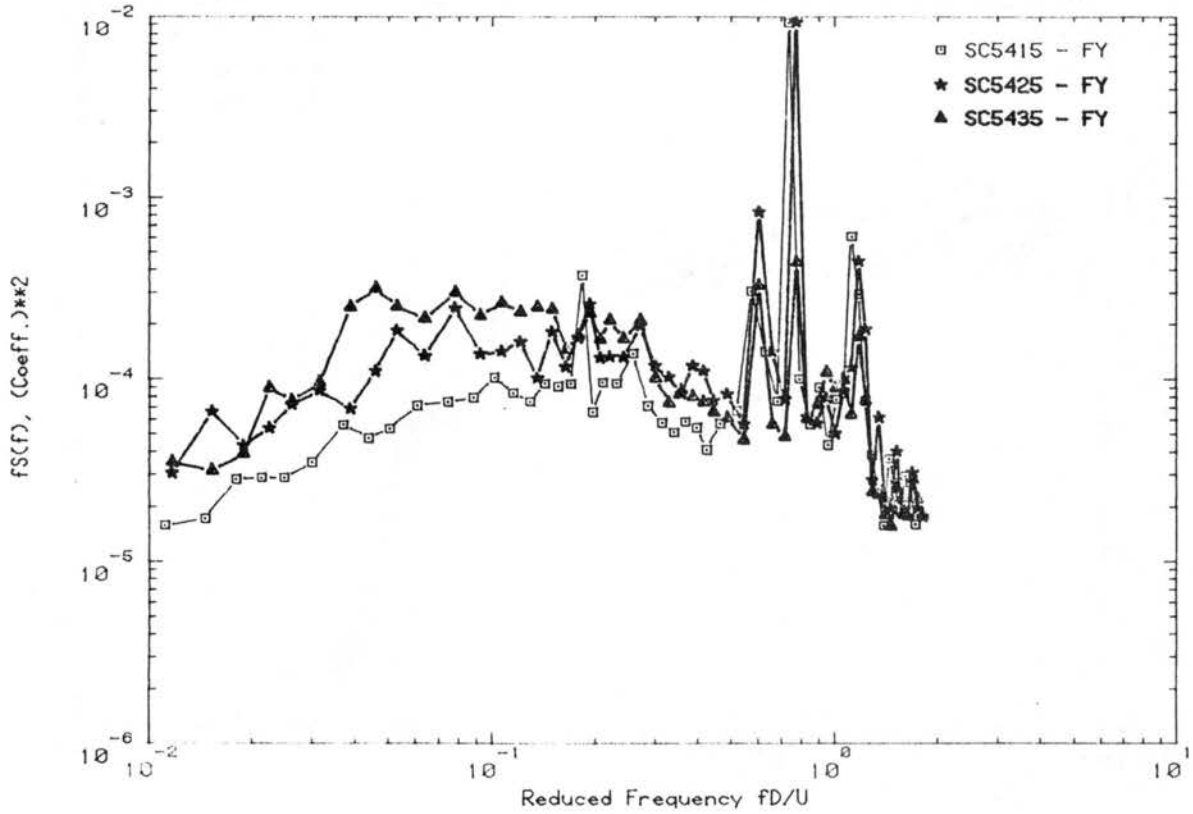


Figure C.3c. Load Spectra for Declination Angle 0°, Hour Angle 60°

RUN NO.541 WIND DIRECTION 60 Deg. VEL. U = 26.3 fps



RUN NO.544 WIND DIRECTION 220 Deg. VEL. U = 24.7 fps

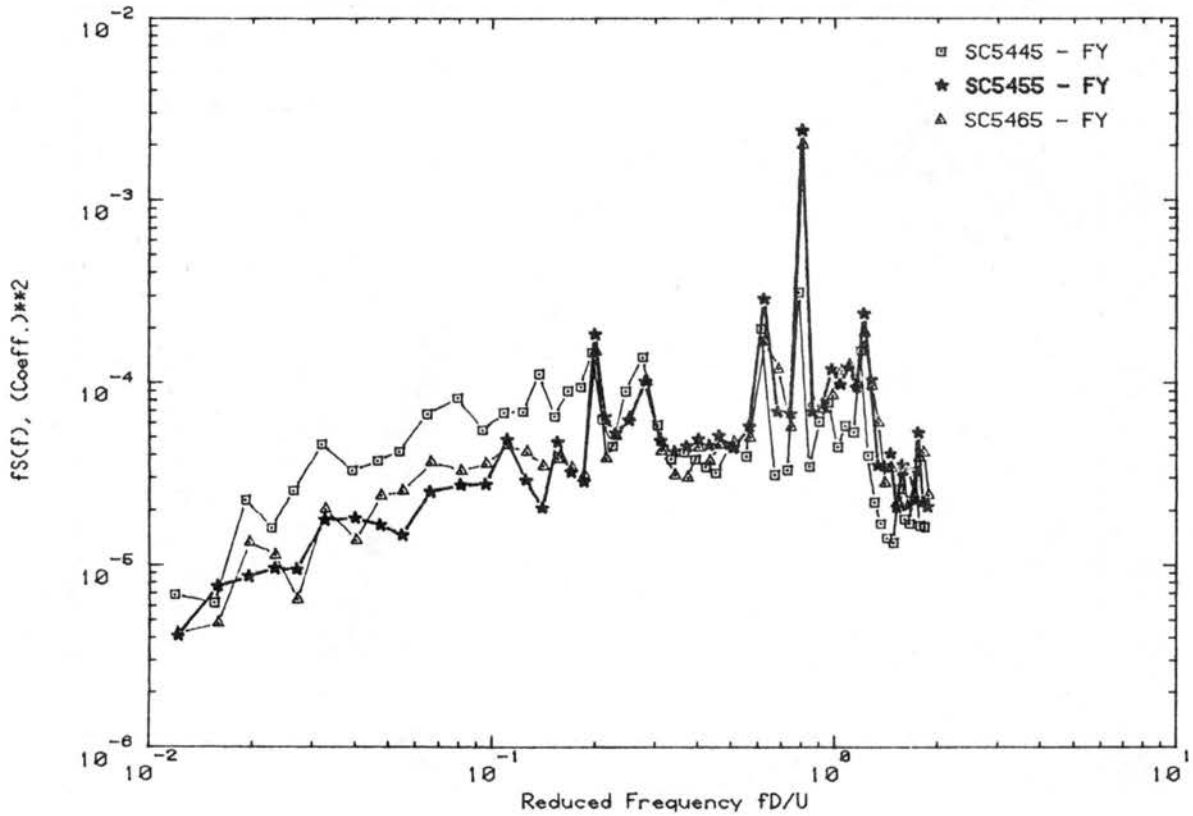
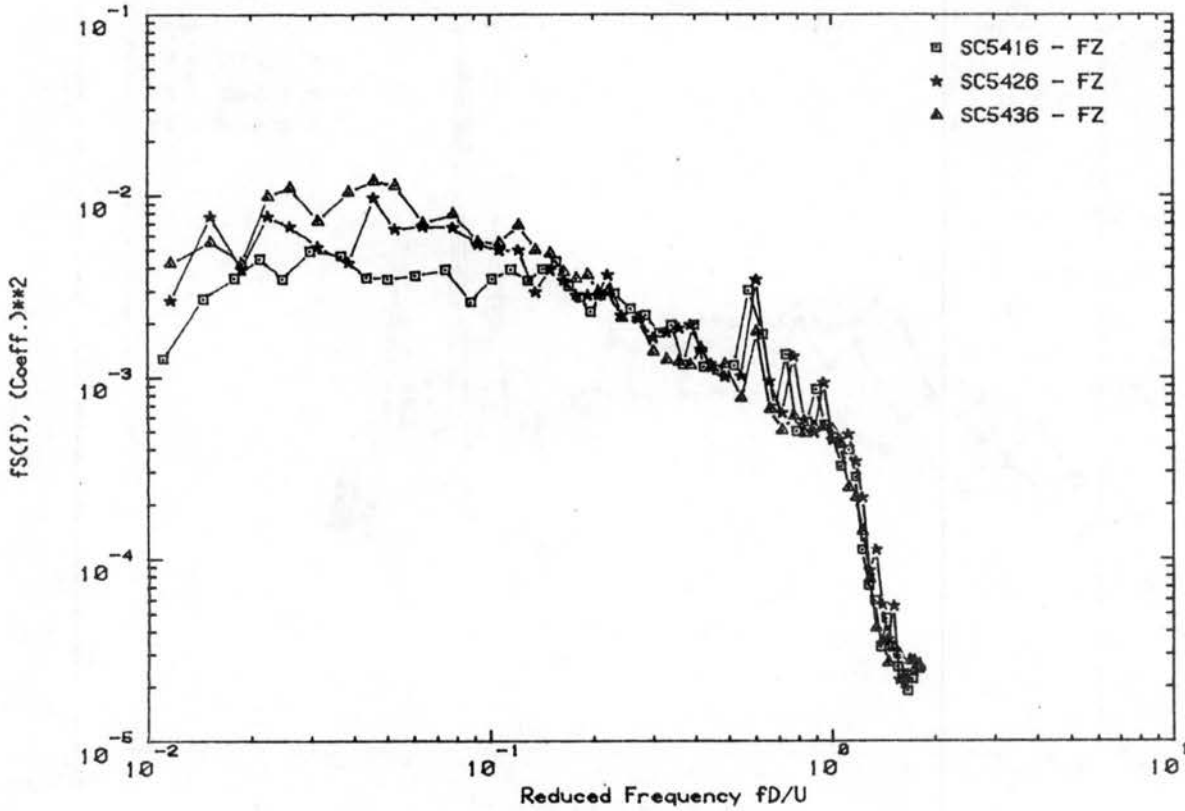


Figure C.3d. Load Spectra for Declination Angle 0°, Hour Angle 60°

RUN NO.541 WIND DIRECTION 60 Deg. VEL. U = 26.3 fps



RUN NO.544 WIND DIRECTION 220 Deg. VEL. U = 24.7 fps

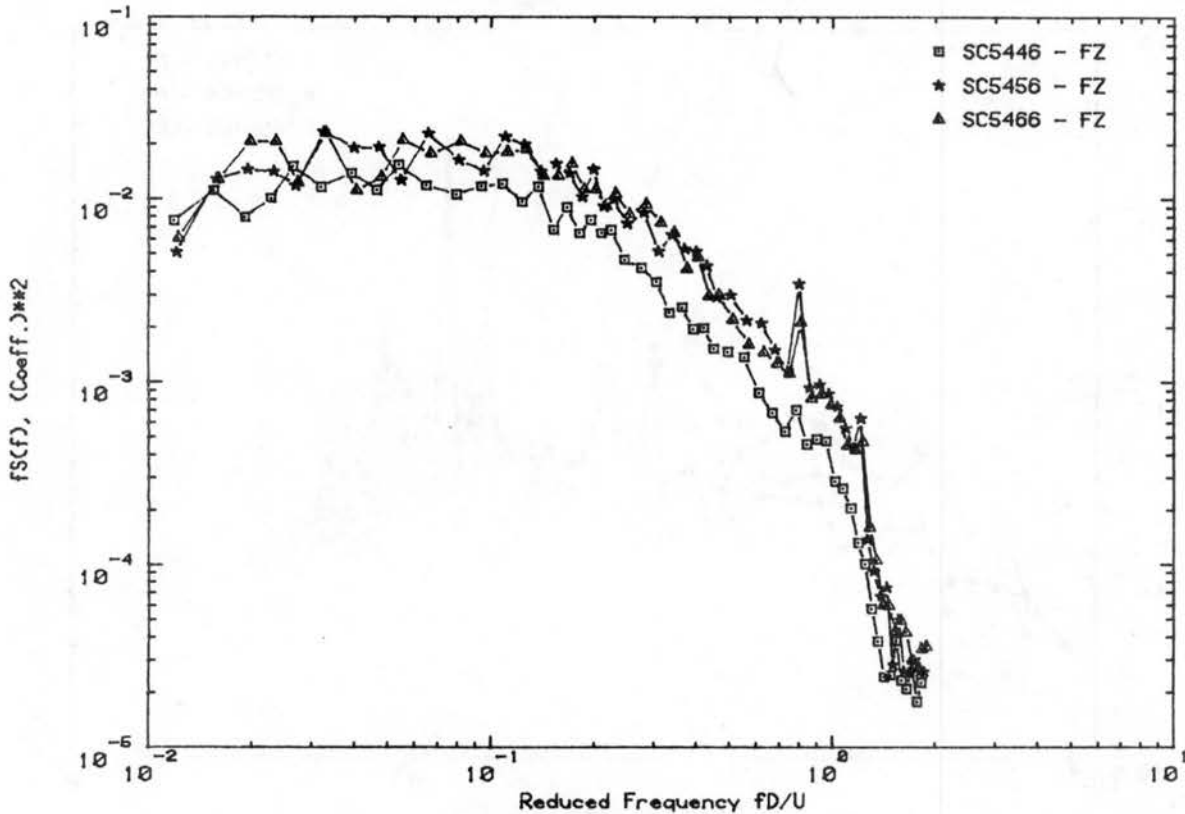


Figure C.3e. Load Spectra for Declination Angle 0°, Hour Angle 60°

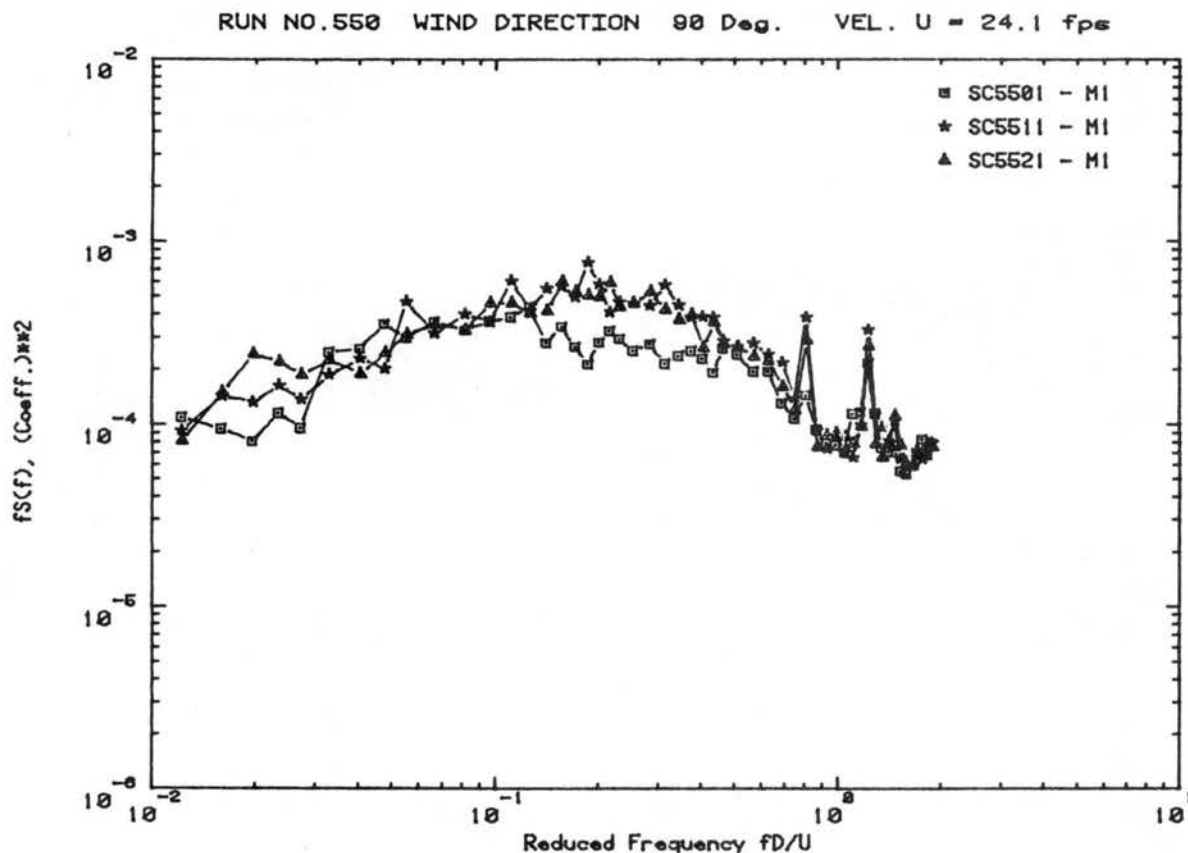
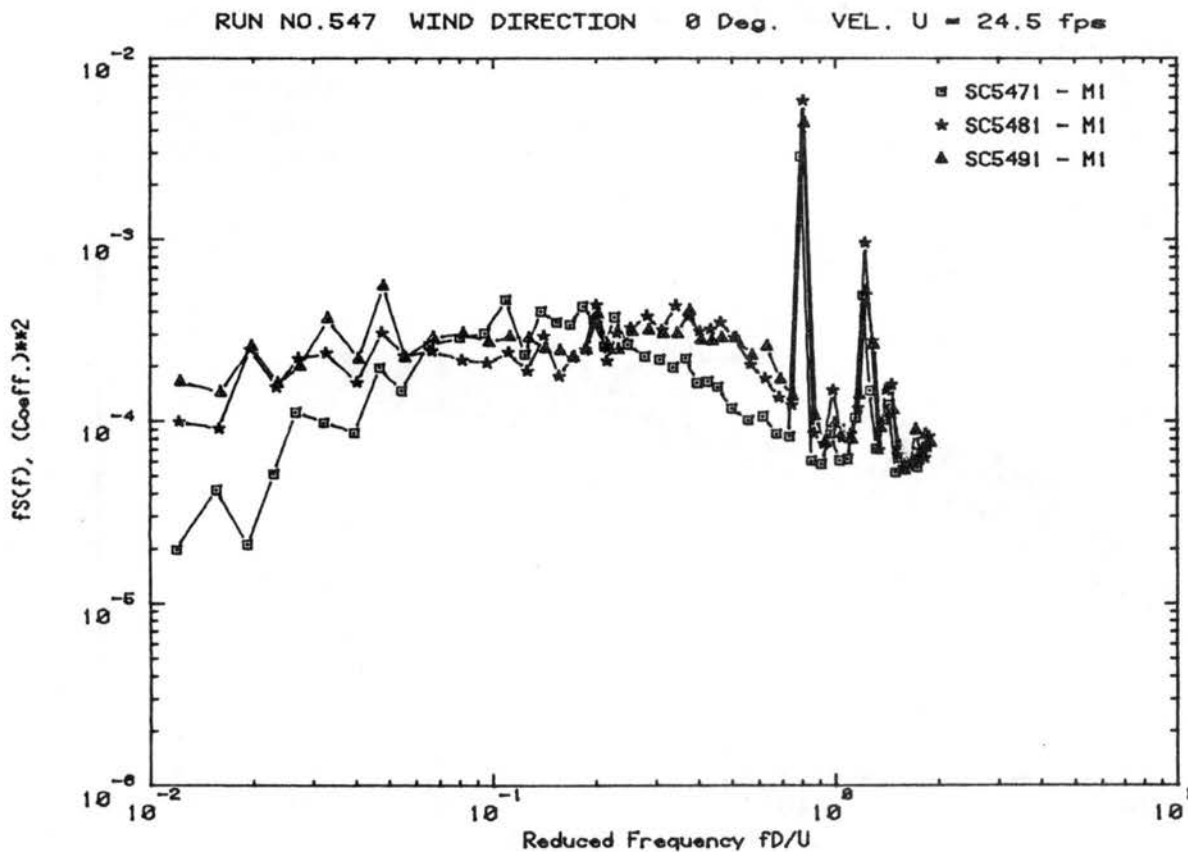
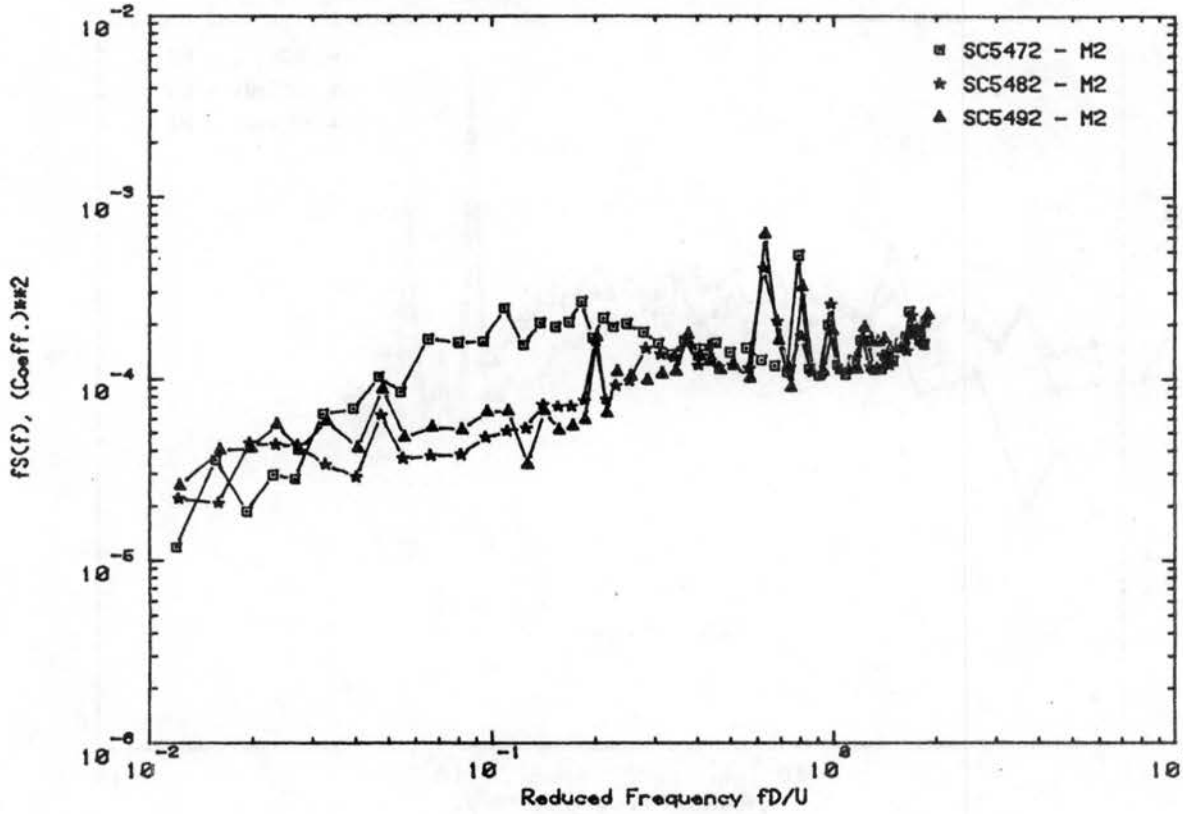


Figure C.4a. Load Spectra for Declination Angle 0°, Hour Angle 45°

RUN NO.547 WIND DIRECTION 0 Deg. VEL. U = 24.5 fps



RUN NO.550 WIND DIRECTION 90 Deg. VEL. U = 24.1 fps

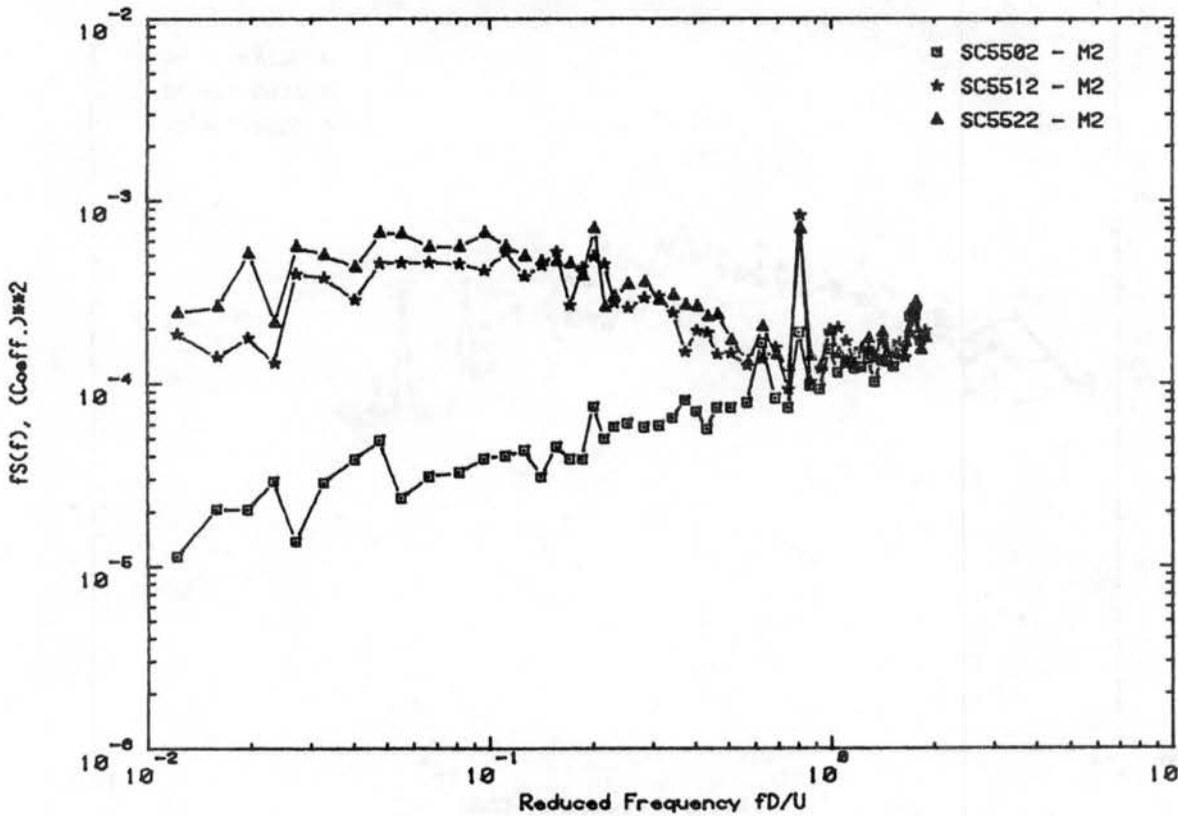


Figure C.4b. Load Spectra for Declination Angle 0°, Hour Angle 45°

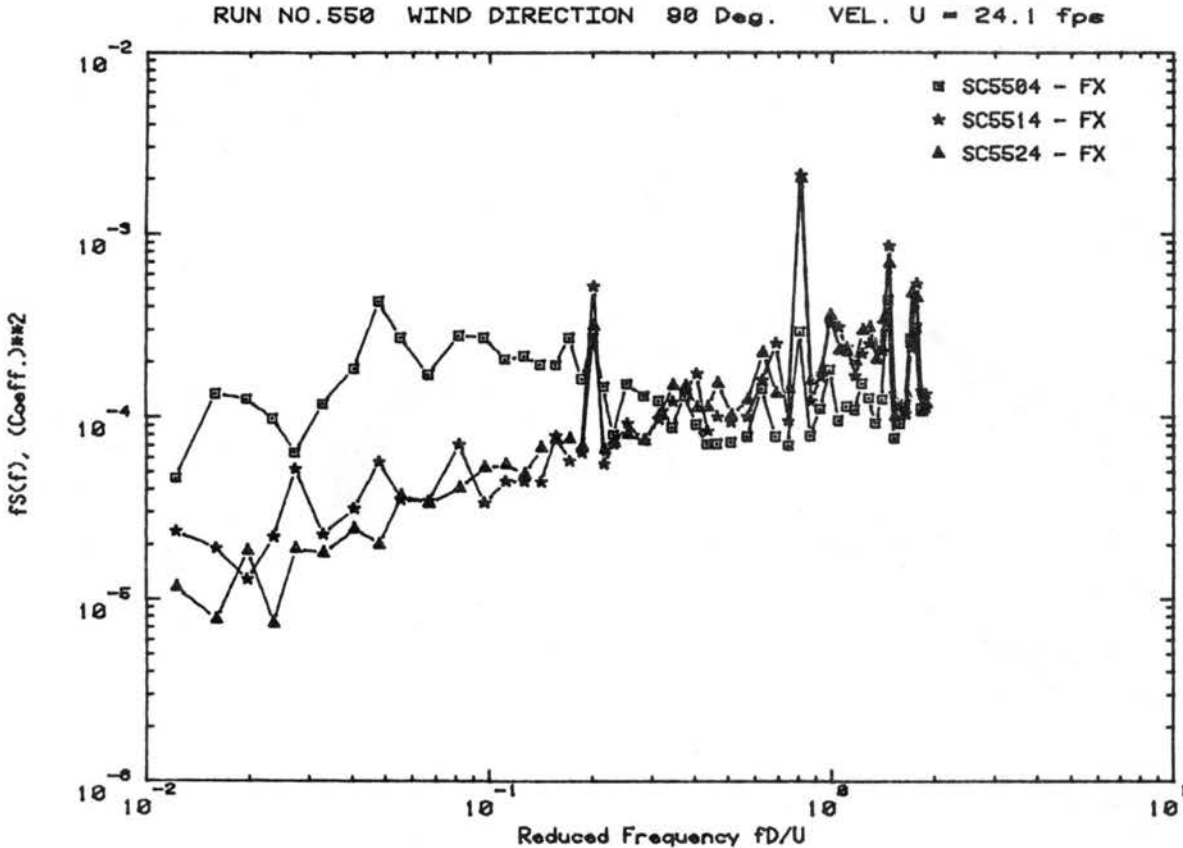
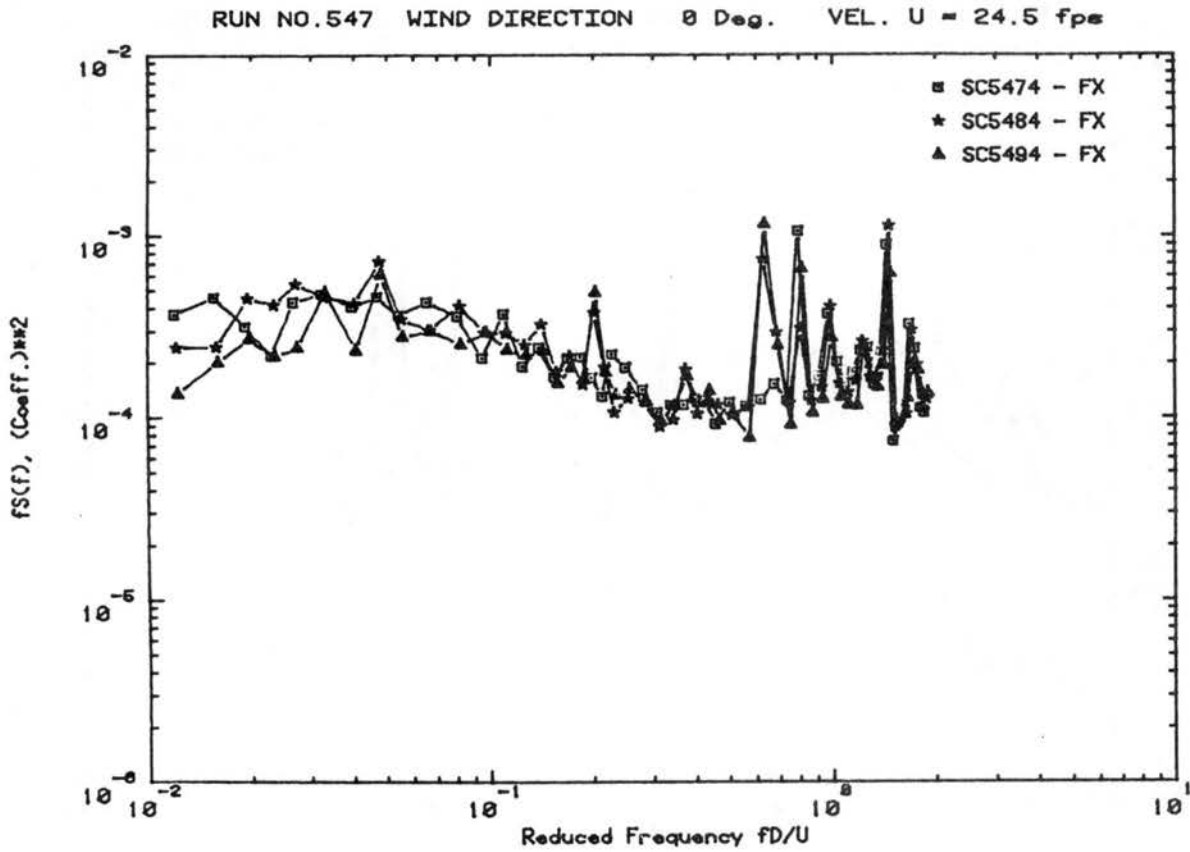
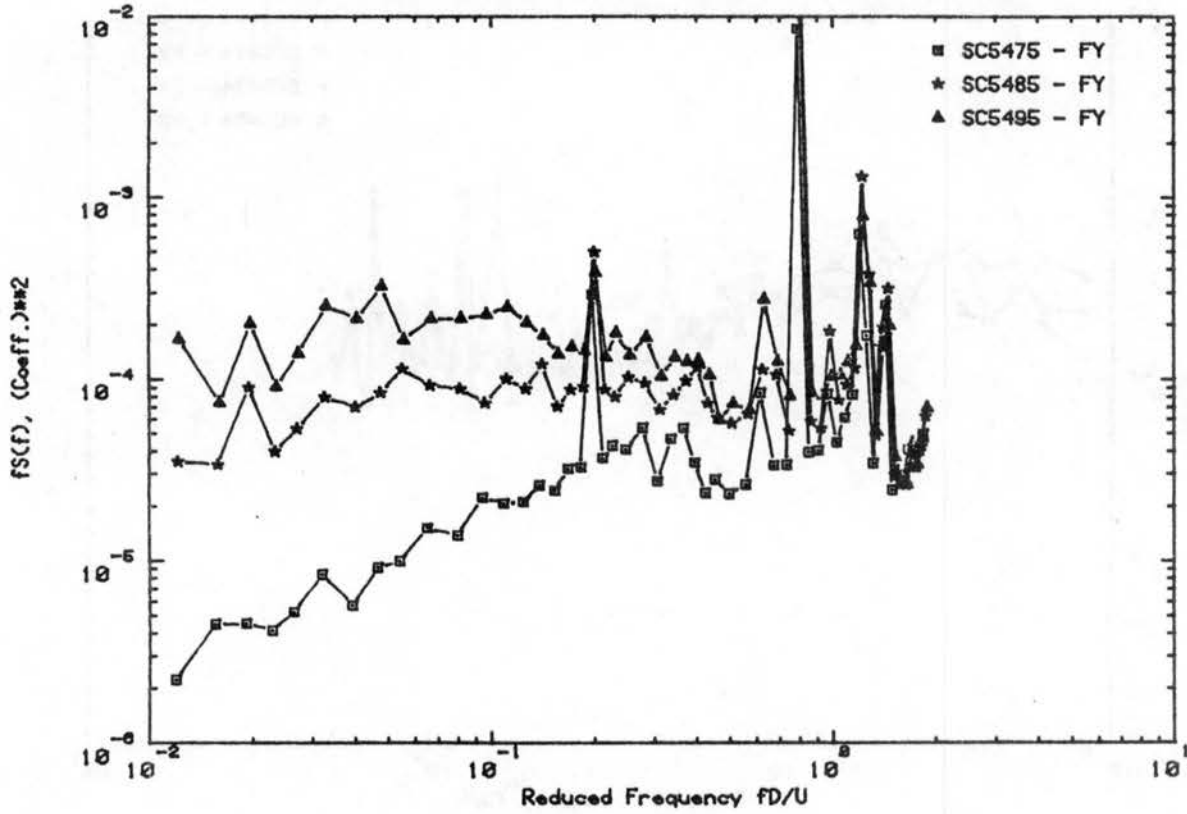


Figure C.4c. Load Spectra for Declination Angle 0° , Hour Angle 45°

RUN NO.547 WIND DIRECTION 0 Deg. VEL. U = 24.5 fps



RUN NO.550 WIND DIRECTION 90 Deg. VEL. U = 24.1 fps

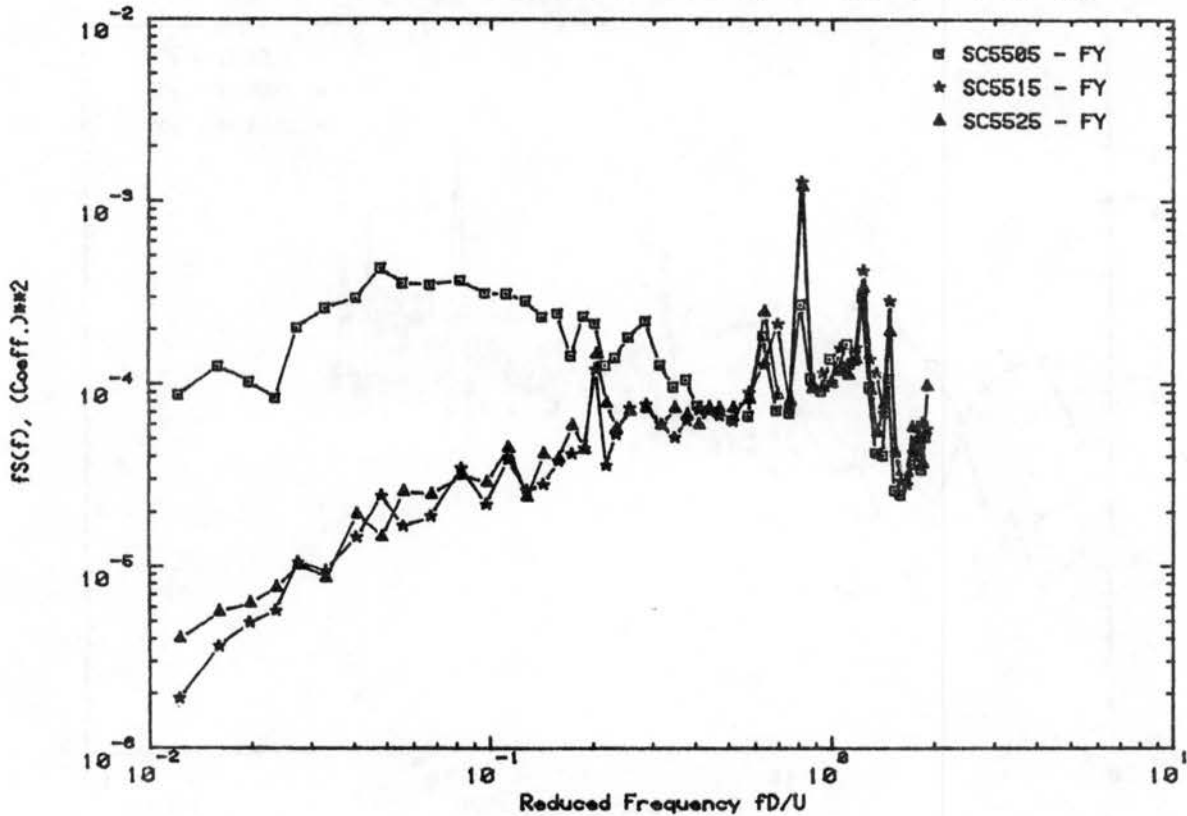
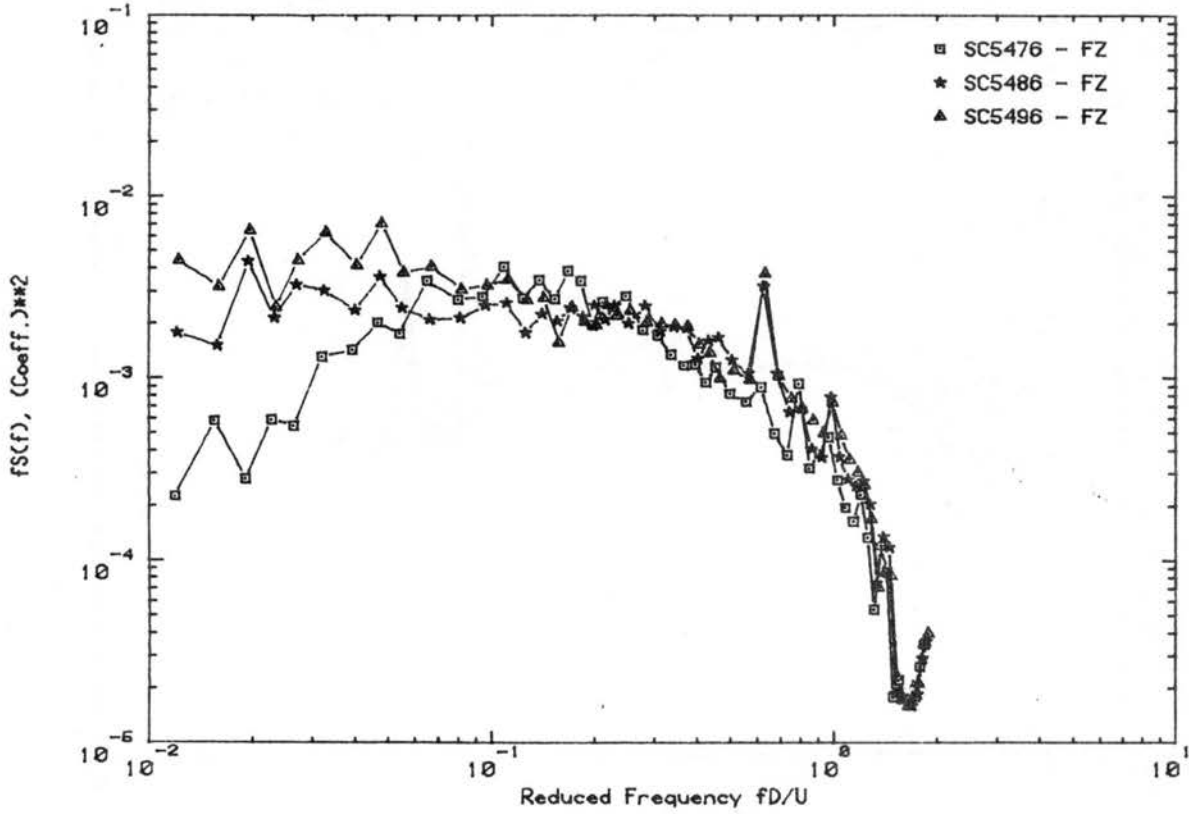


Figure C.4d. Load Spectra for Declination Angle 0°, Hour Angle 45°

RUN NO.547 WIND DIRECTION 0 Deg. VEL. U = 24.5 fps



RUN NO.550 WIND DIRECTION 90 Deg. VEL. U = 24.1 fps

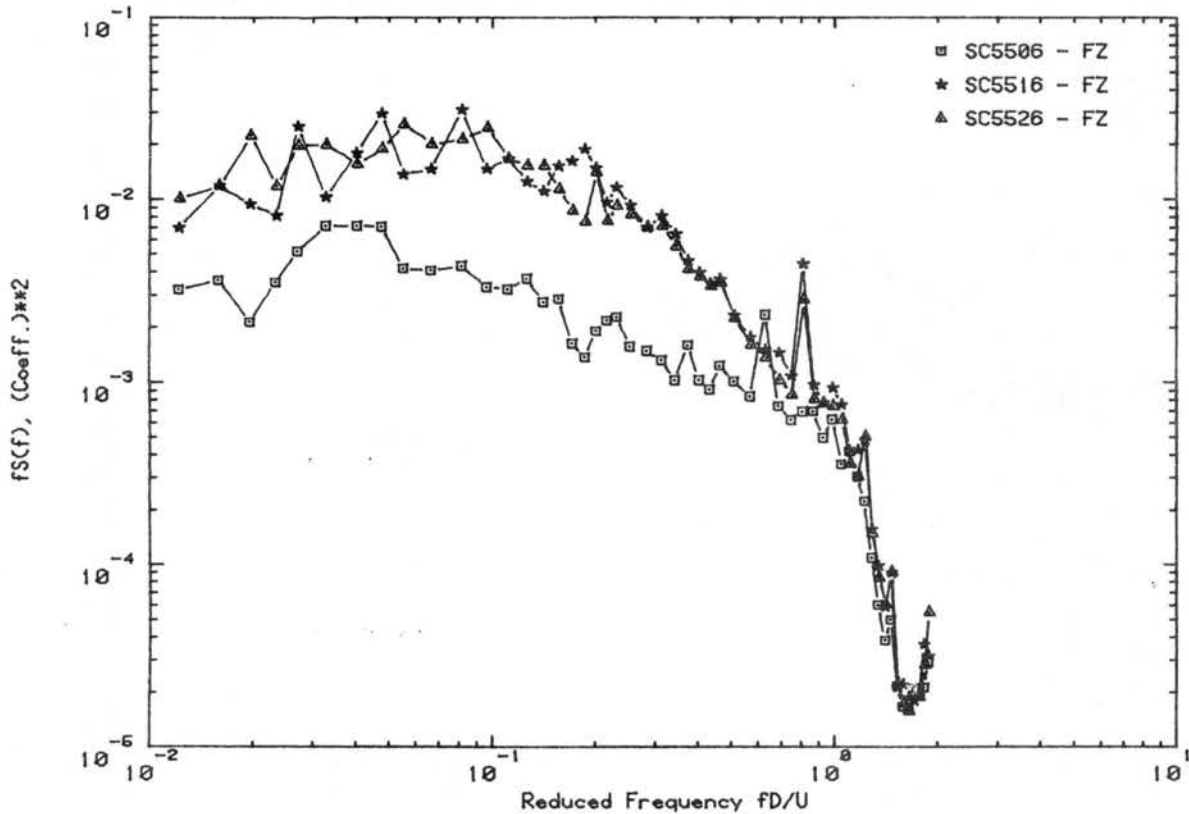
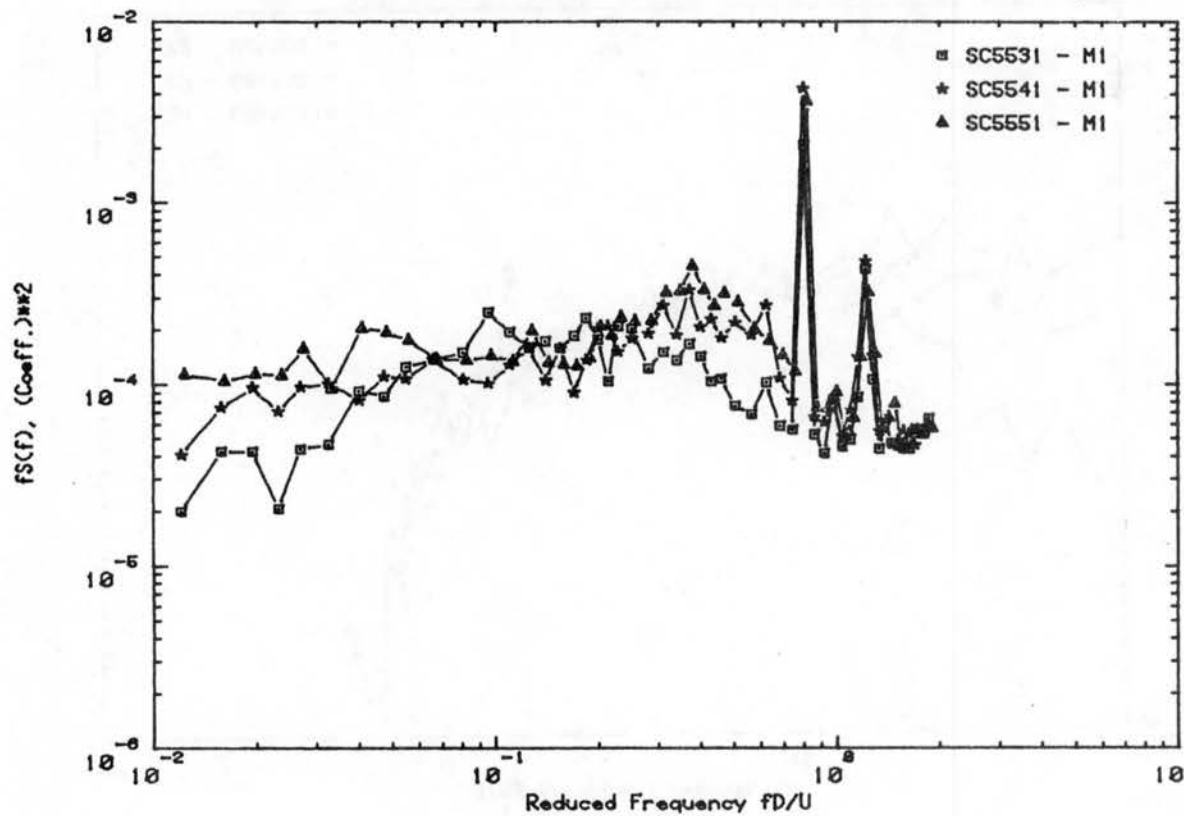


Figure C.4e. Load Spectra for Declination Angle 0°, Hour Angle 45°

RUN NO.553 WIND DIRECTION 0 Deg. VEL. U = 24.2 fps



RUN NO.556 WIND DIRECTION 90 Deg. VEL. U = 24.1 fps

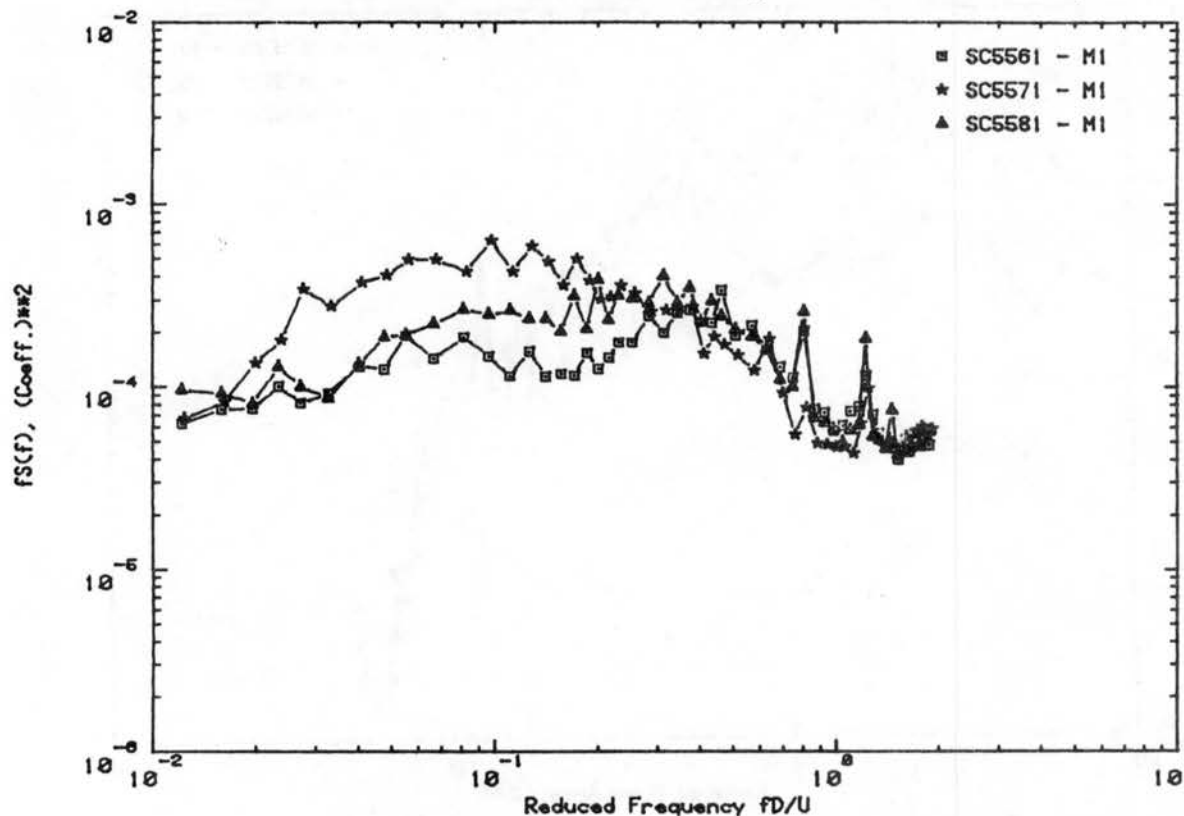
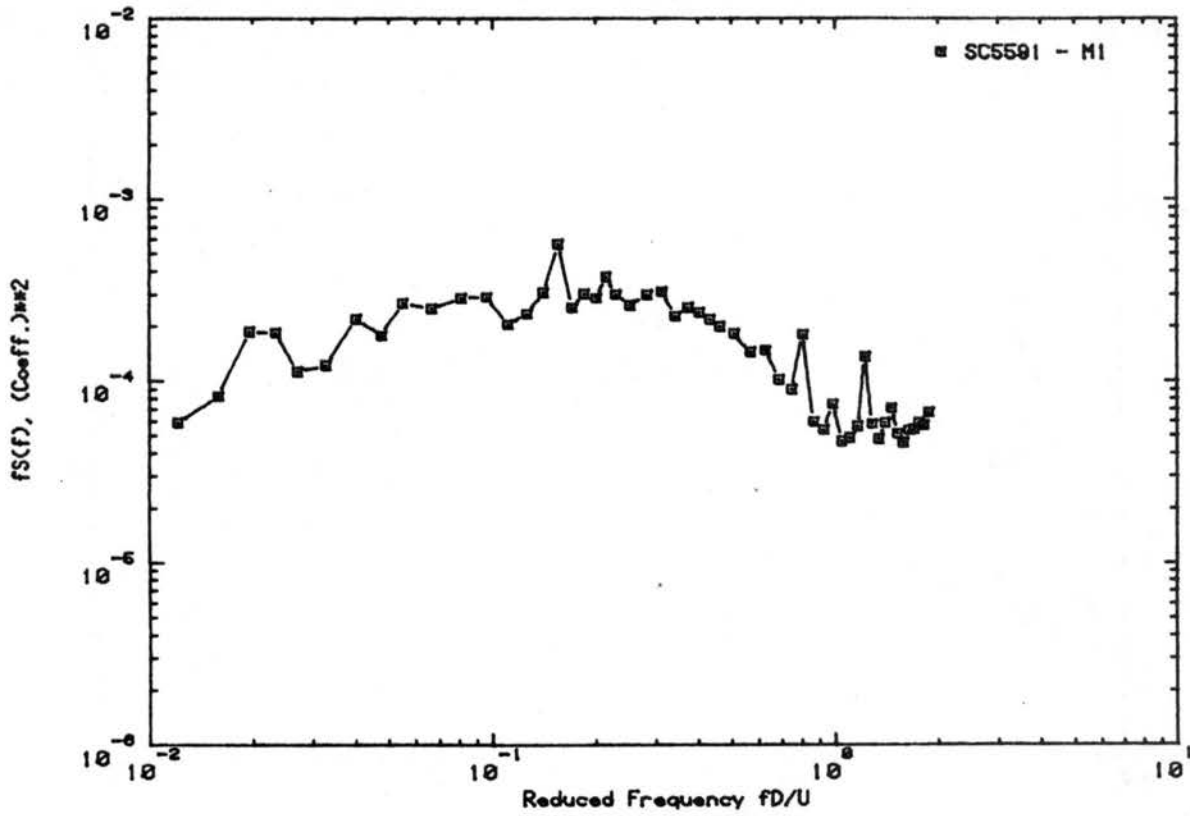


Figure C.5a. Load Spectra for Declination Angle 0°, Hour Angle 30°

RUN NO.550 WIND DIRECTION 290 Deg. VEL. U = 24.1 fps



RUN NO.553 WIND DIRECTION 0 Deg. VEL. U = 24.2 fps

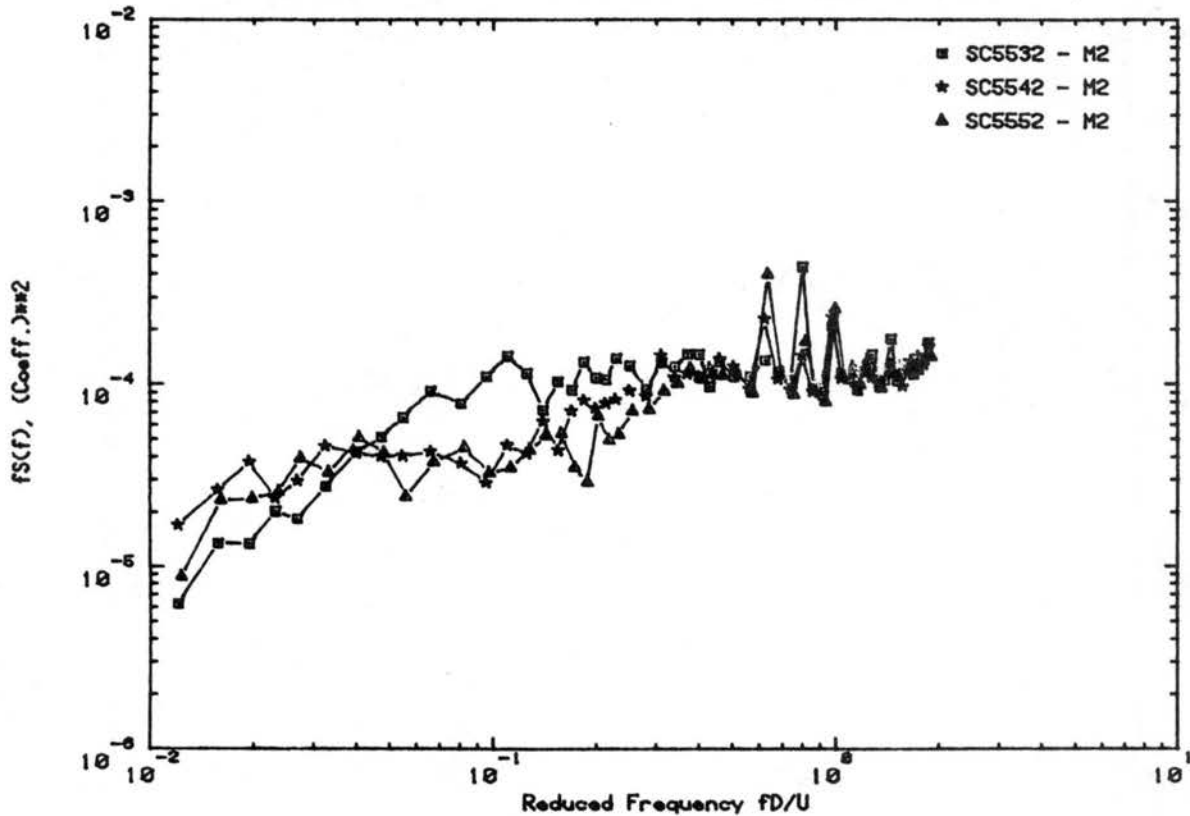
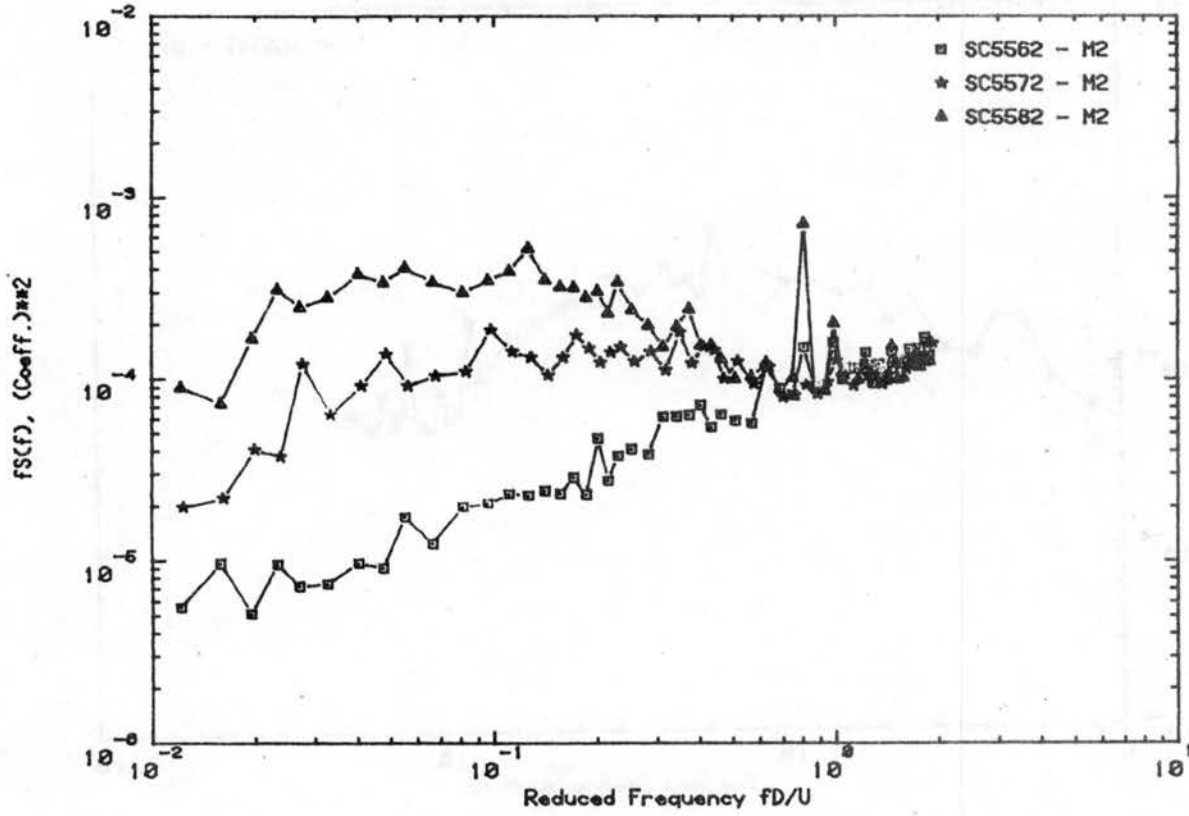


Figure C.5b. Load Spectra for Declination Angle 0°, Hour Angle 30°

RUN NO.556 WIND DIRECTION 90 Deg. VEL. U = 24.1 fps



RUN NO.559 WIND DIRECTION 290 Deg. VEL. U = 24.1 fps

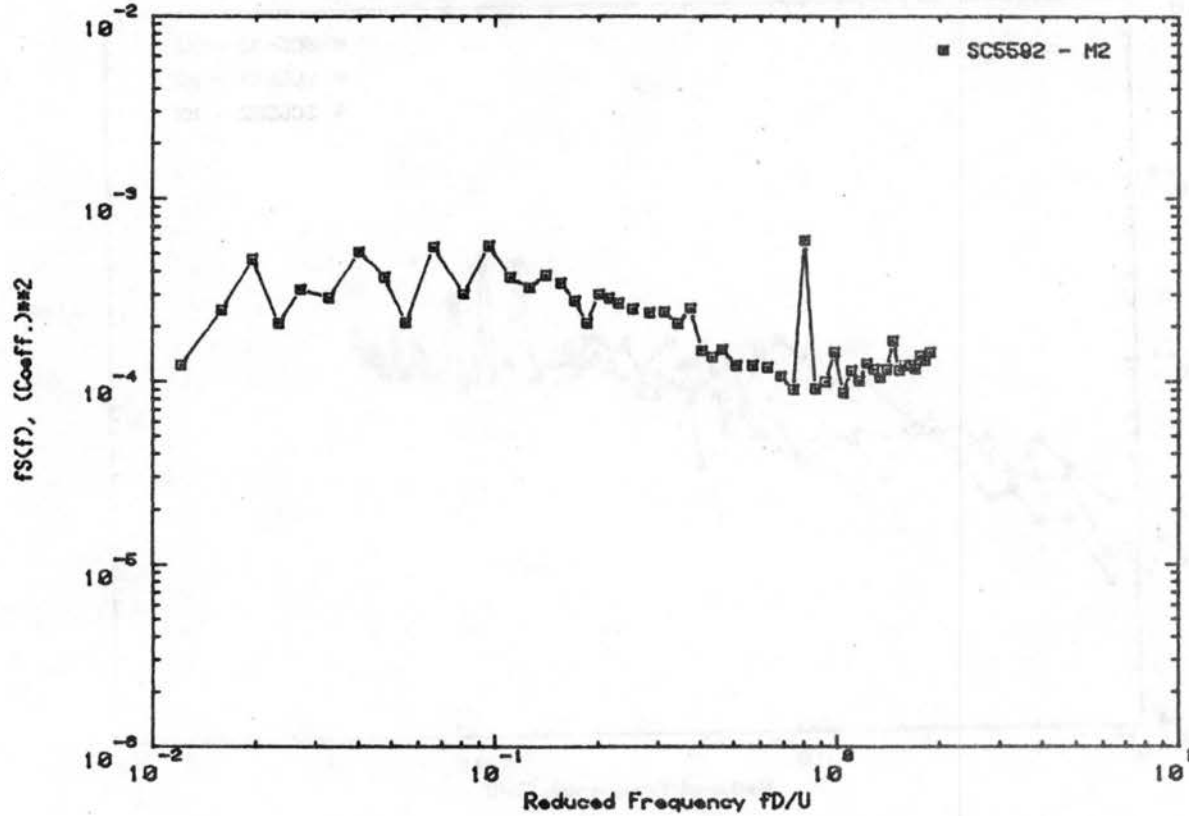
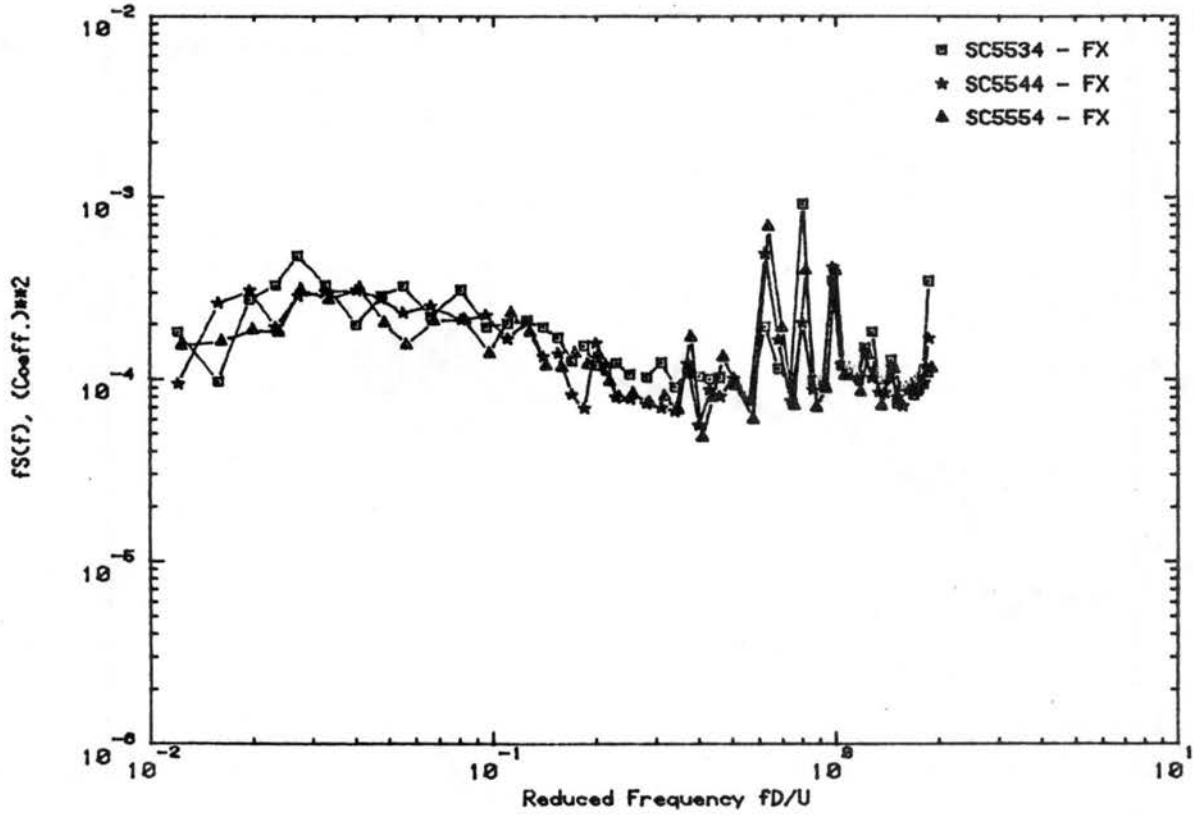


Figure C.5c. Load Spectra for Declination Angle 0°, Hour Angle 30°

RUN NO.553 WIND DIRECTION 0 Deg. VEL. U = 24.2 fps



RUN NO.556 WIND DIRECTION 90 Deg. VEL. U = 24.1 fps

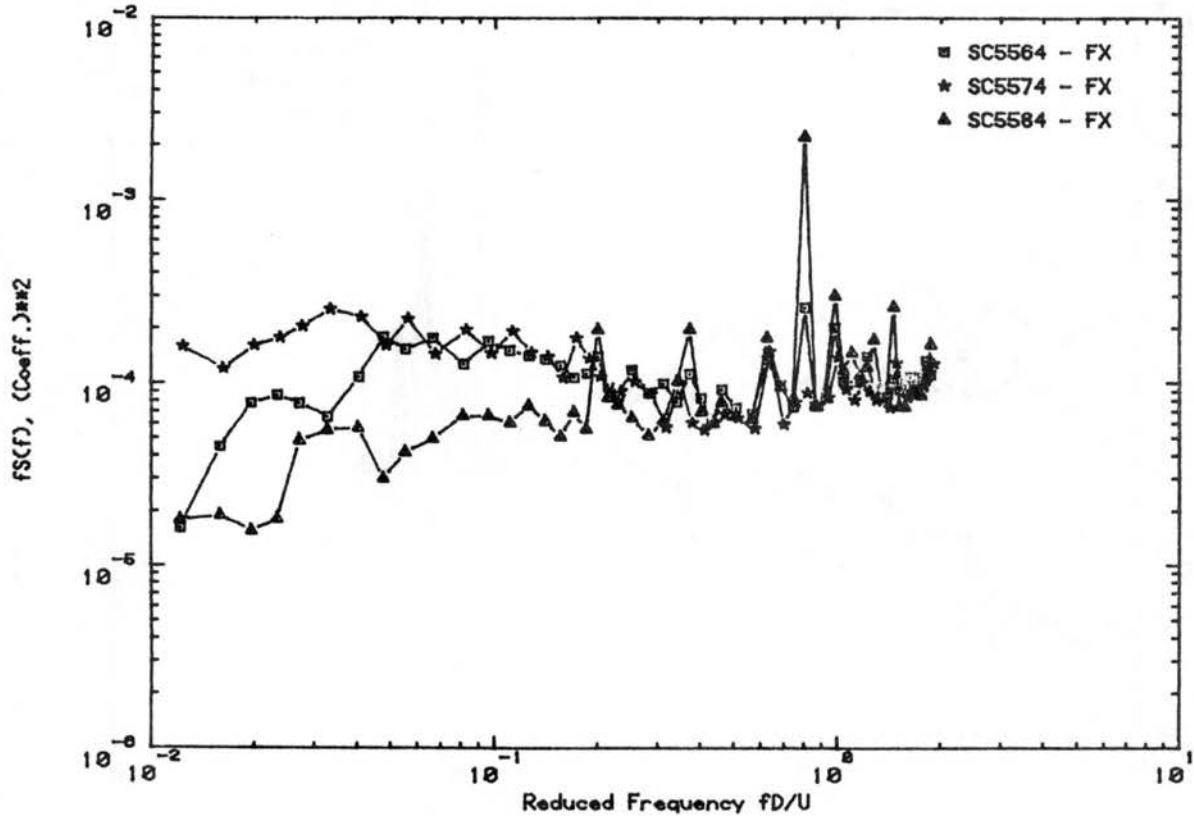
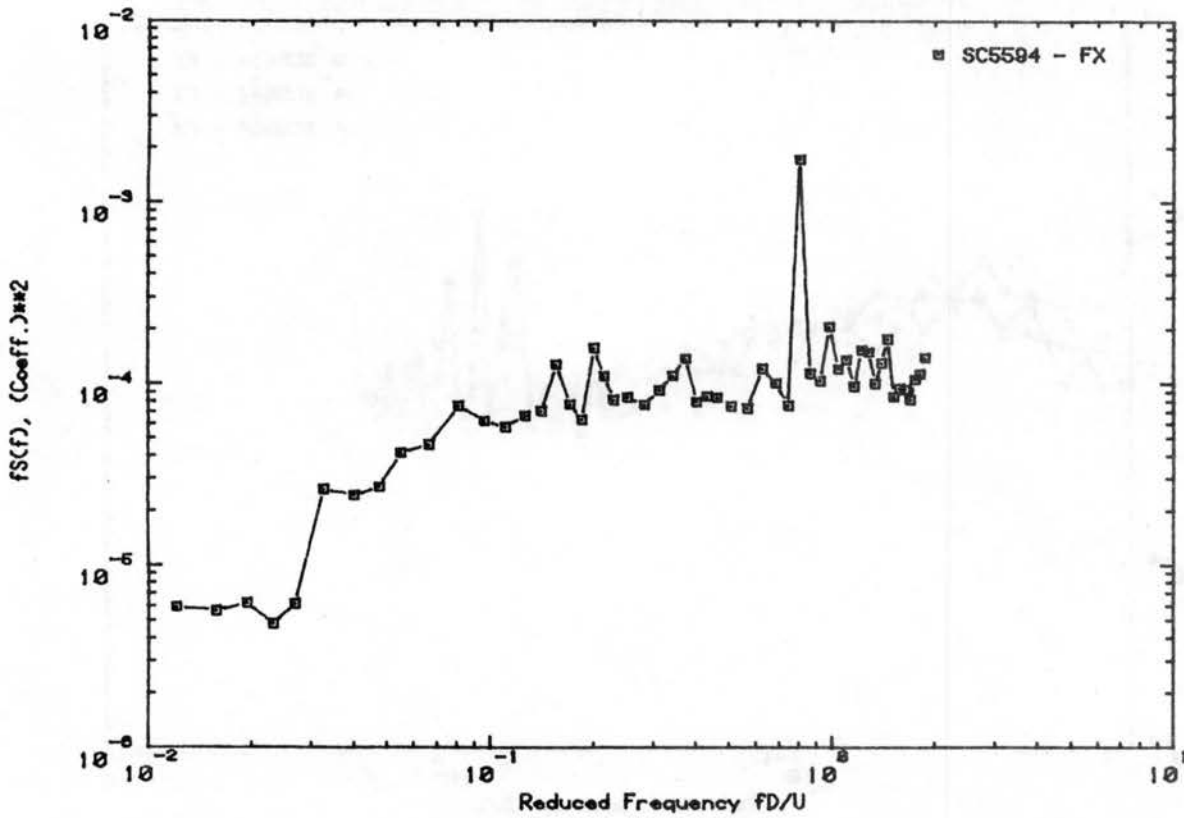


Figure C.5d. Load Spectra for Declination Angle 0°, Hour Angle 30°

RUN NO.559 WIND DIRECTION 290 Deg. VEL. U = 24.1 fps



RUN NO.553 WIND DIRECTION 0 Deg. VEL. U = 24.2 fps

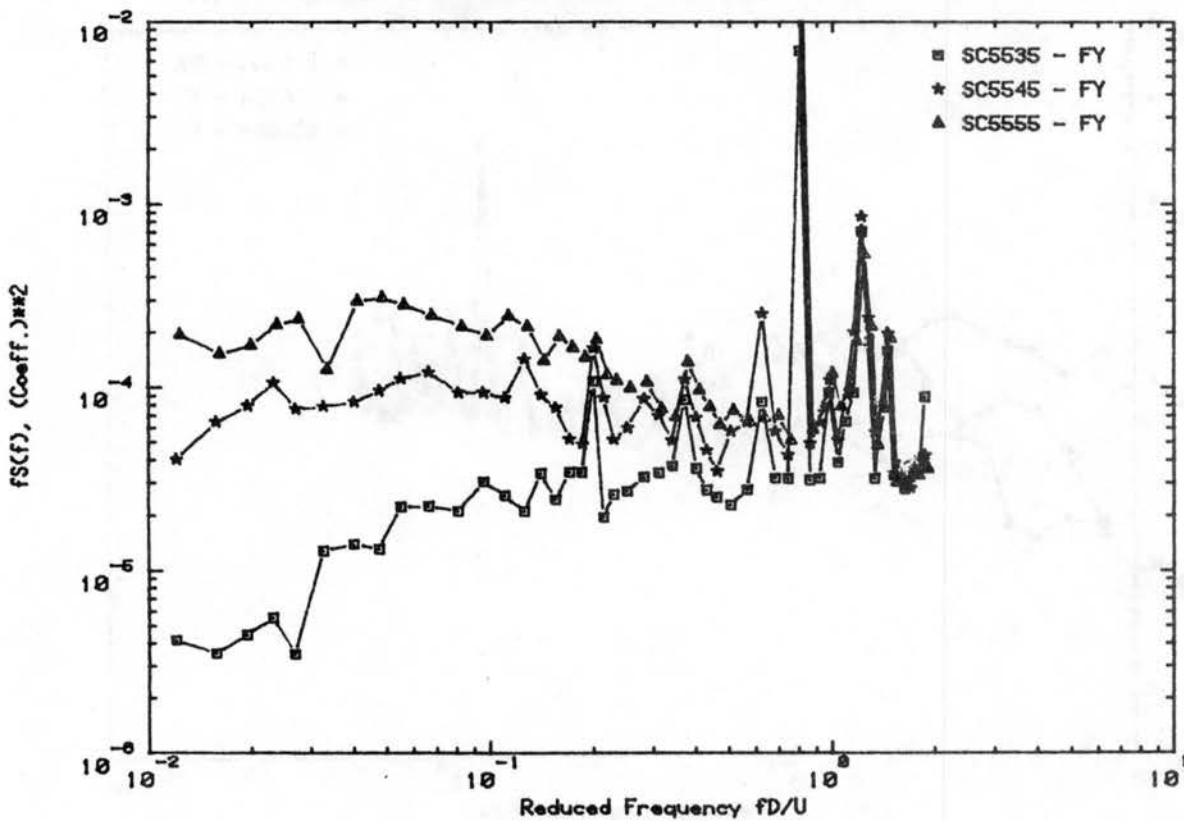


Figure C.5e. Load Spectra for Declination Angle 0°, Hour Angle 30°

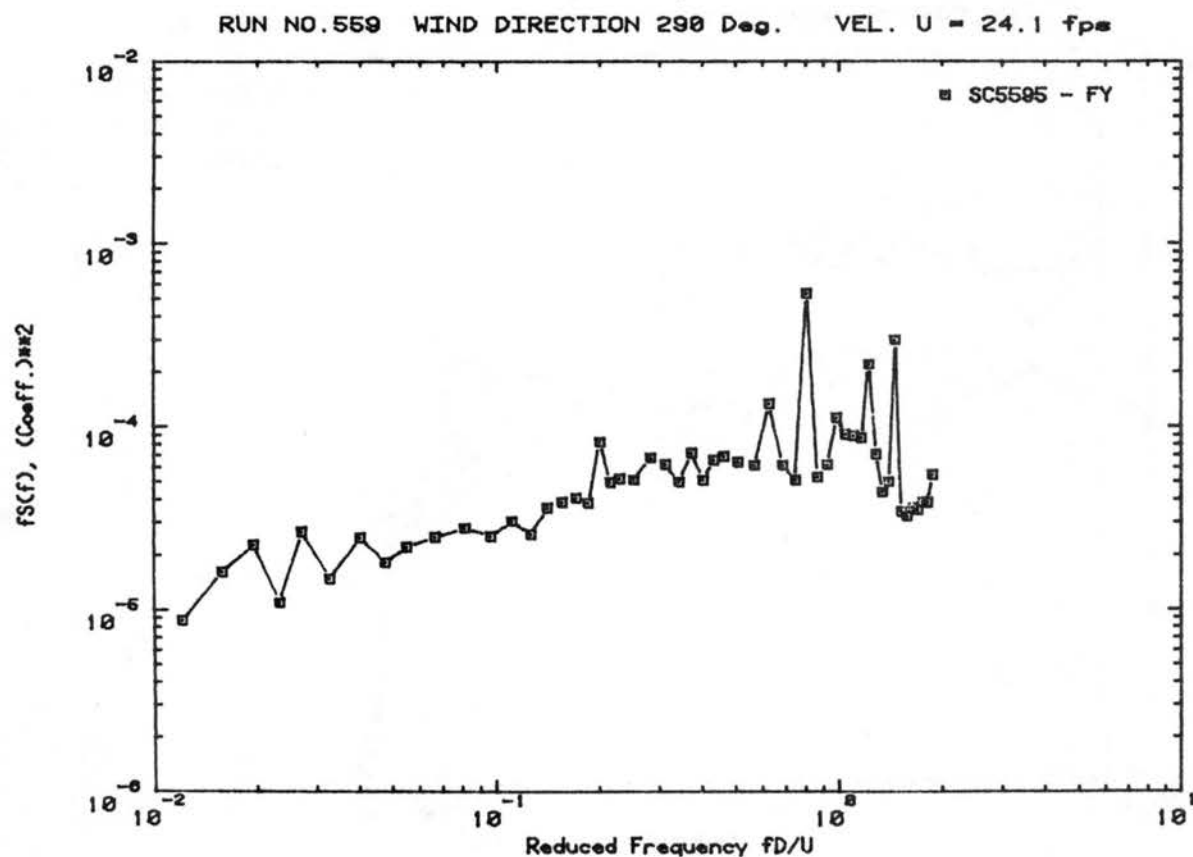
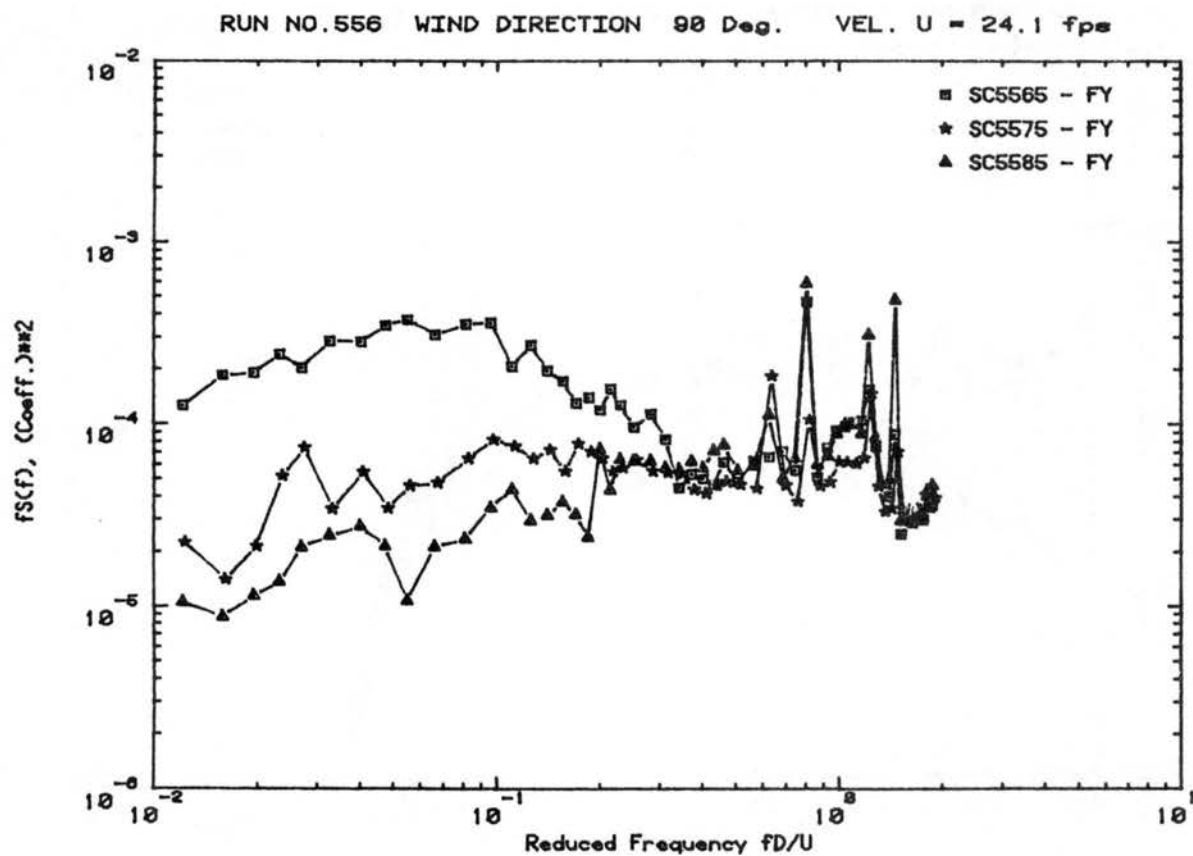
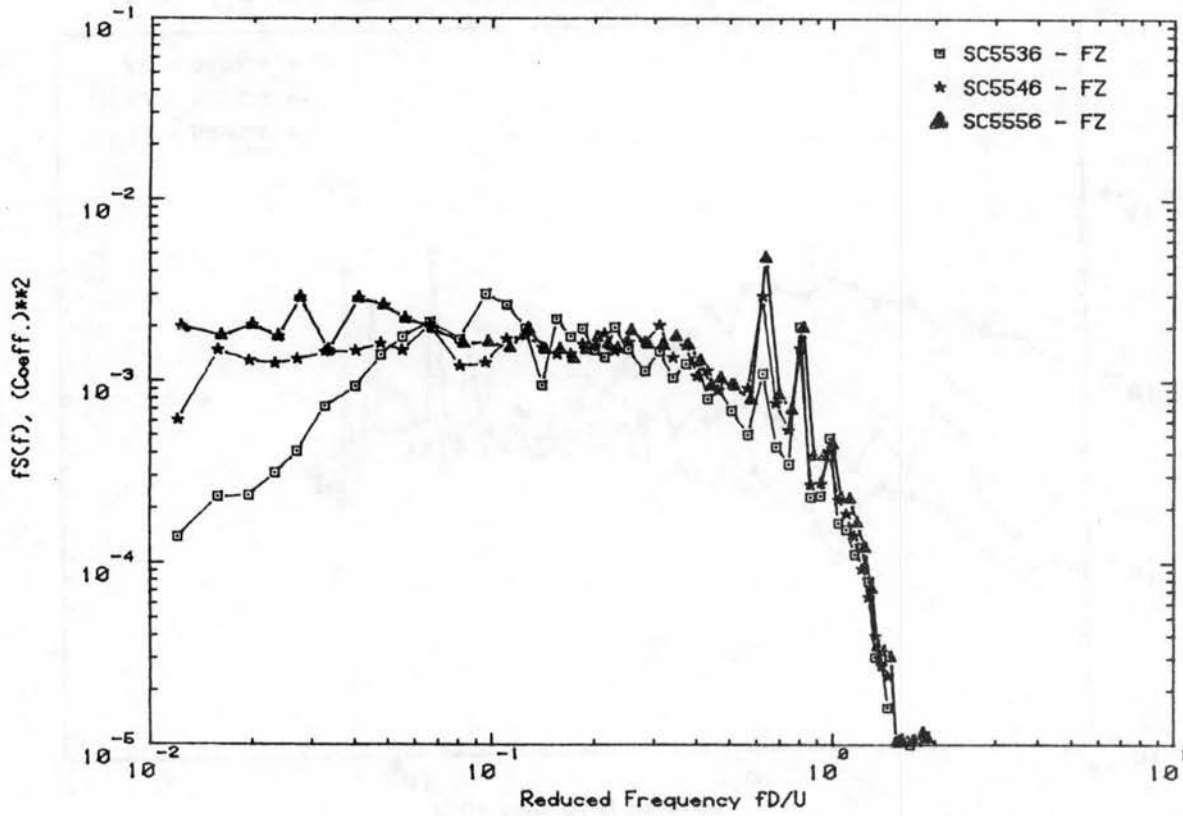


Figure C.5f. Load Spectra for Declination Angle 0° , Hour Angle 30°

RUN NO.553 WIND DIRECTION 0 Deg. VEL. U = 24.2 fps



RUN NO.556 WIND DIRECTION 90 Deg. VEL. U = 24.1 fps

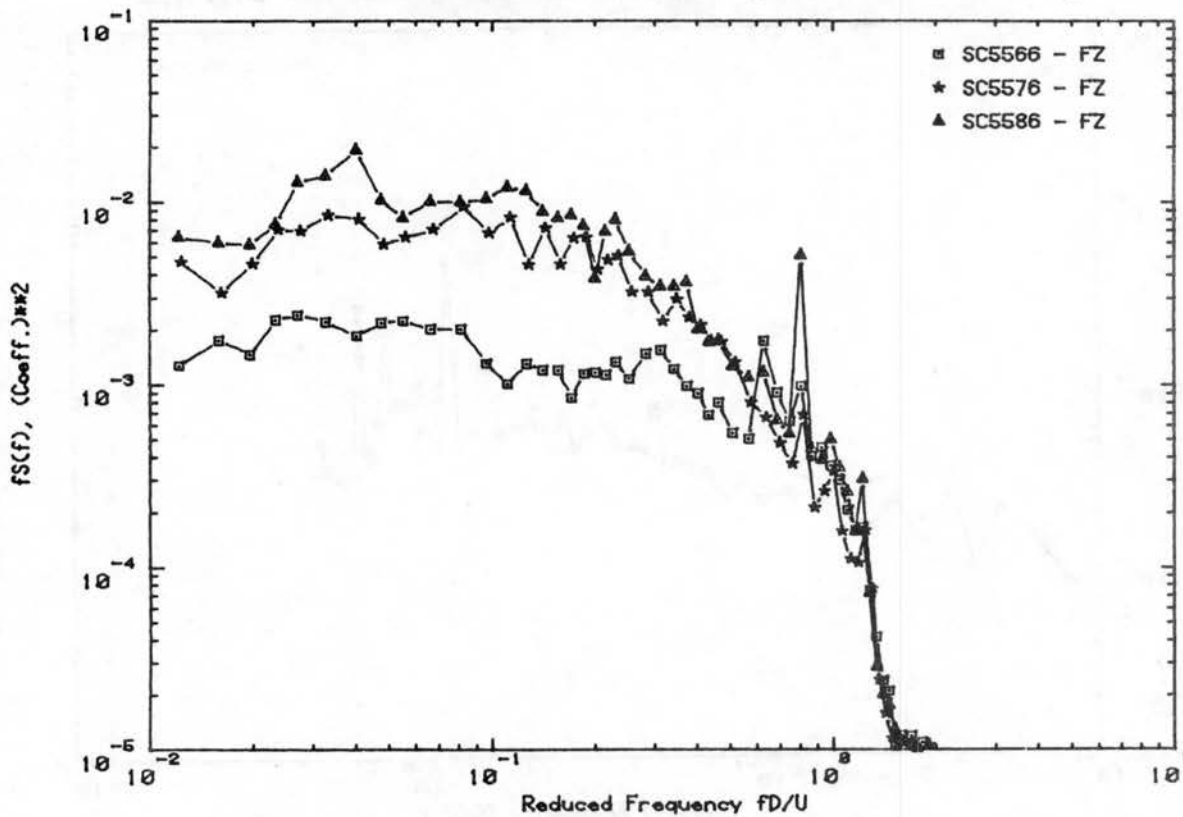


Figure C.5g. Load Spectra for Declination Angle 0°, Hour Angle 30°

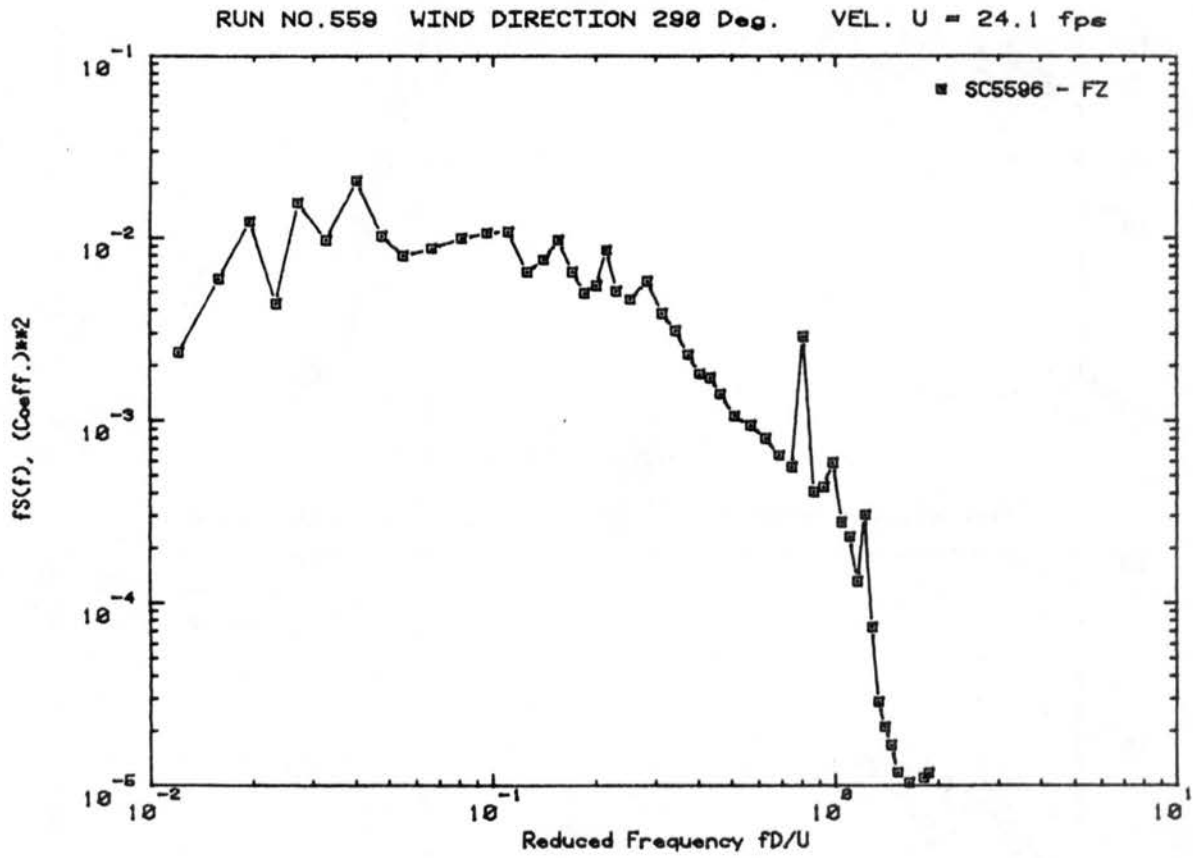
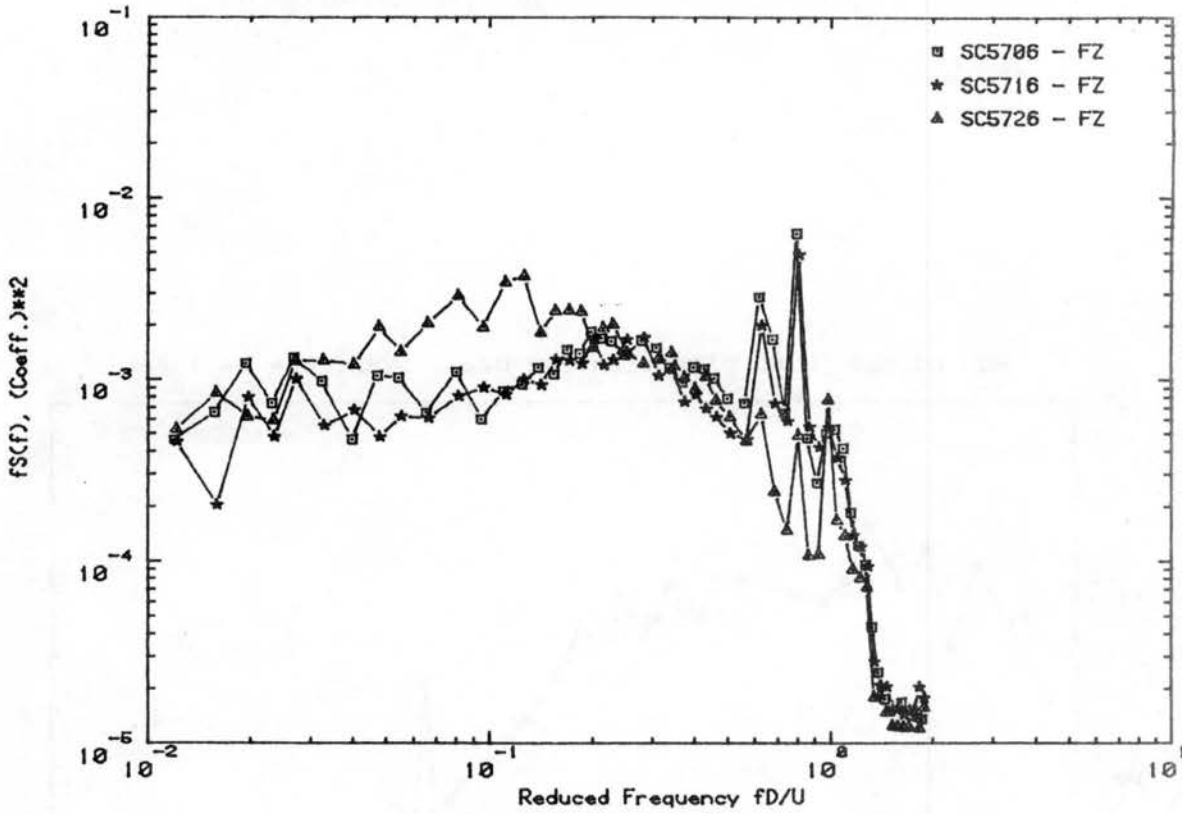


Figure C.5h. Load Spectra for Declination Angle 0° , Hour Angle 30°

RUN NO.570 WIND DIRECTION 60 Deg. VEL. U = 24.4 fps



RUN NO.573 WIND DIRECTION 270 Deg. VEL. U = 24.0 fps

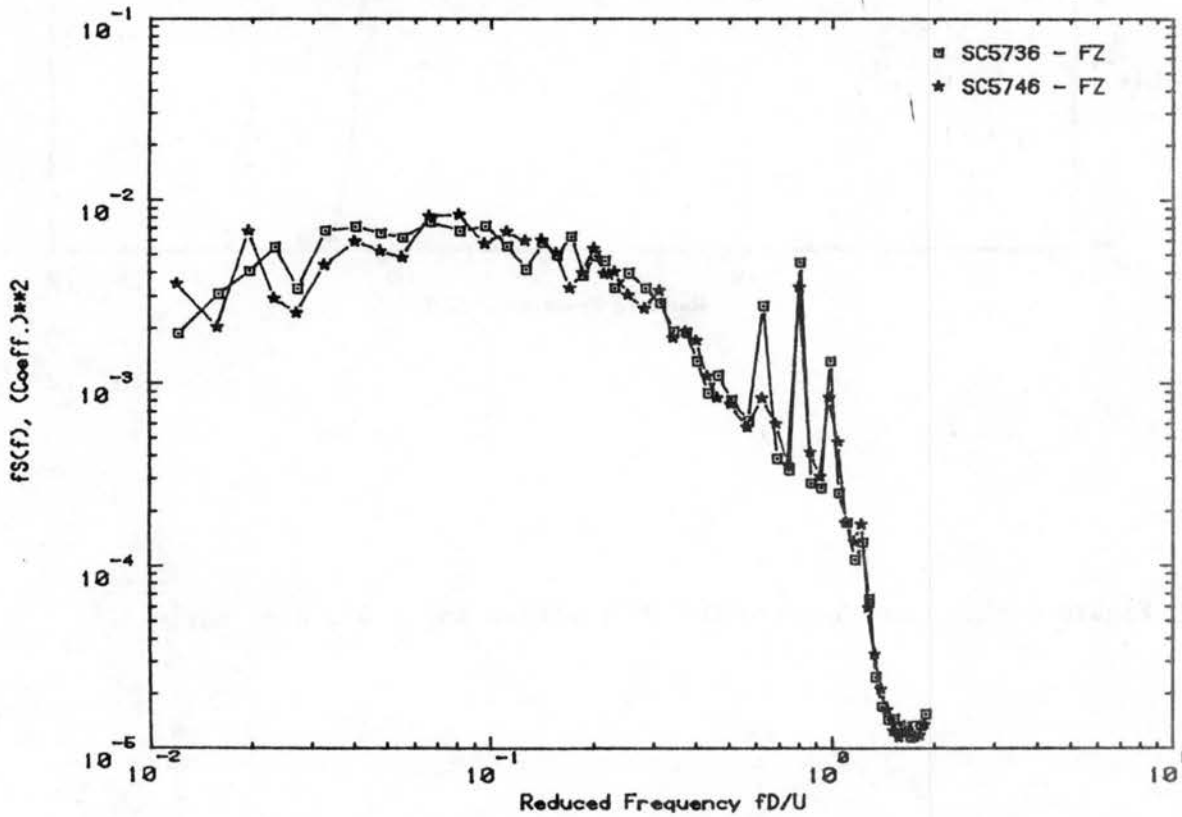
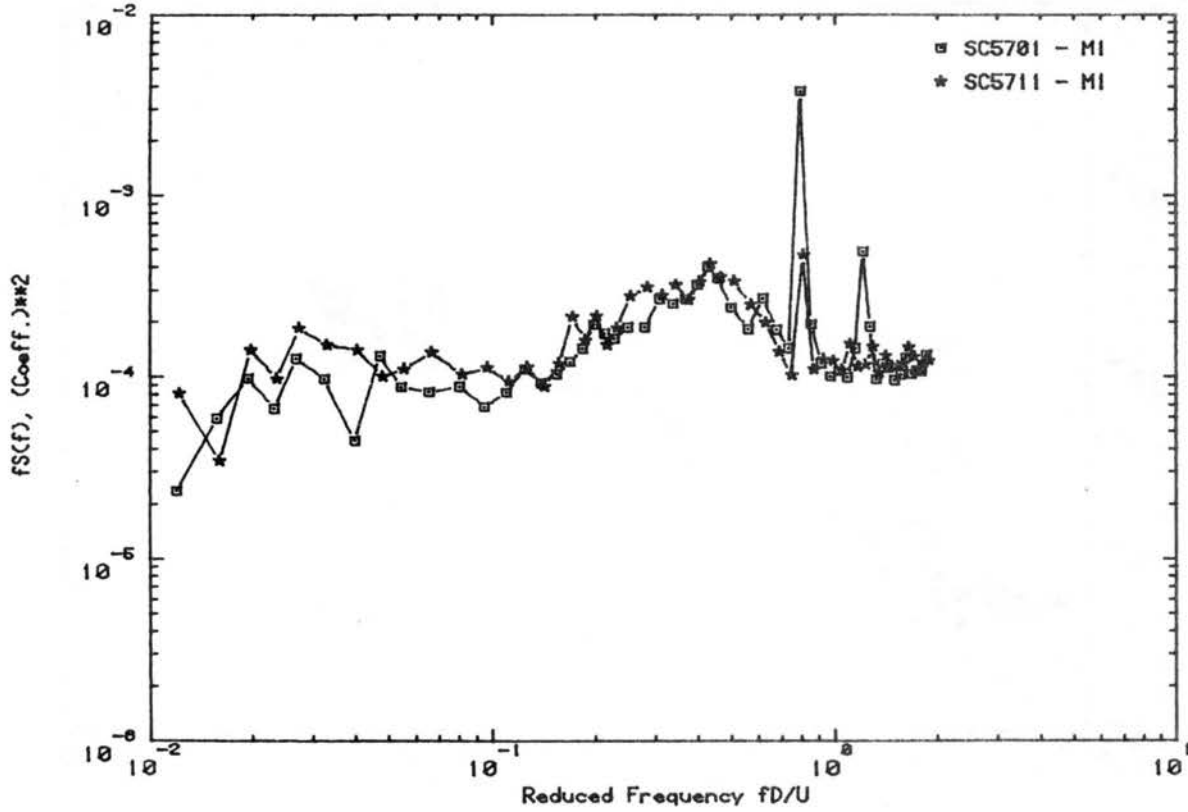


Figure C.6a. Load Spectra for Declination Angle 0°, Hour Angle 15°

RUN NO.570 WIND DIRECTION 60 Deg. VEL. U = 24.4 fps



RUN NO.572 WIND DIRECTION 180 Deg. VEL. U = 24.1 fps

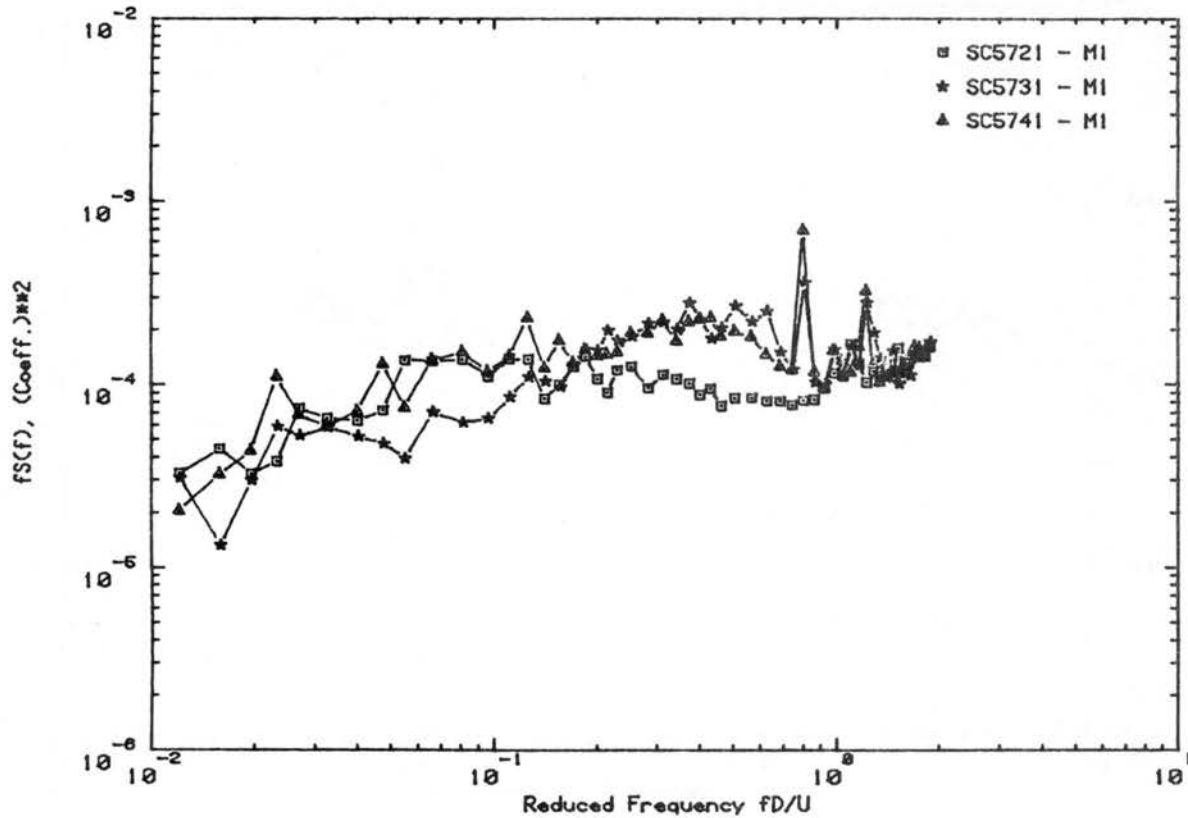
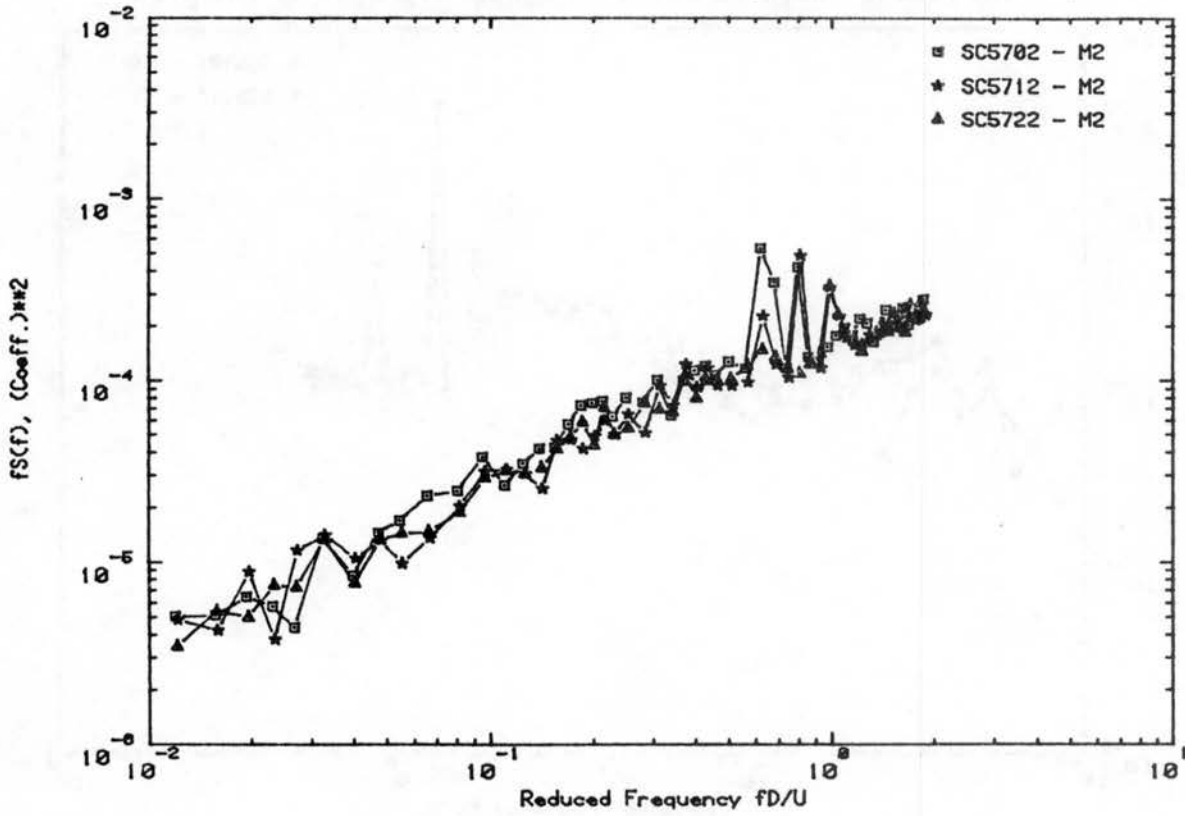


Figure C.6b. Load Spectra for Declination Angle 0°, Hour Angle 15°

RUN NO.570 WIND DIRECTION 60 Deg. VEL. U = 24.4 fps



RUN NO.573 WIND DIRECTION 270 Deg. VEL. U = 24.8 fps

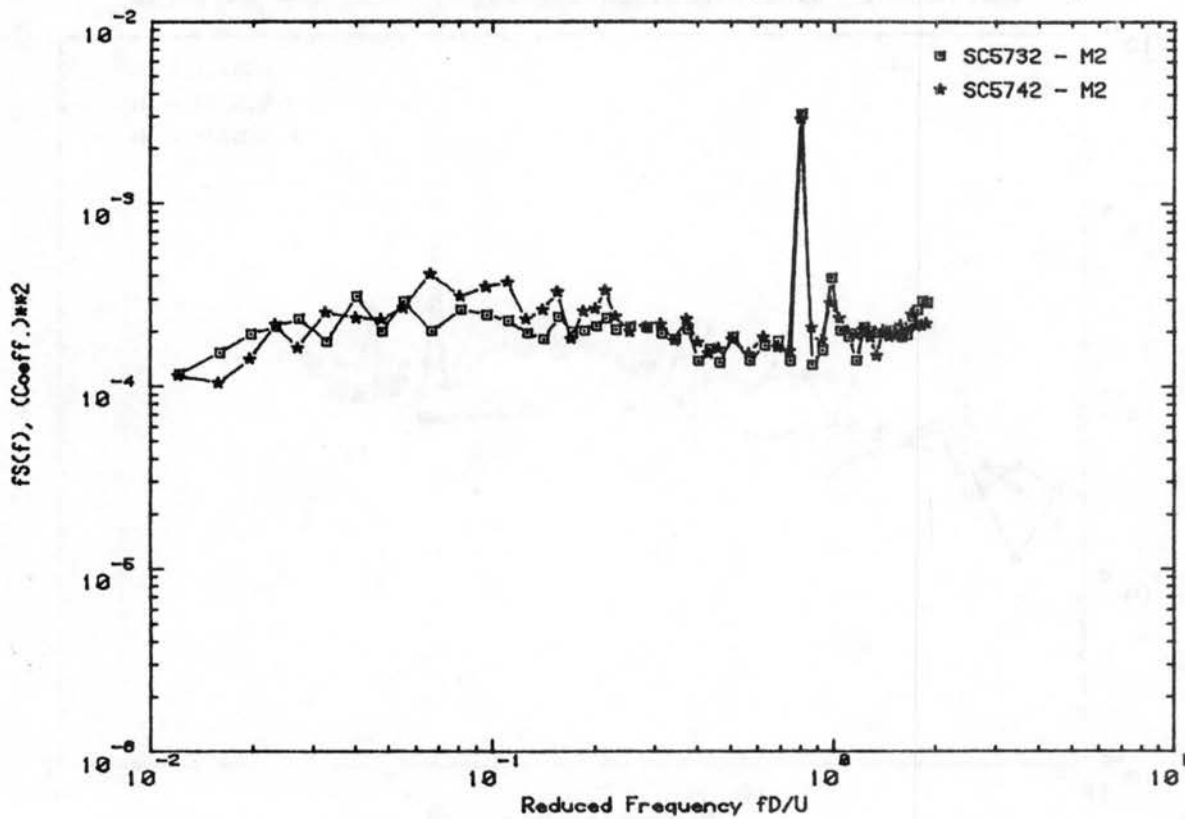


Figure C.6c. Load Spectra for Declination Angle 0°, Hour Angle 15°

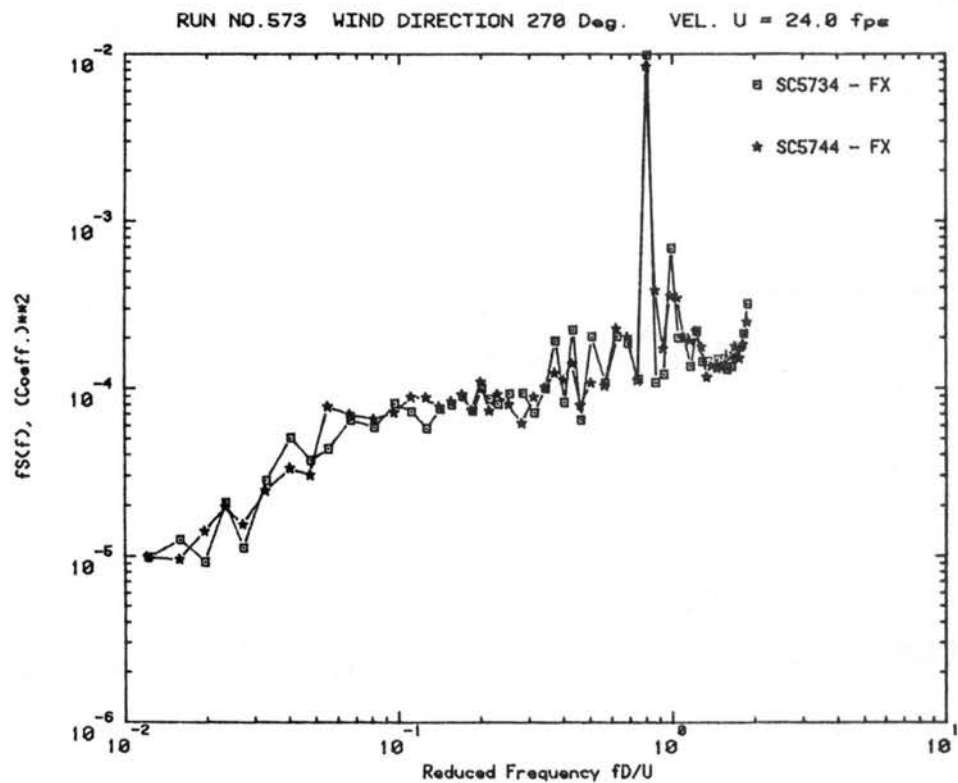
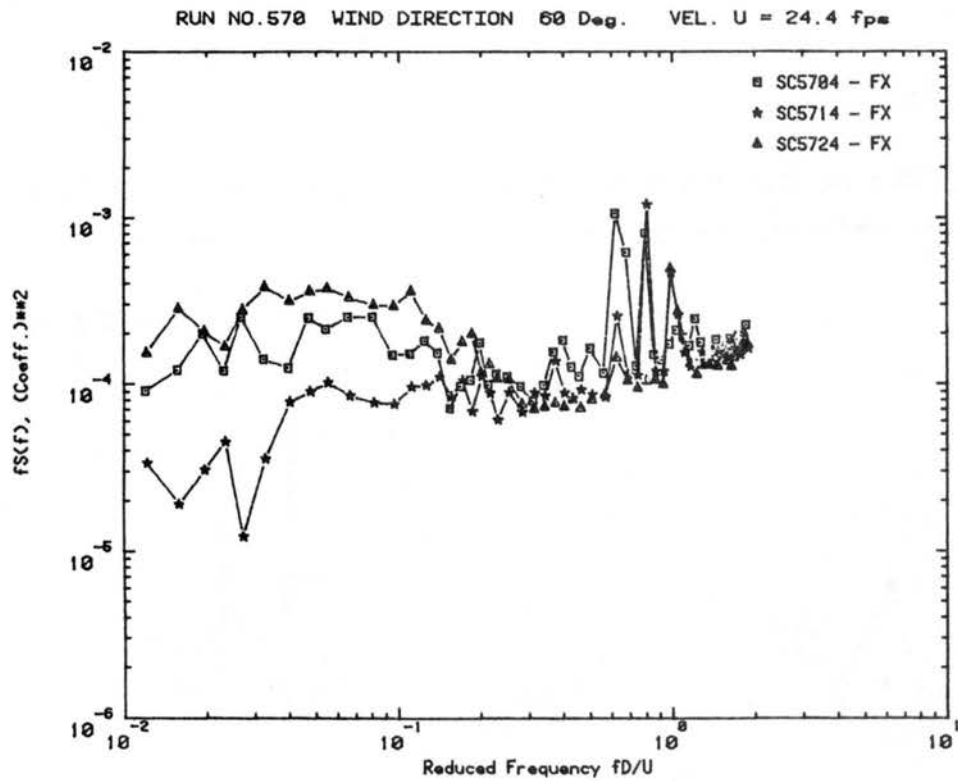


Figure C.6d. Load Spectra for Declination Angle 0° , Hour Angle 15°

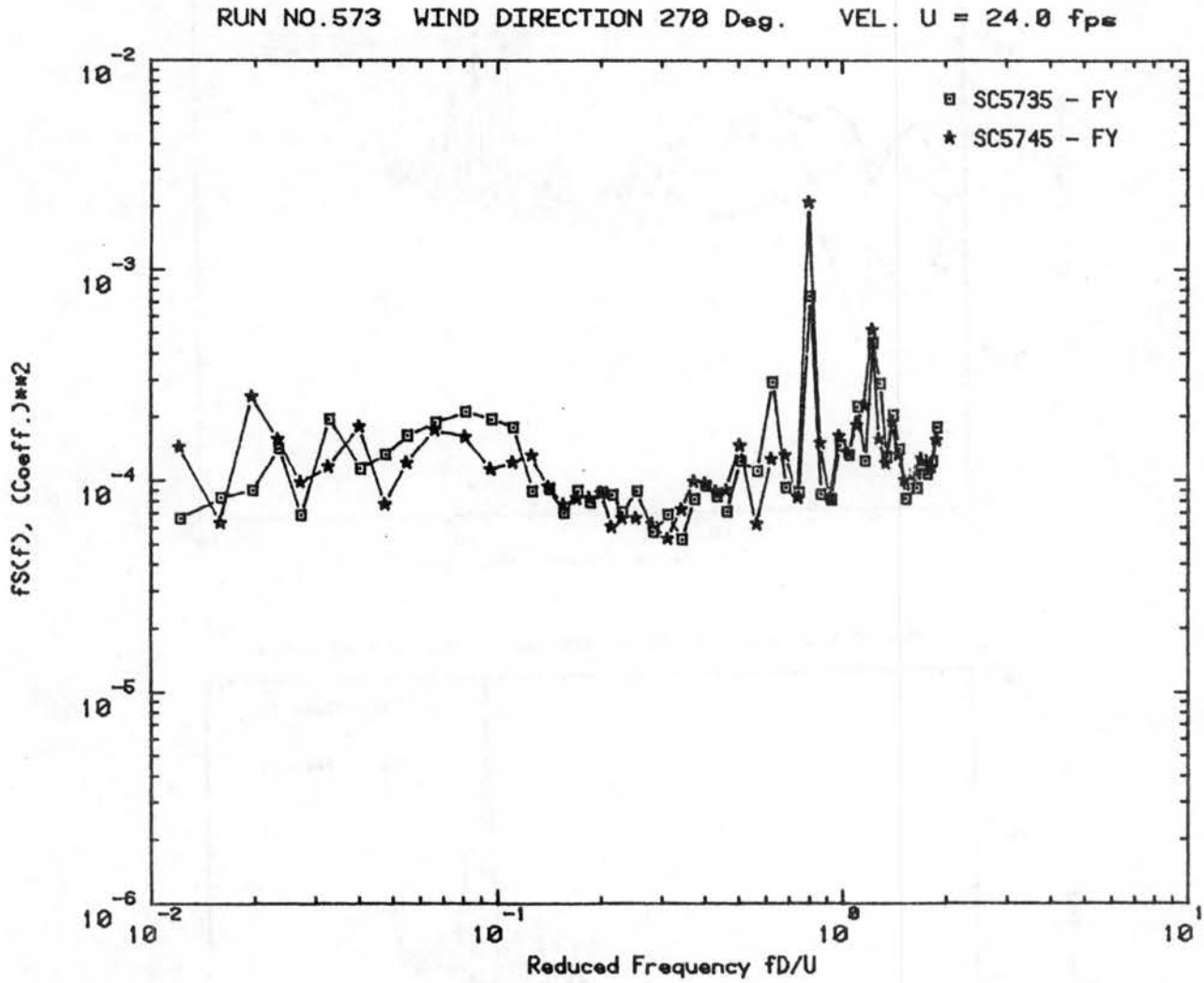
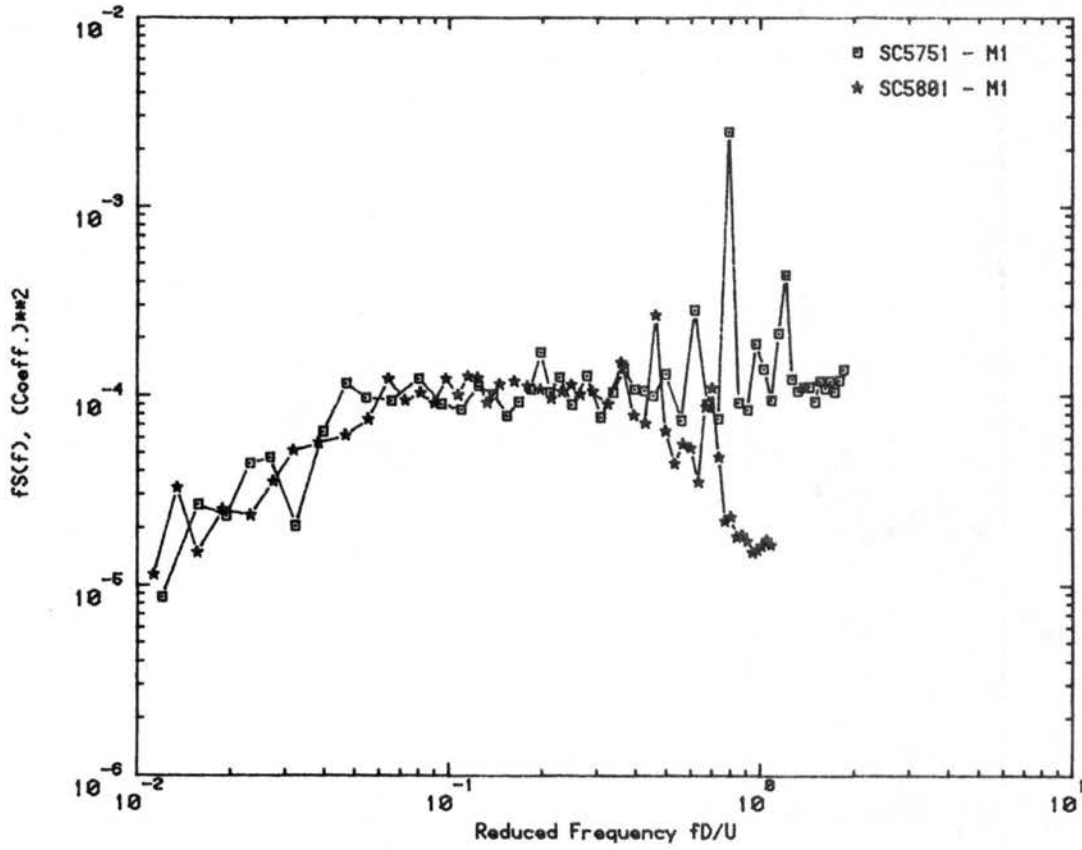


Figure C.6e. Load Spectra for Declination Angle 0° , Hour Angle 15°

RUN NO.575 WIND DIRECTION 0 Deg. VEL. U = 24.4 fps



RUN NO.576 WIND DIRECTION 20 Deg. VEL. U = 24.7 fps

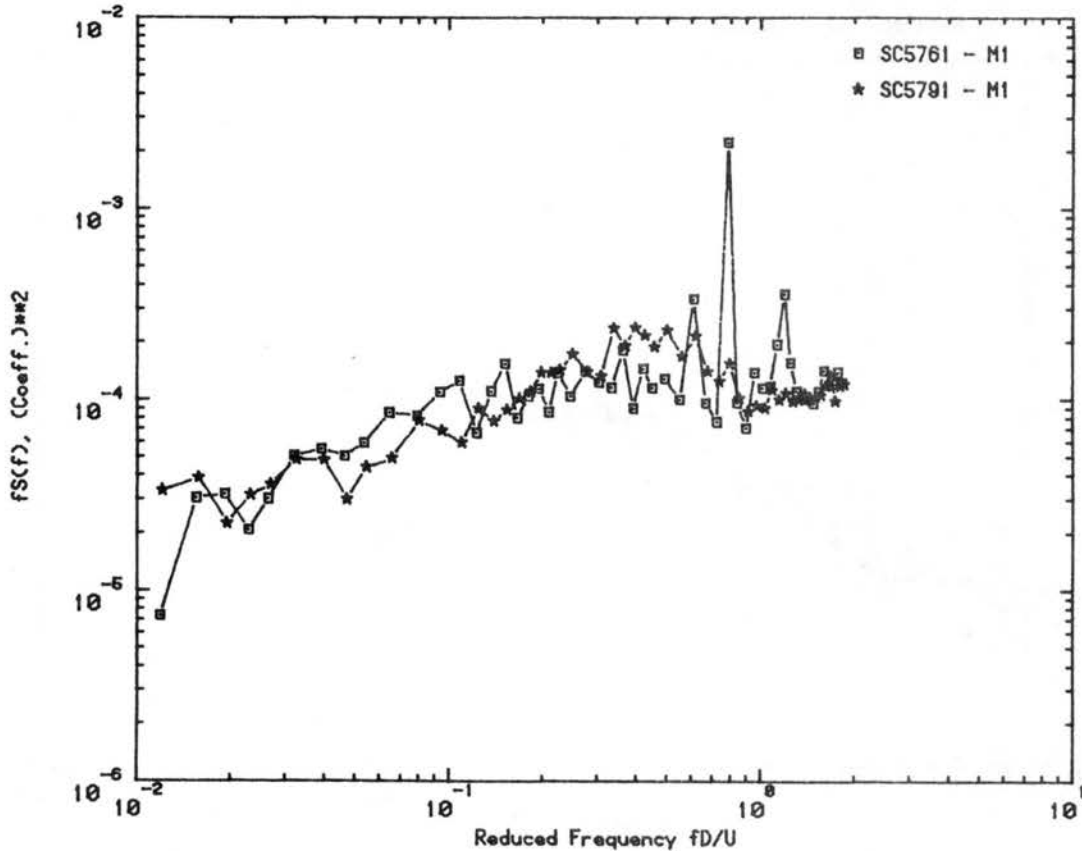
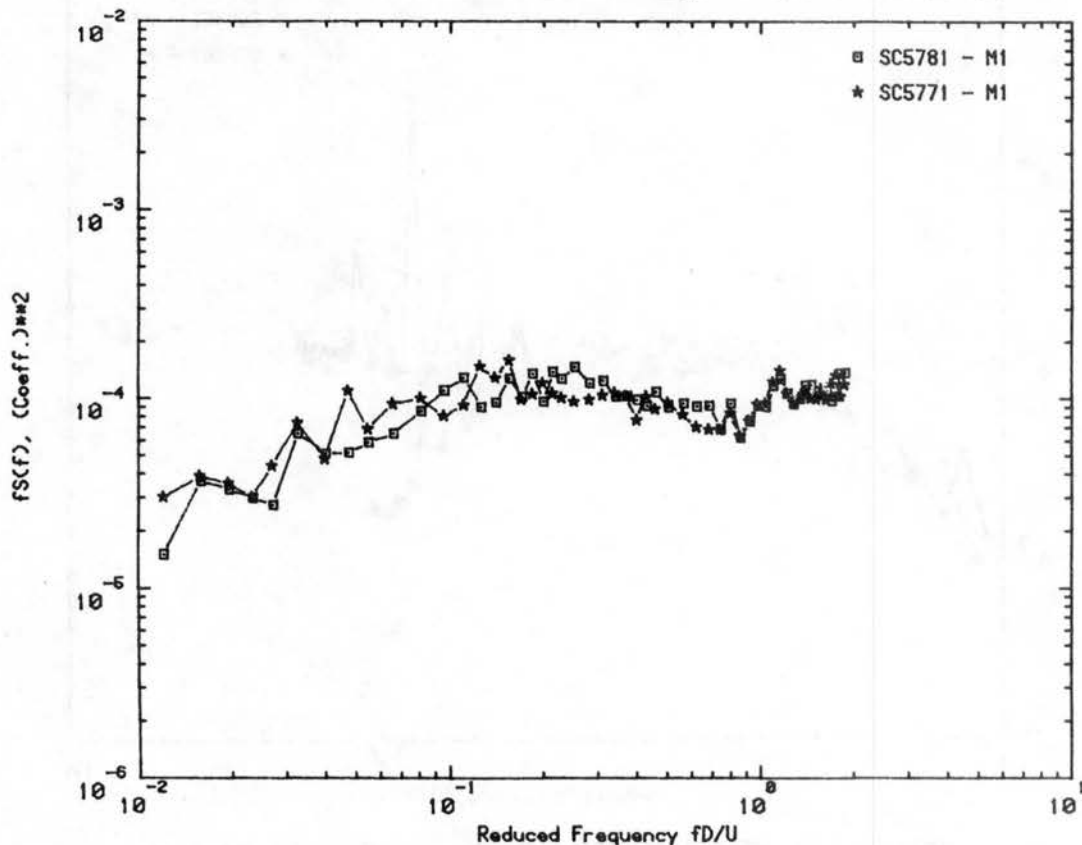


Figure C.7a. Load Spectra for Declination Angle 0°, Hour Angle 0°

RUN NO.578 WIND DIRECTION 160 Deg. VEL. U = 24.2 fps



RUN NO.575 WIND DIRECTION 0 Deg. VEL. U = 24.4 fps

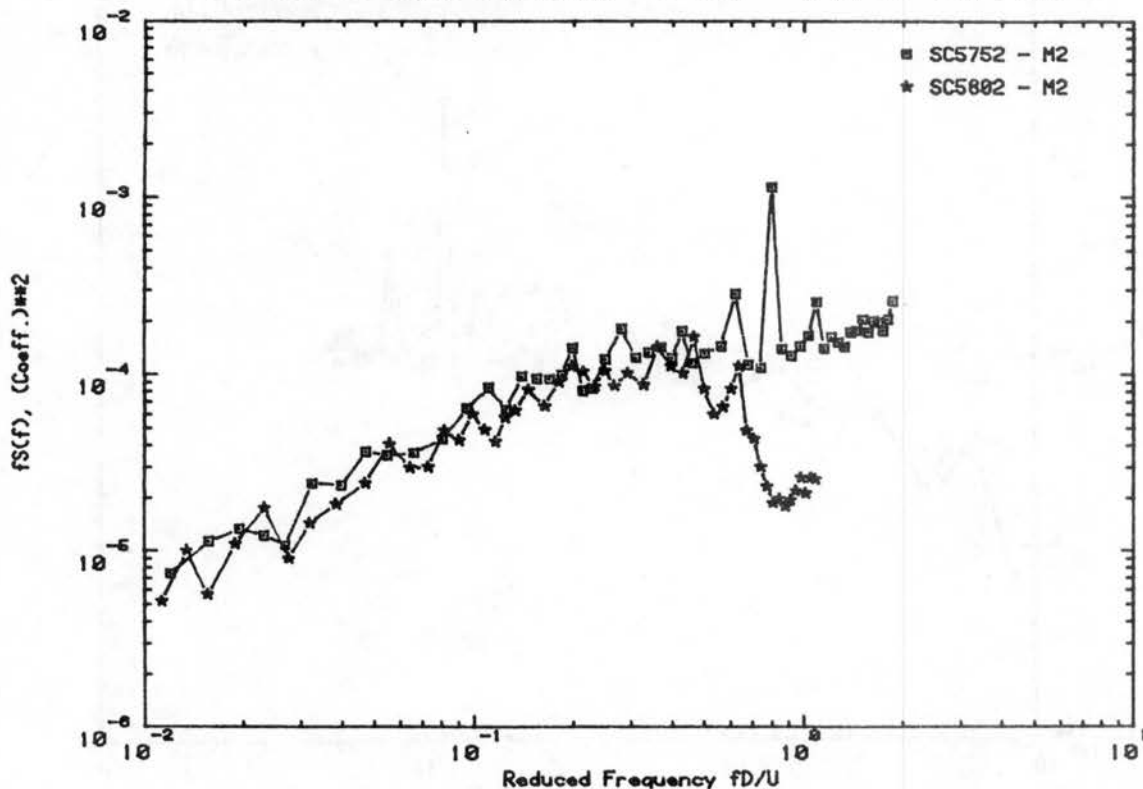
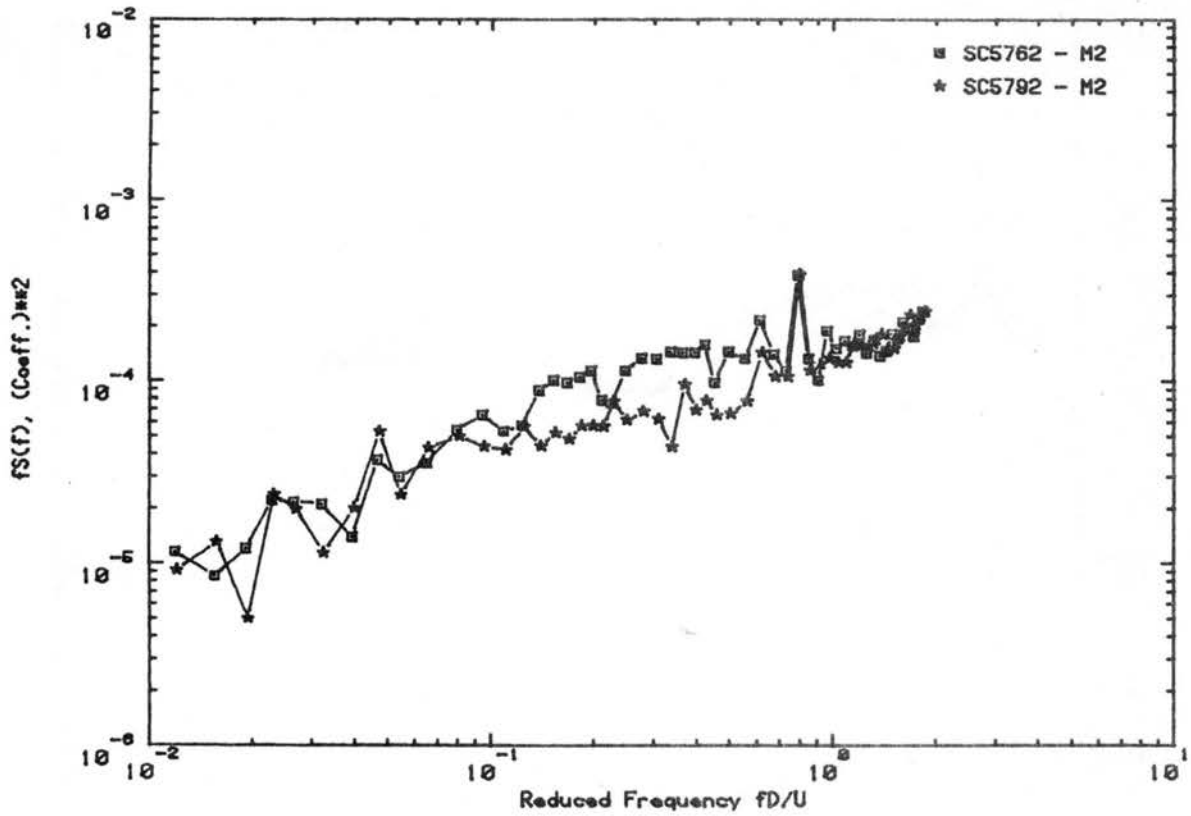


Figure C.7b. Load Spectra for Declination Angle 0°, Hour Angle 0°

RUN NO.576 WIND DIRECTION 20 Deg. VEL. U = 24.7 fps



RUN NO.576 WIND DIRECTION 160 Deg. VEL. U = 24.2 fps

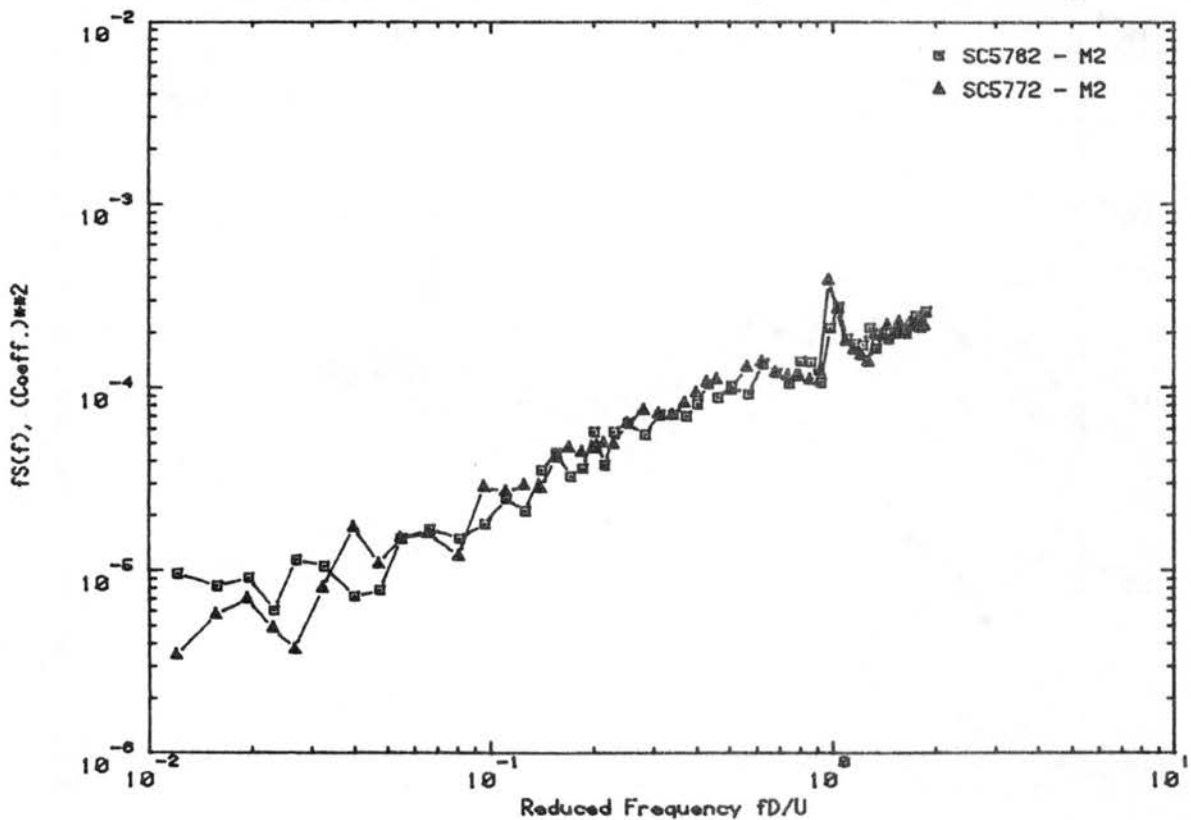
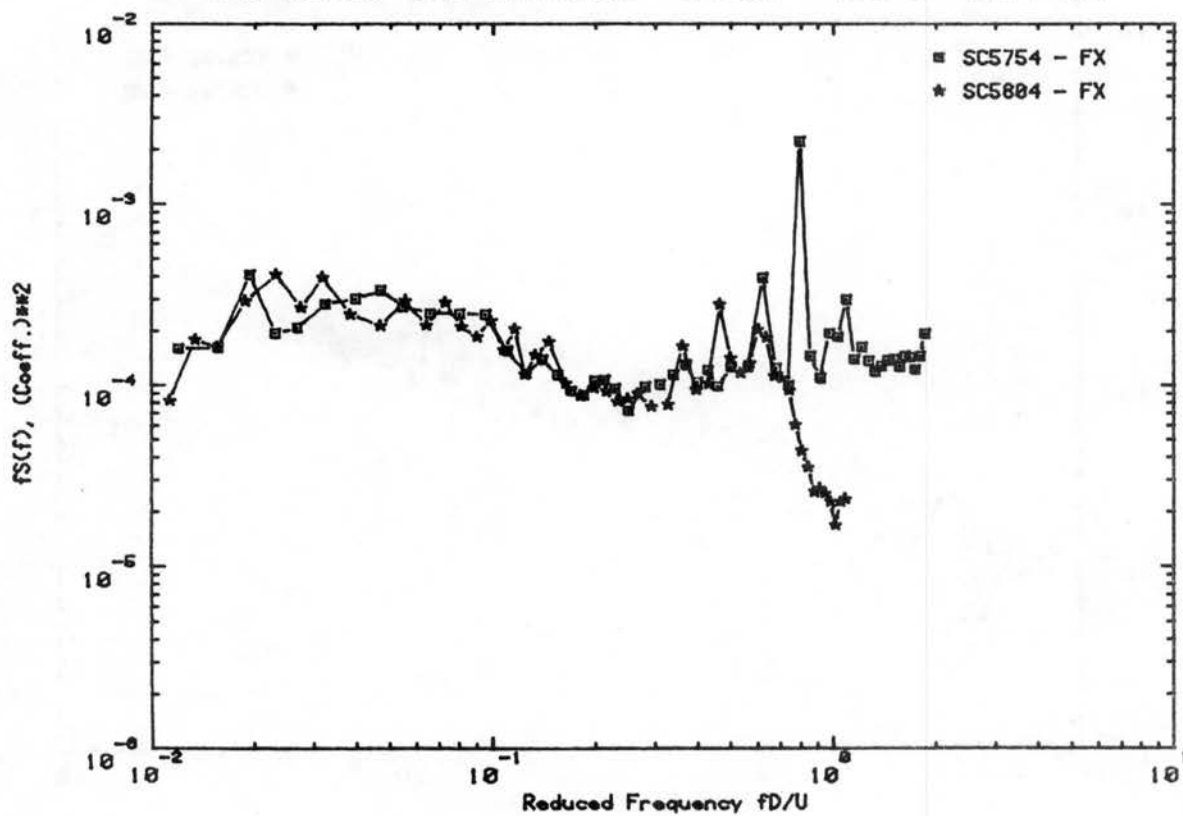
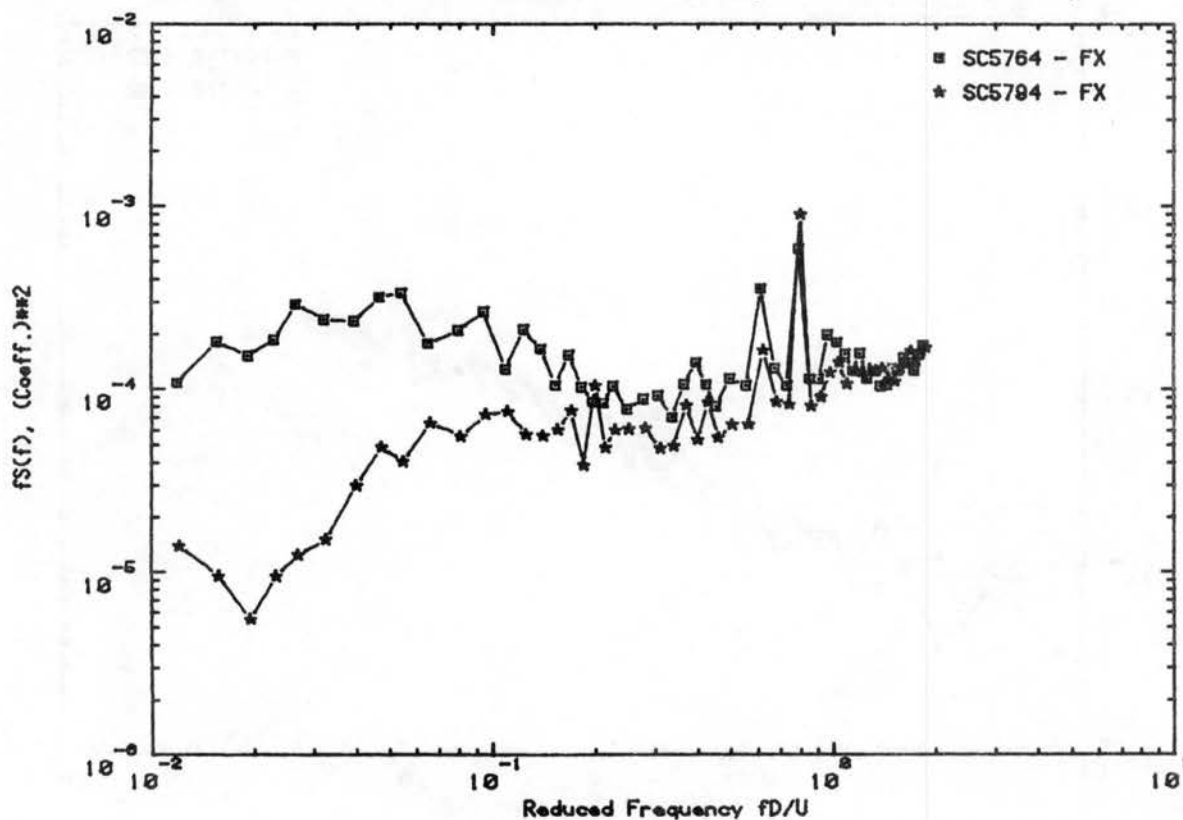


Figure C.7c. Load Spectra for Declination Angle 0°, Hour Angle 0°

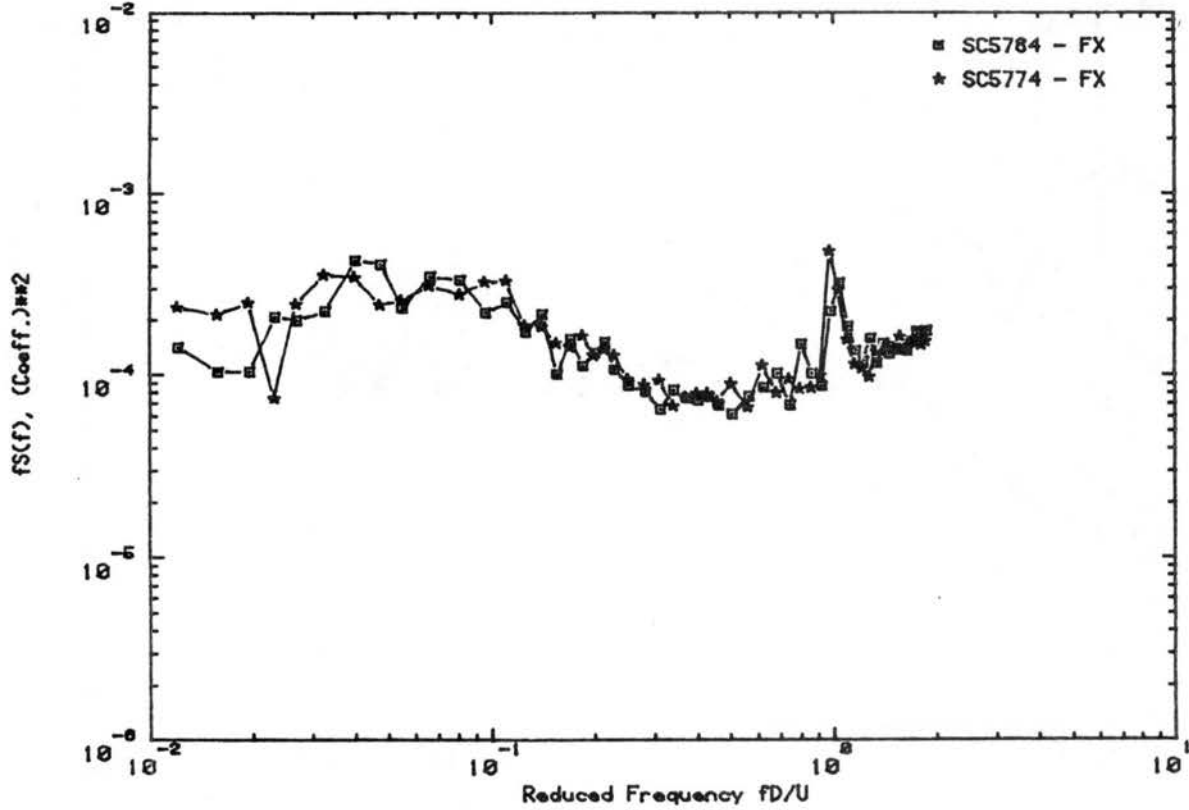
RUN NO.575 WIND DIRECTION 0 Deg. VEL. U = 24.4 fps



RUN NO.576 WIND DIRECTION 20 Deg. VEL. U = 24.7 fps

Figure C.7d. Load Spectra for Declination Angle 0° , Hour Angle 0°

RUN NO.578 WIND DIRECTION 160 Deg. VEL. U = 24.2 fps



RUN NO.575 WIND DIRECTION 0 Deg. VEL. U = 24.4 fps

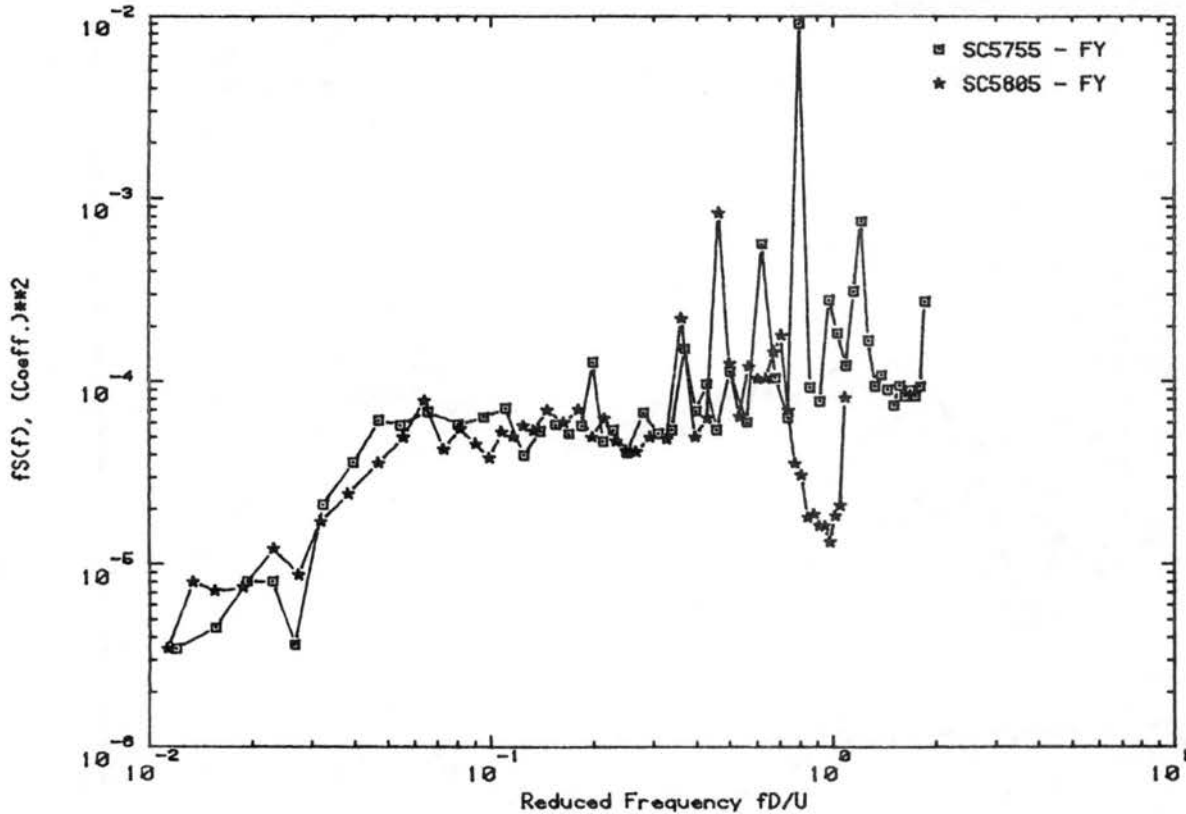
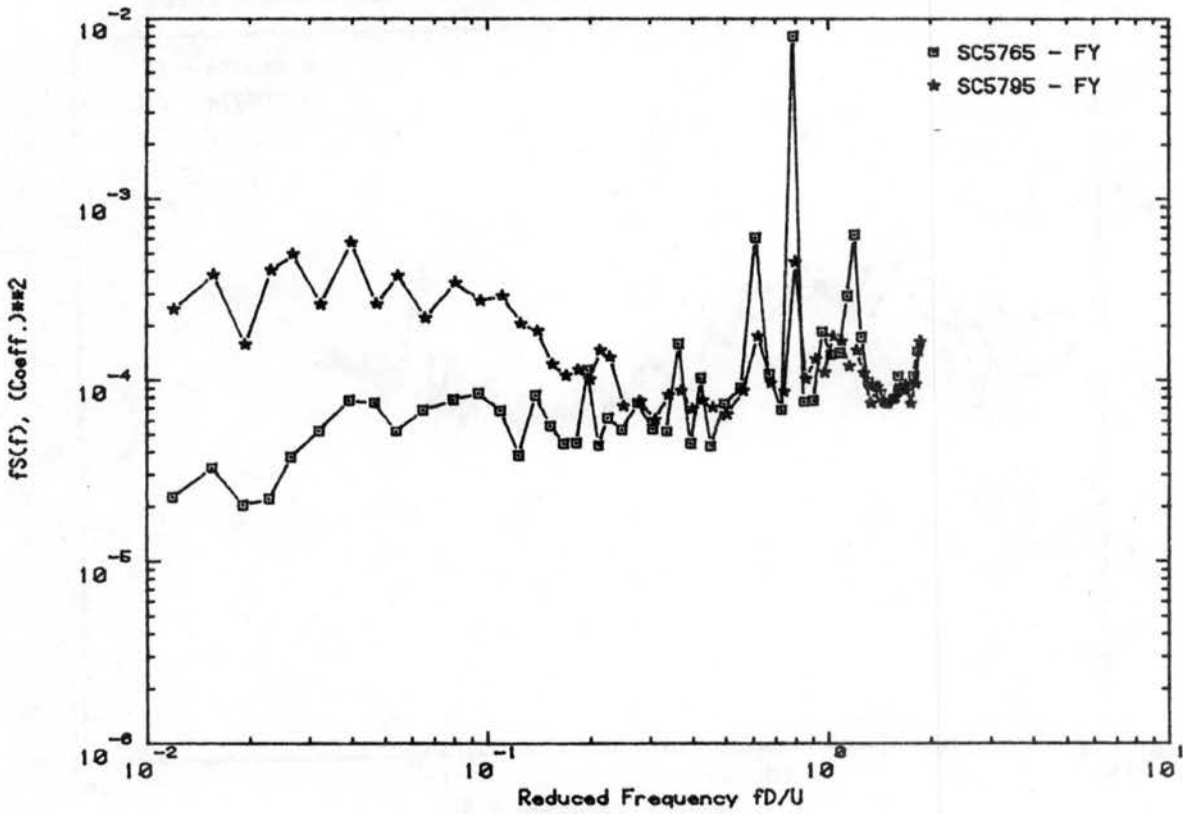


Figure C.7e. Load Spectra for Declination Angle 0°, Hour Angle 0°

RUN NO.576 WIND DIRECTION 20 Deg. VEL. U = 24.7 fps



RUN NO.578 WIND DIRECTION 160 Deg. VEL. U = 24.2 fps

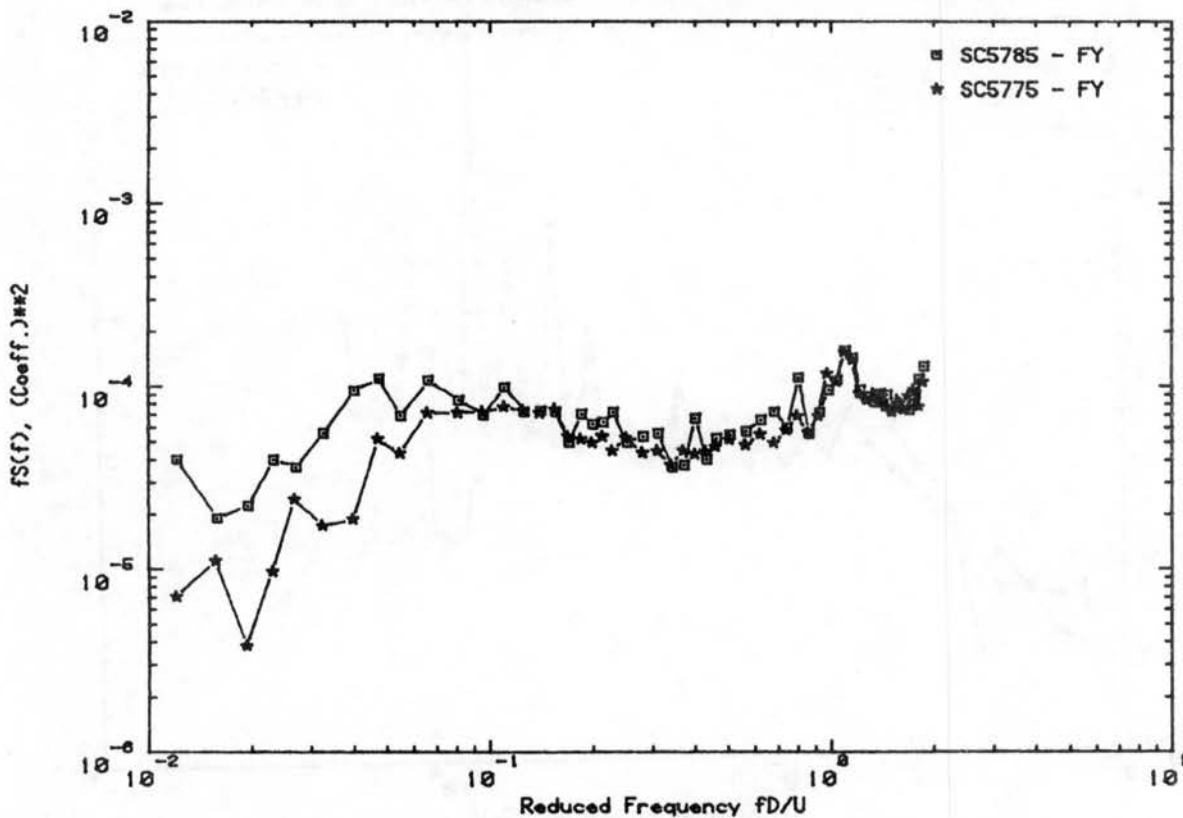
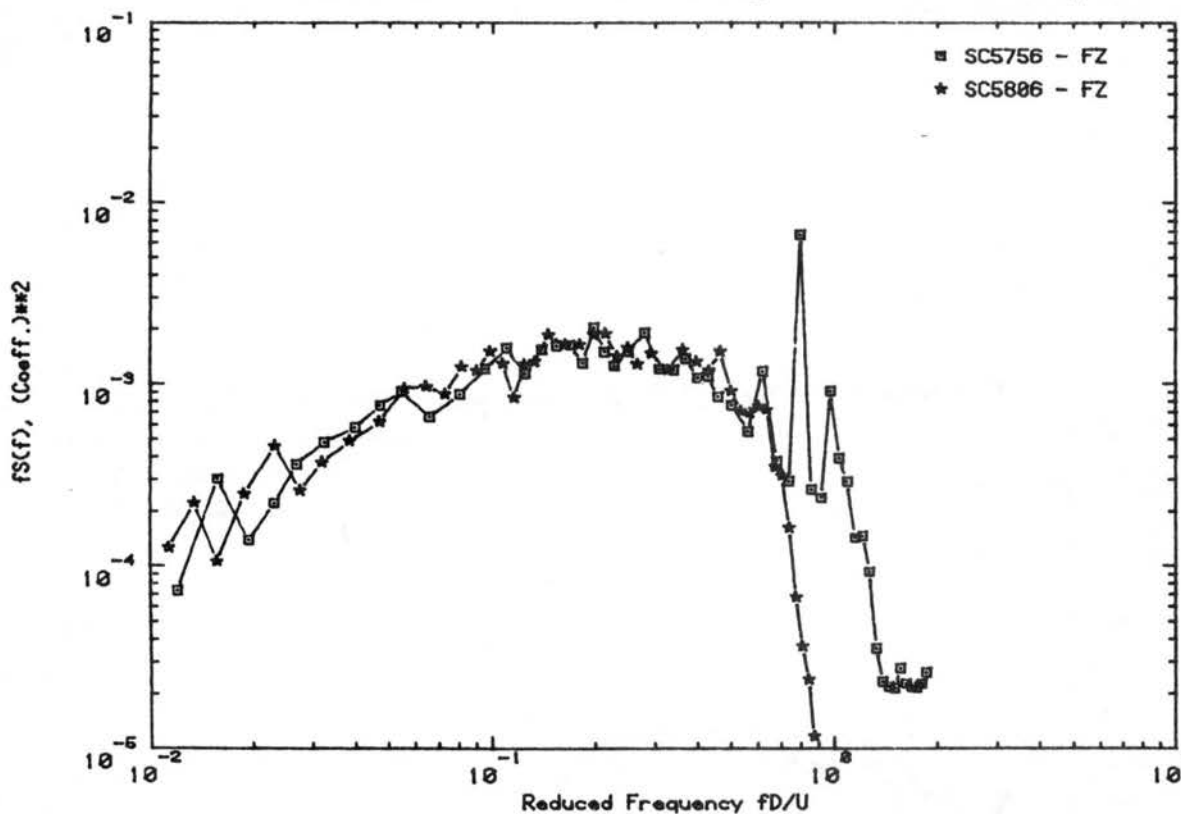


Figure C.7f. Load Spectra for Declination Angle 0°, Hour Angle 0°

RUN NO.575 WIND DIRECTION 0 Deg. VEL. U = 24.4 fps



RUN NO.576 WIND DIRECTION 20 Deg. VEL. U = 24.7 fps

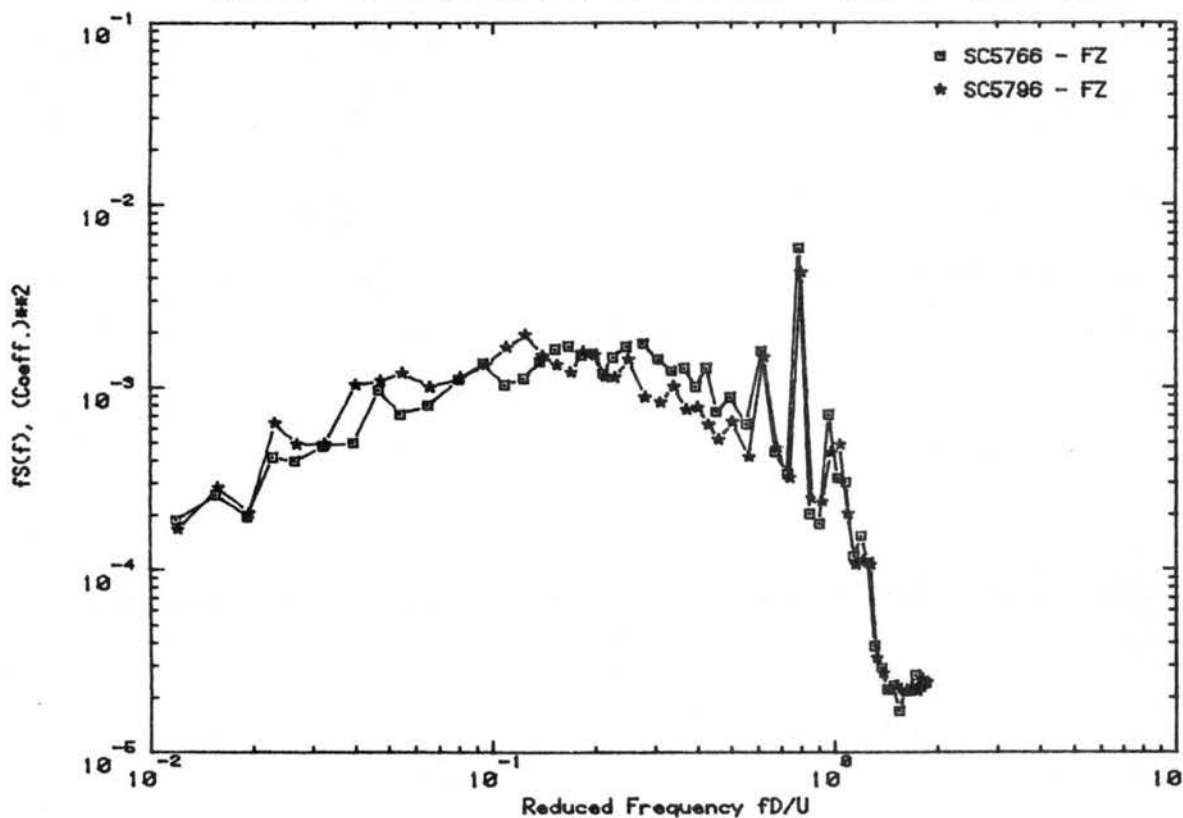


Figure C.7g. Load Spectra for Declination Angle 0°, Hour Angle 0°

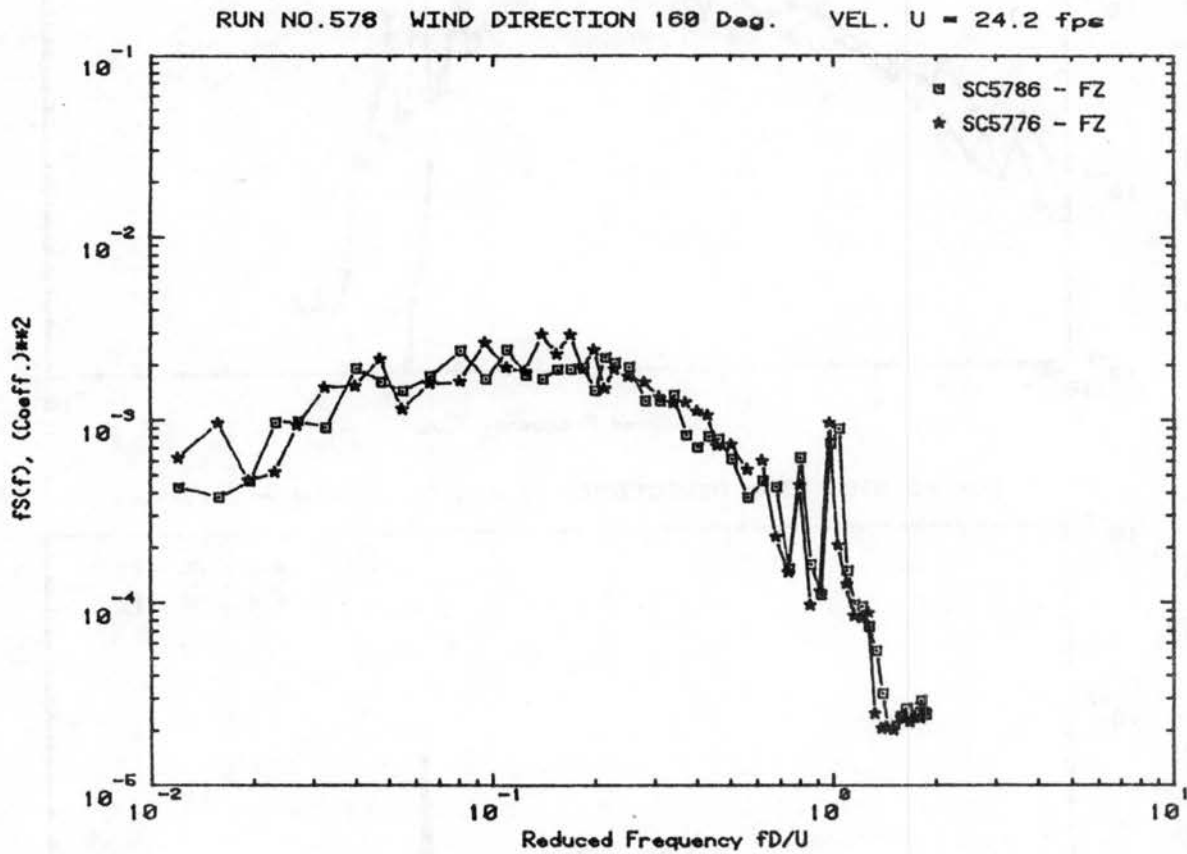
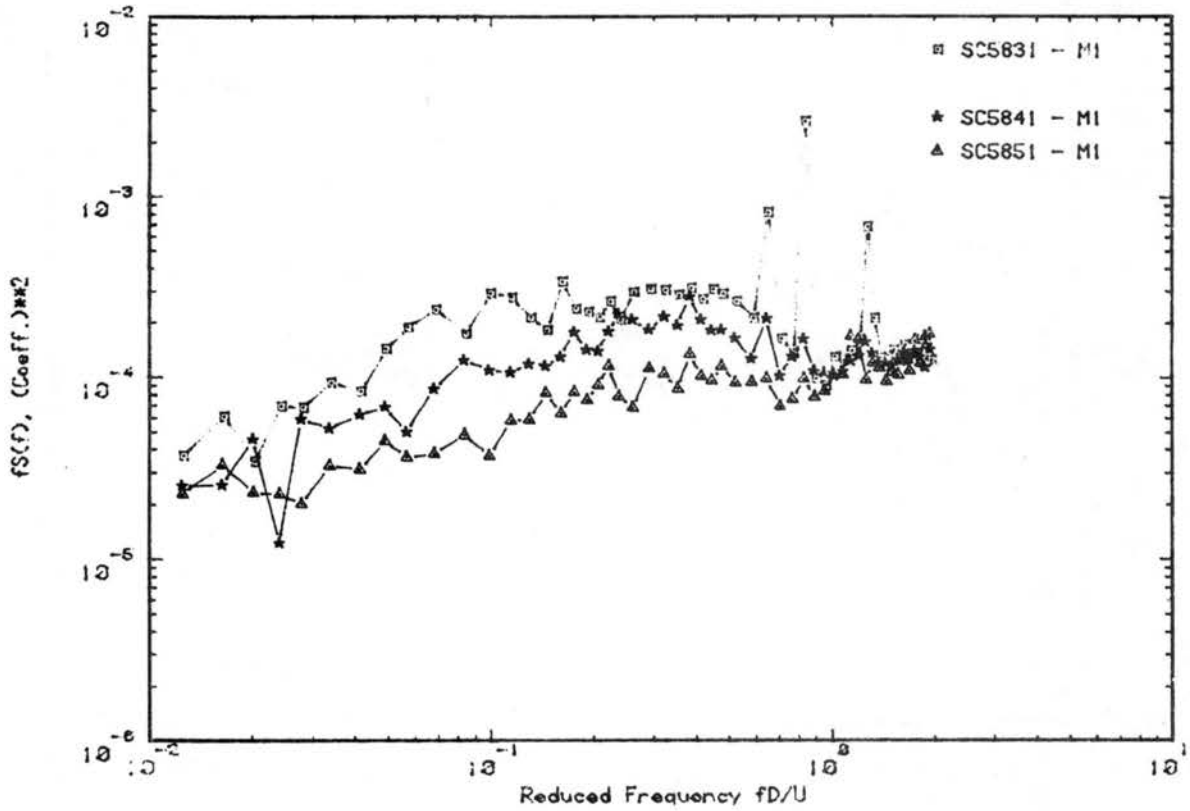


Figure C.7h. Load Spectra for Declination Angle 0° , Hour Angle 0°

RUN NO.583 WIND DIRECTION 60 Deg. VEL. U = 23.1 fps



RUN NO.583 WIND DIRECTION 60 Deg. VEL. U = 23.1 fps

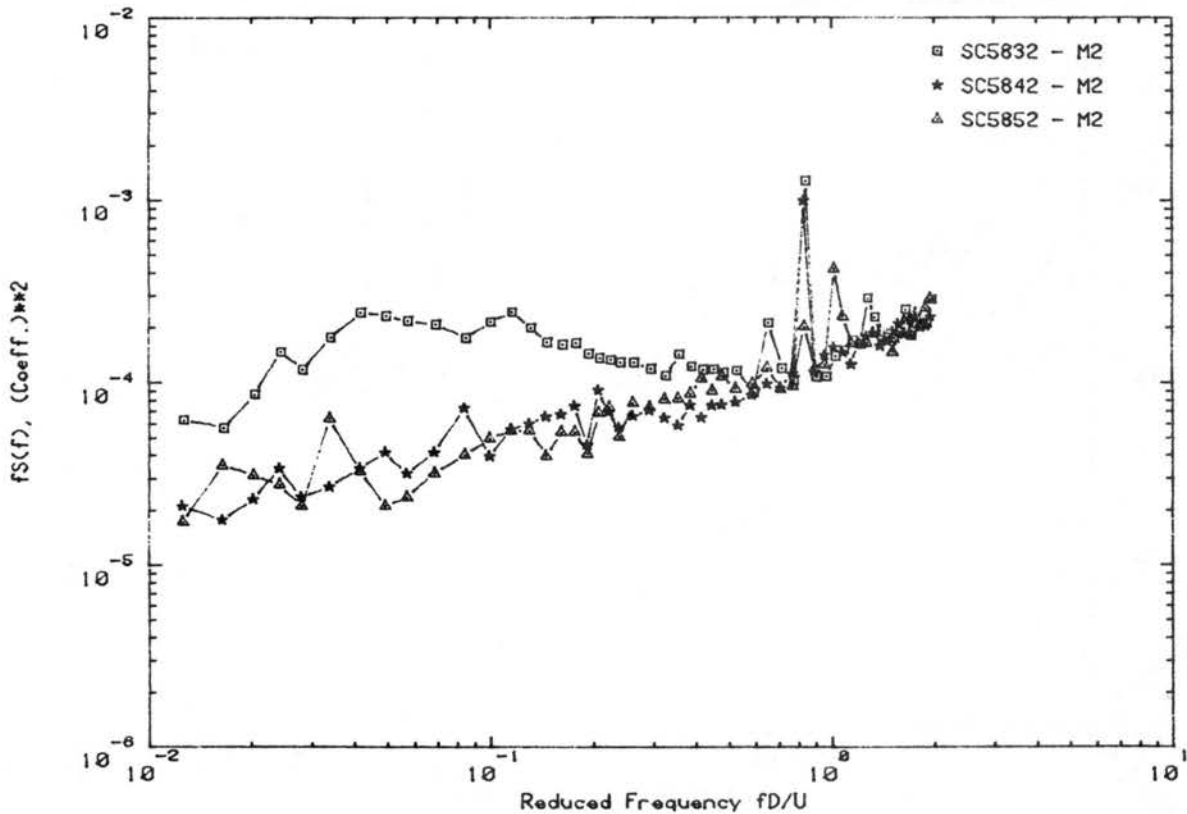
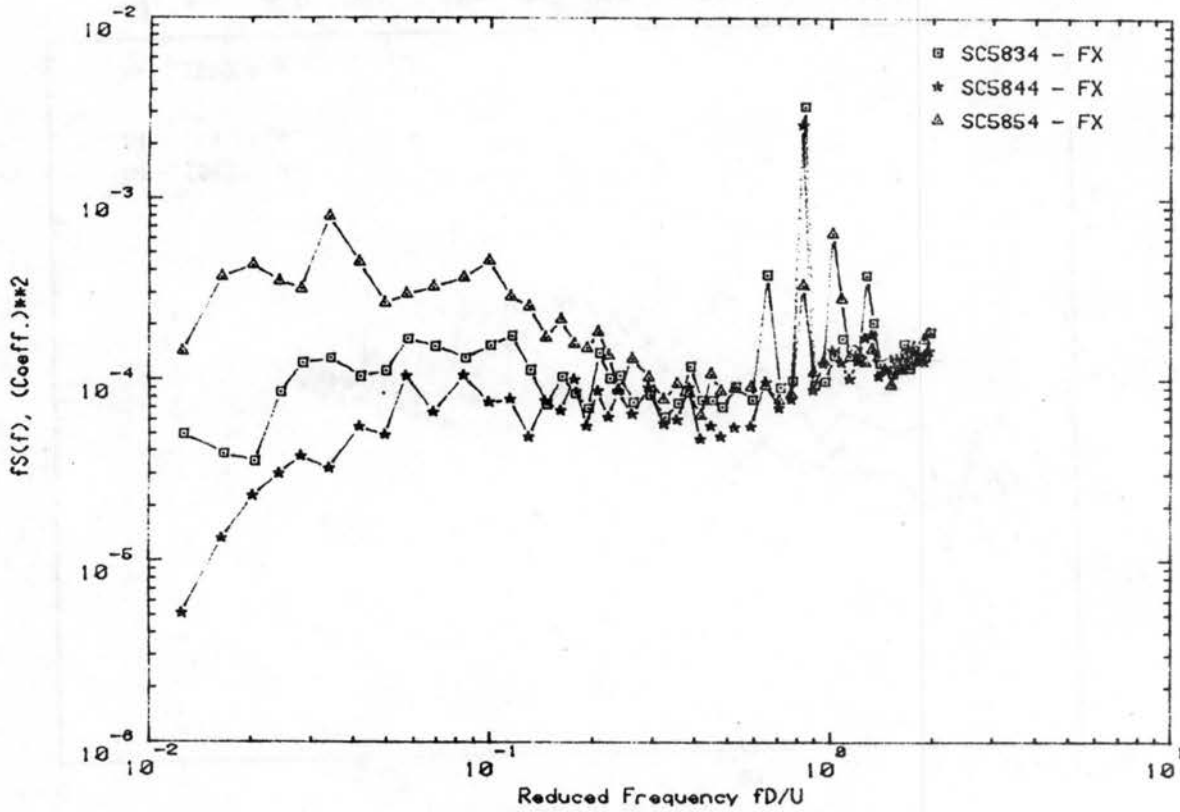


Figure C.8a. Load Spectra for Declination Angle -20° , Hour Angle 0°

RUN NO.583 WIND DIRECTION 60 Deg. VEL. U = 23.1 fps



RUN NO.583 WIND DIRECTION 60 Deg. VEL. U = 23.1 fps

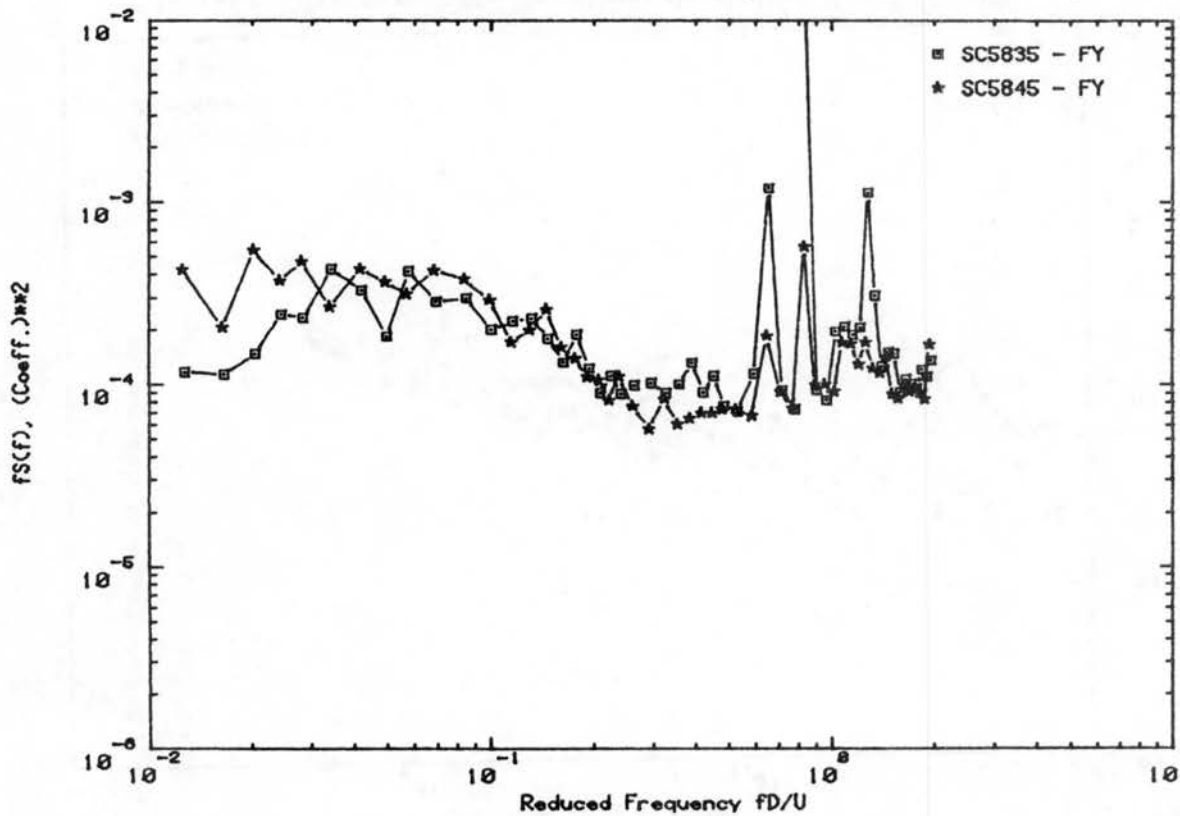
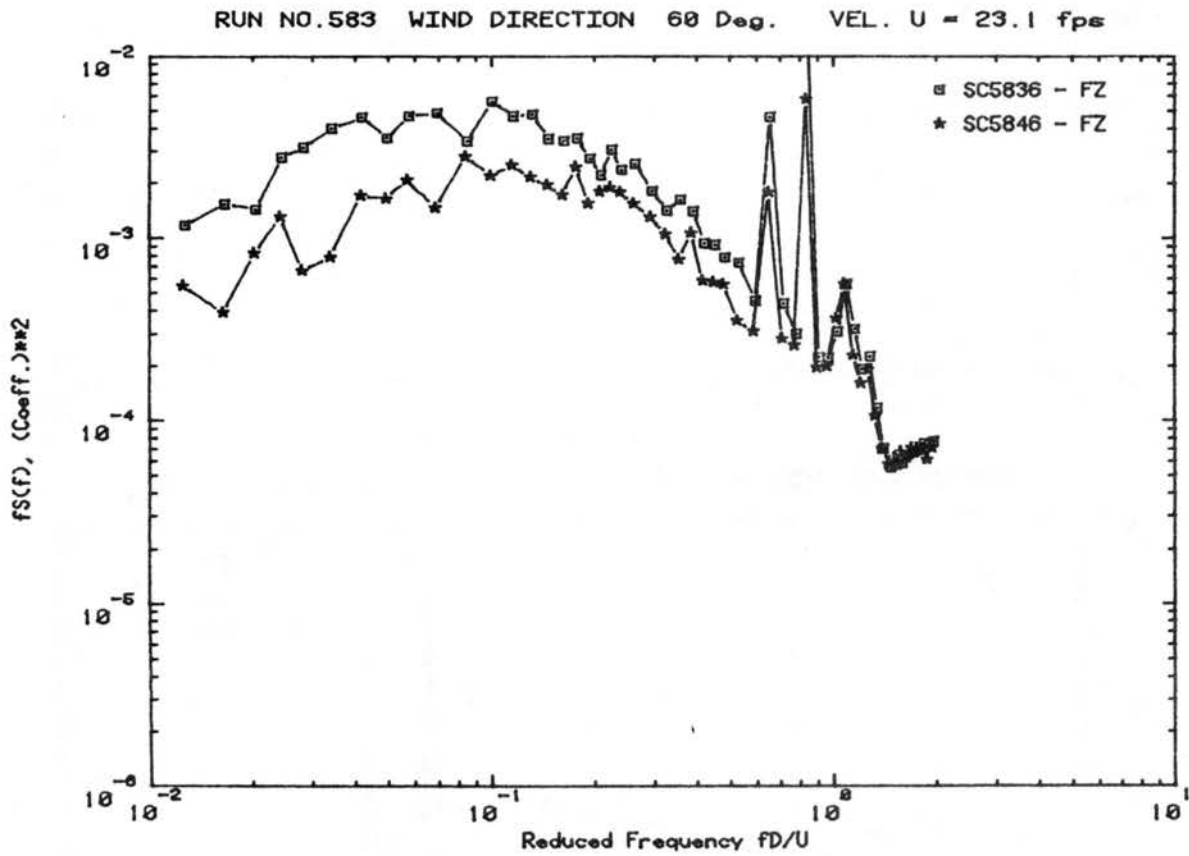
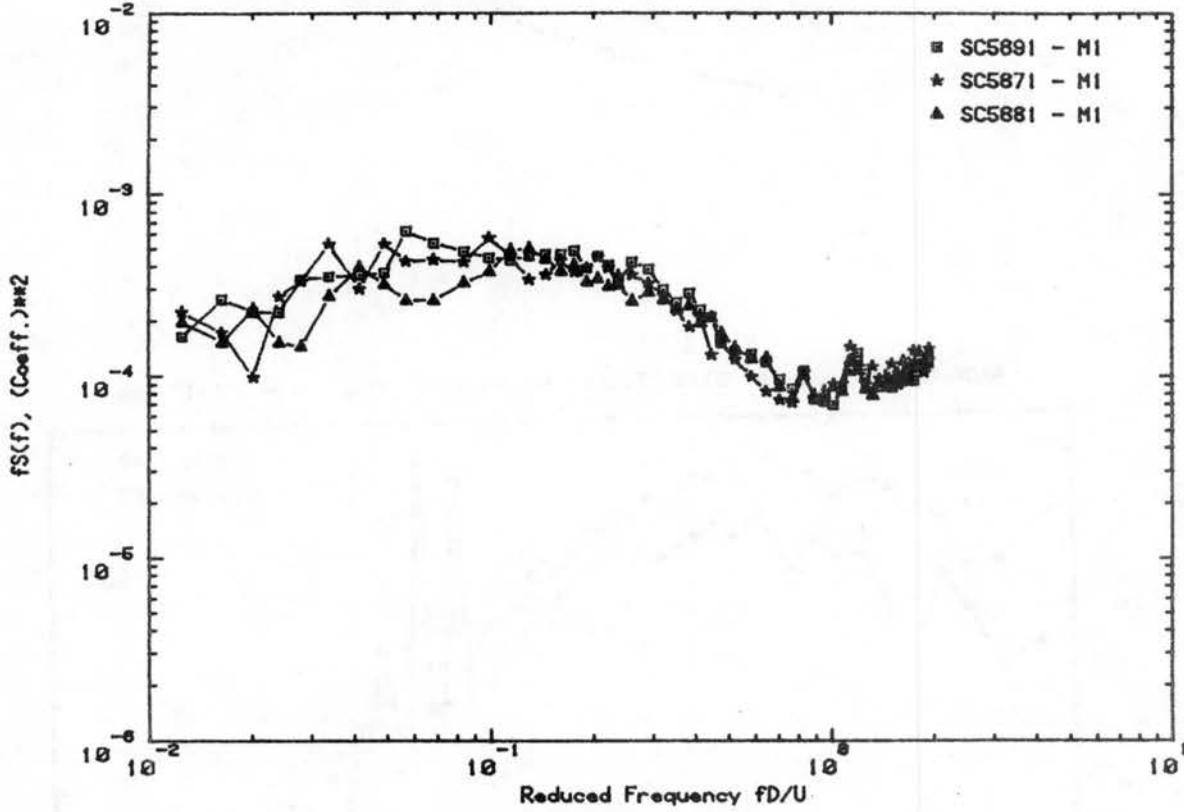


Figure C.8b. Load Spectra for Declination Angle -20° , Hour Angle 0°

Figure C.8c. Load Spectra for Declination Angle -20° , Hour Angle 0°

RUN NO.589 WIND DIRECTION 160 Deg. VEL. U = 23.4 fps



RUN NO.592 WIND DIRECTION 0 Deg. VEL. U = 23.0 fps

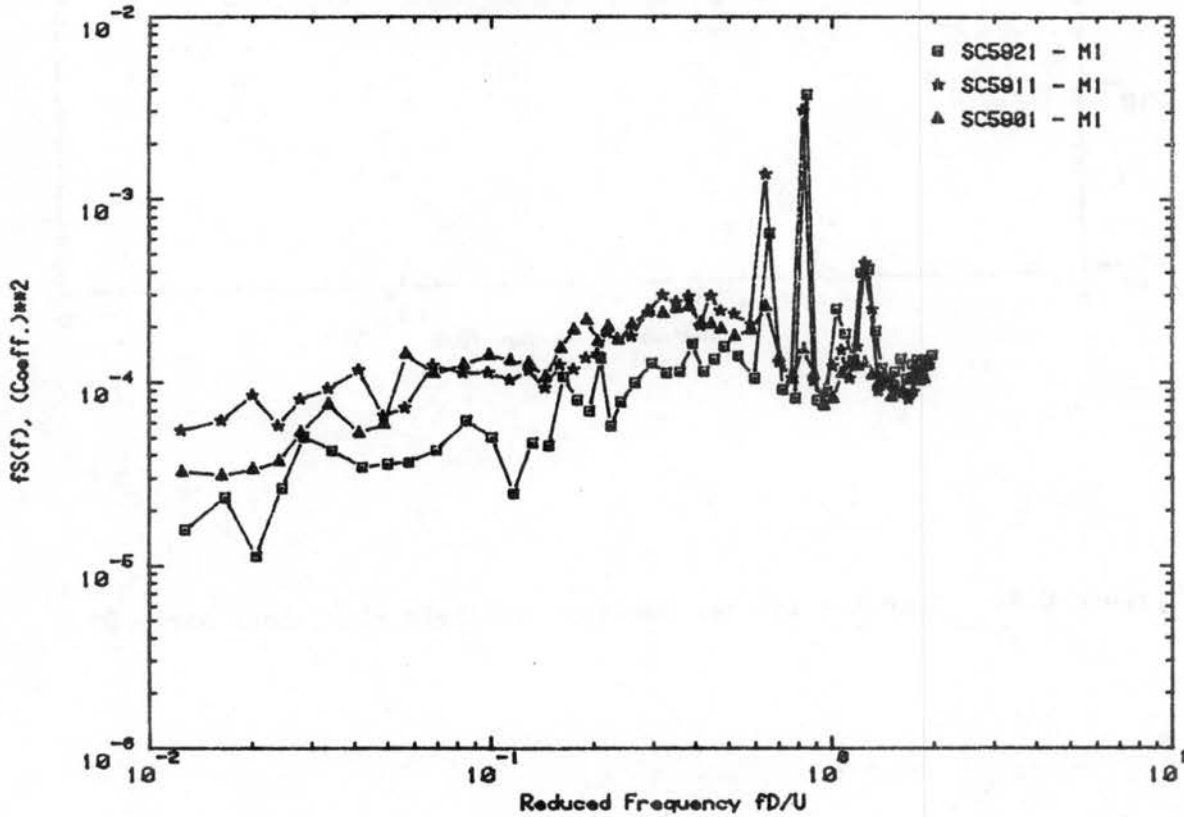


Figure C.9a. Load Spectra for Declination Angle 20°, Hour Angle 0°

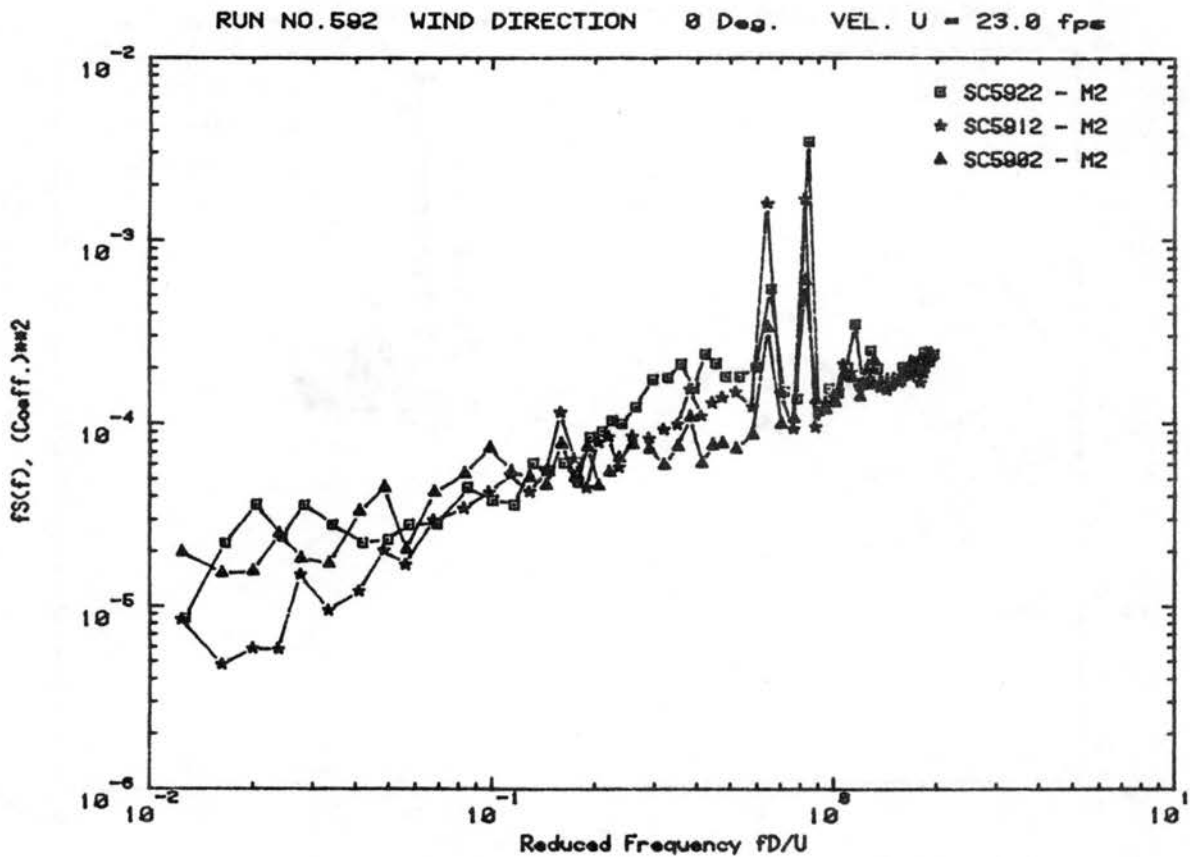
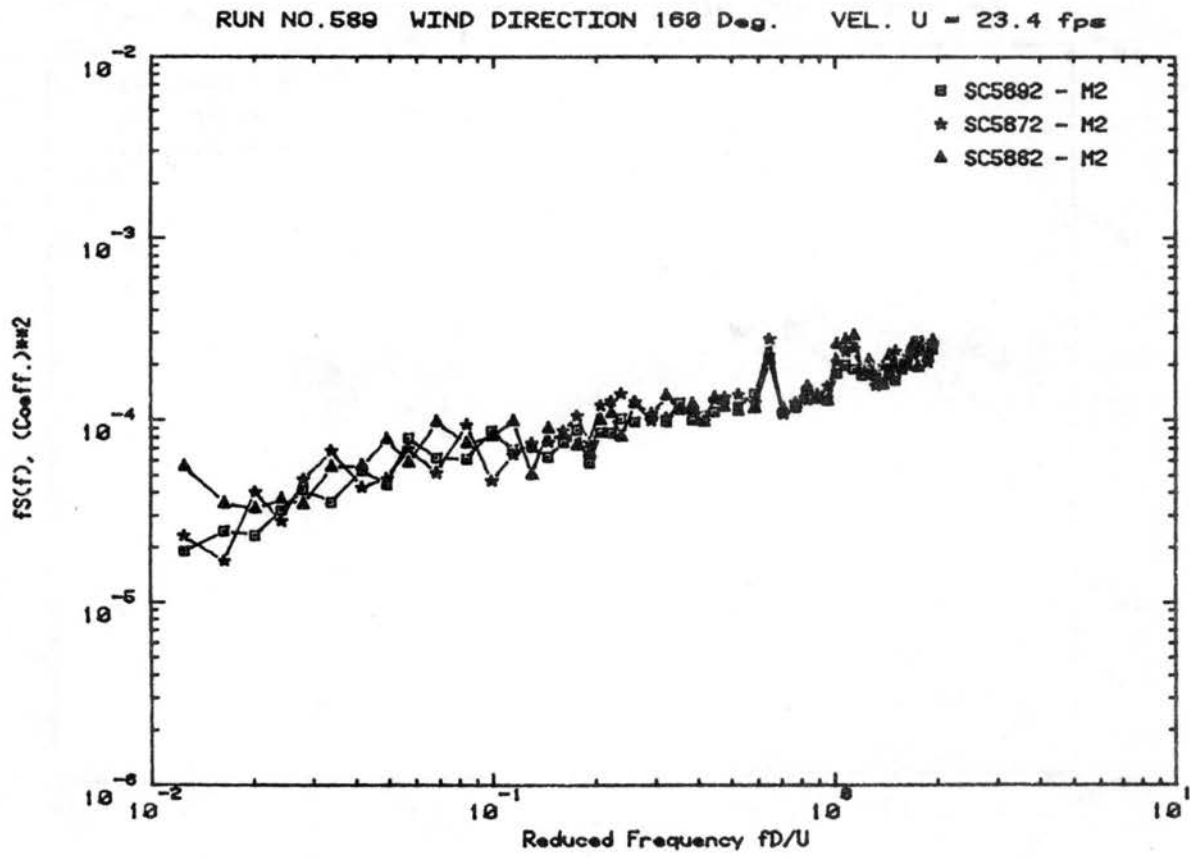
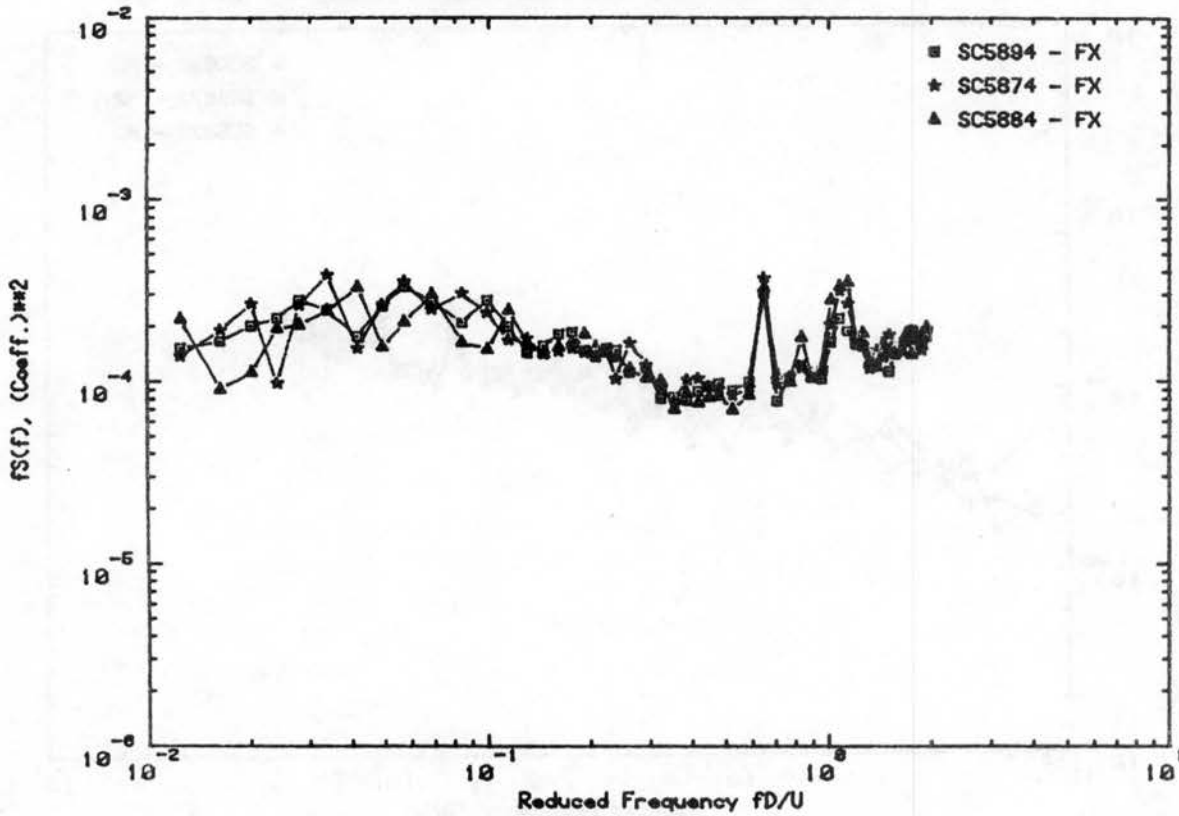


Figure C.9b. Load Spectra for Declination Angle 20° , Hour Angle 0°

RUN NO.589 WIND DIRECTION 160 Deg. VEL. U = 23.4 fps



RUN NO.592 WIND DIRECTION 0 Deg. VEL. U = 23.8 fps

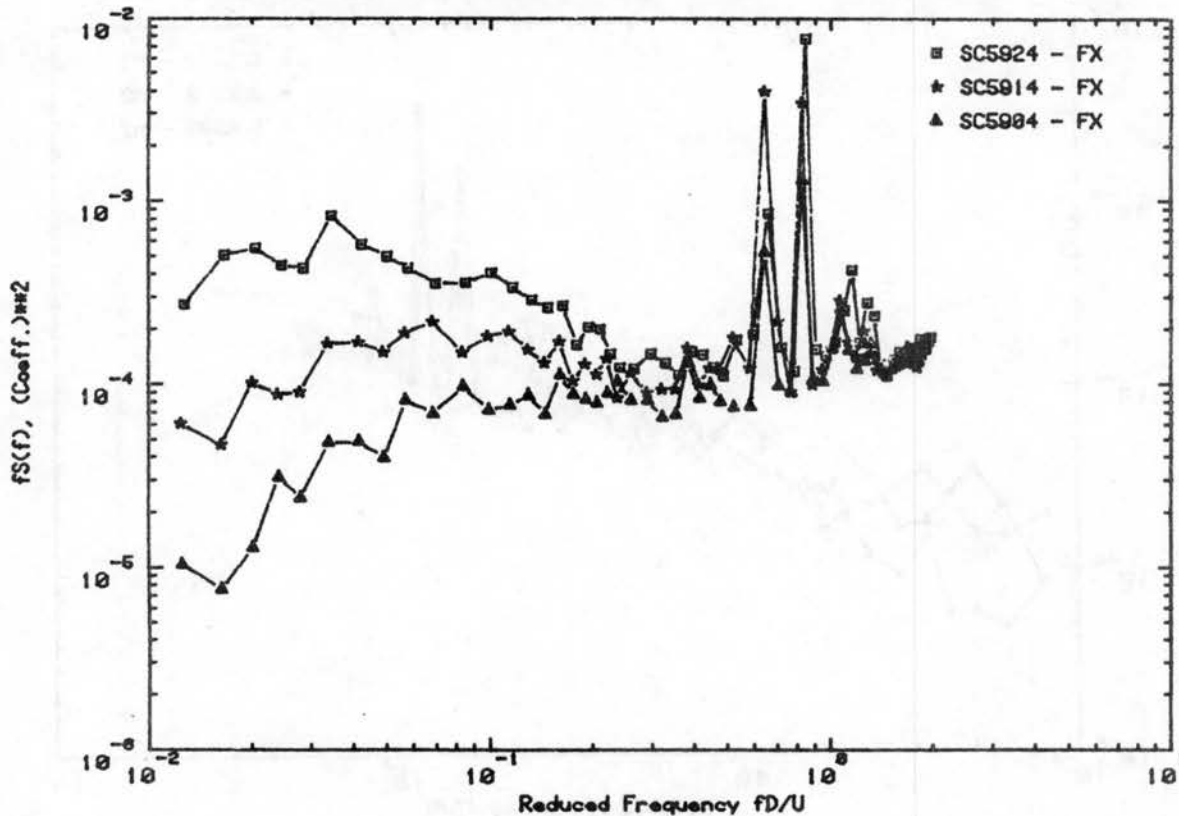


Figure C.9c. Load Spectra for Declination Angle 20°, Hour Angle 0°

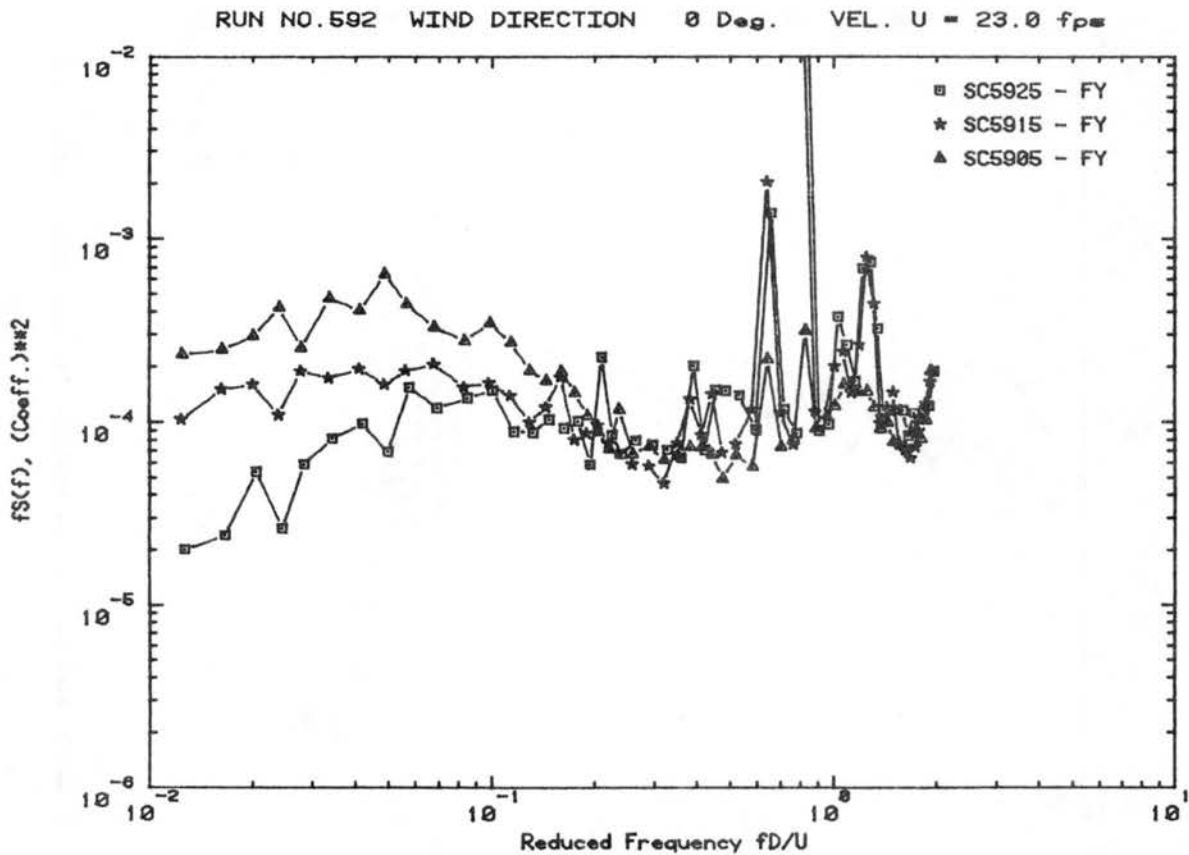
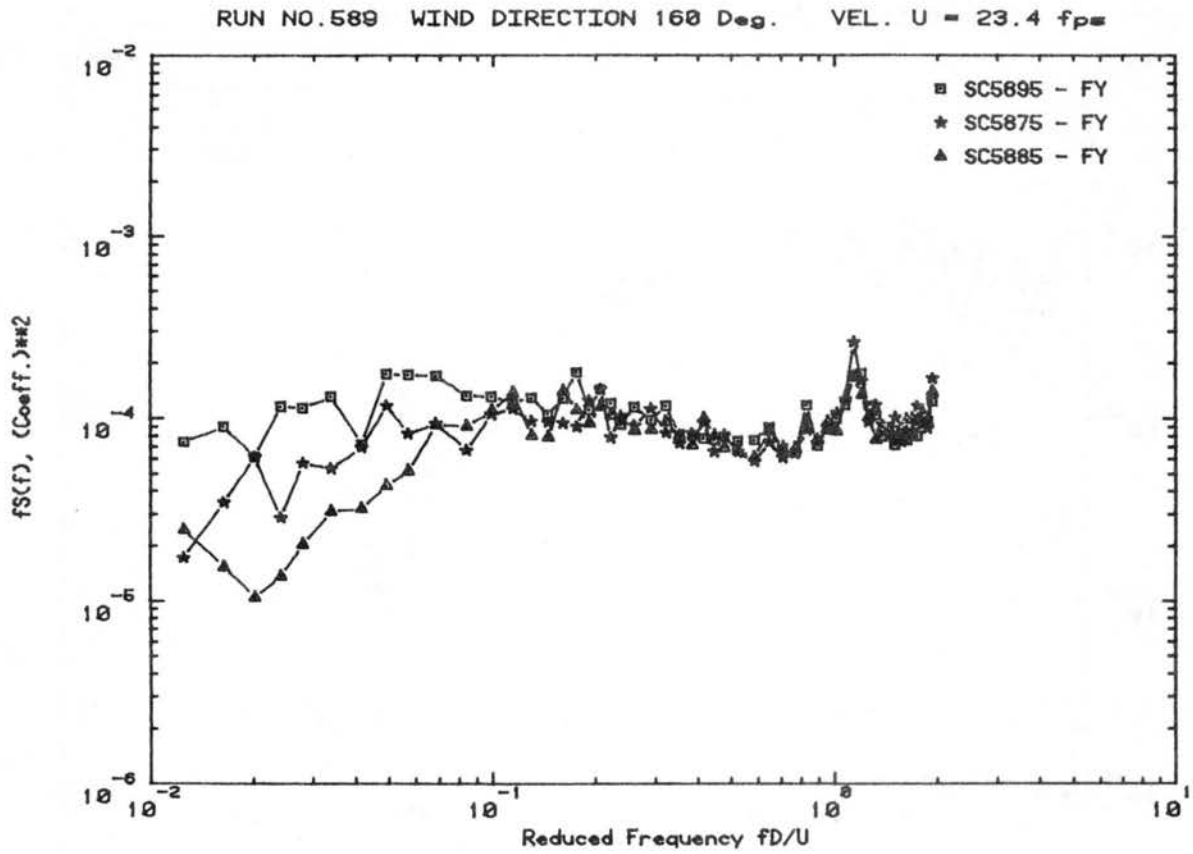
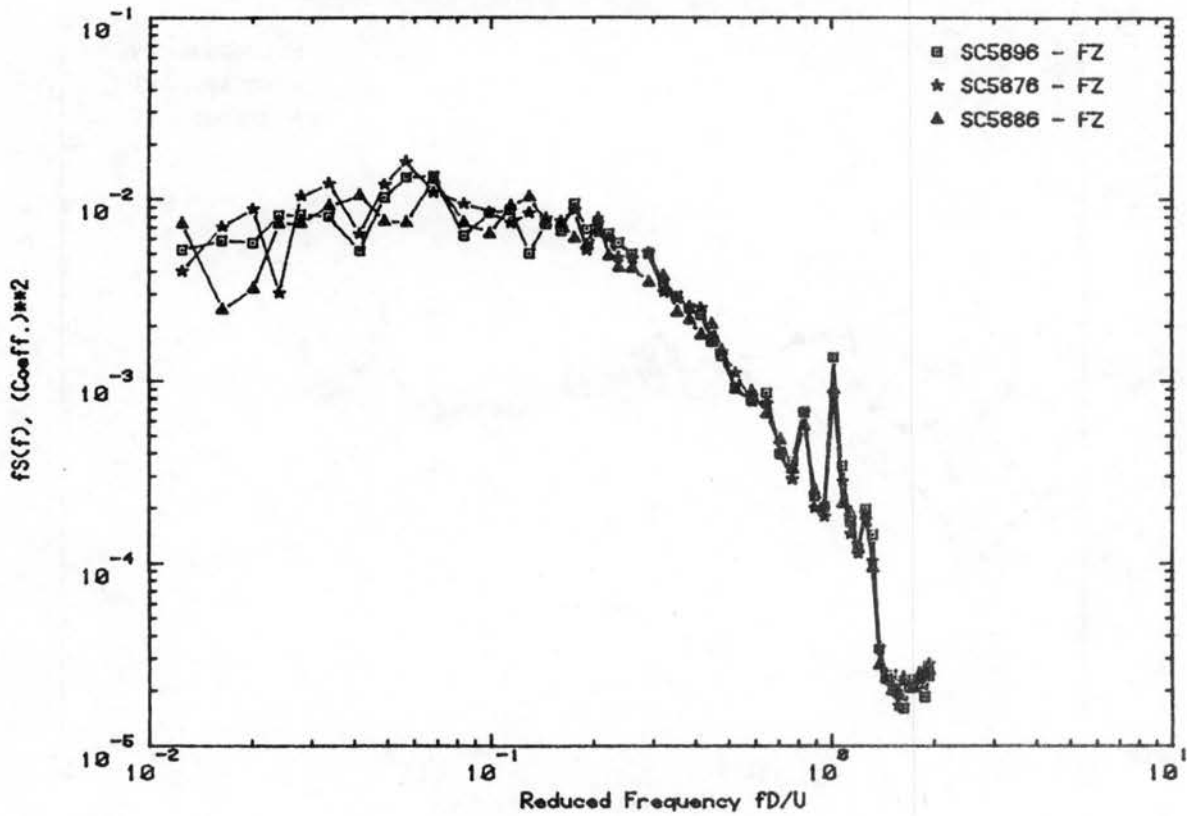


Figure C.9d. Load Spectra for Declination Angle 20° , Hour Angle 0°

RUN NO.589 WIND DIRECTION 160 Deg. VEL. U = 23.4 fps



RUN NO.592 WIND DIRECTION 0 Deg. VEL. U = 23.0 fps

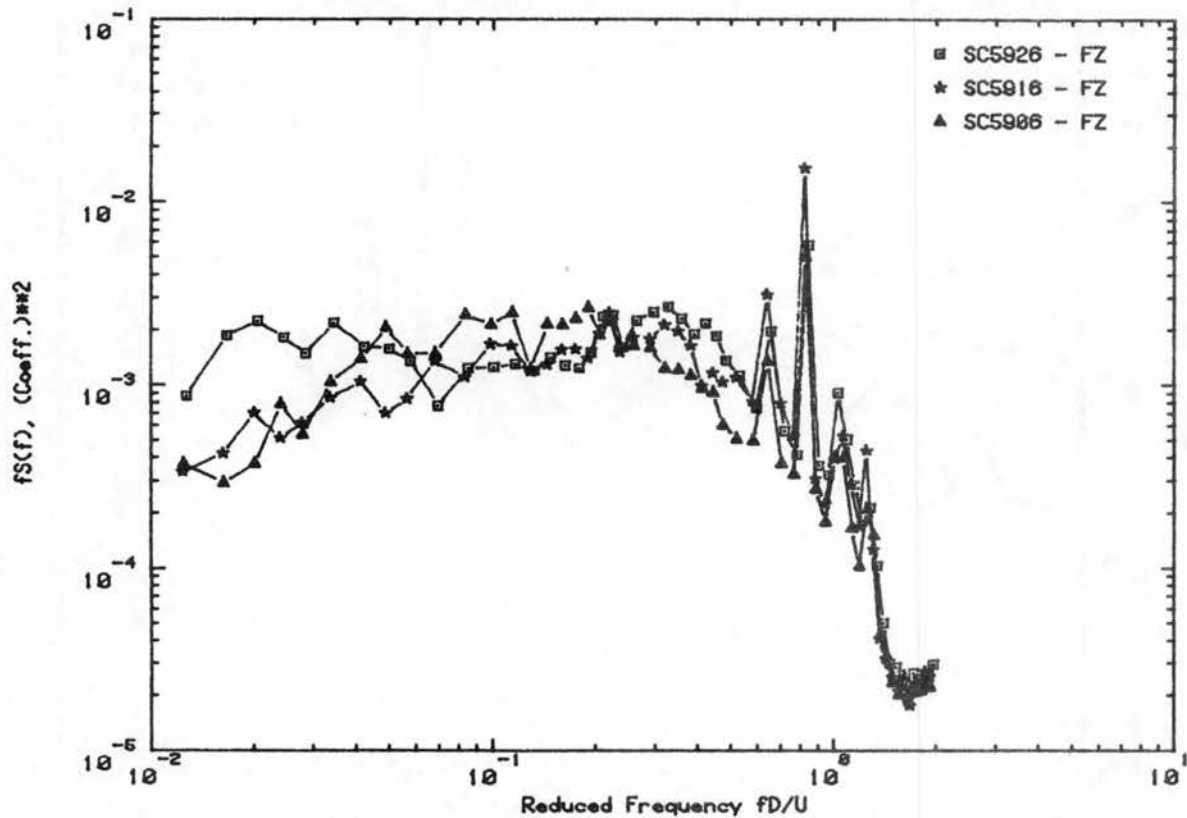


Figure C.9e. Load Spectra for Declination Angle 20°, Hour Angle 0°

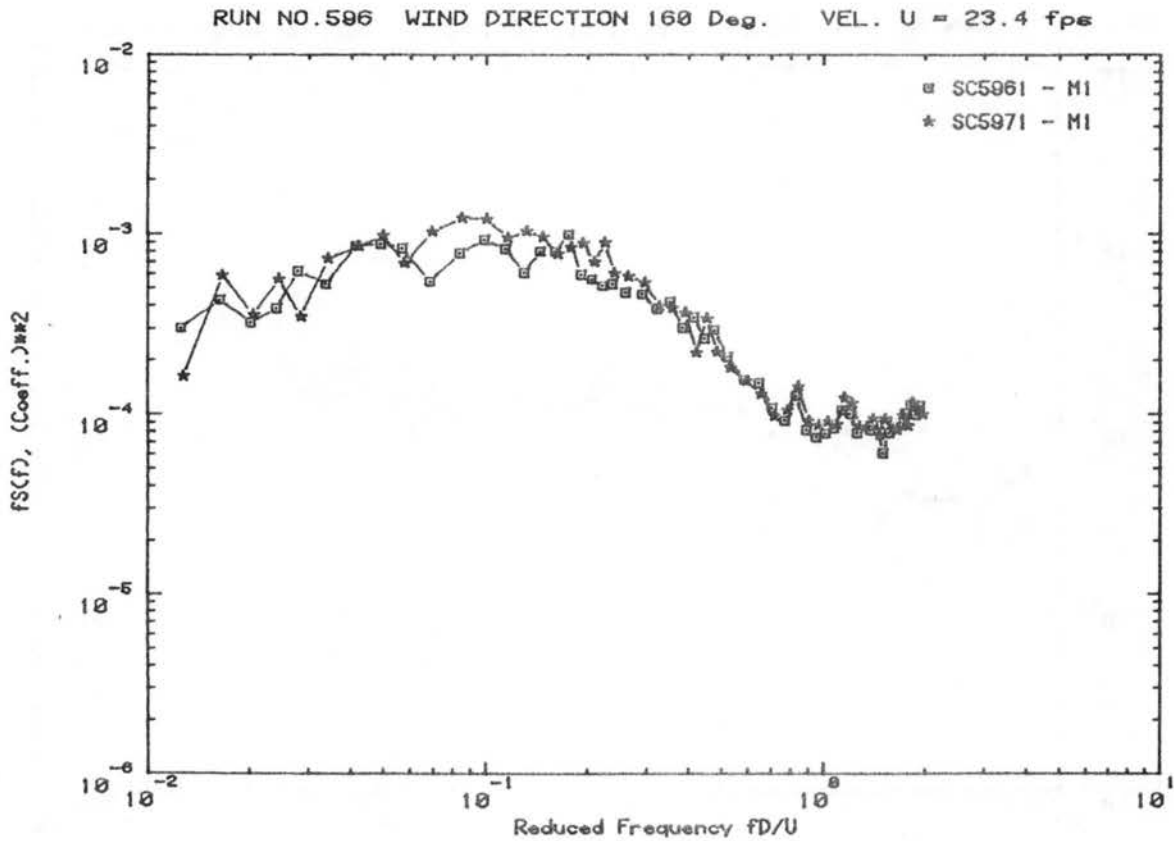
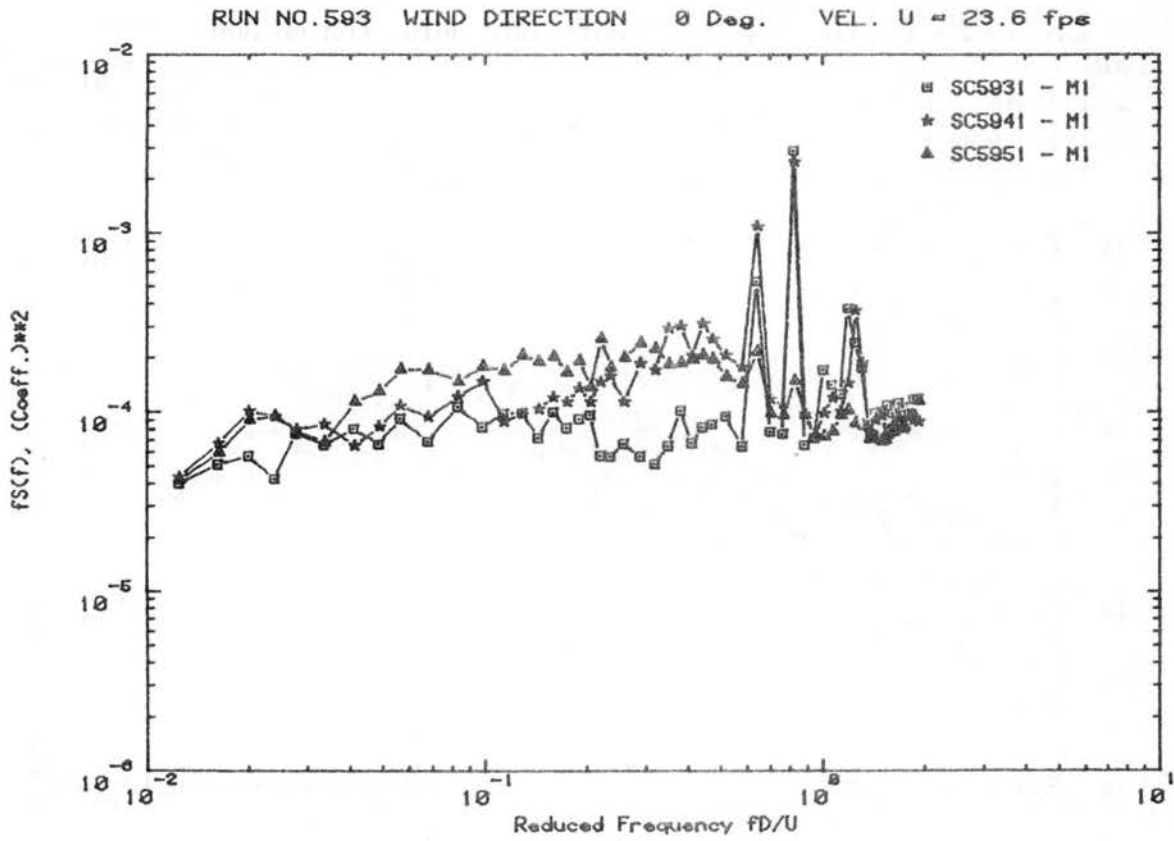
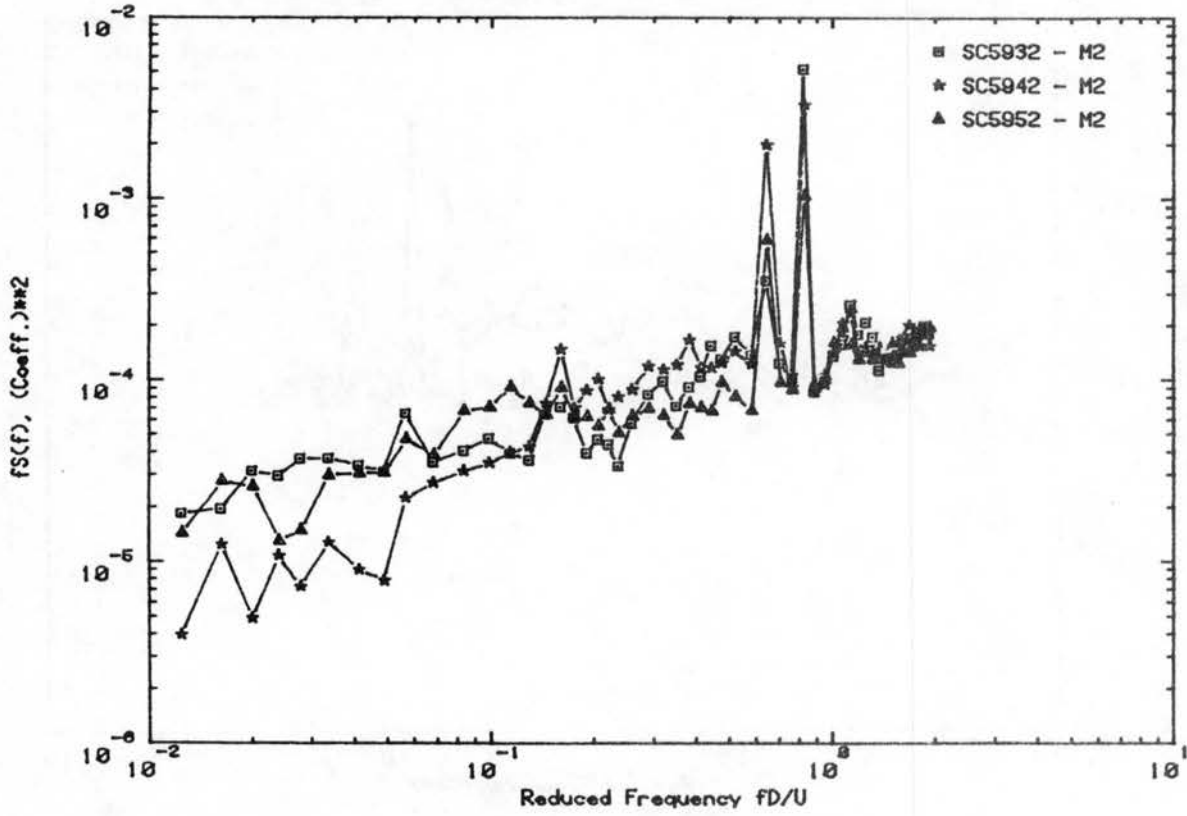


Figure C.10a. Load Spectra for Declination Angle 40° , Hour Angle 0°

RUN NO.593 WIND DIRECTION 0 Deg. VEL. U = 23.6 fps



RUN NO.596 WIND DIRECTION 160 Deg. VEL. U = 23.4 fps

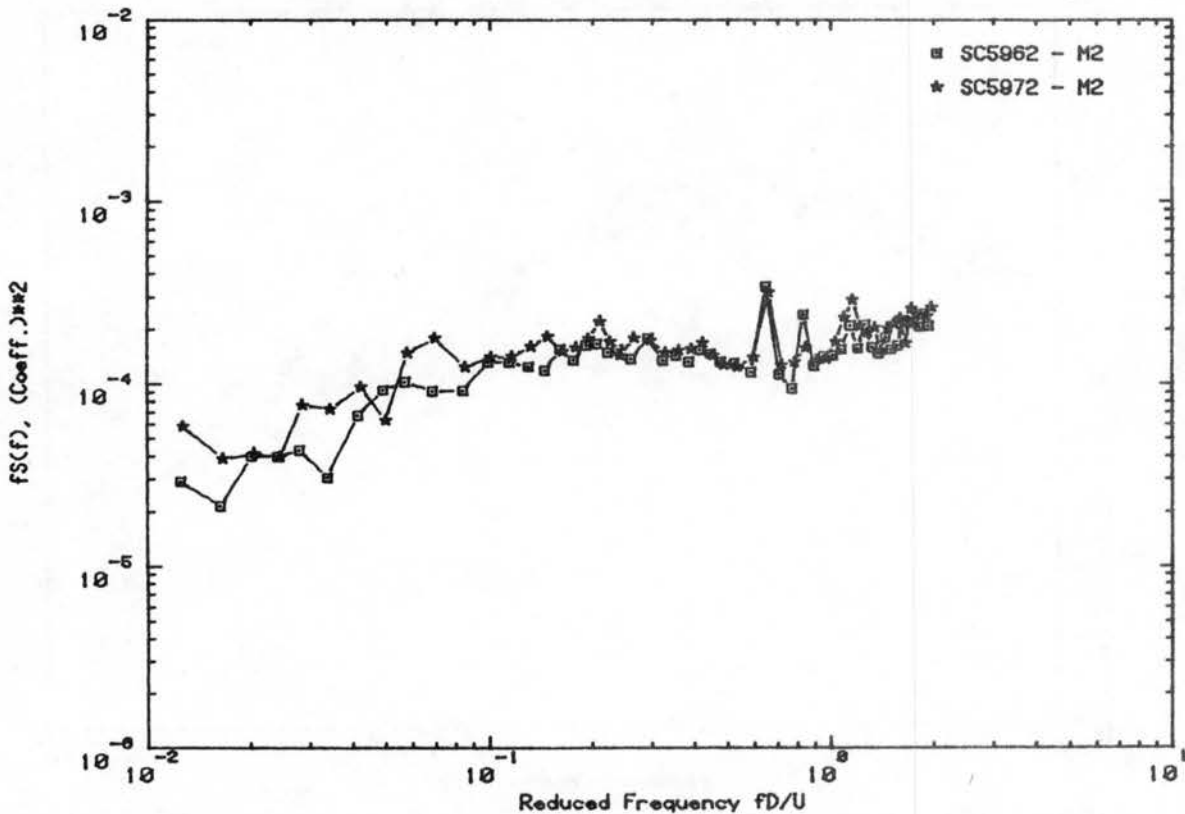


Figure C.10b. Load Spectra for Declination Angle 40°, Hour Angle 0°

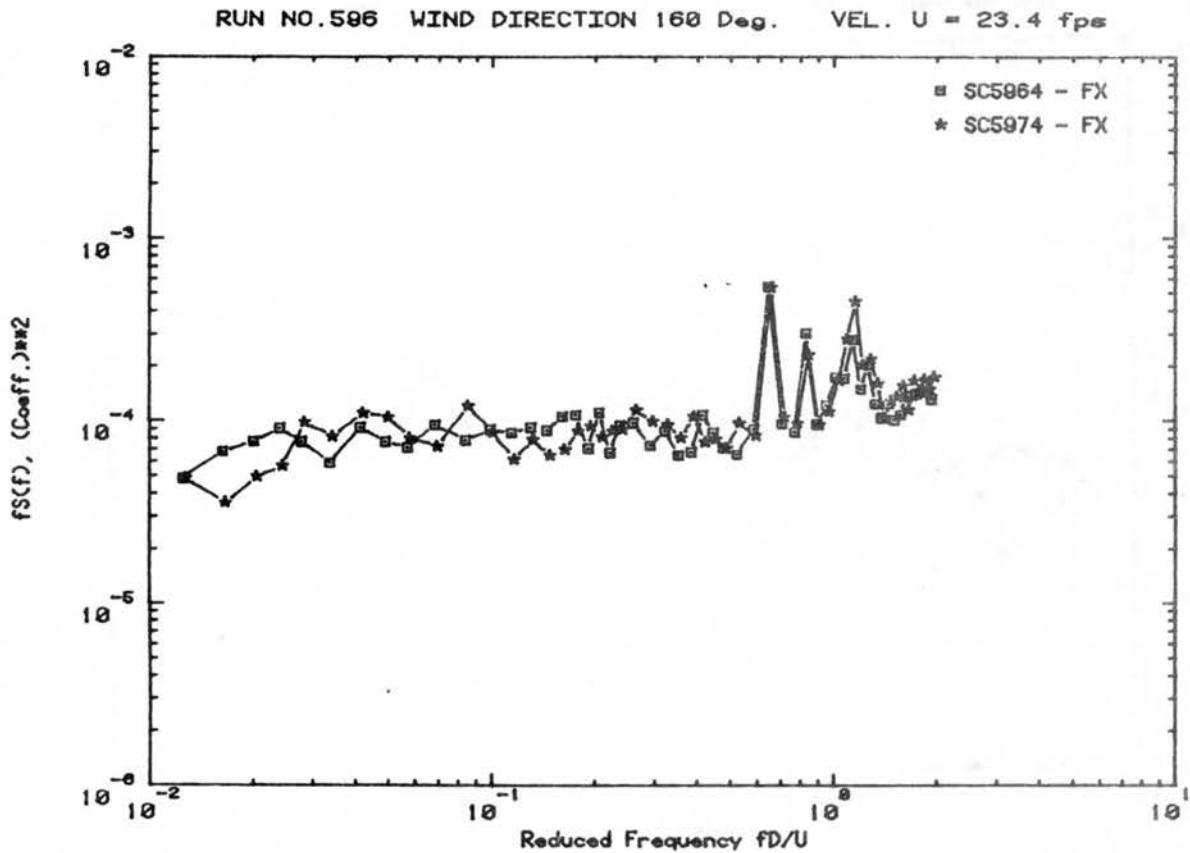
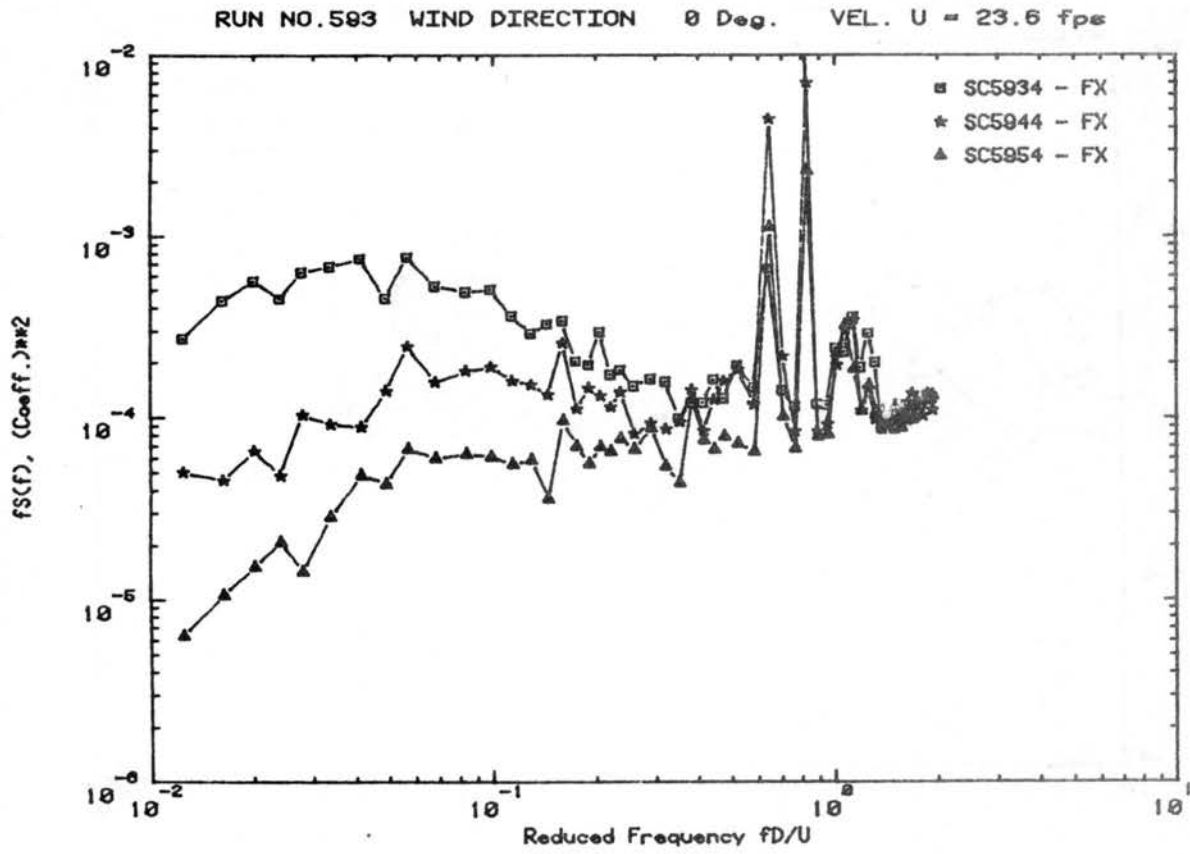
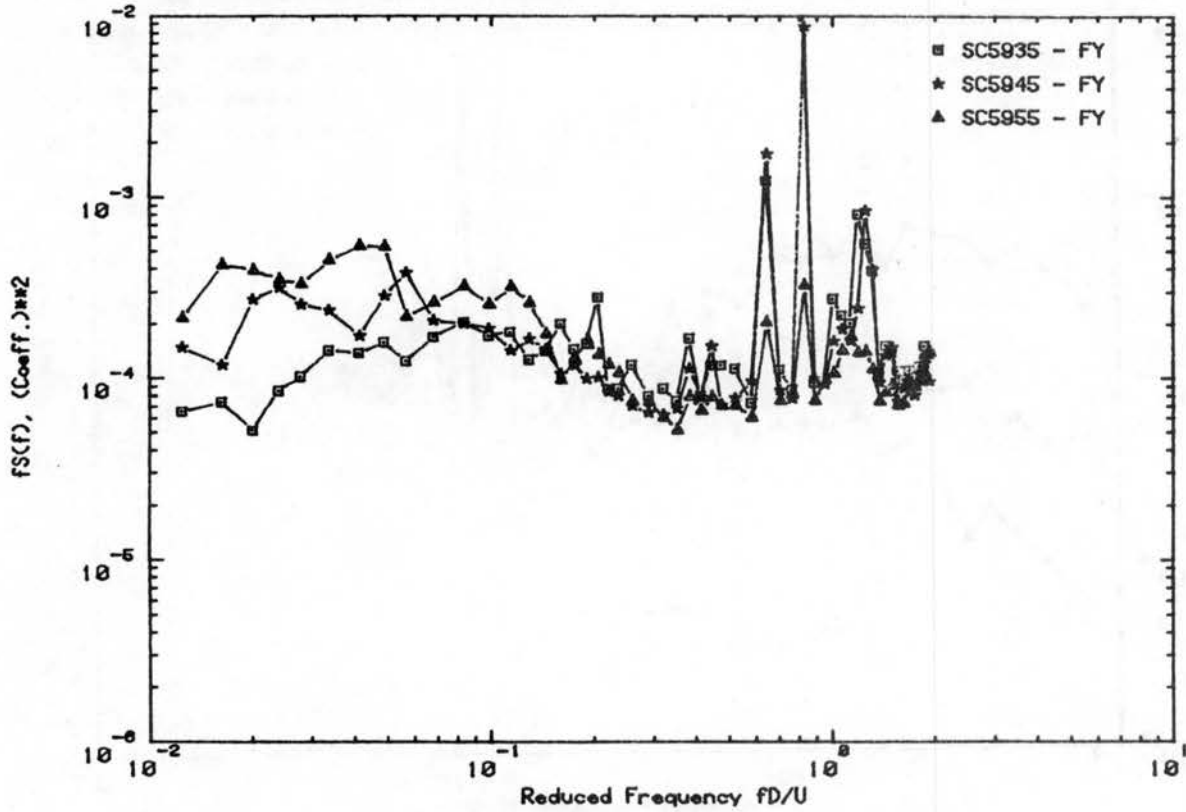


Figure C.10c. Load Spectra for Declination Angle 40° , Hour Angle 0°

RUN NO.593 WIND DIRECTION 0 Deg. VEL. U = 23.6 fps



RUN NO.596 WIND DIRECTION 160 Deg. VEL. U = 23.4 fps

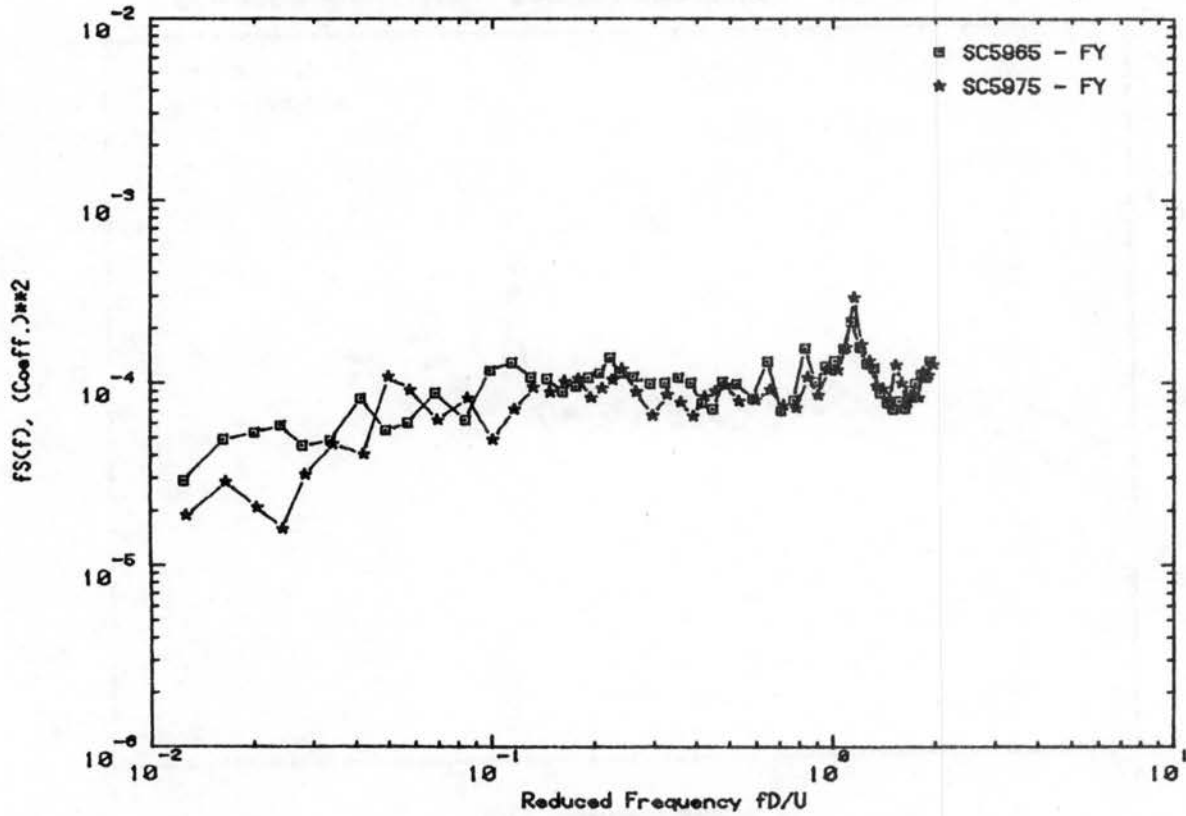


Figure C.10d. Load Spectra for Declination Angle 40°, Hour Angle 0°

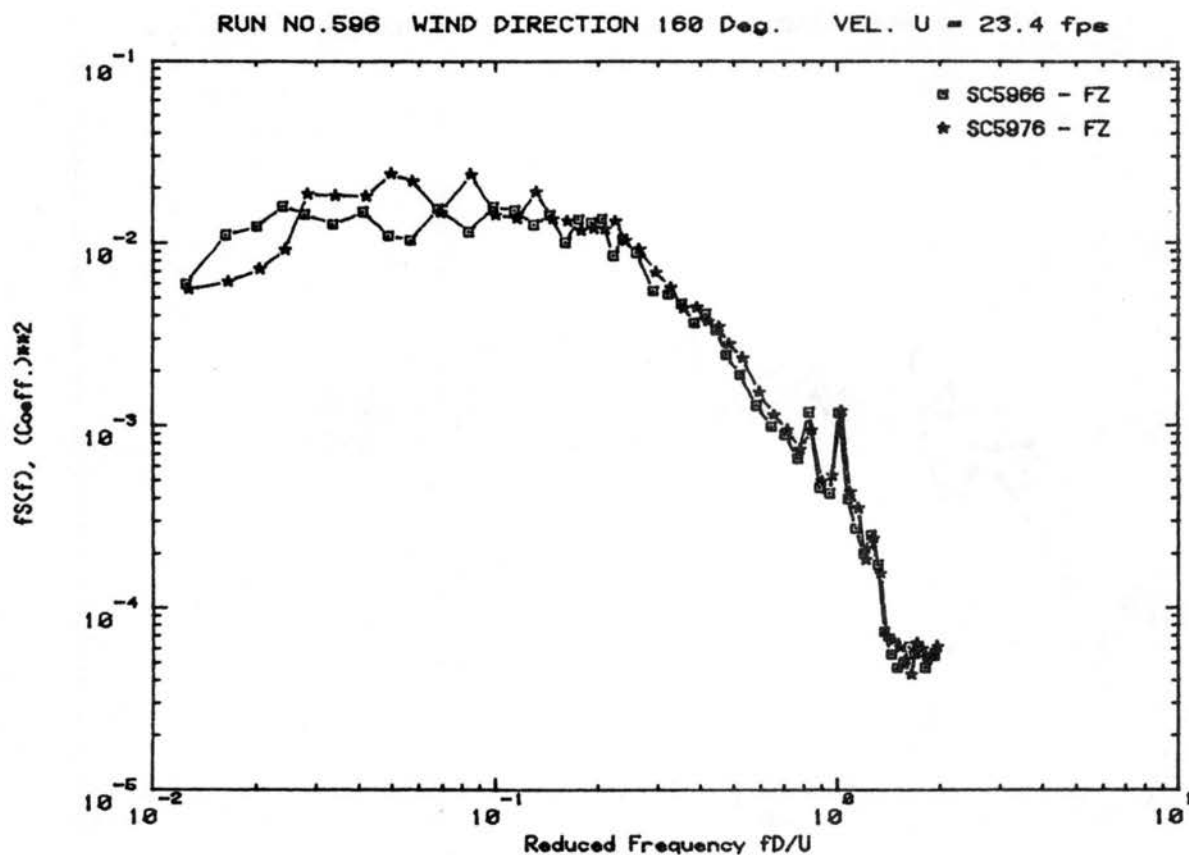
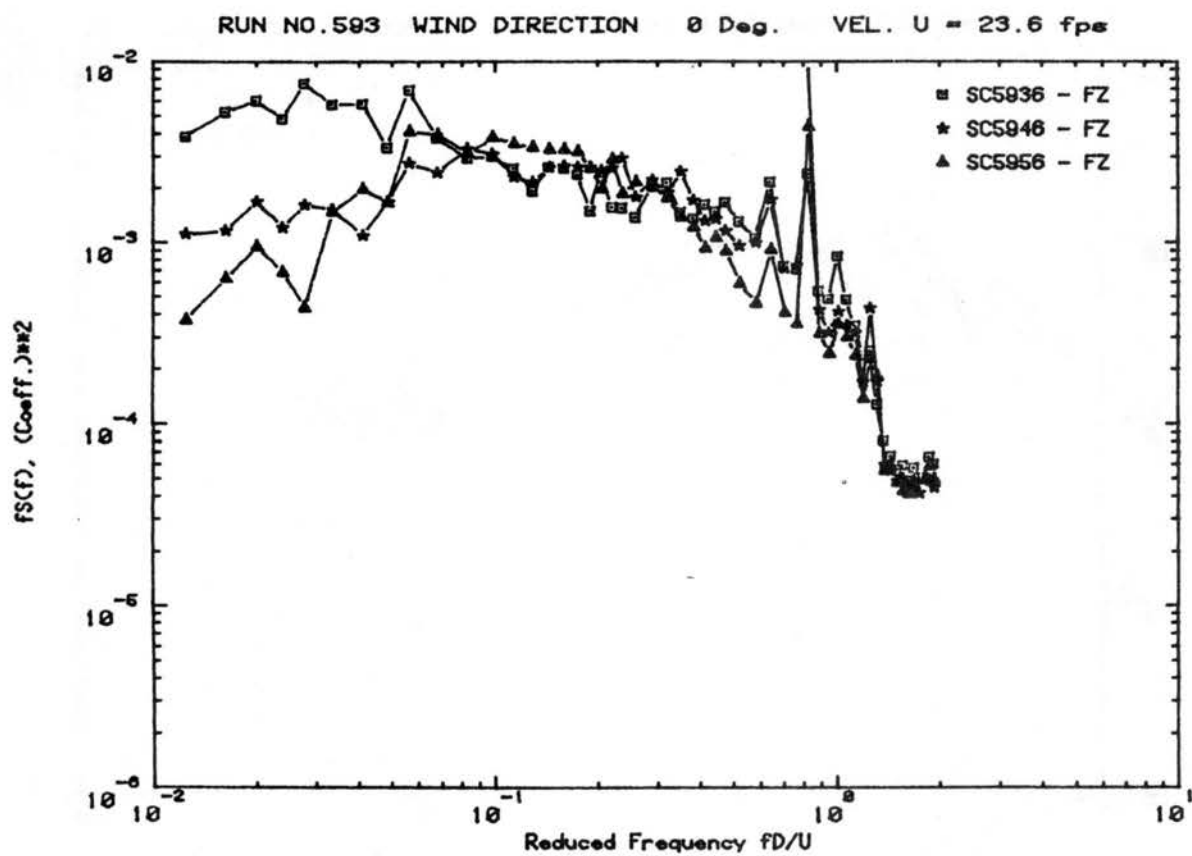
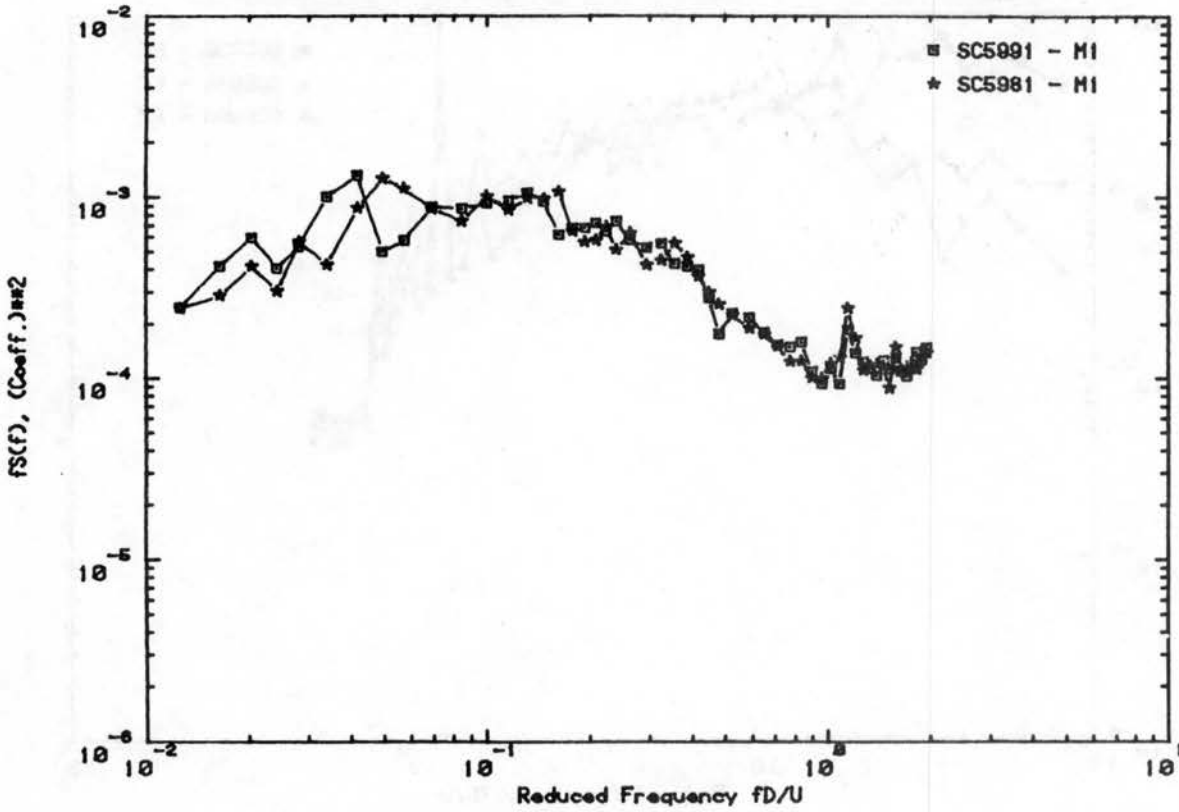


Figure C.10e. Load Spectra for Declination Angle 40° , Hour Angle 0°

RUN NO.599 WIND DIRECTION 160 Deg. VEL. U = 23.2 fps



RUN NO.600 WIND DIRECTION 90 Deg. VEL. U = 23.4 fps

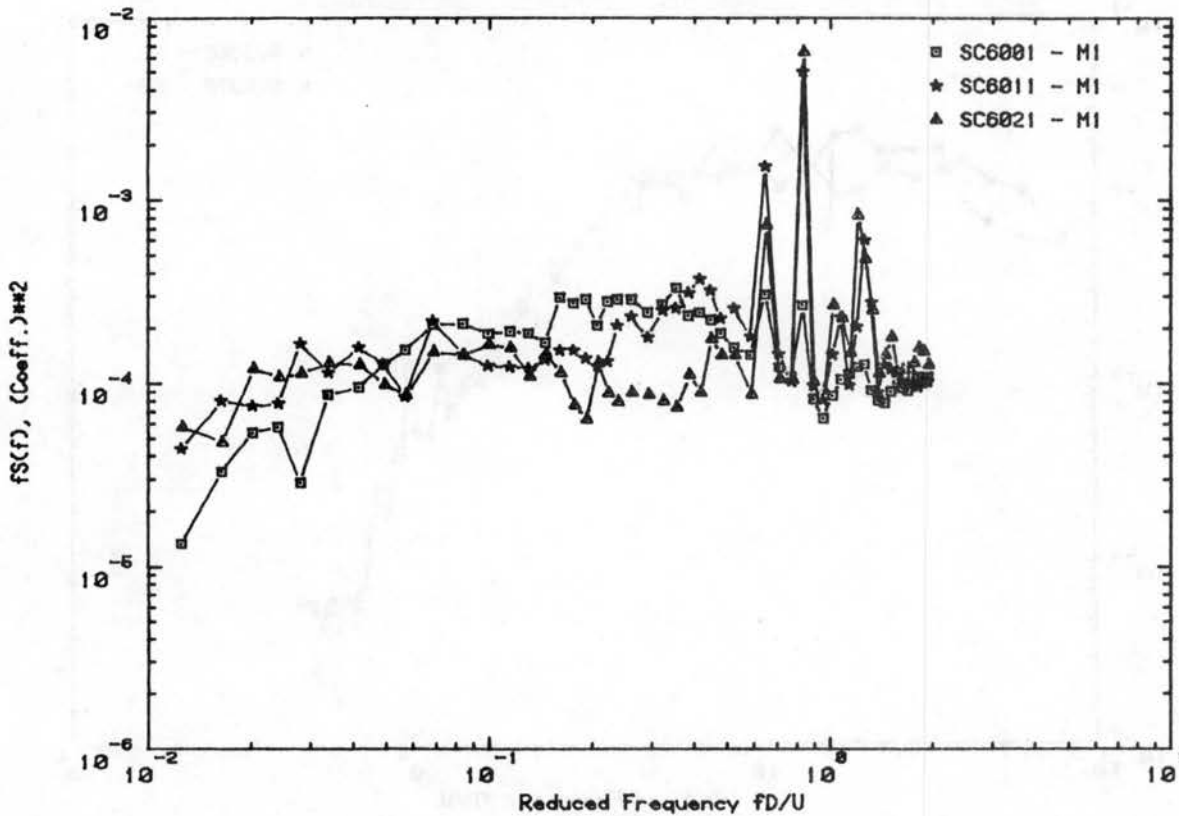


Figure C.11a. Load Spectra for Declination Angle 50°, Hour Angle 0°

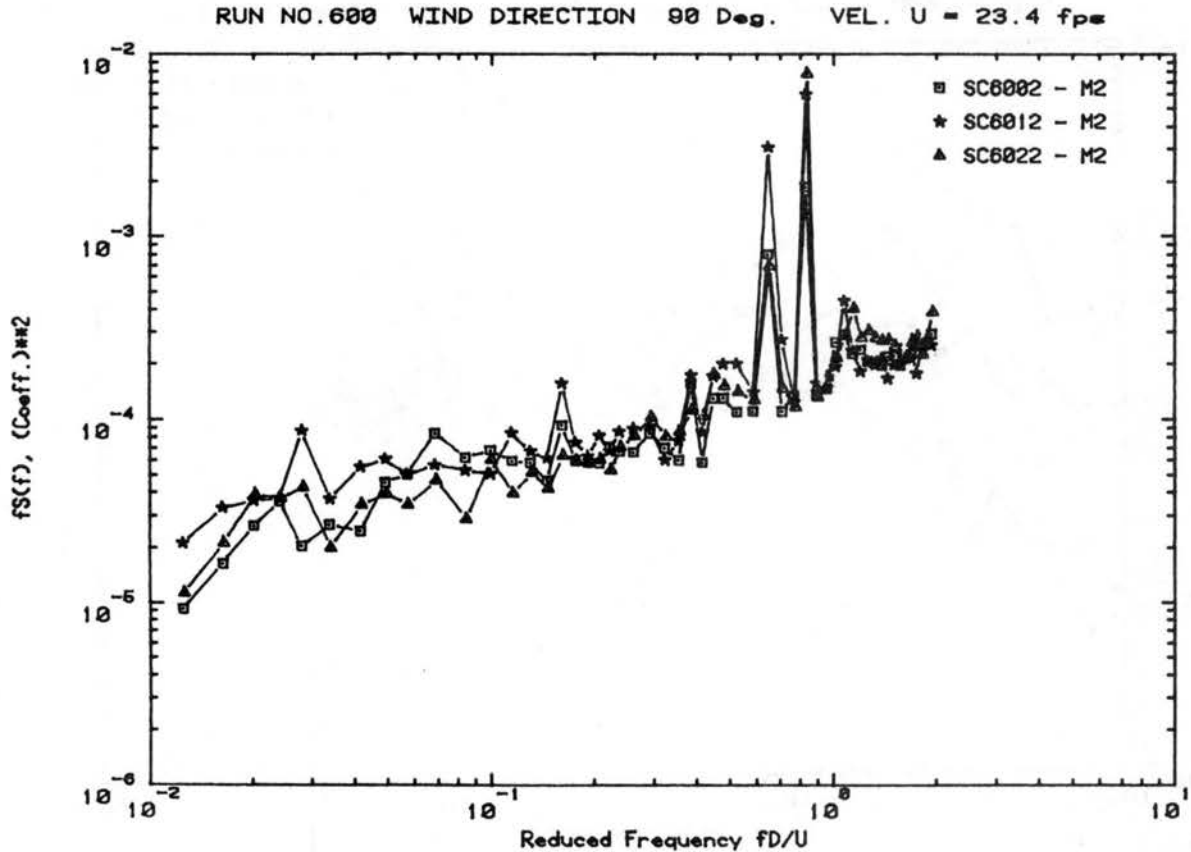
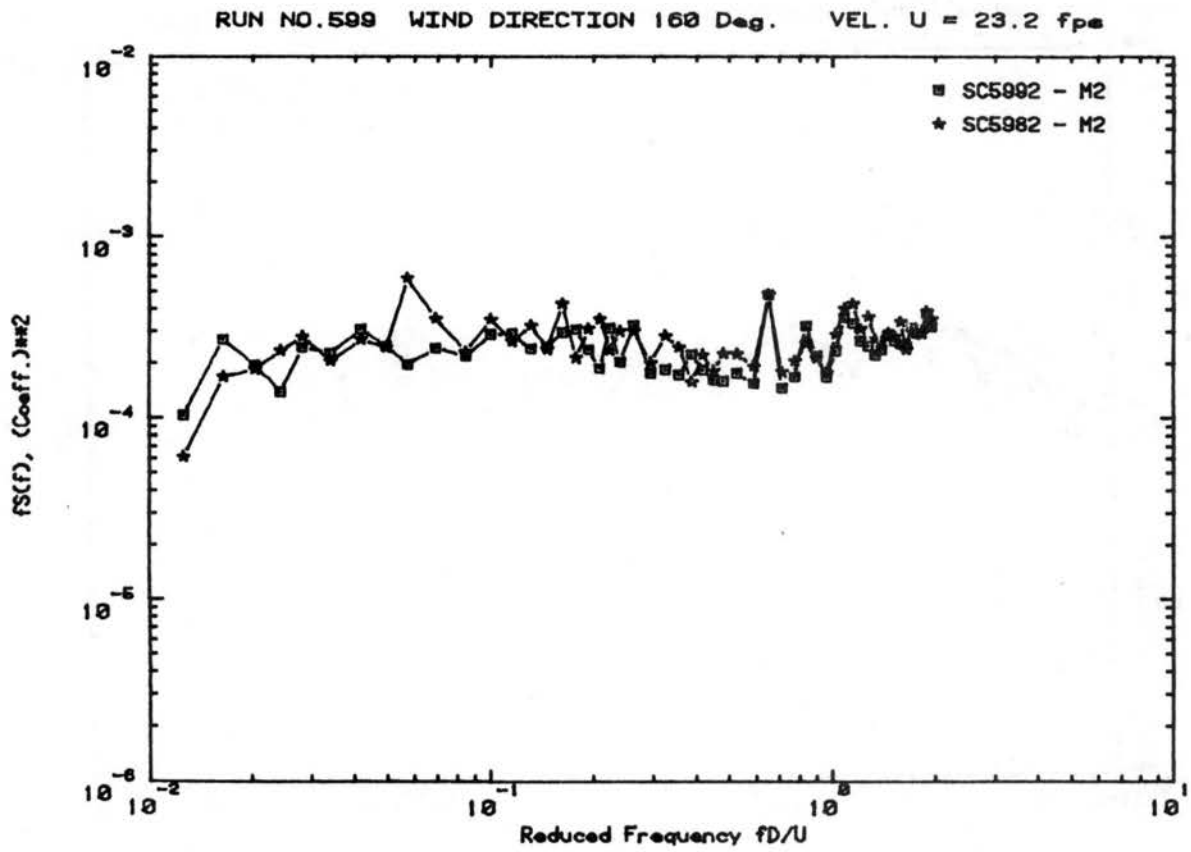


Figure C.11b. Load Spectra for Declination Angle 50° , Hour Angle 0°

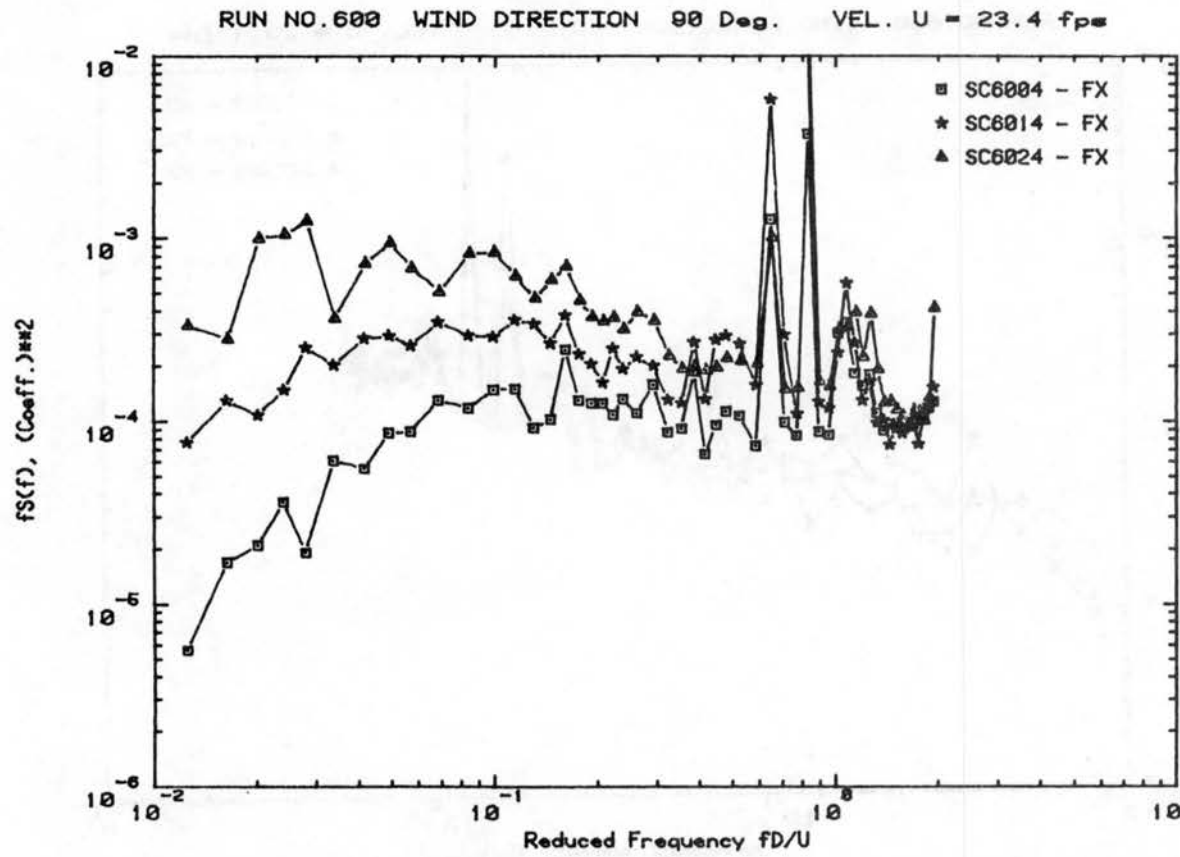
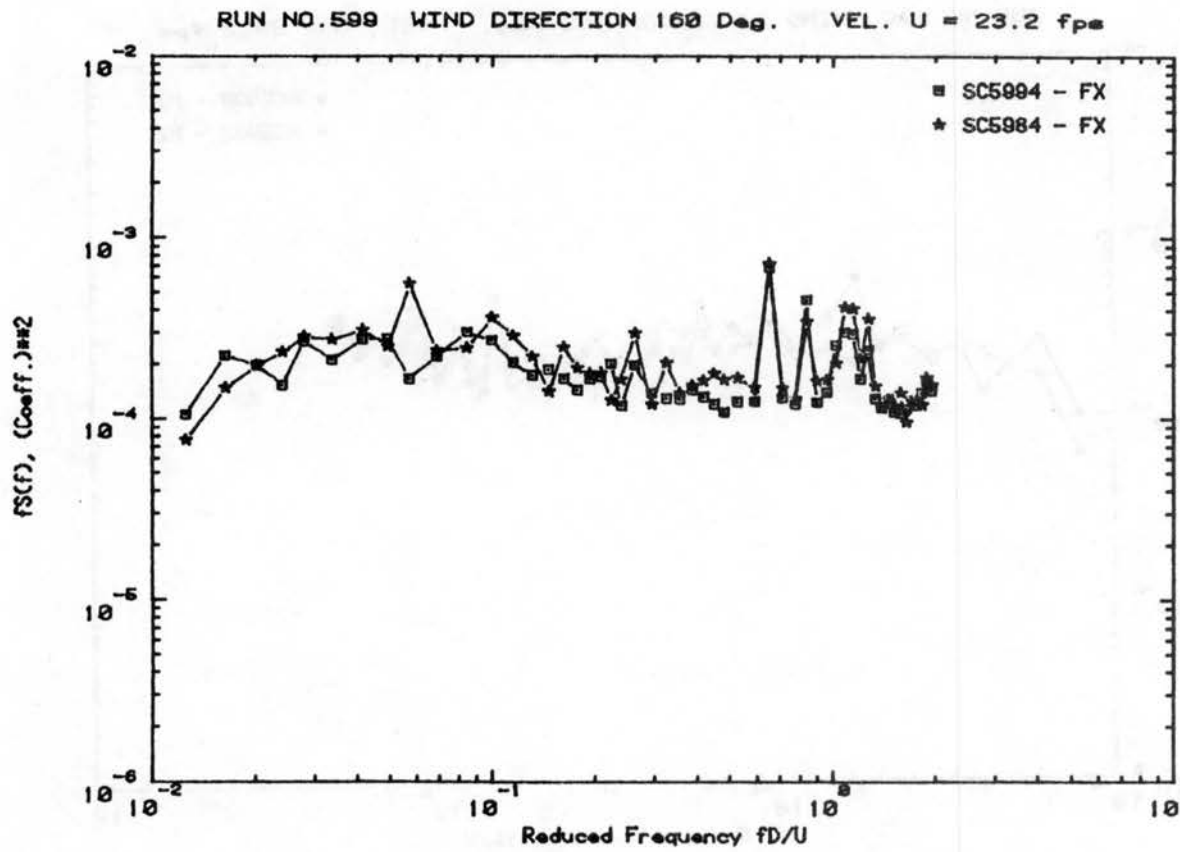


Figure C.11c. Load Spectra for Declination Angle 50°, Hour Angle 0°

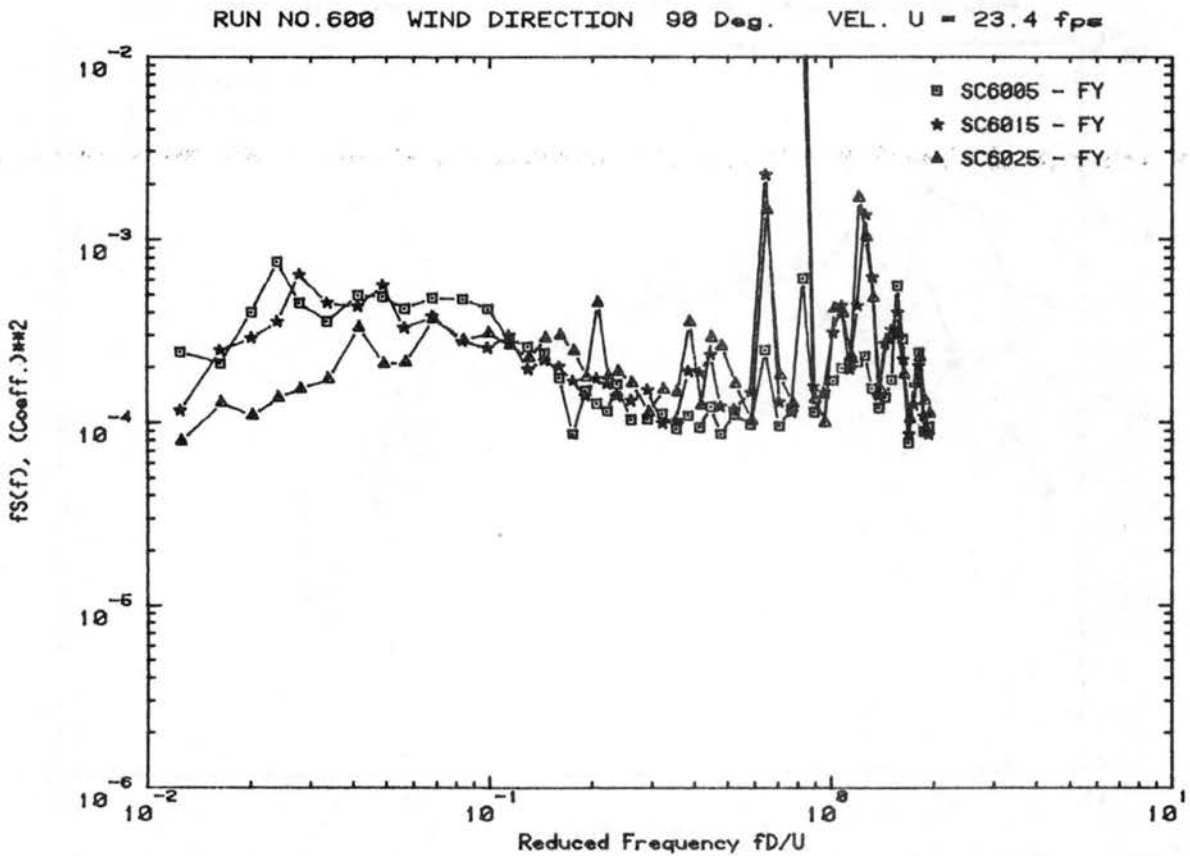
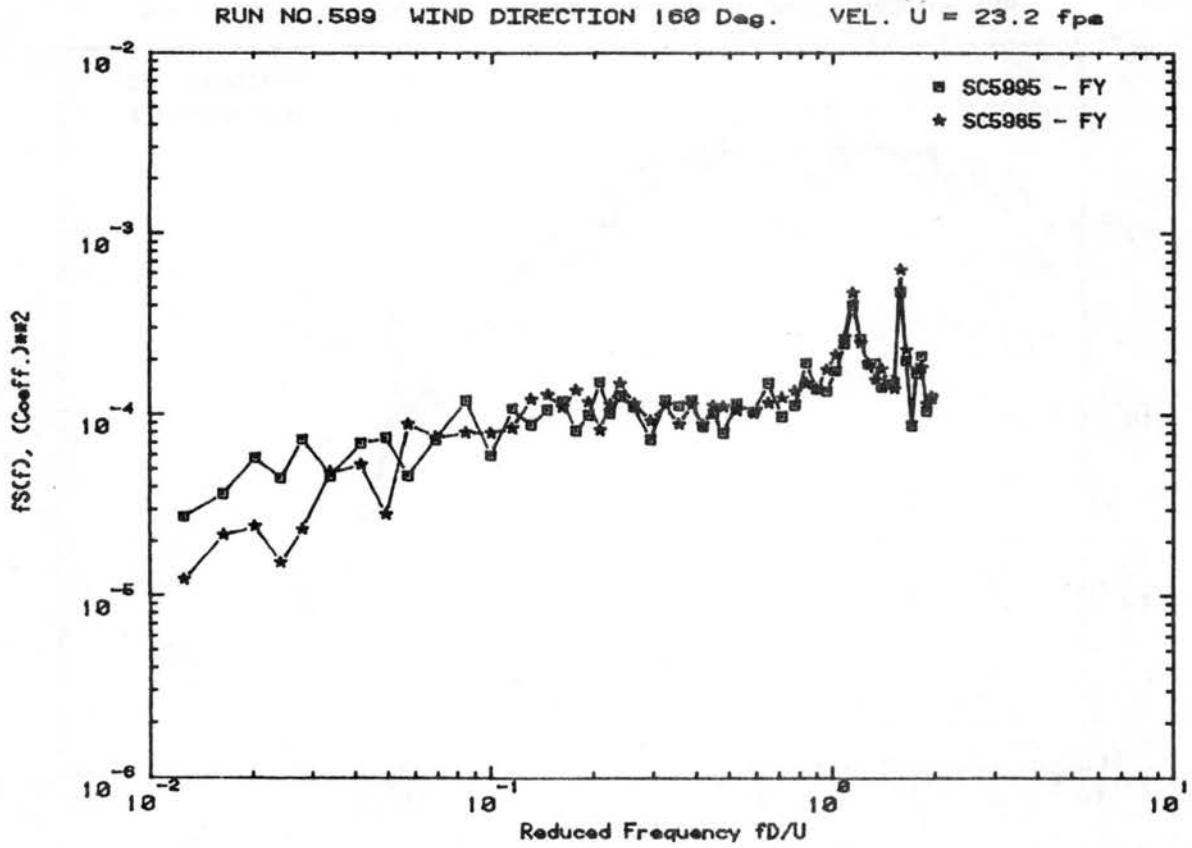
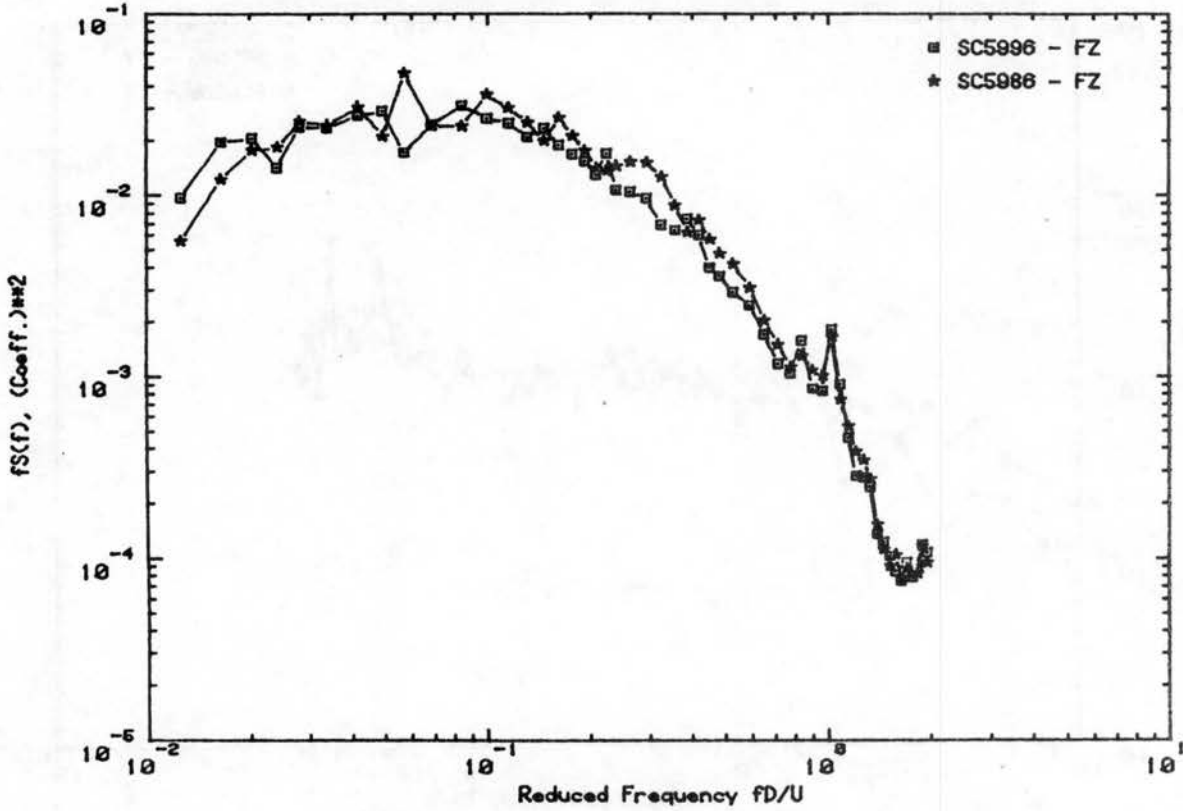


Figure C.11d. Load Spectra for Declination Angle 50° , Hour Angle 0°

RUN NO. 599 WIND DIRECTION 160 Deg. VEL. U = 23.2 fps



RUN NO. 600 WIND DIRECTION 90 Deg. VEL. U = 23.4 fps

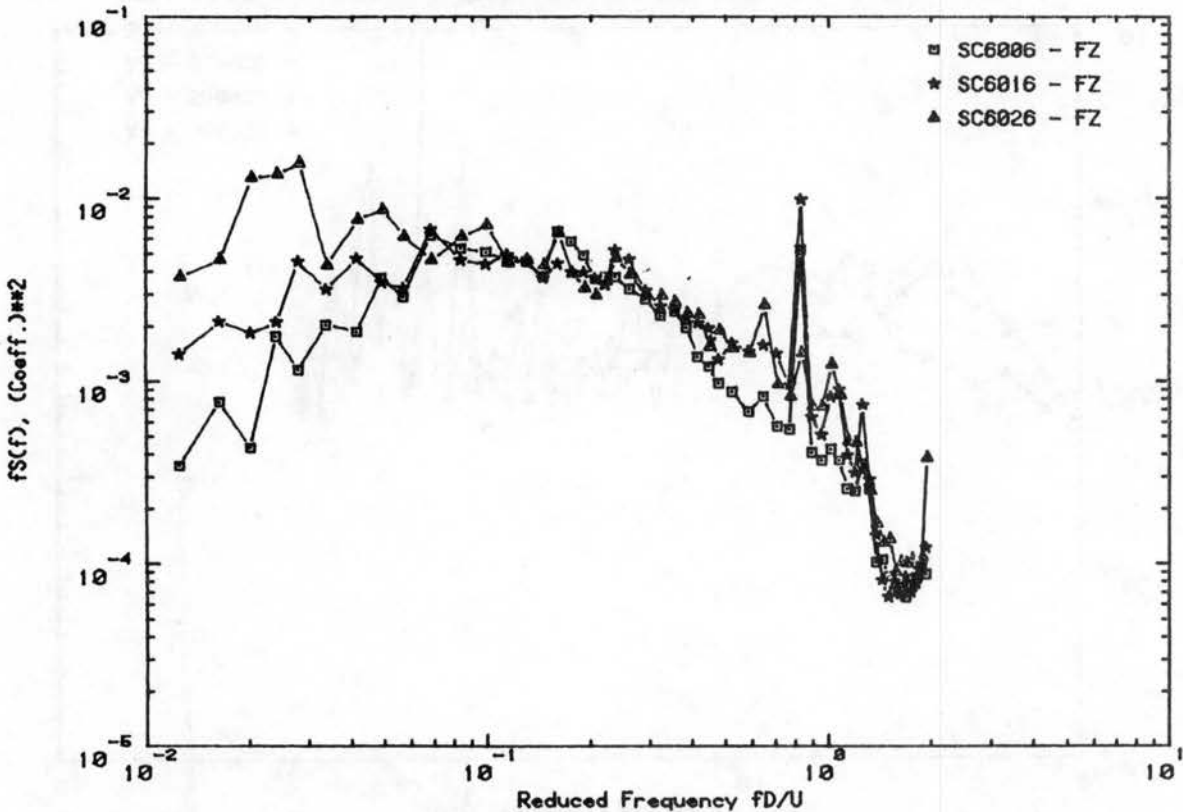


Figure C.11e. Load Spectra for Declination Angle 50°, Hour Angle 0°

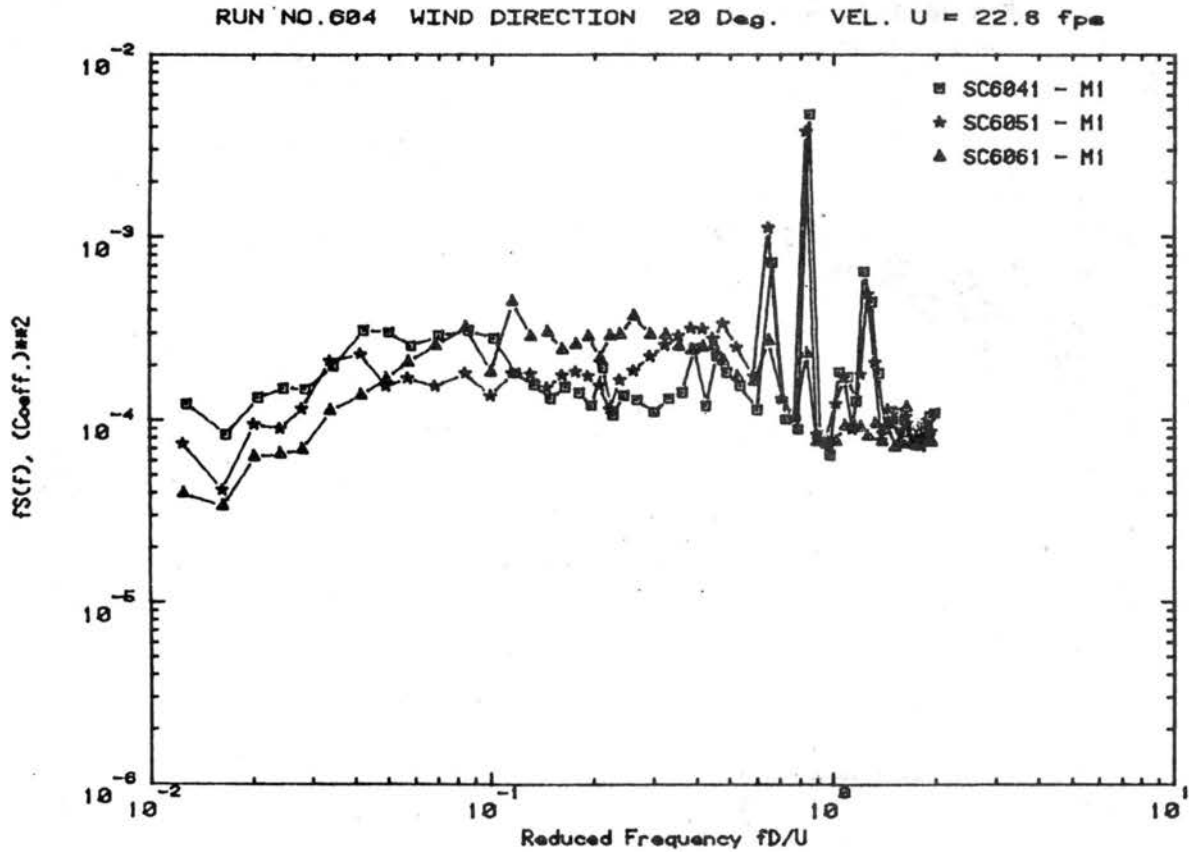
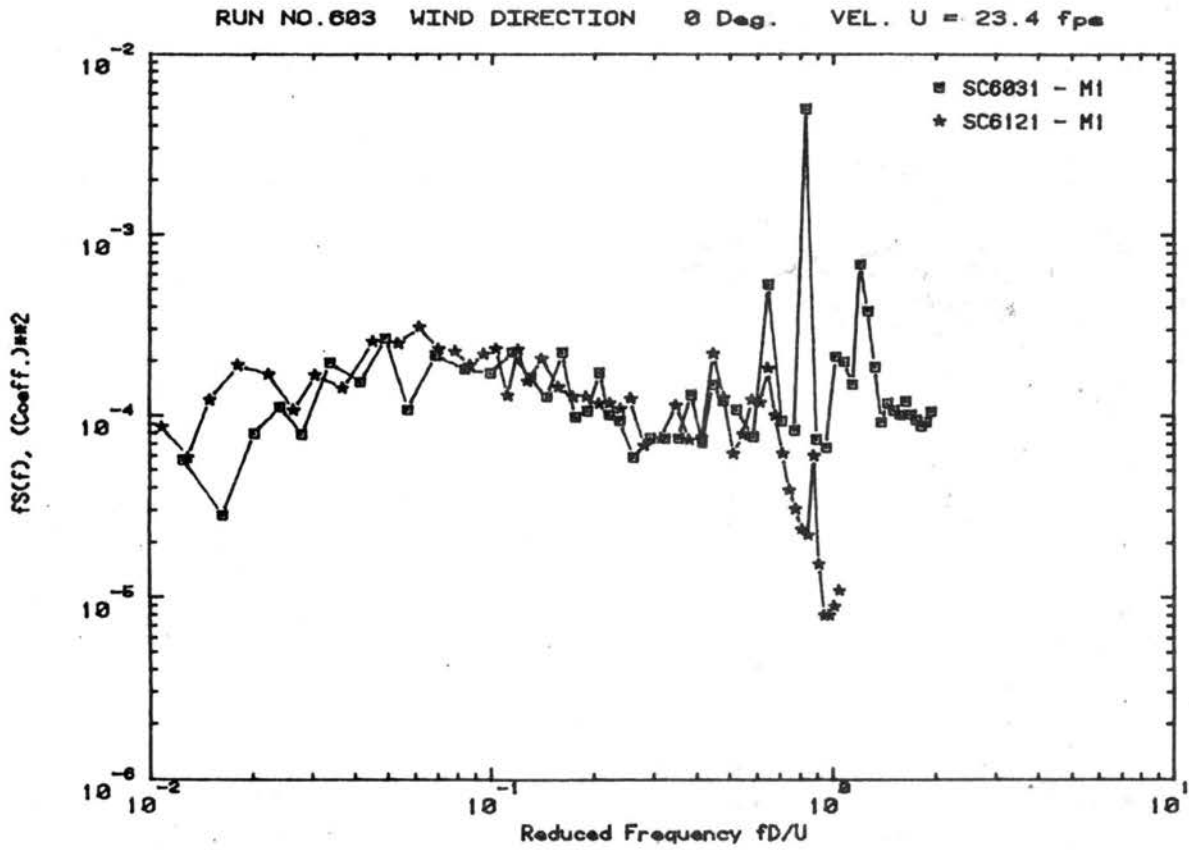
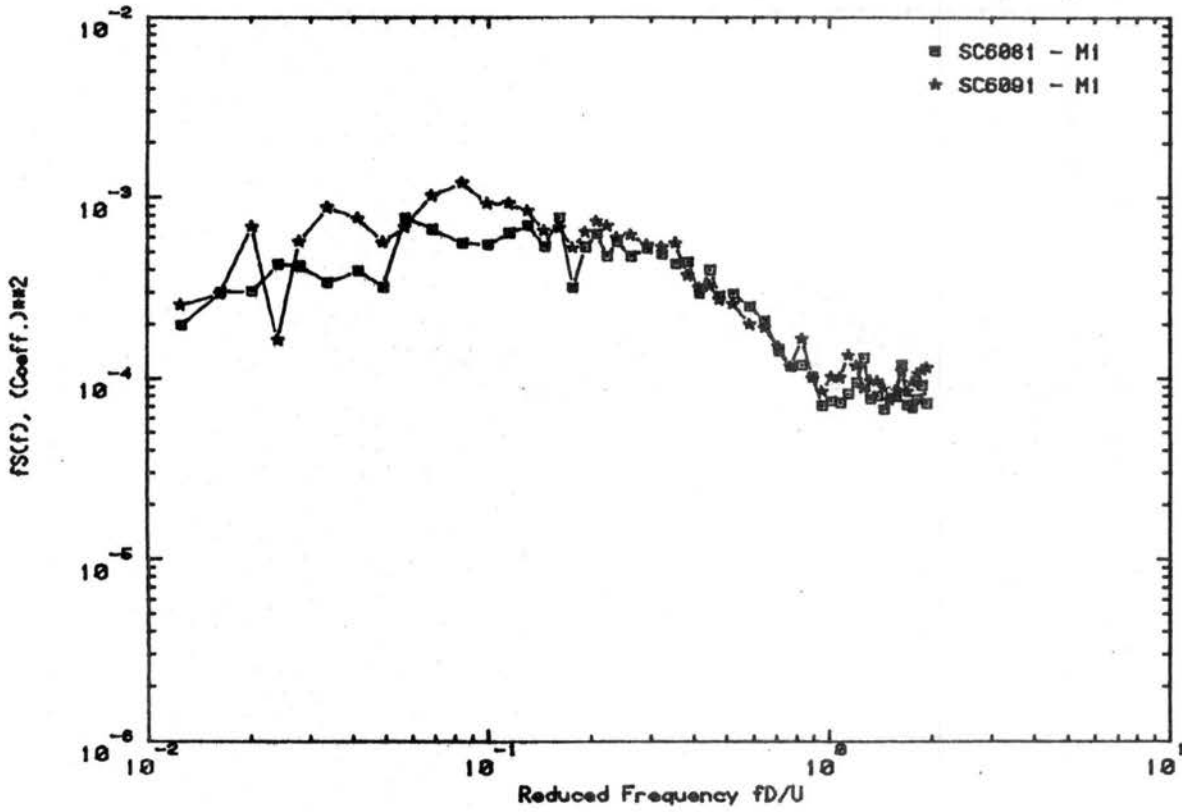


Figure C.12a. Load Spectra for Declination Angle 60° , Hour Angle 0°

RUN NO. 688 WIND DIRECTION 120 Deg. VEL. U = 23.3 fps



RUN NO. 618 WIND DIRECTION 180 Deg. VEL. U = 22.7 fps

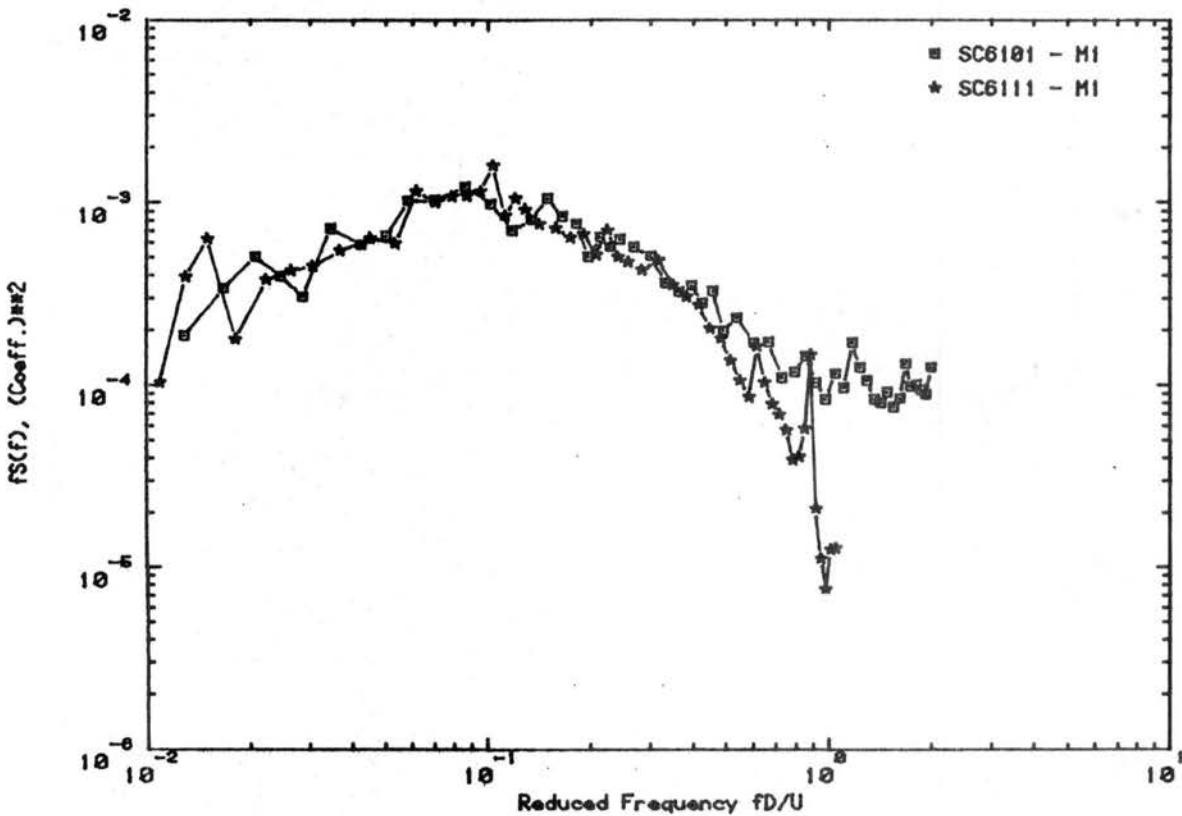
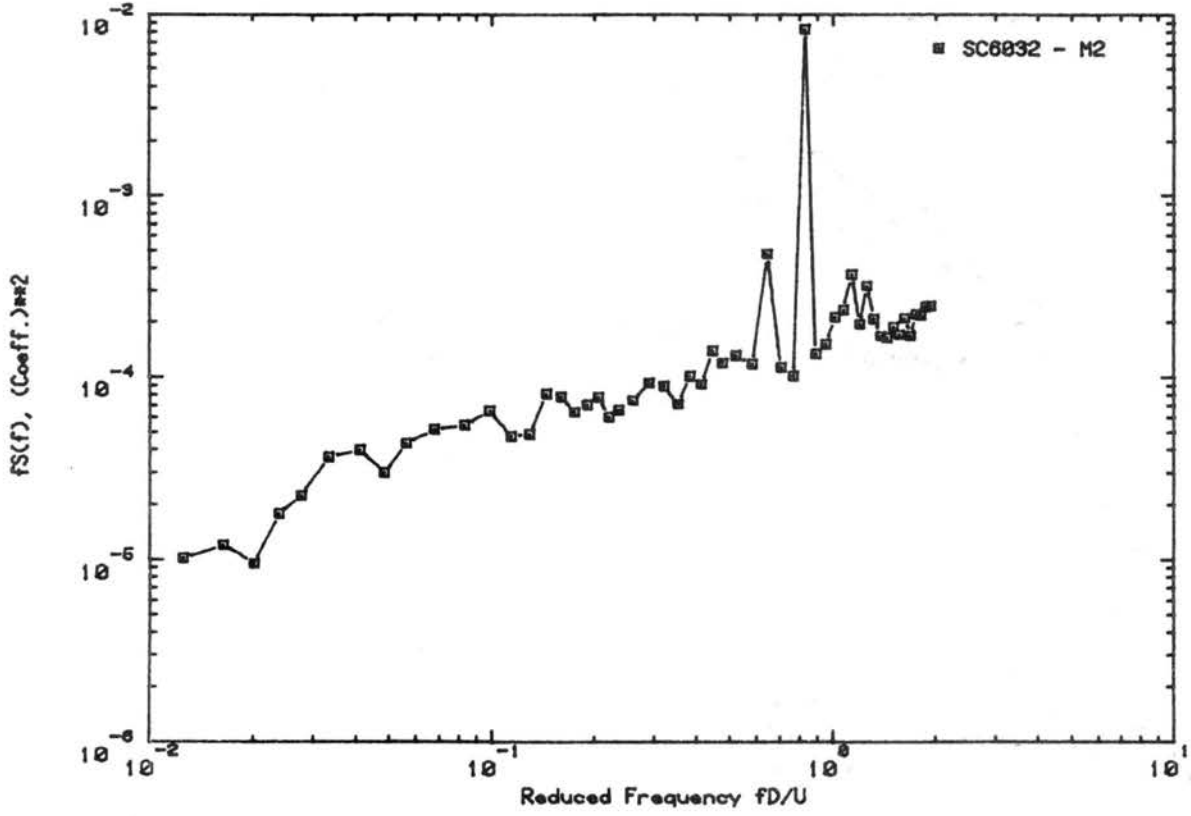


Figure C.12b. Load Spectra for Declination Angle 60° , Hour Angle 0°

RUN NO. 603 WIND DIRECTION 0 Deg. VEL. U = 23.4 fps



RUN NO. 604 WIND DIRECTION 20 Deg. VEL. U = 22.8 fps

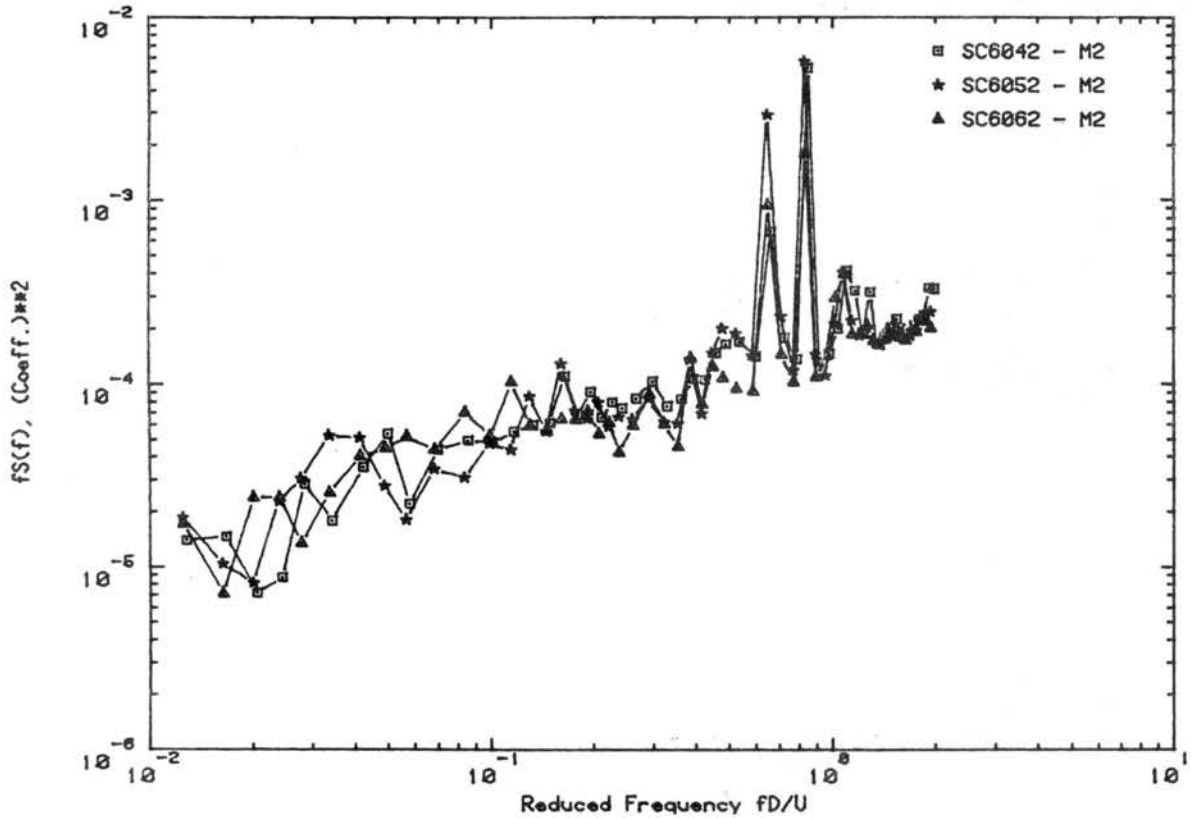
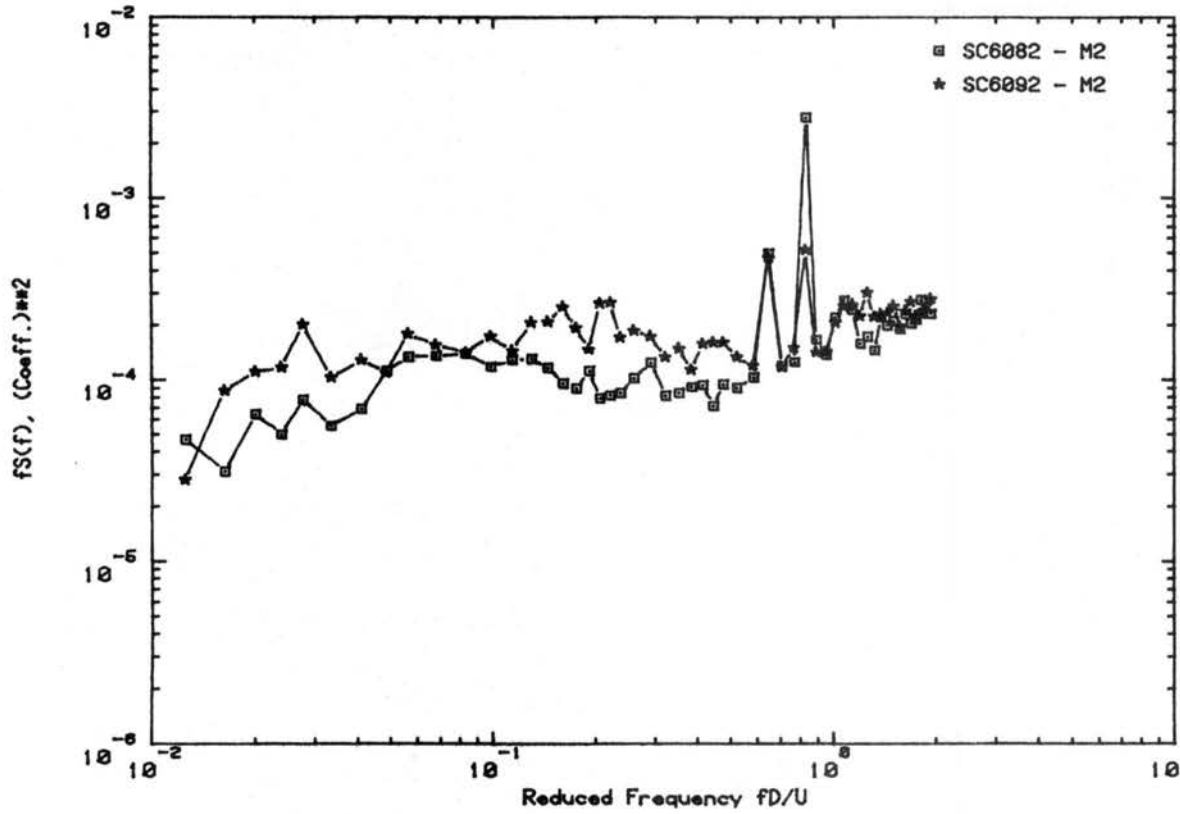


Figure C.12c. Load Spectra for Declination Angle 60°, Hour Angle 0°

RUN NO. 608 WIND DIRECTION 120 Deg. VEL. U = 23.3 fps



RUN NO. 610 WIND DIRECTION 180 Deg. VEL. U = 22.7 fps

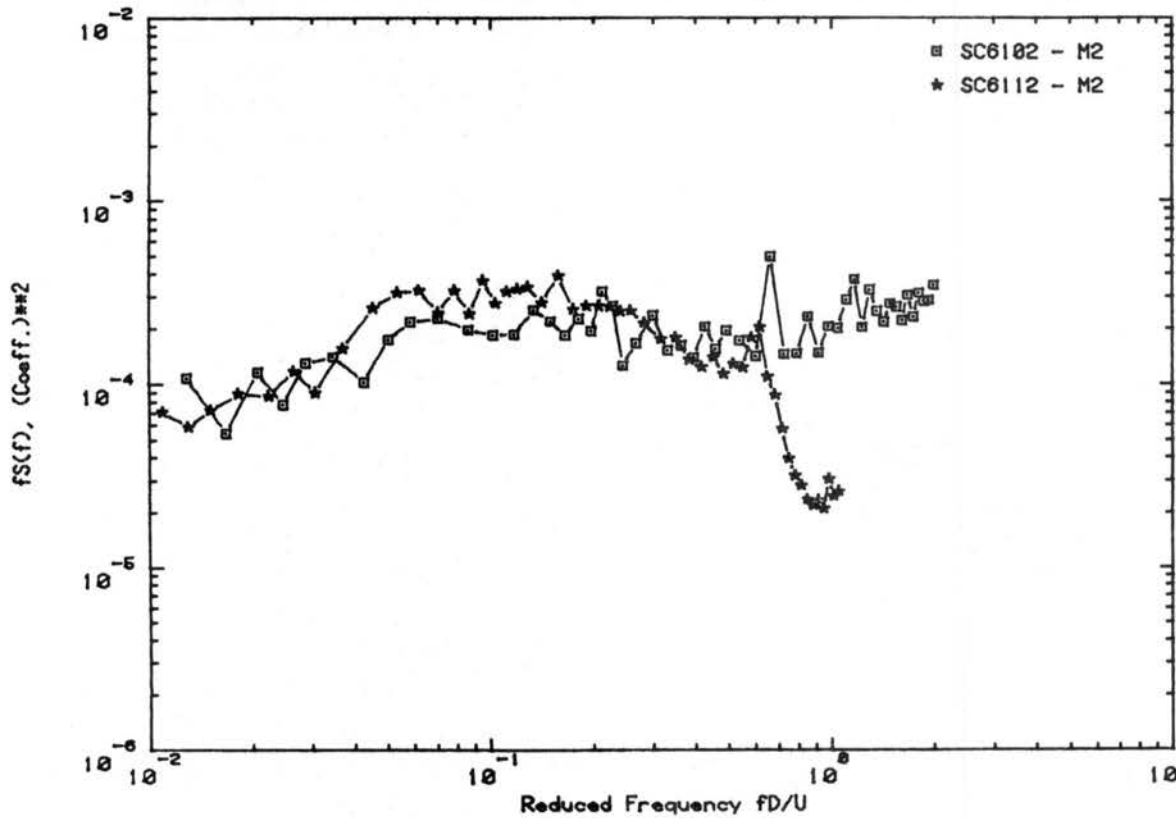


Figure C.12d. Load Spectra for Declination Angle 60°, Hour Angle 0°

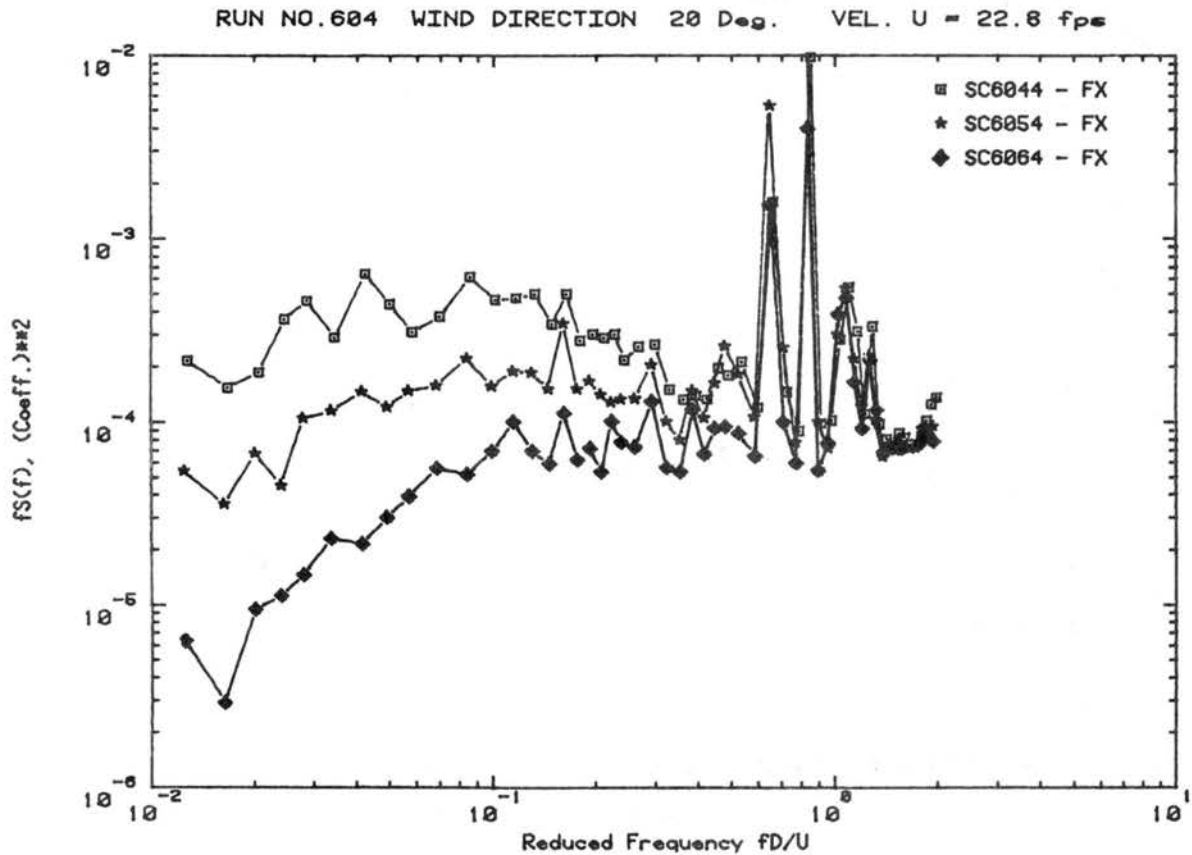
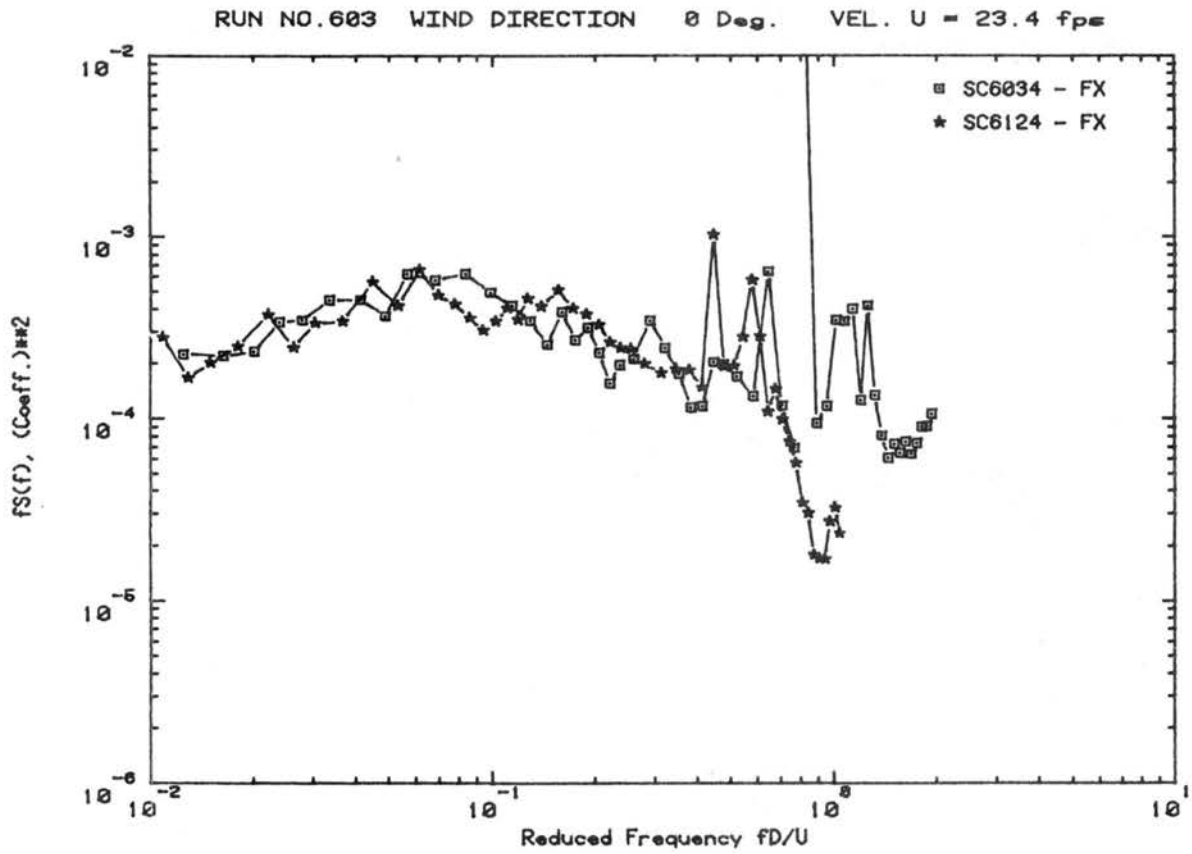
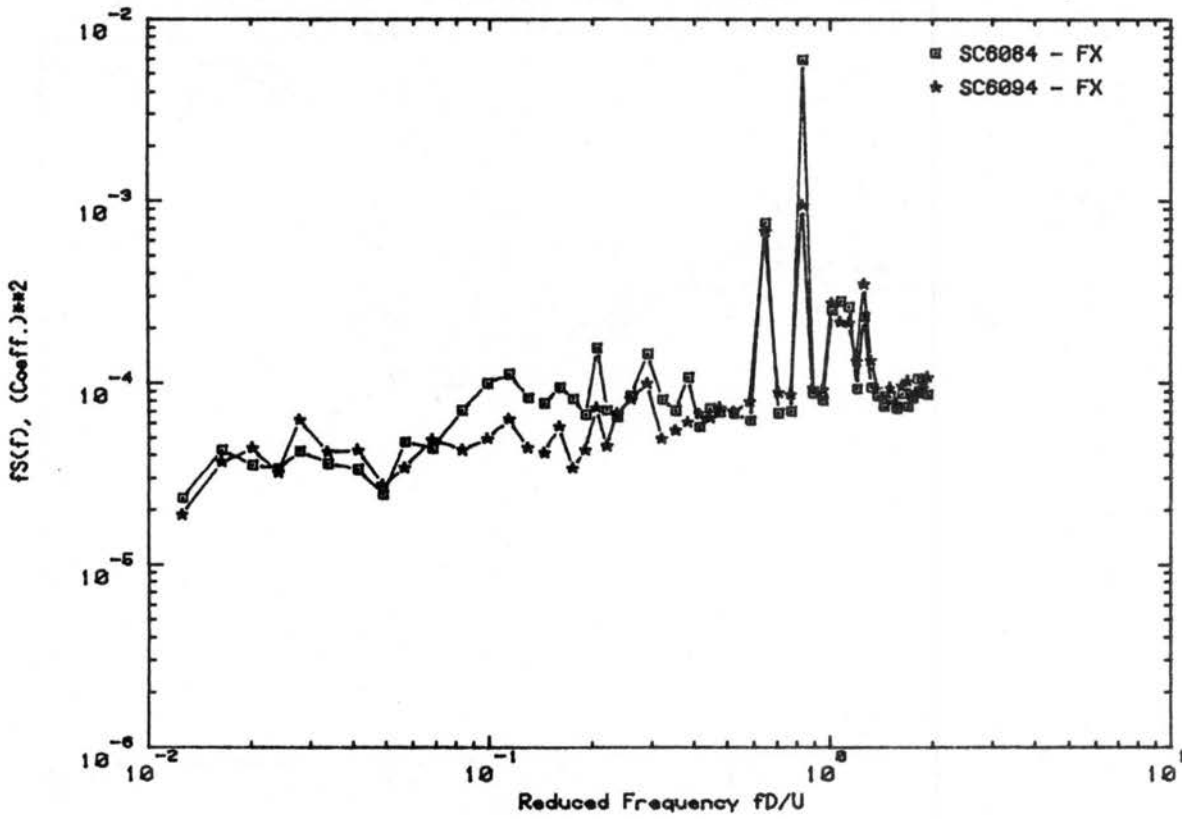


Figure C.12e. Load Spectra for Declination Angle 60° , Hour Angle 0°

RUN NO.608 WIND DIRECTION 120 Deg. VEL. U = 23.3 fps



RUN NO.610 WIND DIRECTION 180 Deg. VEL. U = 22.7 fps

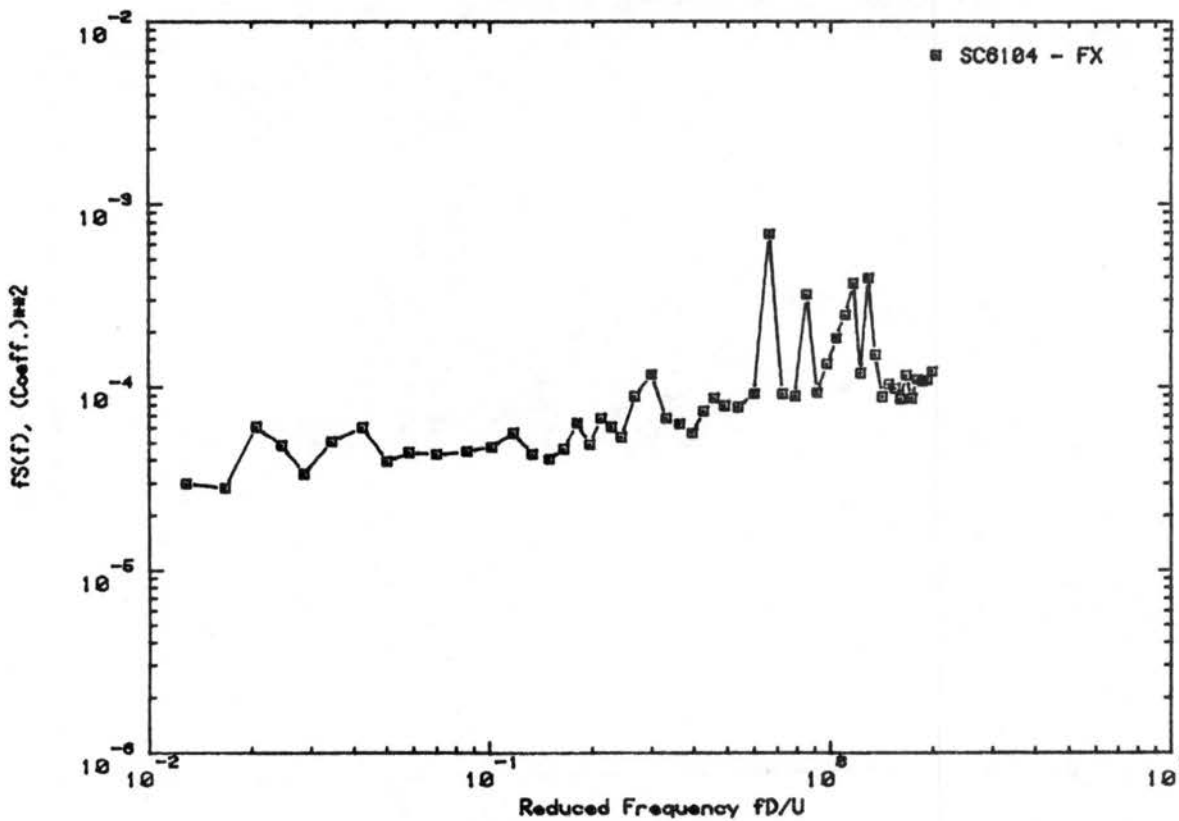
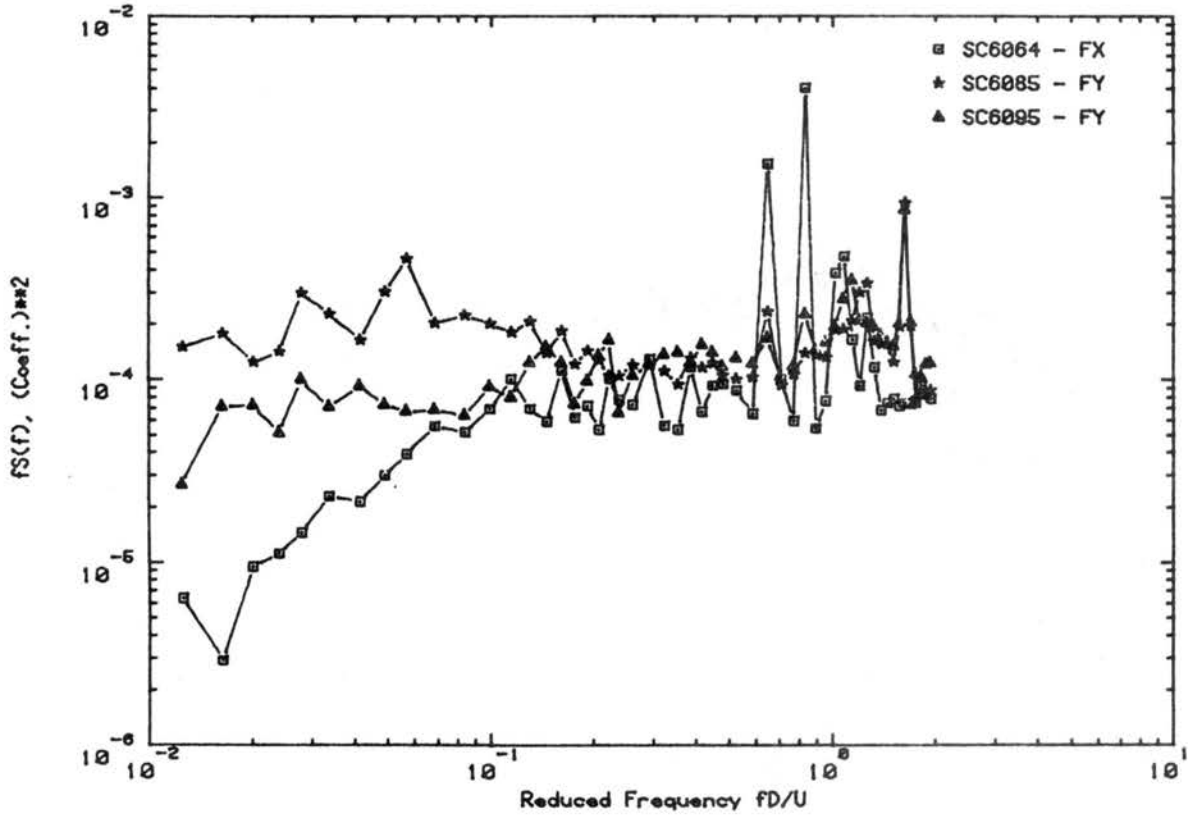


Figure C.12f. Load Spectra for Declination Angle 60°, Hour Angle 0°

RUN NO.606 WIND DIRECTION 90 Deg. VEL. U = 23.3 fps



RUN NO.604 WIND DIRECTION 20 Deg. VEL. U = 22.8 fps

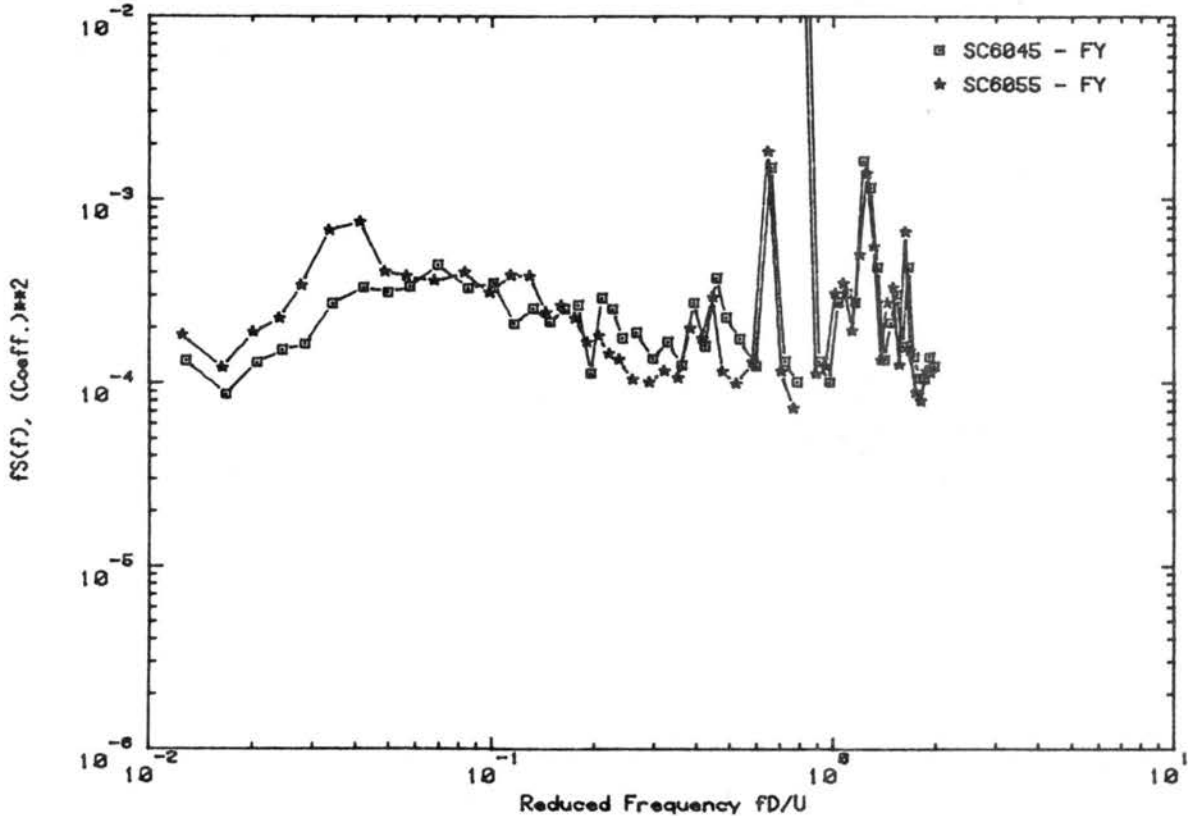
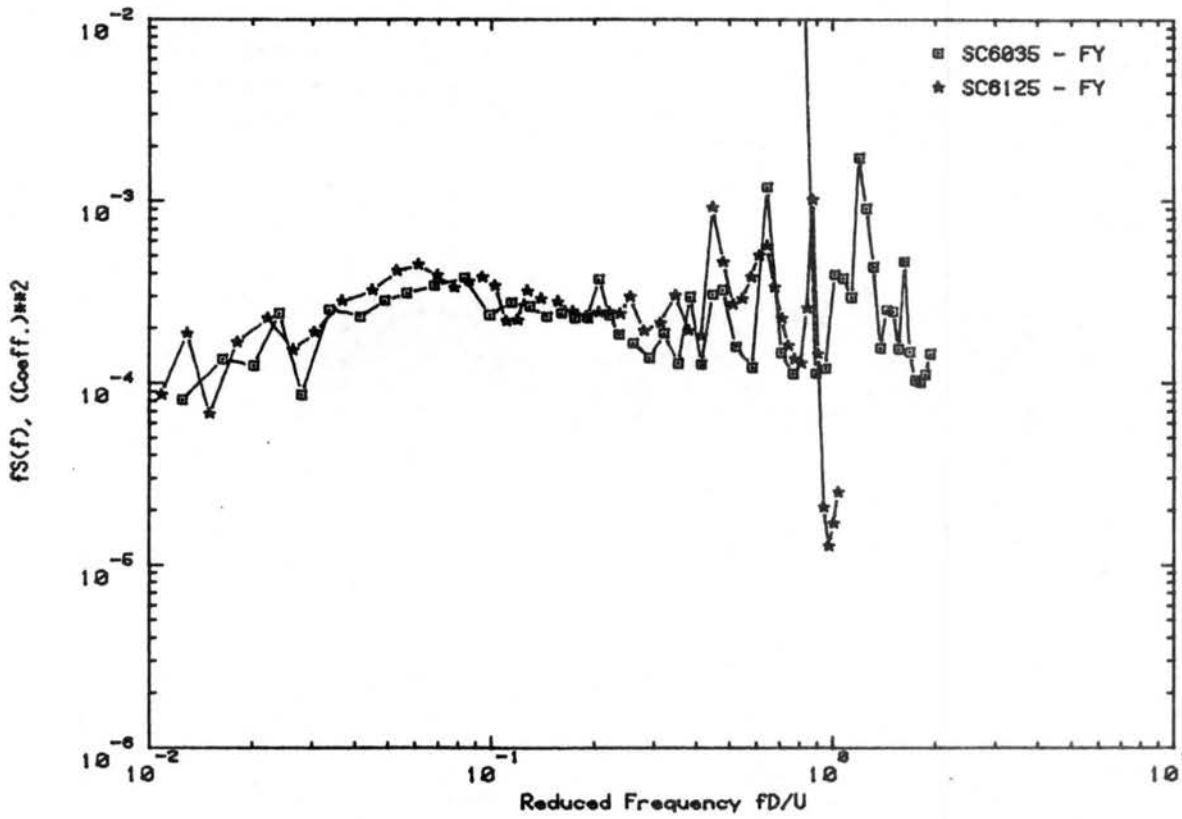


Figure C.12g. Load Spectra for Declination Angle 60°, Hour Angle 0°

RUN NO.603 WIND DIRECTION 0 Deg. VEL. U = 23.4 fps



RUN NO.610 WIND DIRECTION 180 Deg. VEL. U = 22.7 fps

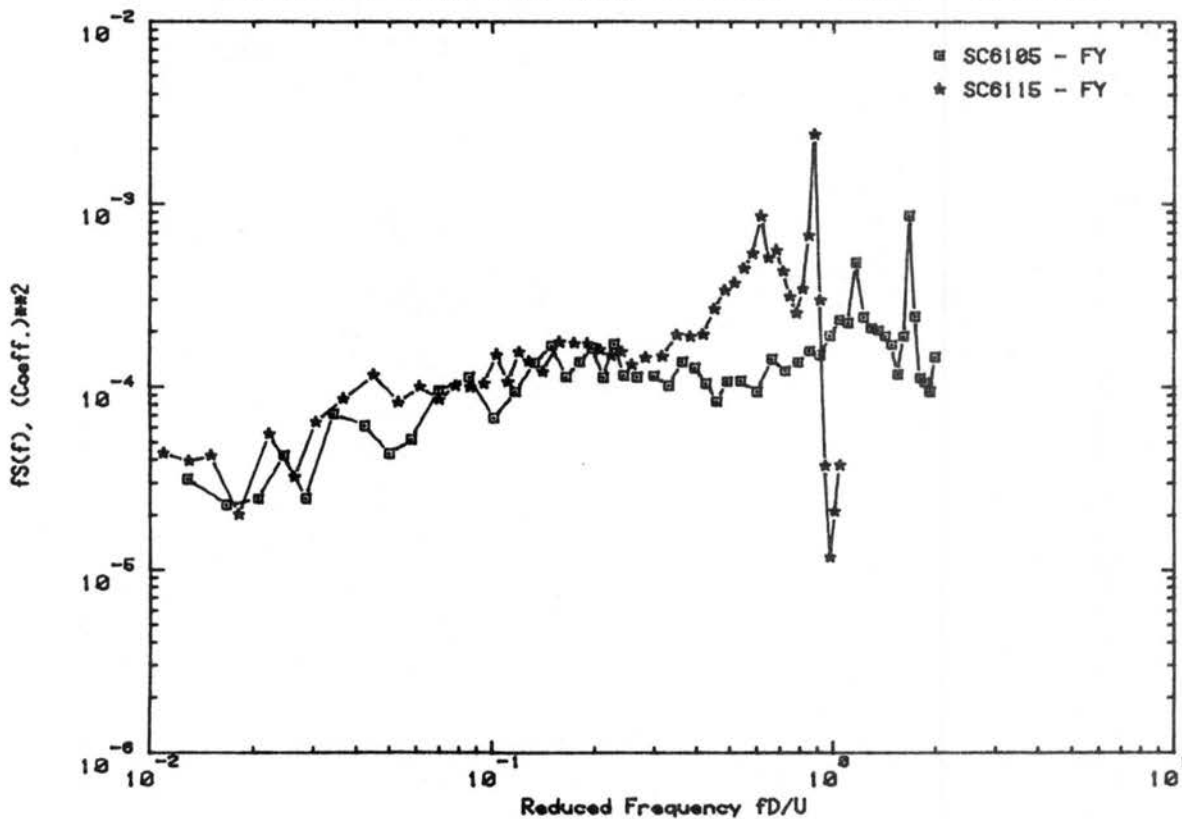


Figure C.12h. Load Spectra for Declination Angle 60°, Hour Angle 0°

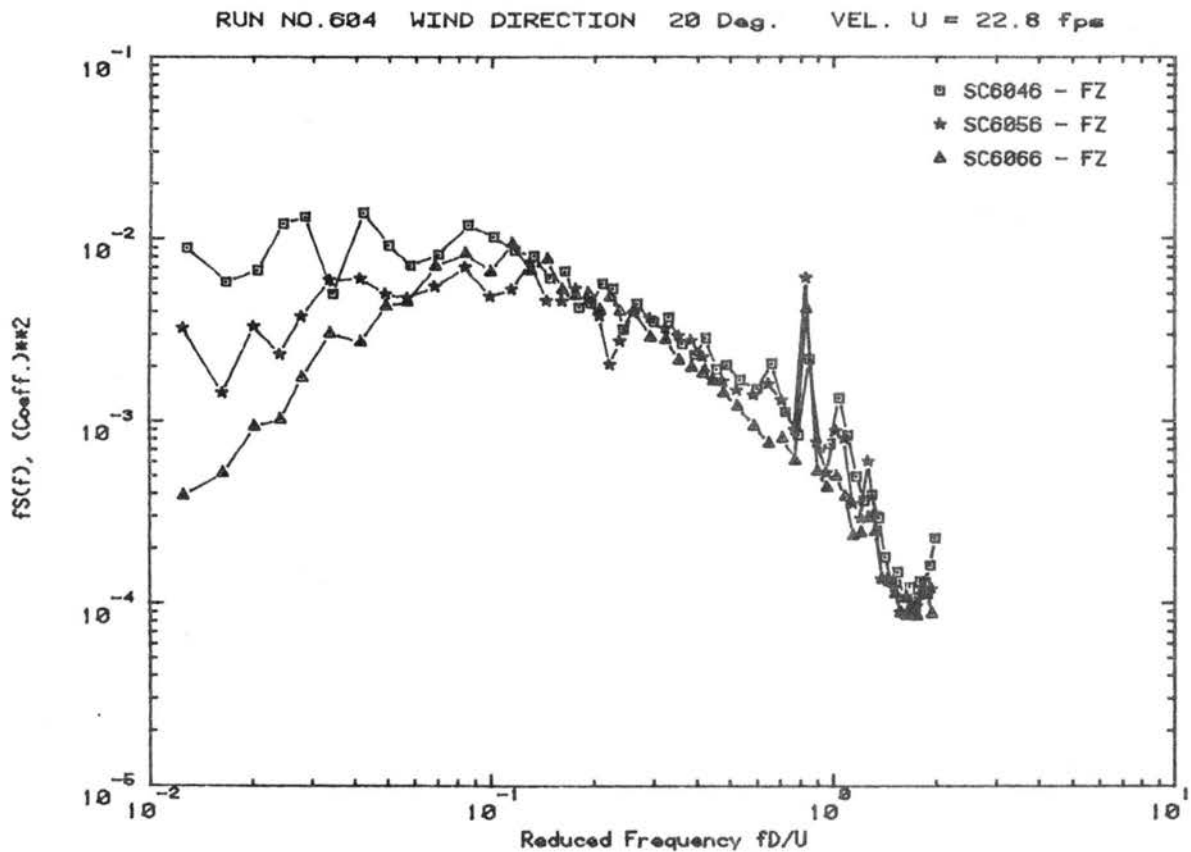
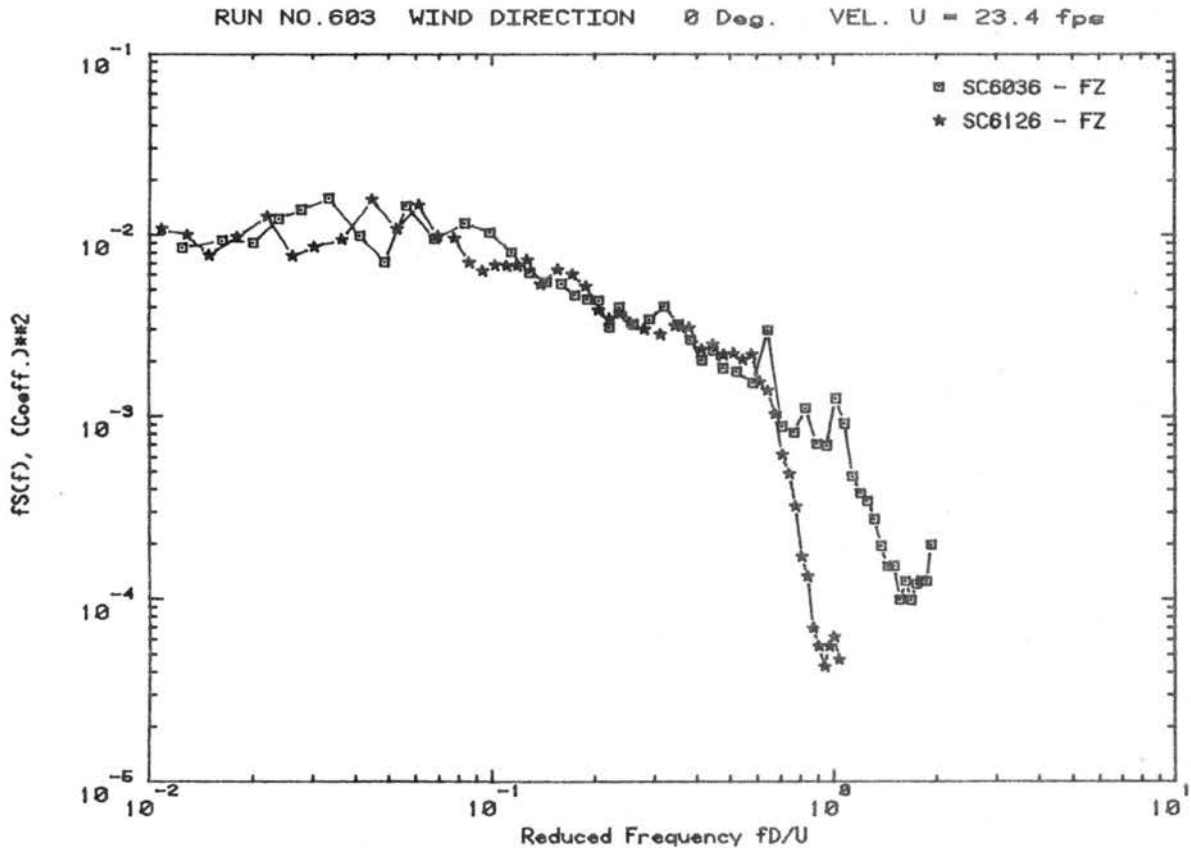
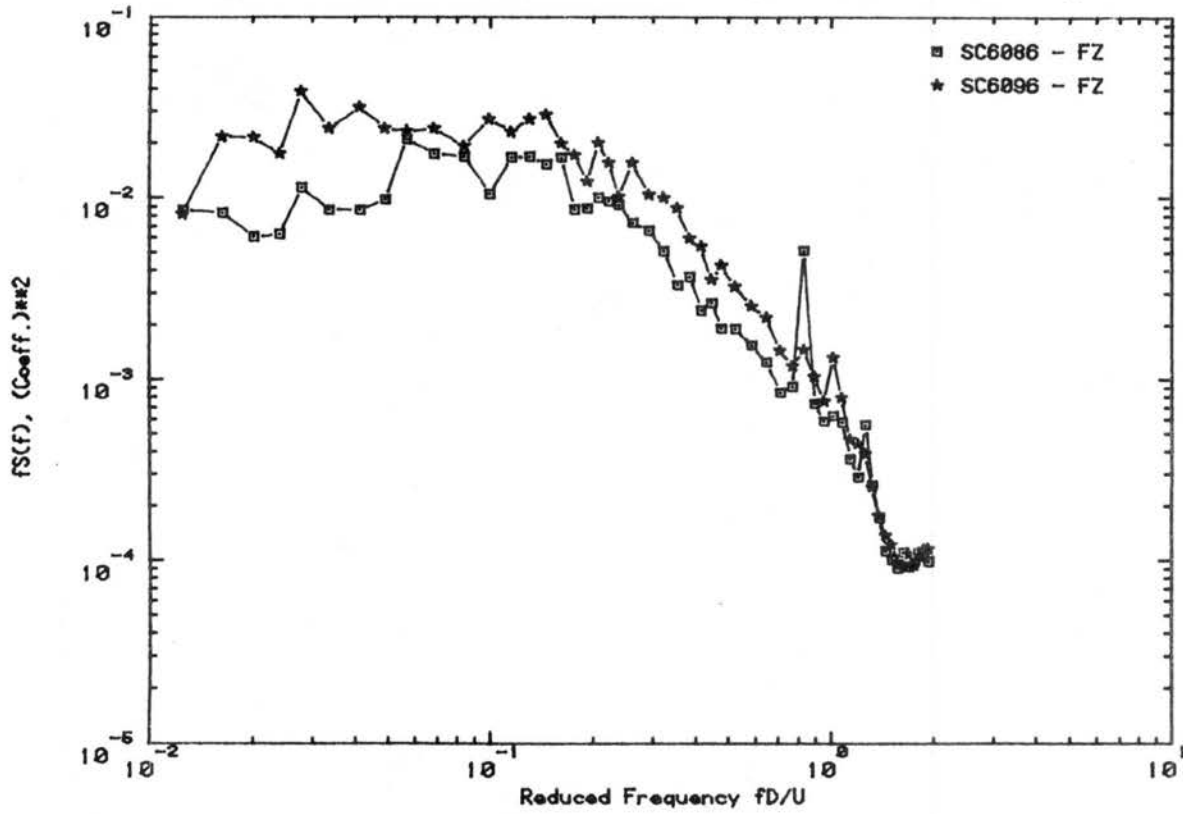


Figure C.12i. Load Spectra for Declination Angle 60° , Hour Angle 0°

RUN NO.608 WIND DIRECTION 120 Deg. VEL. U = 23.3 fps



RUN NO.610 WIND DIRECTION 180 Deg. VEL. U = 22.7 fps

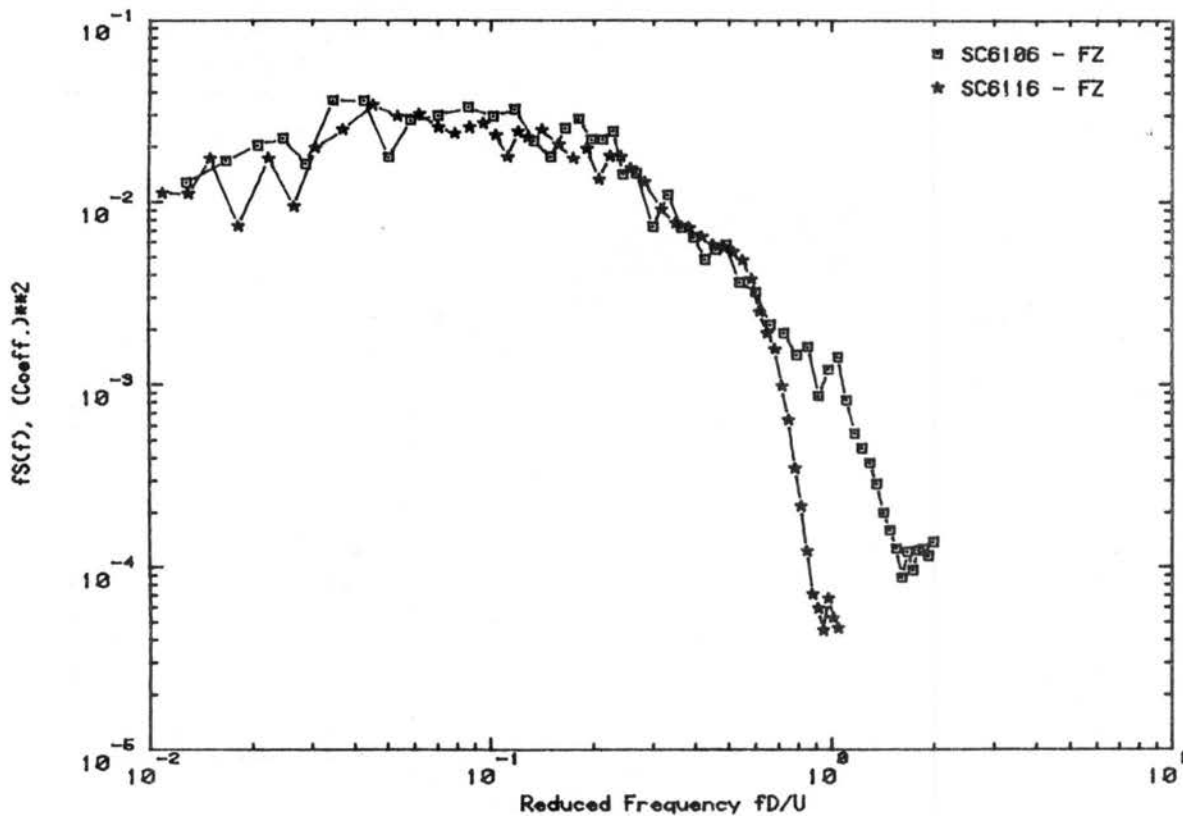


Figure C.12j. Load Spectra for Declination Angle 60°, Hour Angle 0°

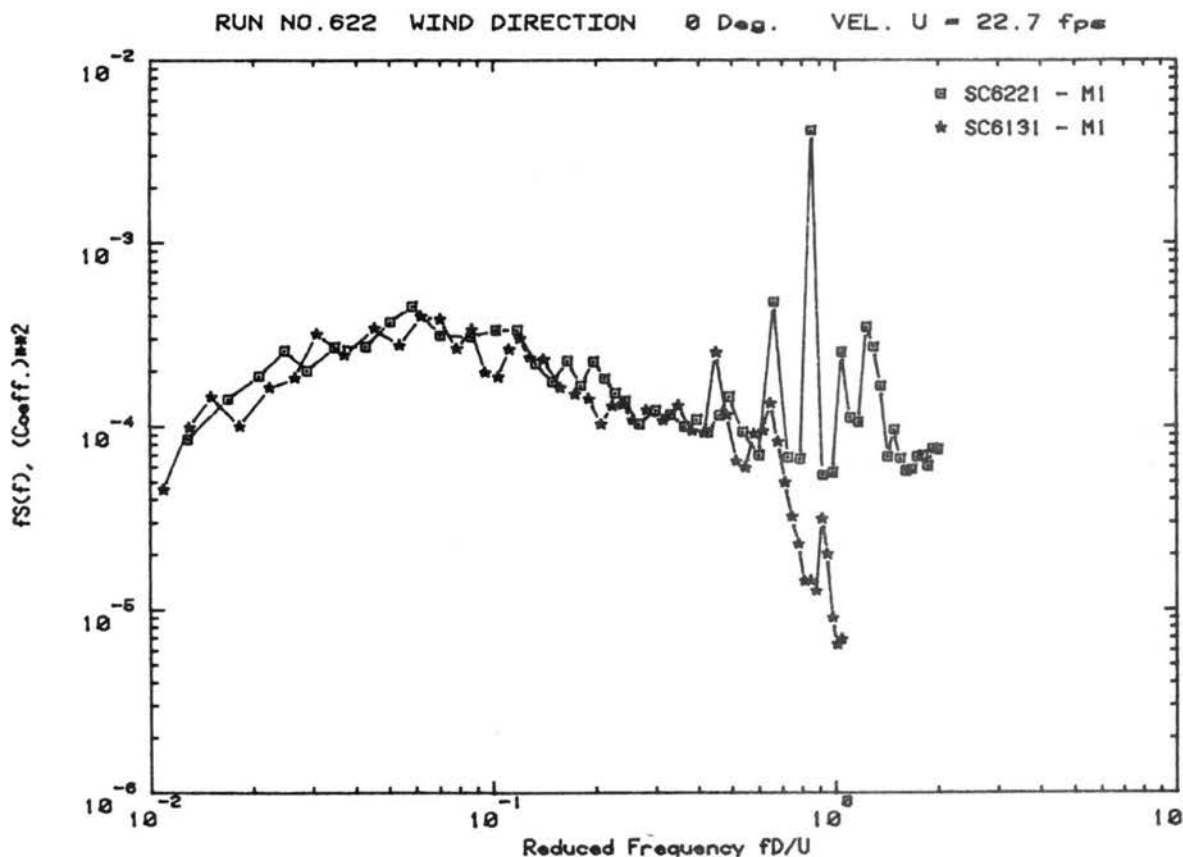
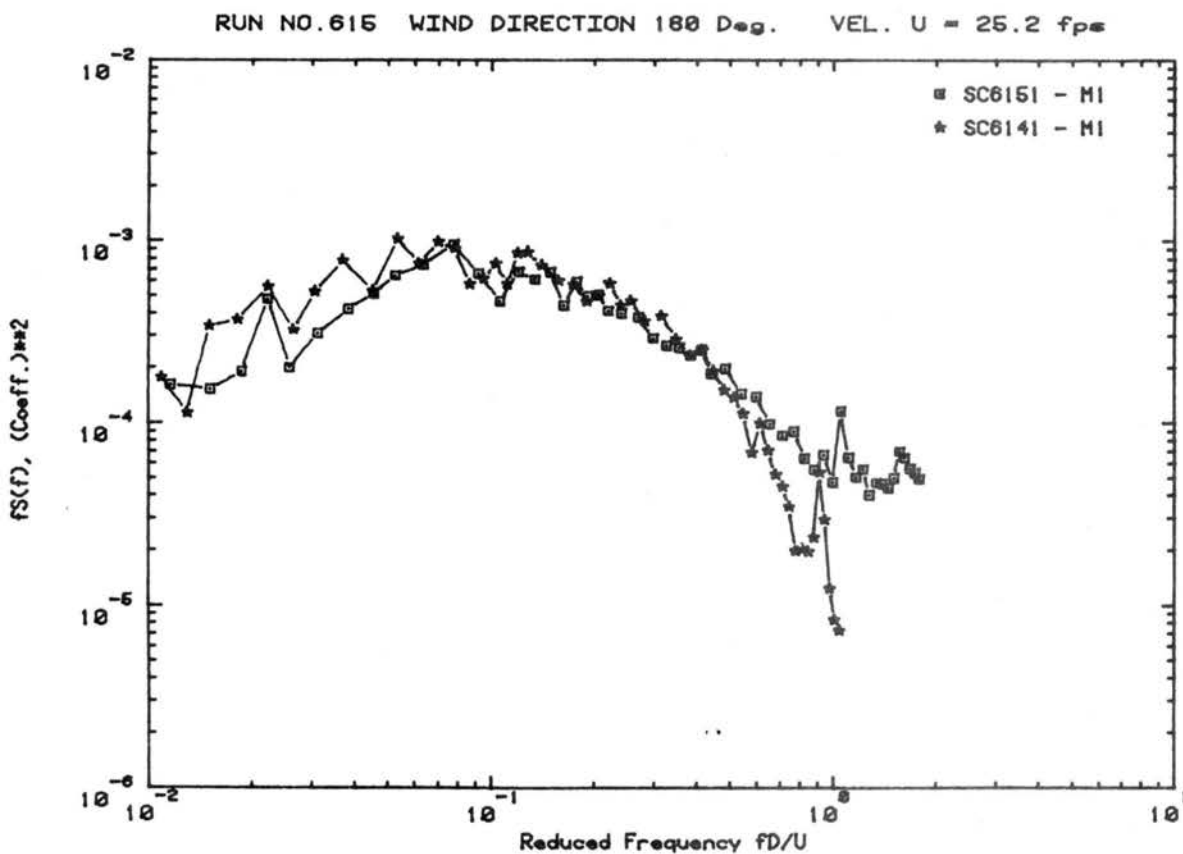
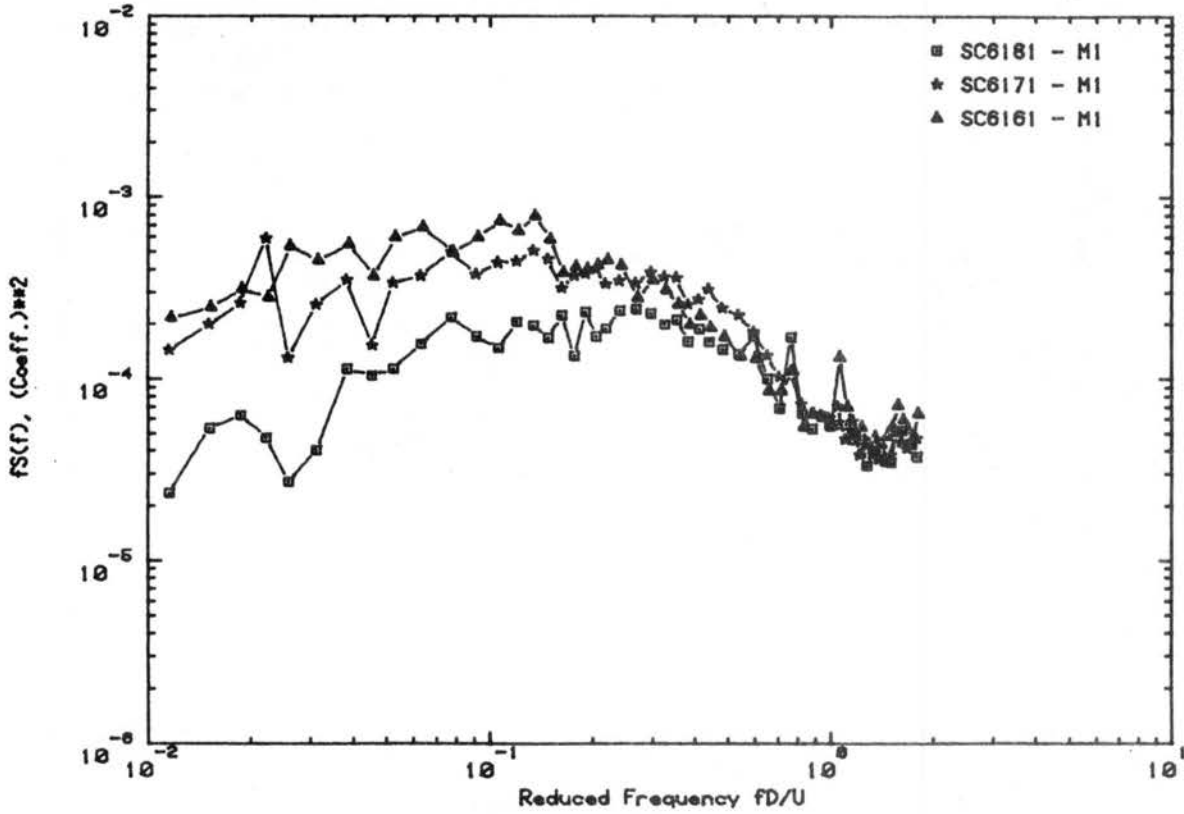


Figure C.13a. Load Spectra for Declination Angle 75° , Hour Angle 0°

RUN NO.618 WIND DIRECTION 90 Deg. VEL. U = 25.3 fps



RUN NO.621 WIND DIRECTION 20 Deg. VEL. U = 22.4 fps

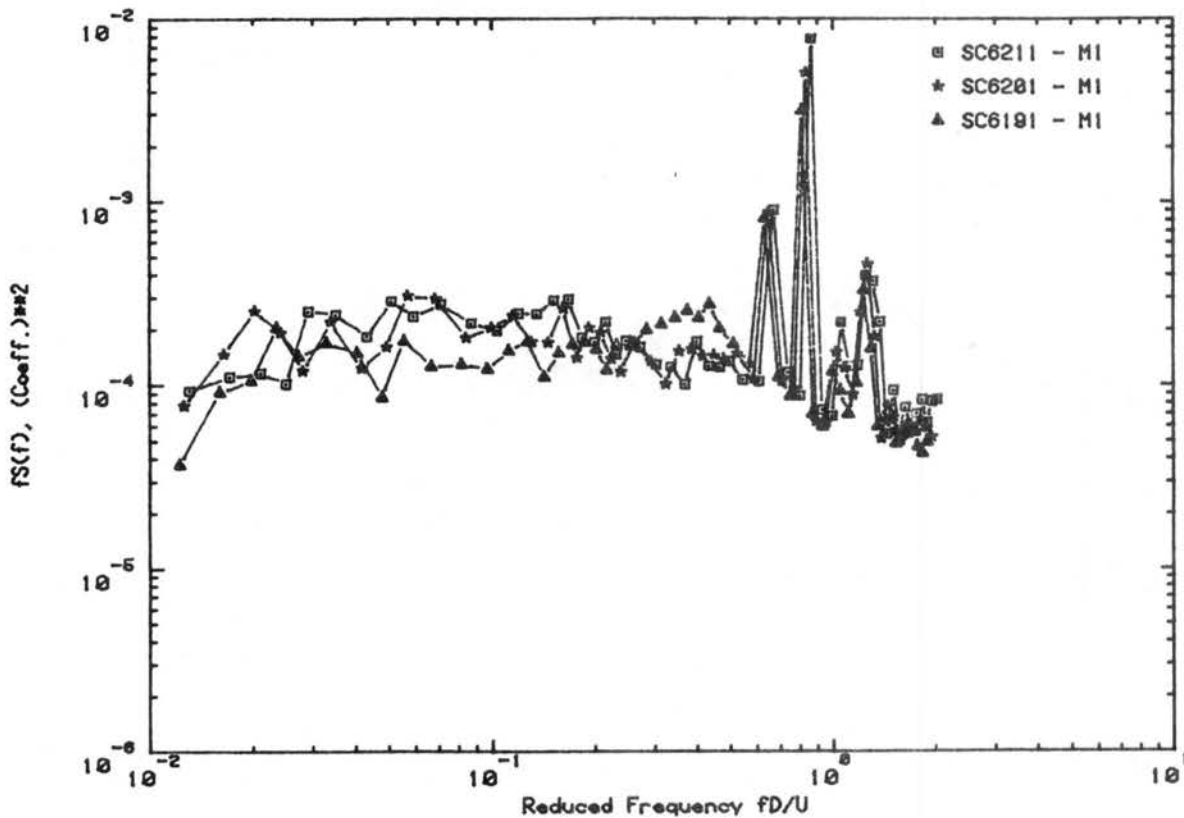
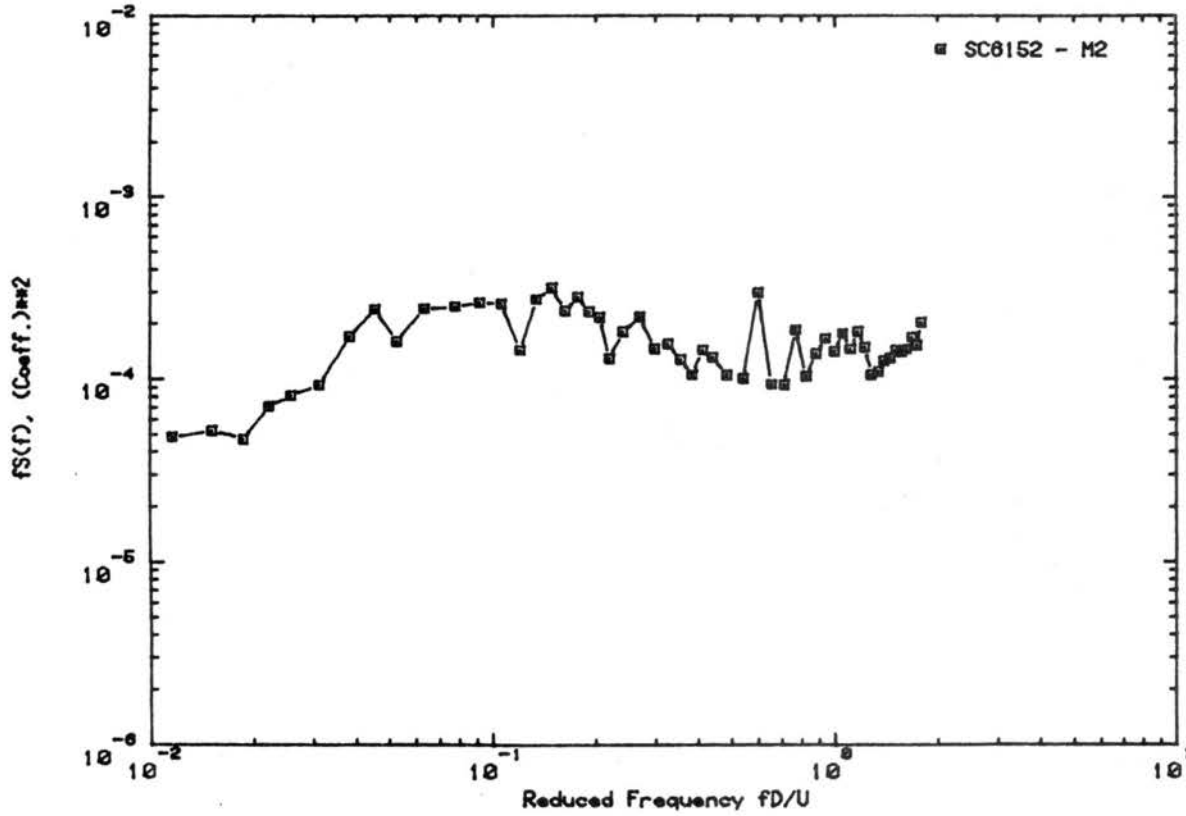


Figure C.13b. Load Spectra for Declination Angle 75°, Hour Angle 0°

RUN NO.615 WIND DIRECTION 180 Deg. VEL. U = 25.2 fps



RUN NO.616 WIND DIRECTION 180 Deg. VEL. U = 25.0 fps

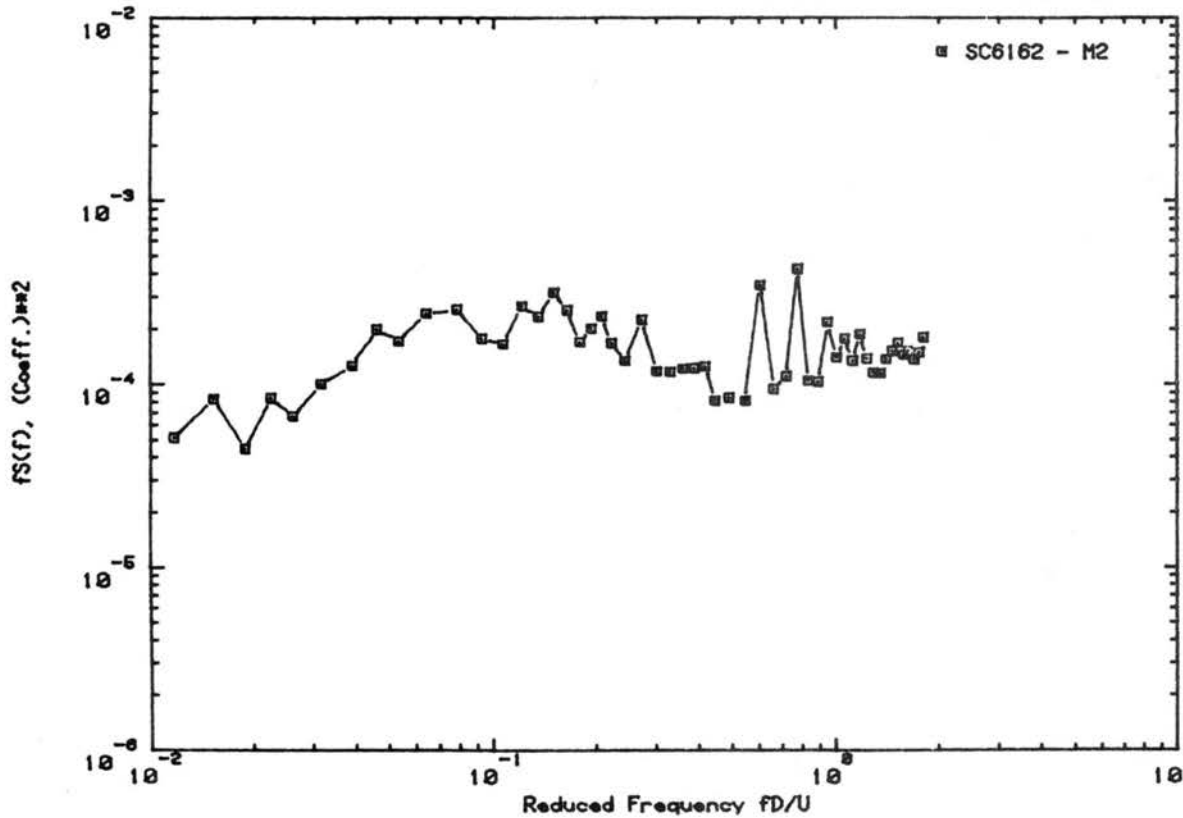
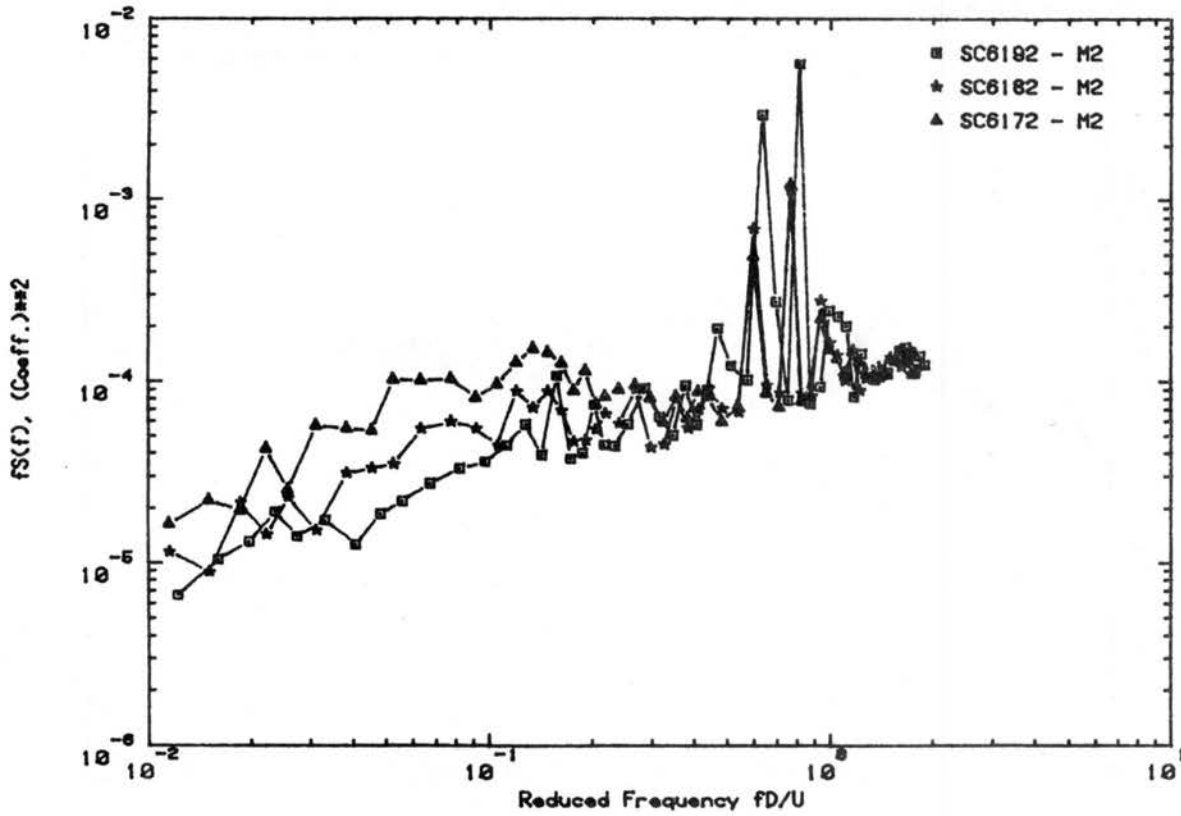


Figure C.13c. Load Spectra for Declination Angle 75° , Hour Angle 0°

RUN NO.619 WIND DIRECTION 60 Deg. VEL. U = 23.9 fps



RUN NO.622 WIND DIRECTION 0 Deg. VEL. U = 22.7 fps

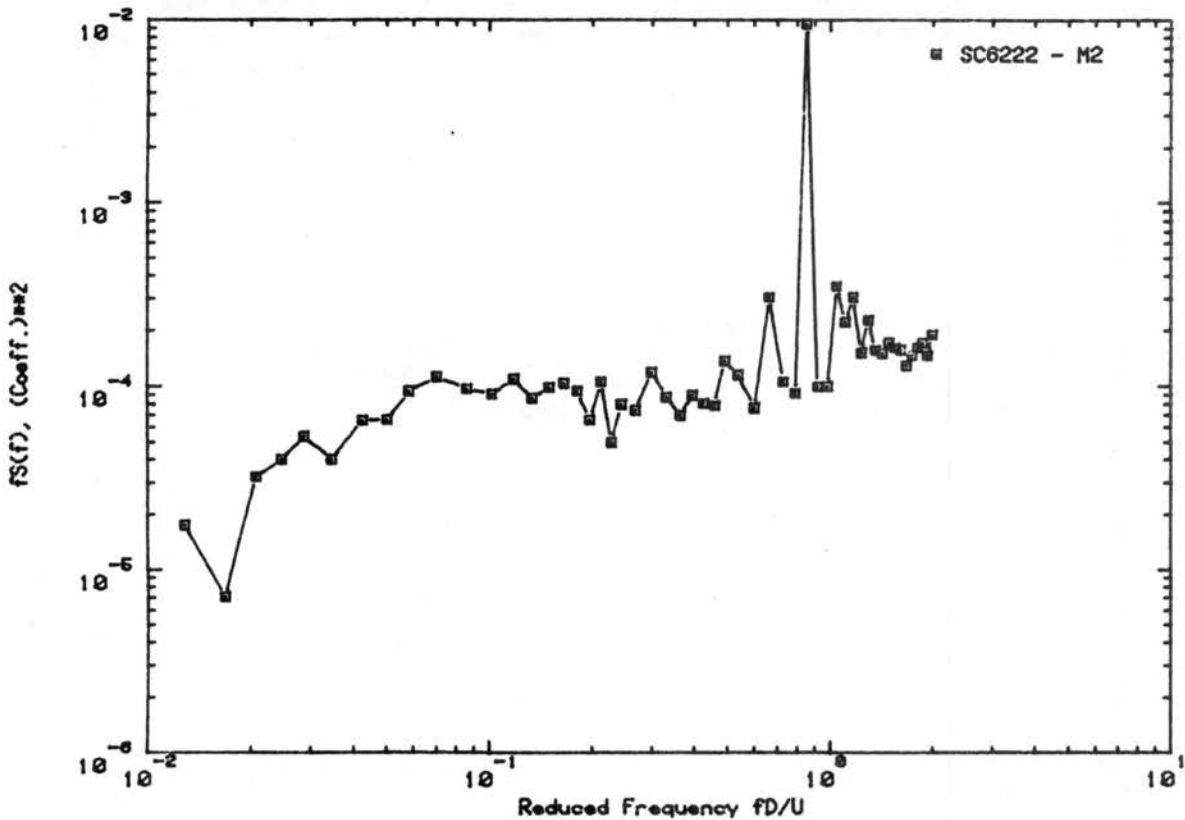


Figure C.13d. Load Spectra for Declination Angle 75°, Hour Angle 0°

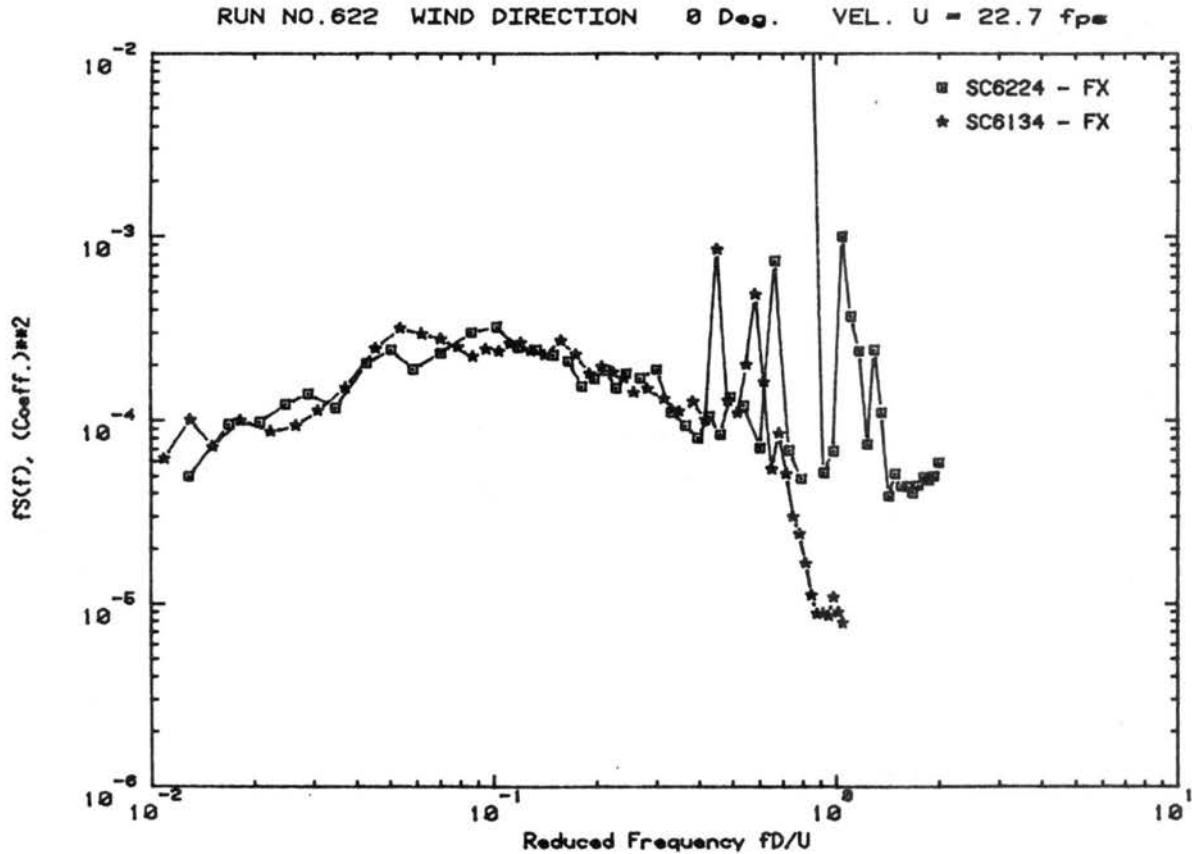
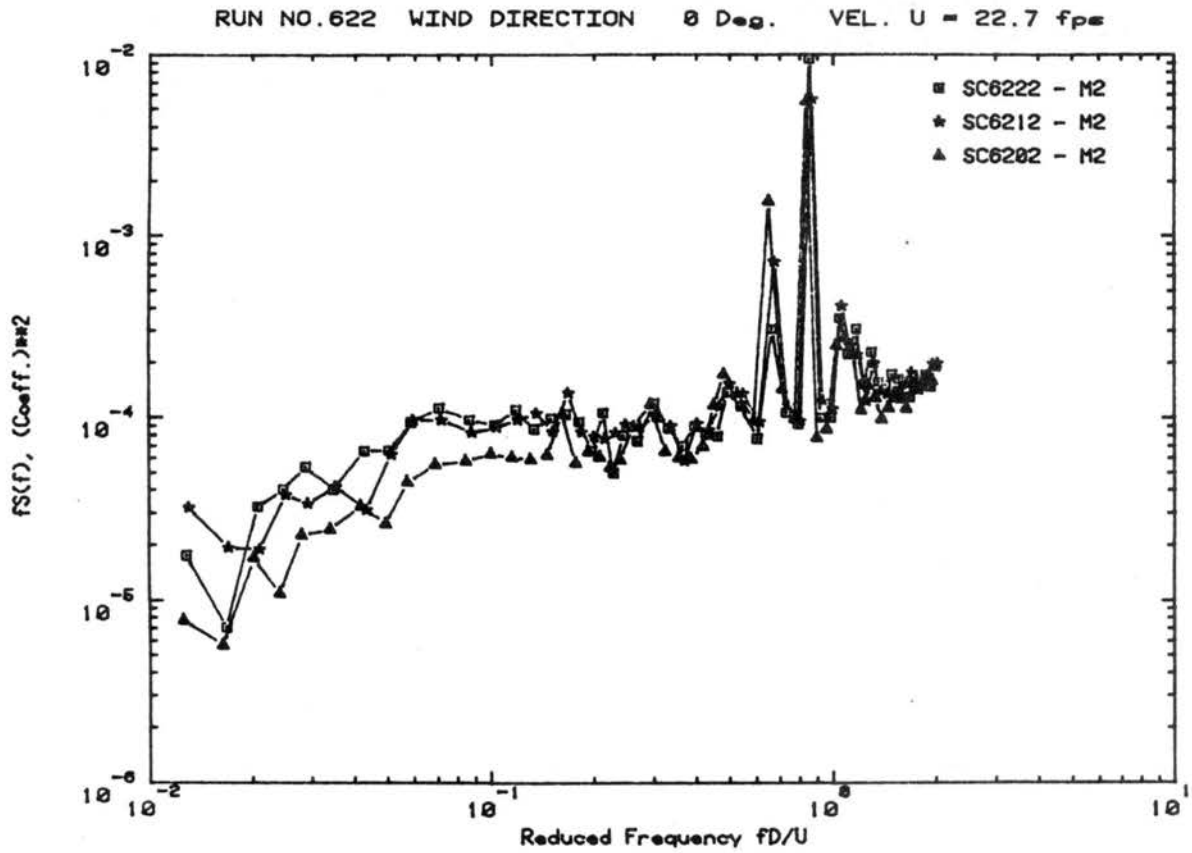
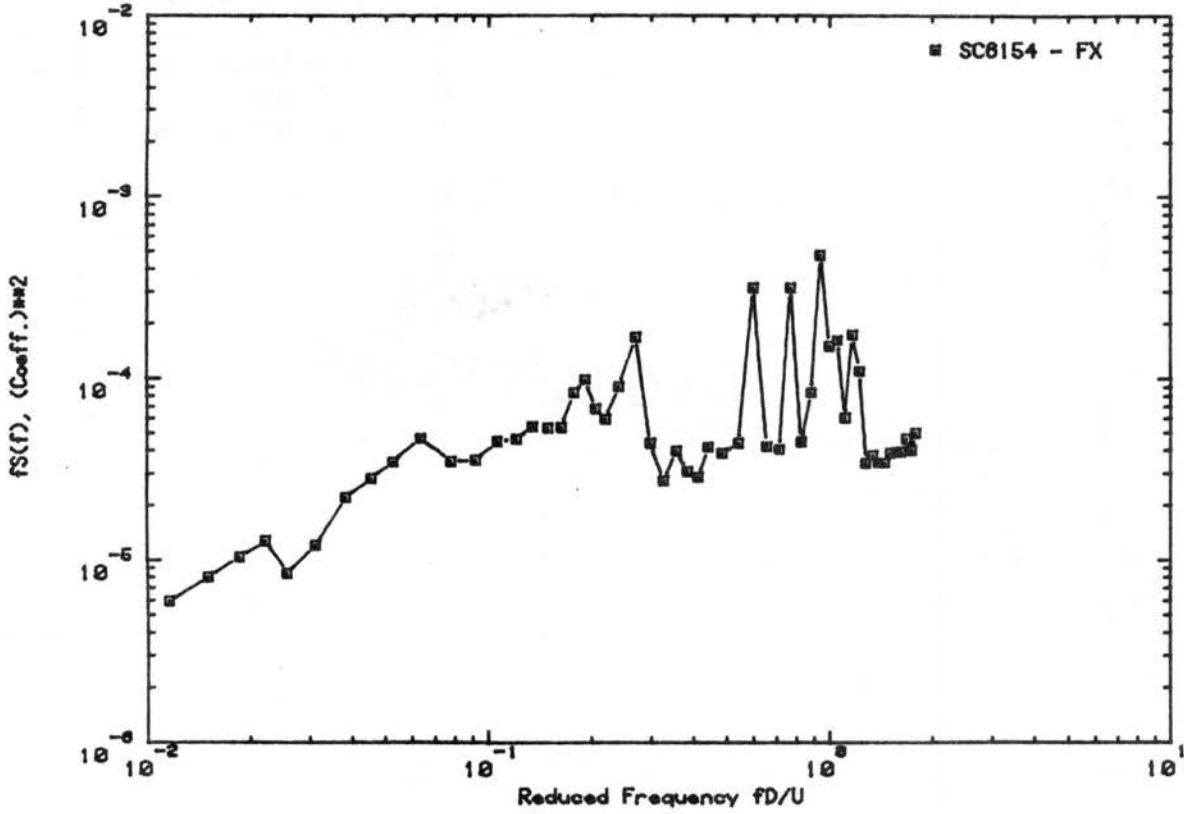


Figure C.13e. Load Spectra for Declination Angle 75° , Hour Angle 0°

RUN NO.615 WIND DIRECTION 180 Deg. VEL. U = 25.2 fps



RUN NO.618 WIND DIRECTION 90 Deg. VEL. U = 25.3 fps

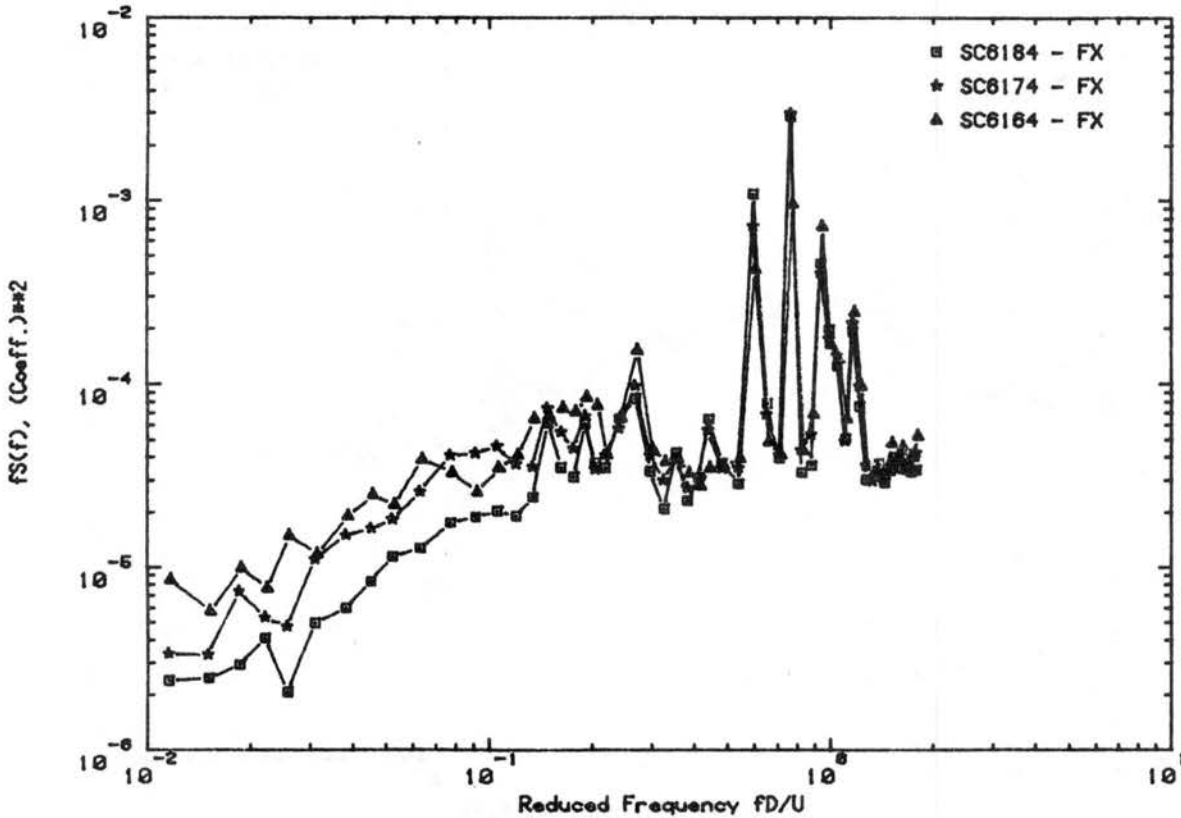


Figure C.13f. Load Spectra for Declination Angle 75°, Hour Angle 0°

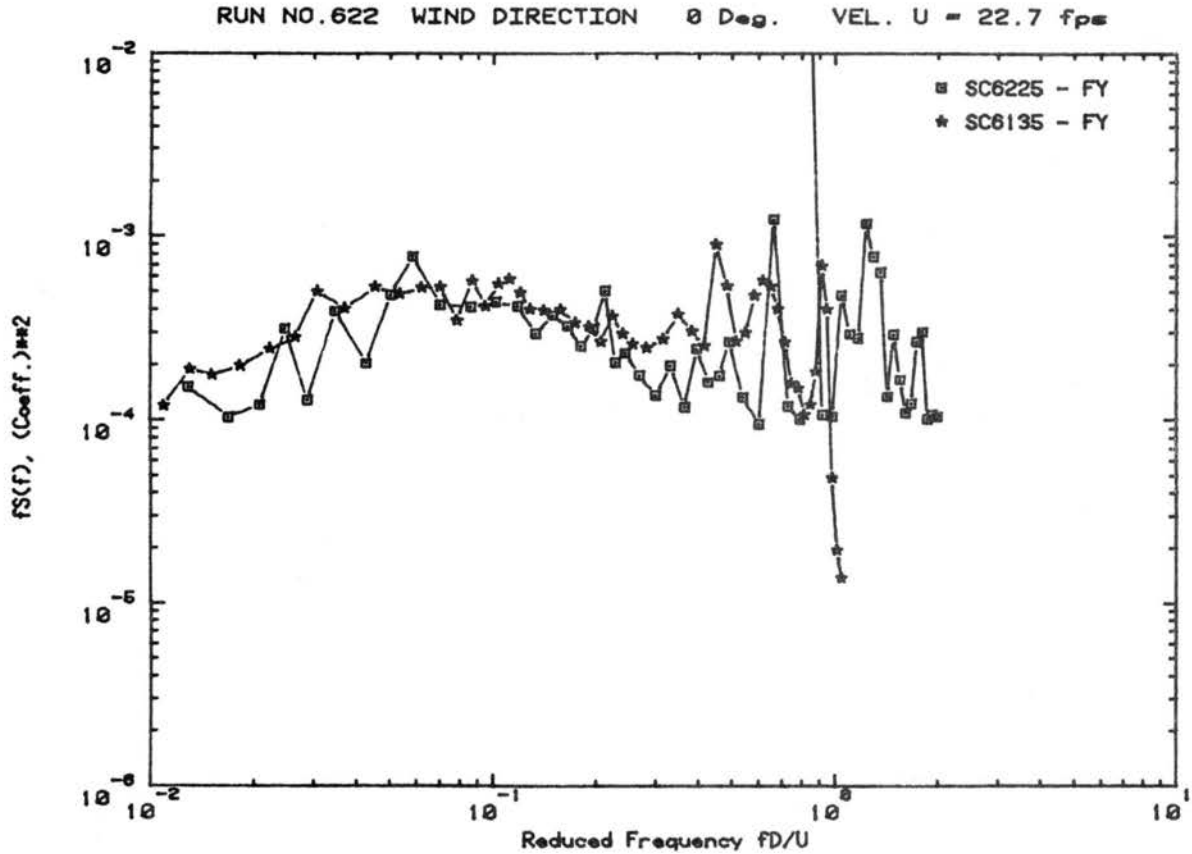
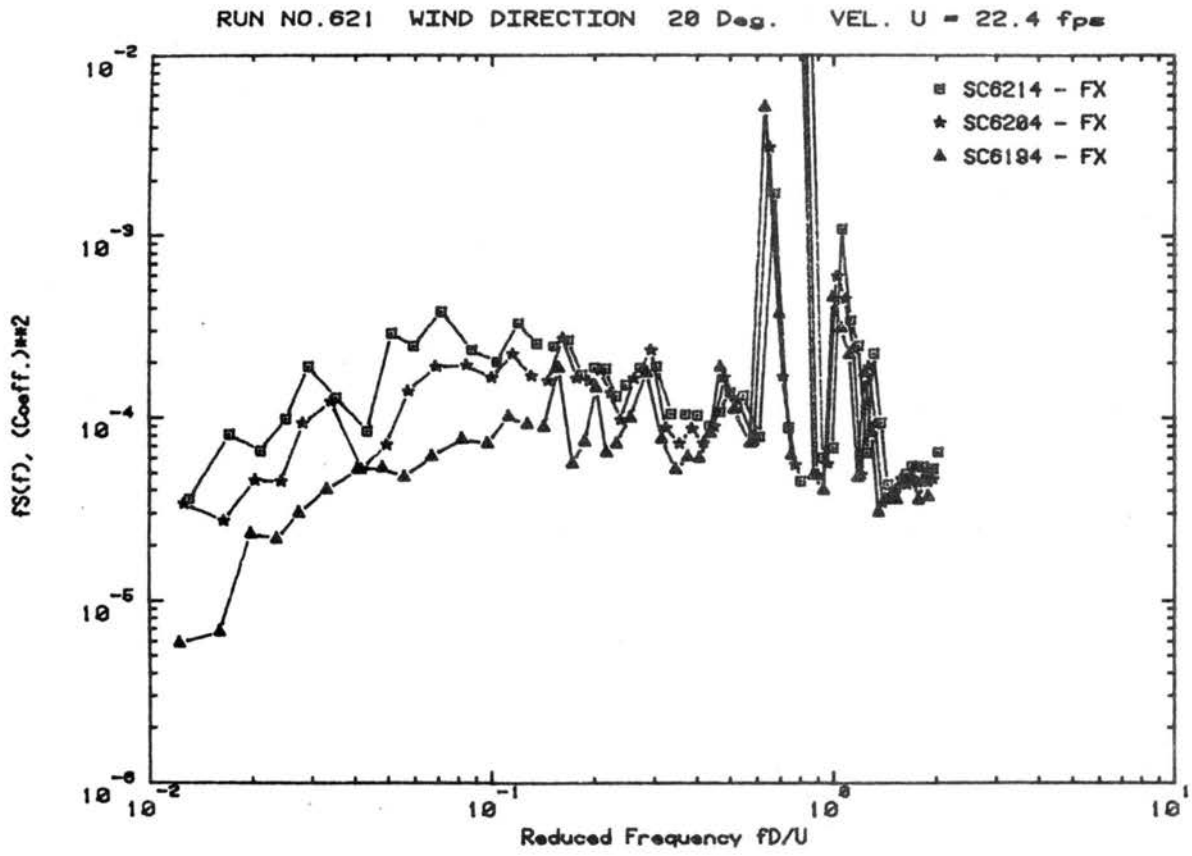


Figure C.13g. Load Spectra for Declination Angle 75° , Hour Angle 0°

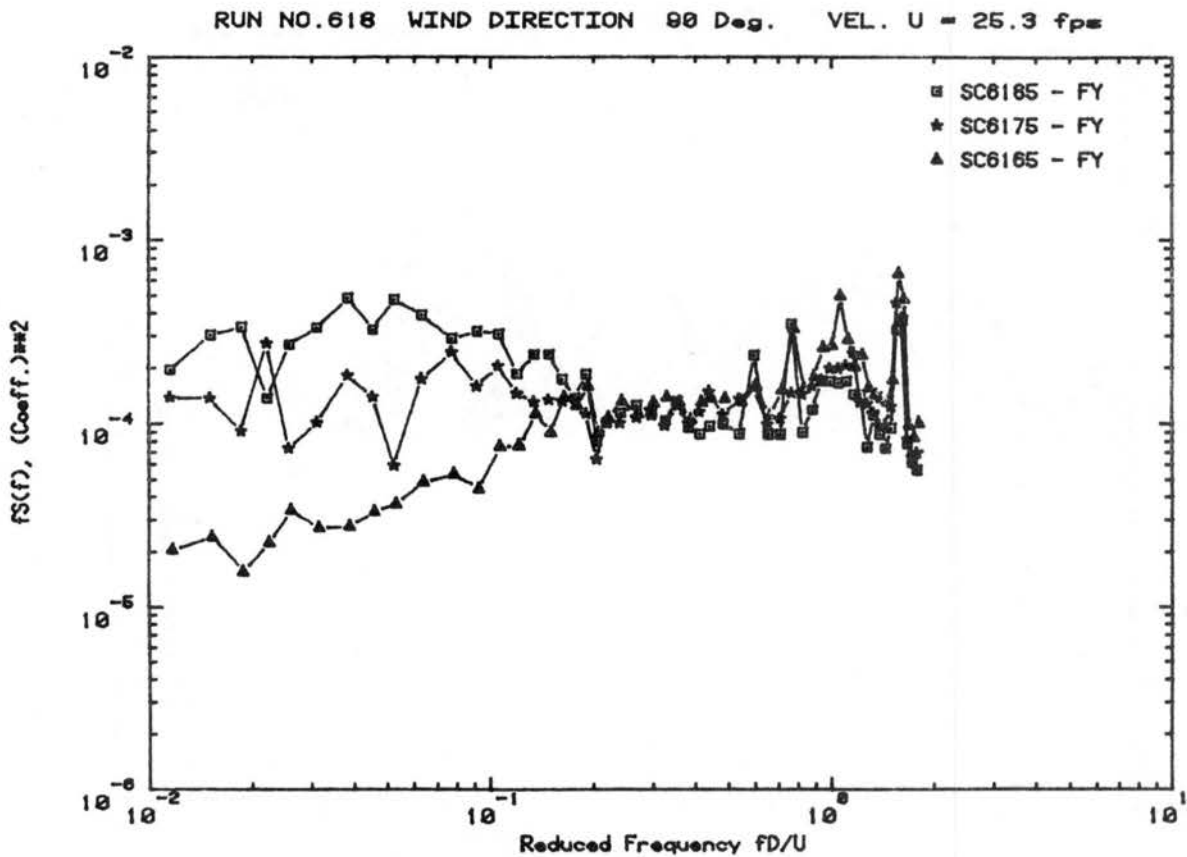
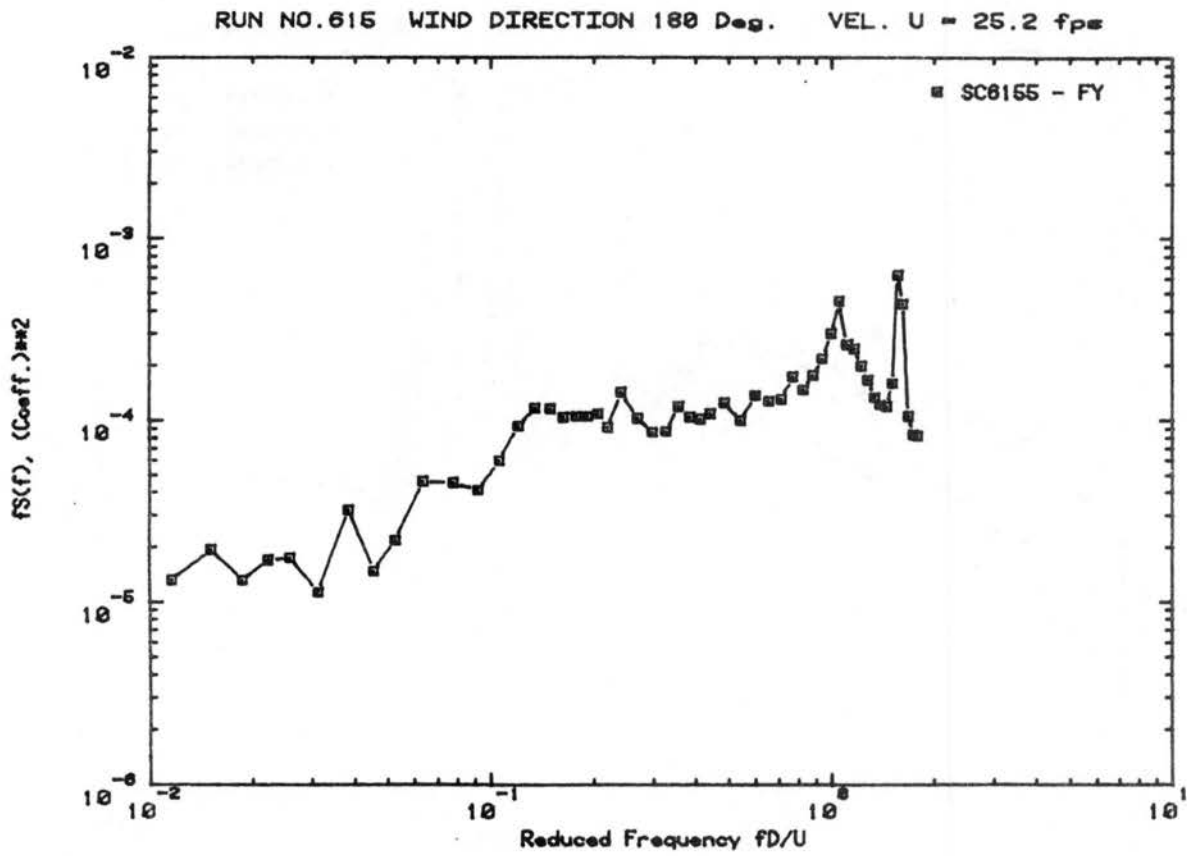


Figure C.13h. Load Spectra for Declination Angle 75° , Hour Angle 0°

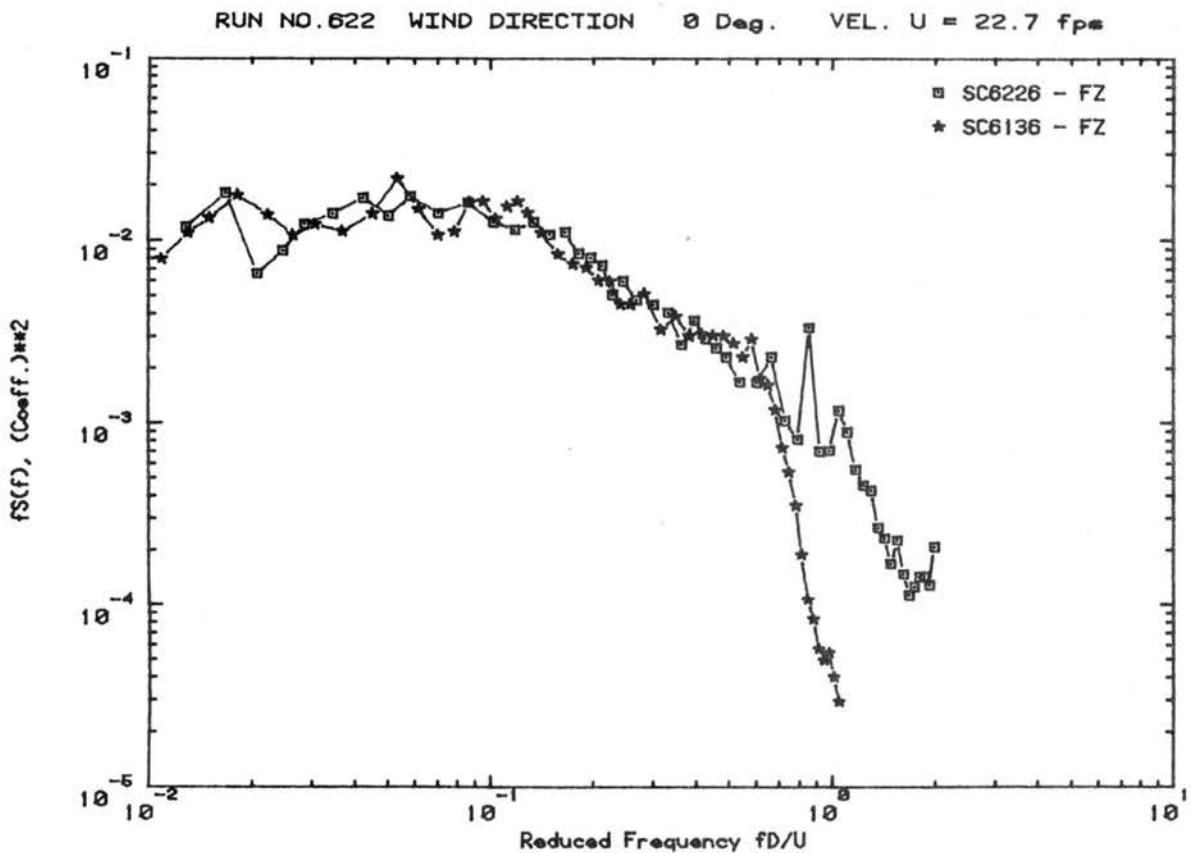
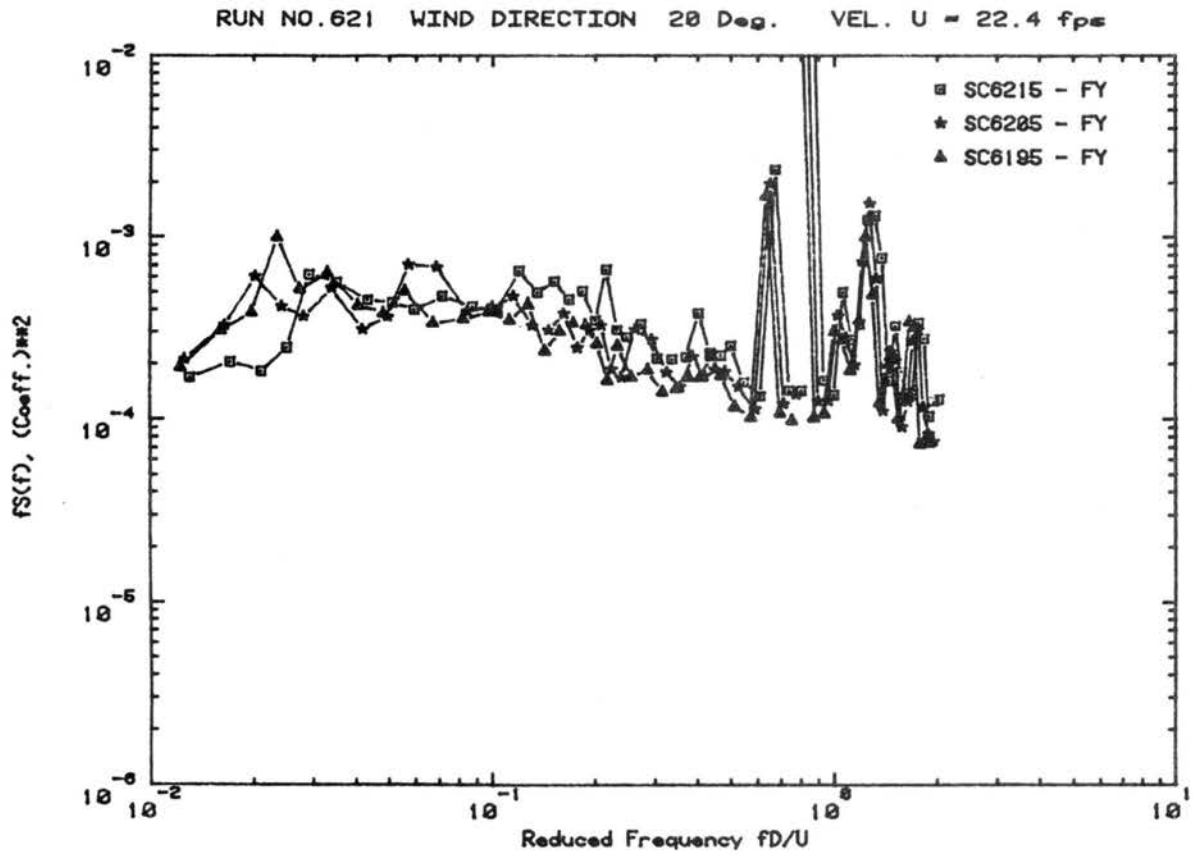


Figure C.13i. Load Spectra for Declination Angle 75° , Hour Angle 0°

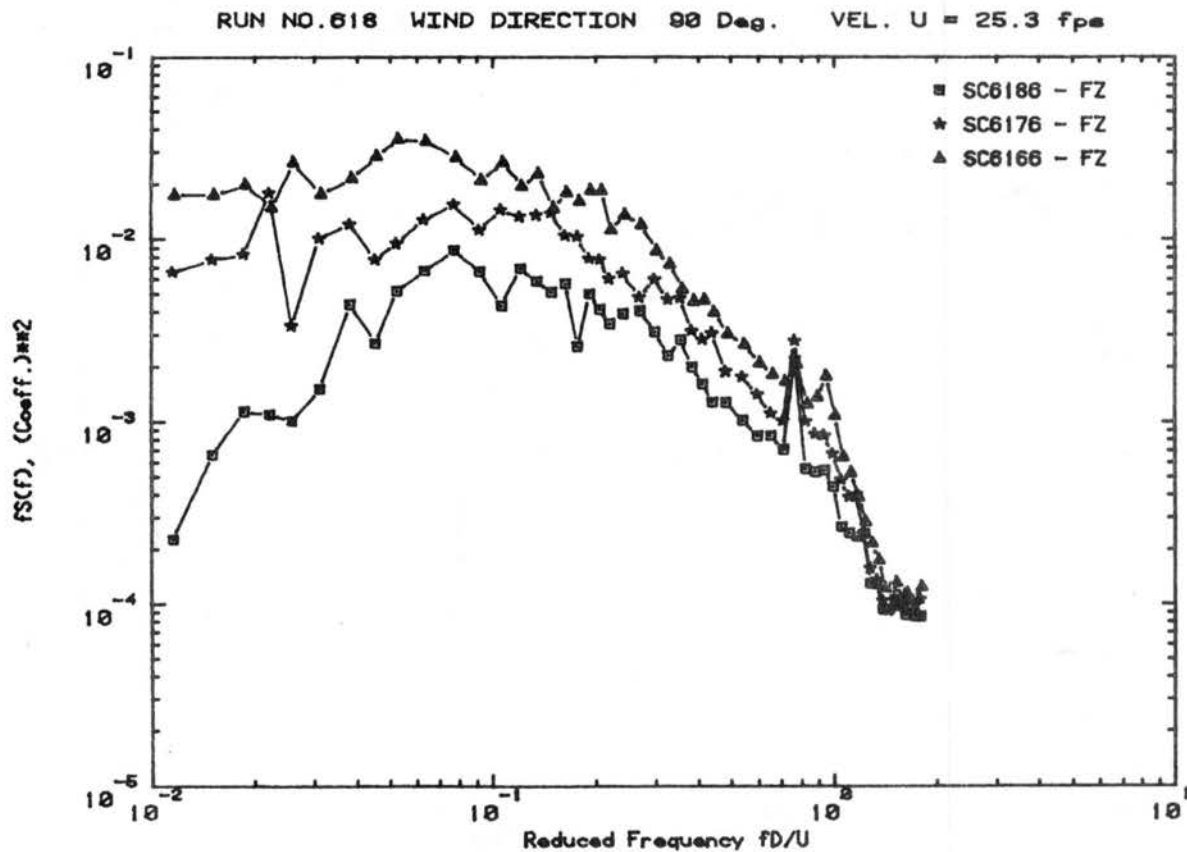
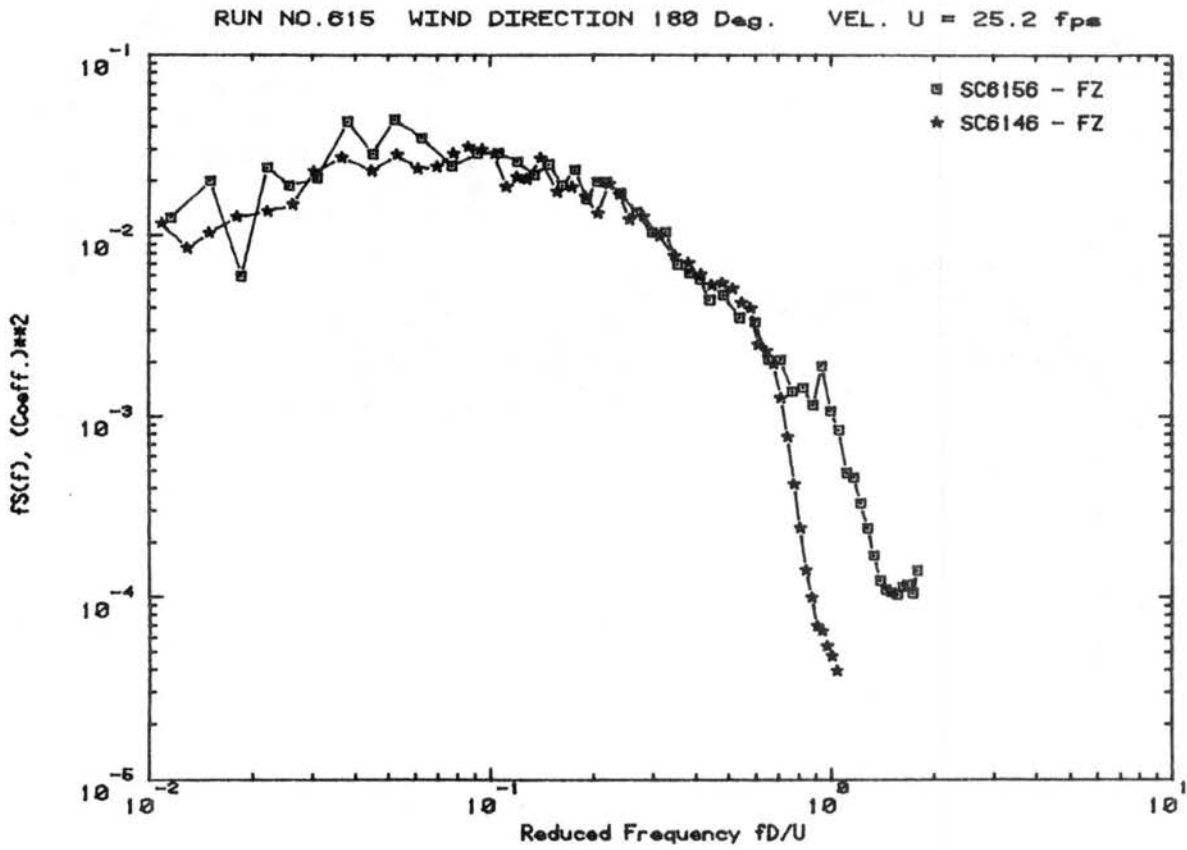


Figure C.13j. Load Spectra for Declination Angle 75° , Hour Angle 0°

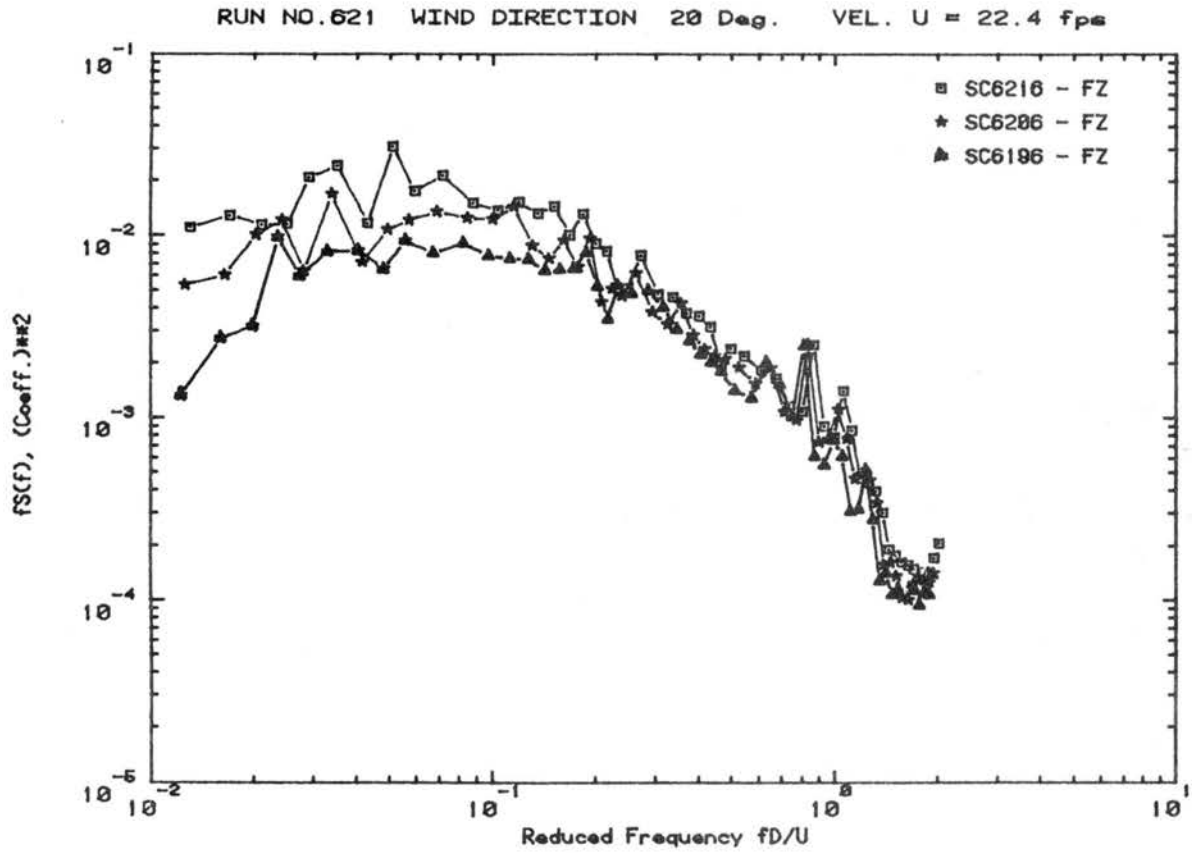
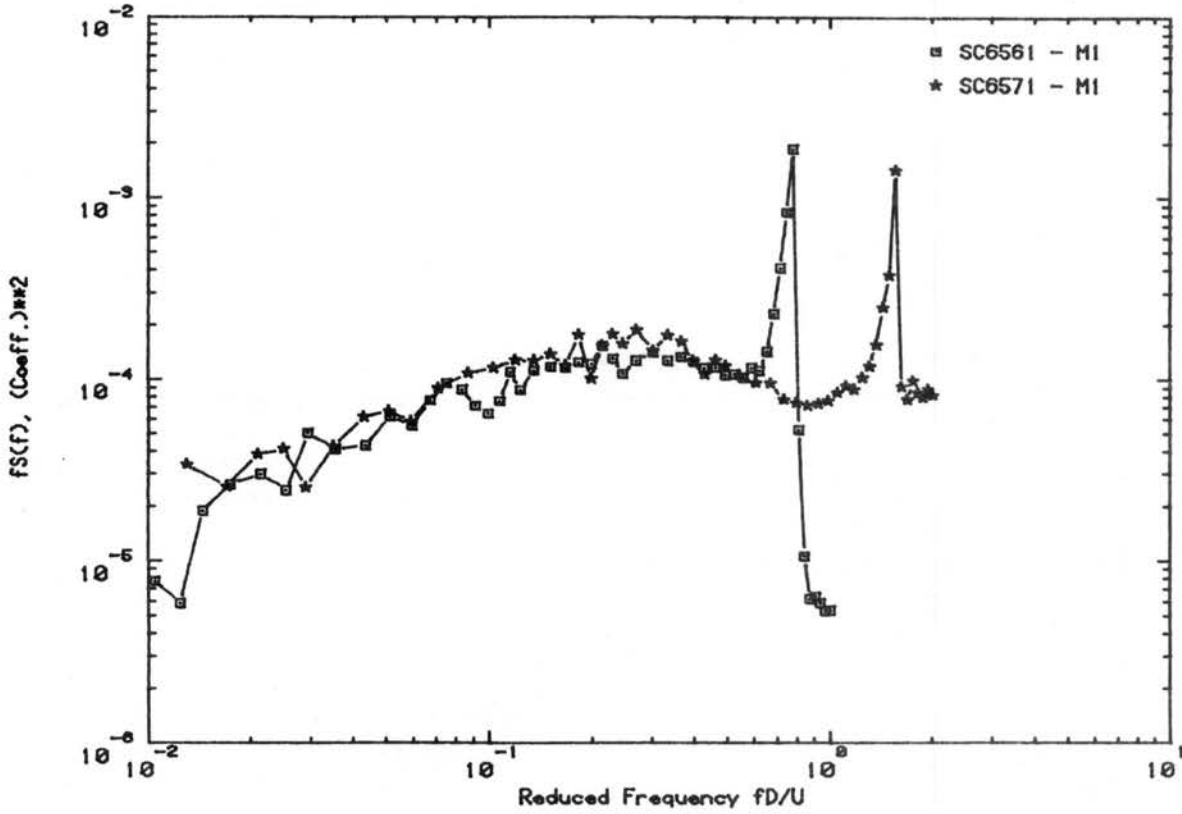


Figure C.13k. Load Spectra for Declination Angle 75° , Hour Angle 0°

RUN NO.656 WIND DIRECTION 180 Deg. VEL. U = 45.1 fps



RUN NO.658 WIND DIRECTION 140 Deg. VEL. U = 22.3 fps

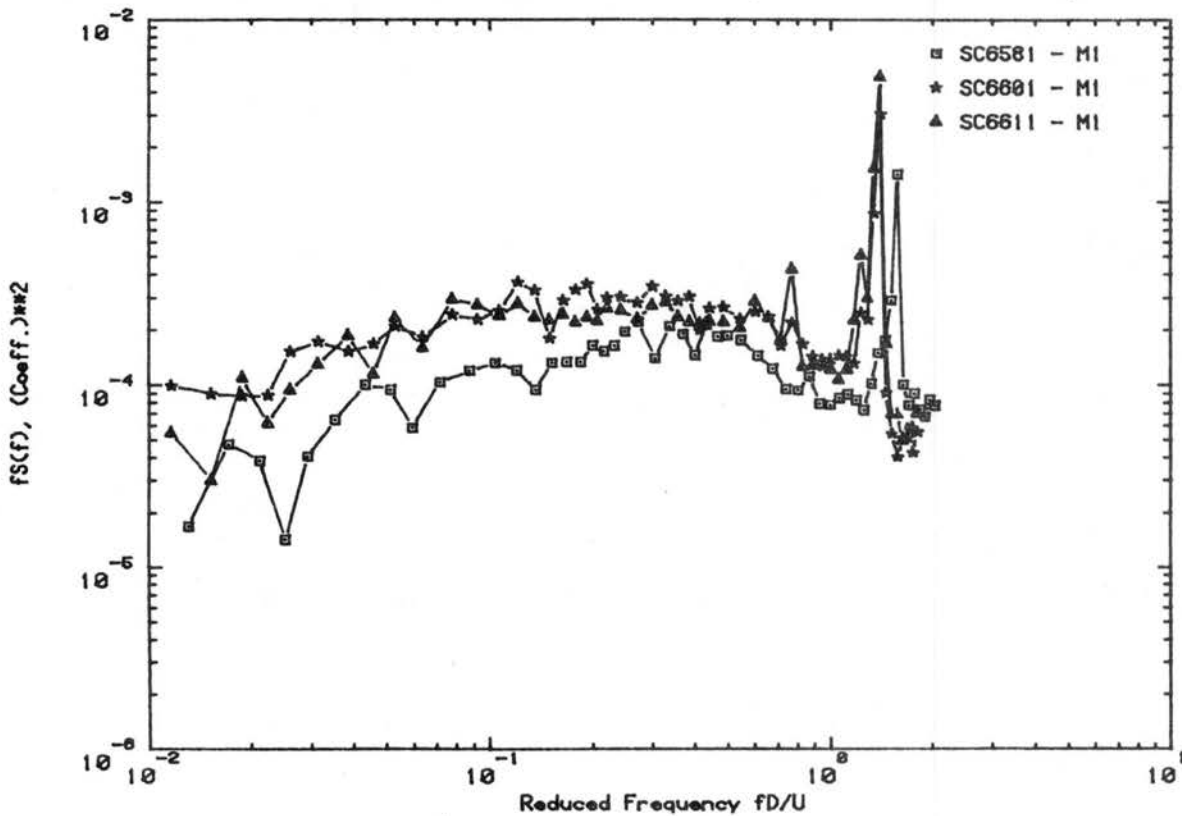


Figure C.14a. Load Spectra for Umbrella Stowed Position,
 Declination Angle 0° , Hour Angle 0°

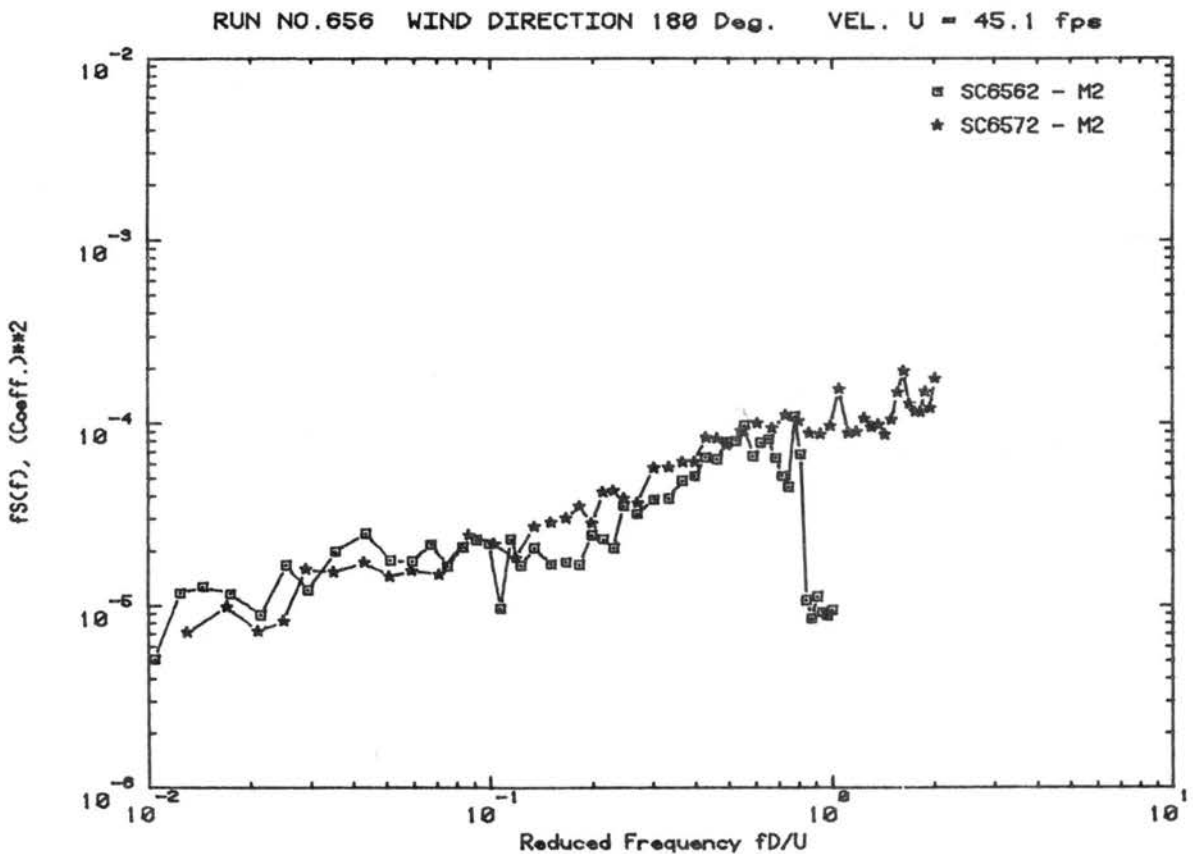
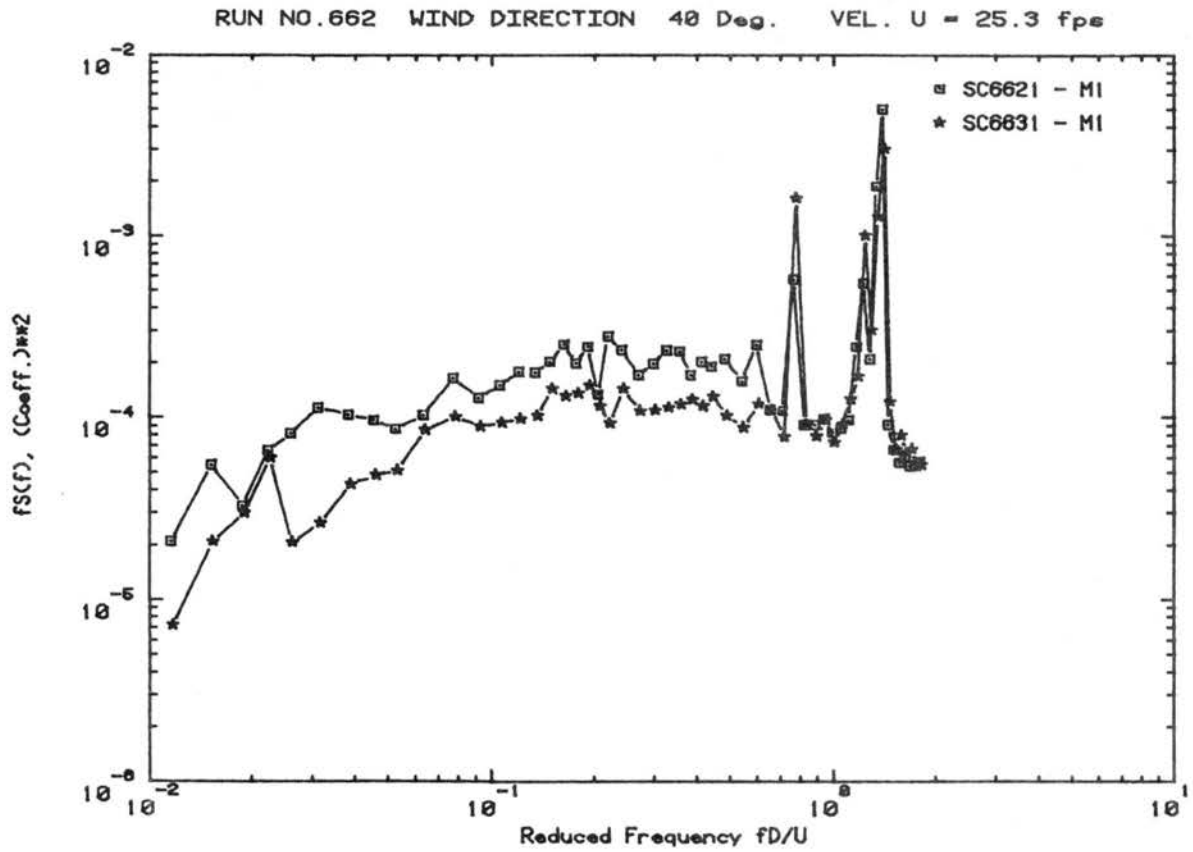
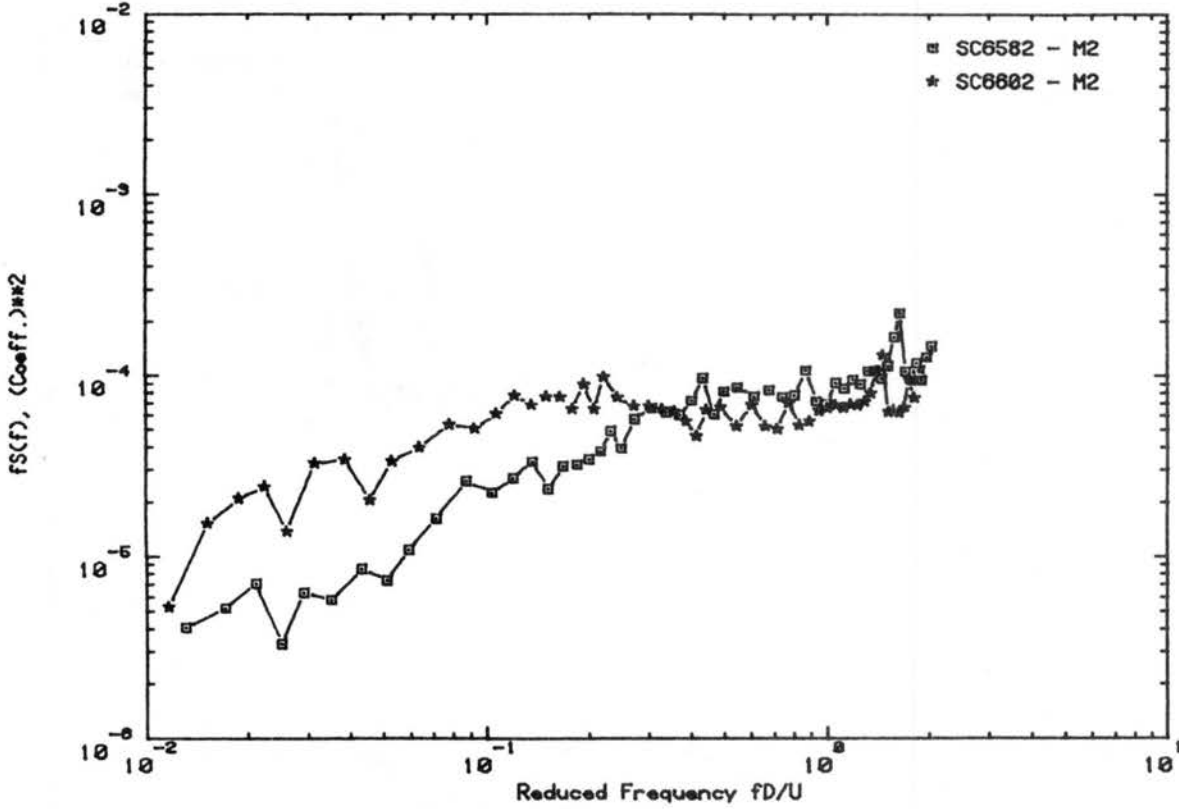


Figure C.14b. Load Spectra for Umbrella Stowed Position, Declination Angle 0° , Hour Angle 0°

RUN NO.658 WIND DIRECTION 140 Deg. VEL. U = 22.3 fps



RUN NO.661 WIND DIRECTION 60 Deg. VEL. U = 25.1 fps

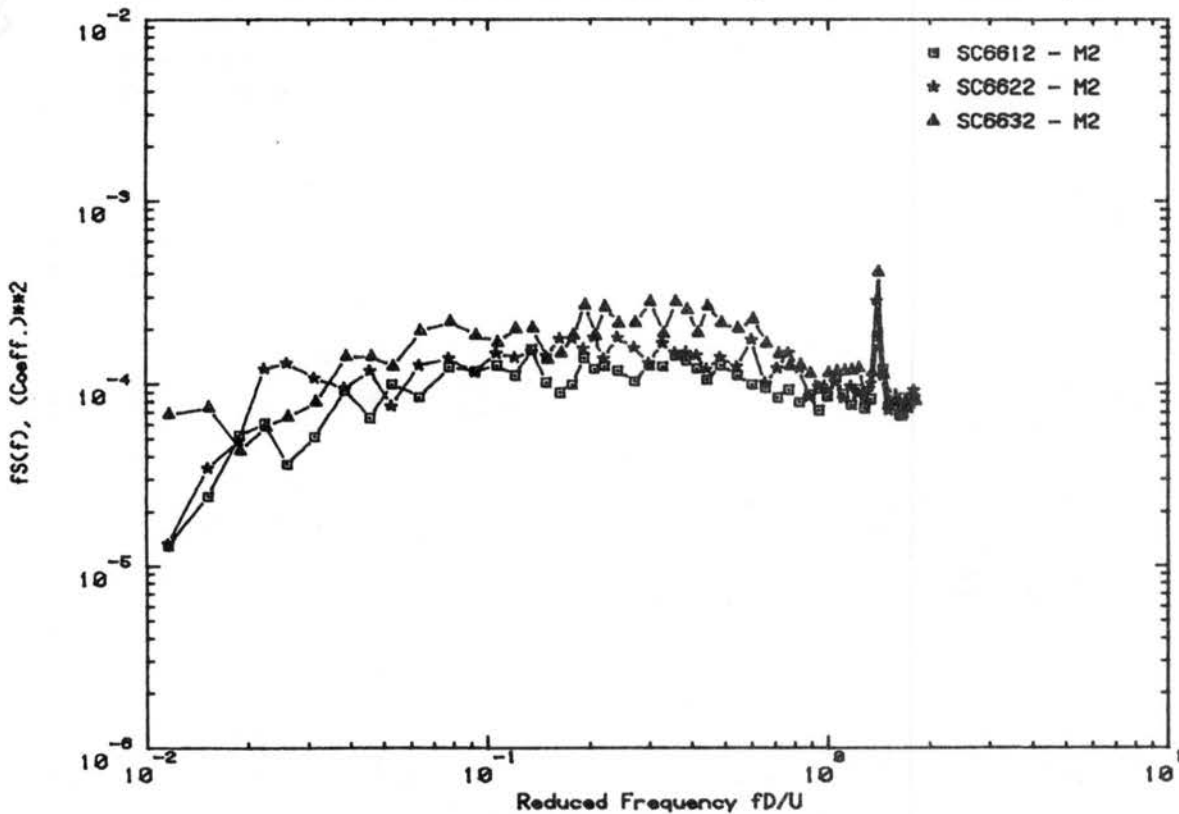


Figure C.14c. Load Spectra for Umbrella Stowed Position, Declination Angle 0°, Hour Angle 0°

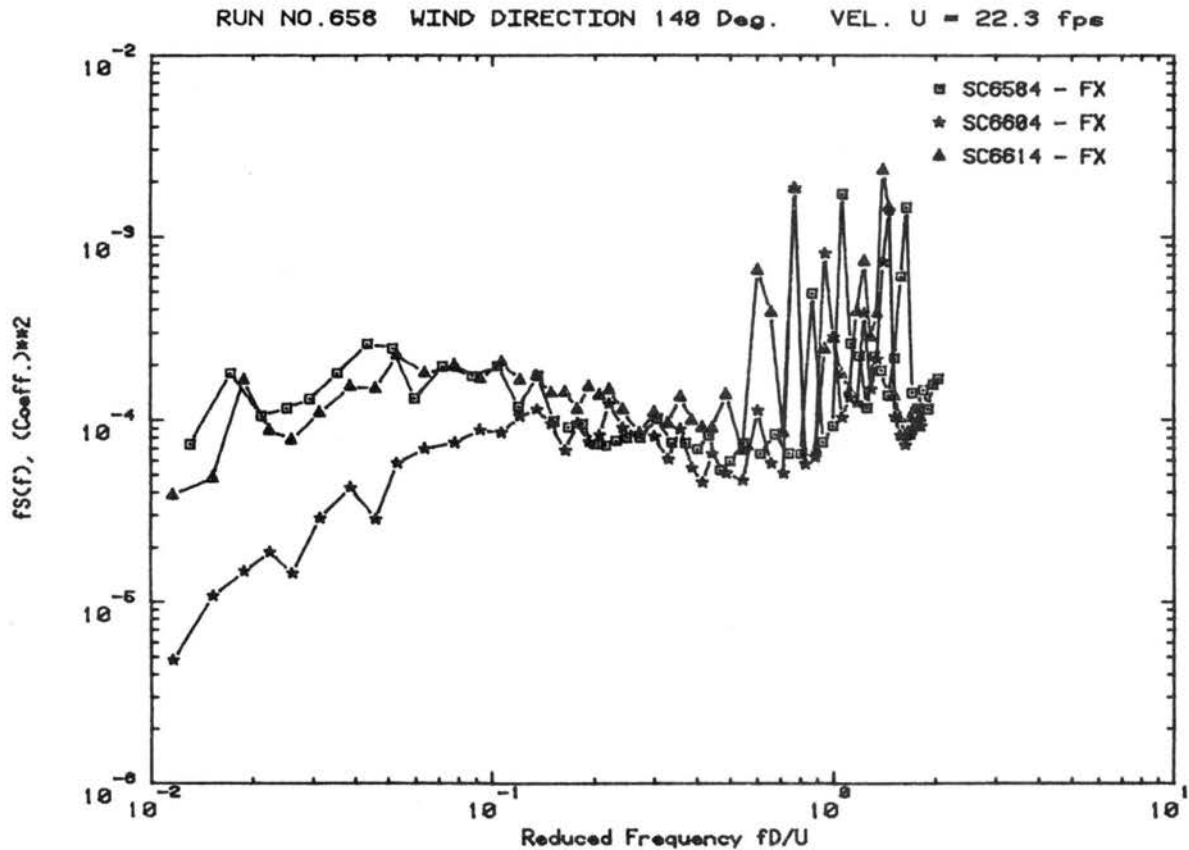
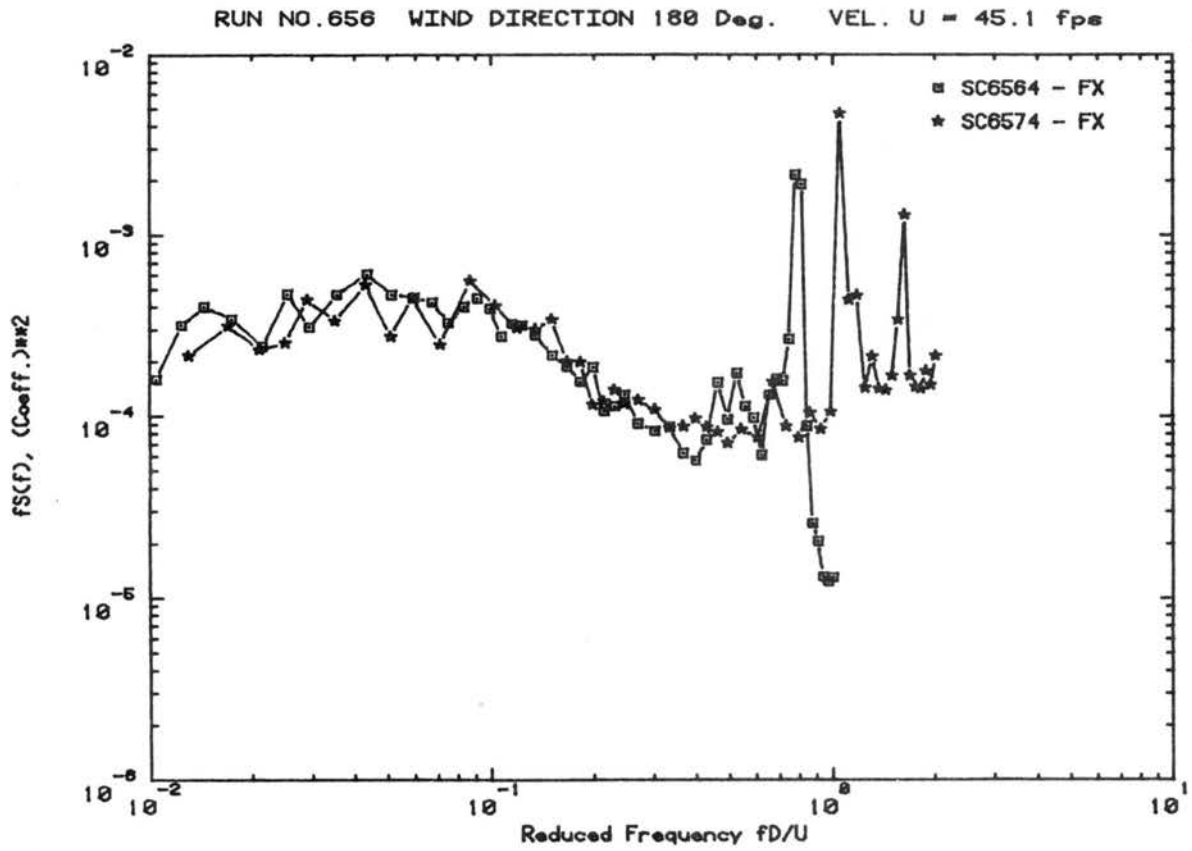
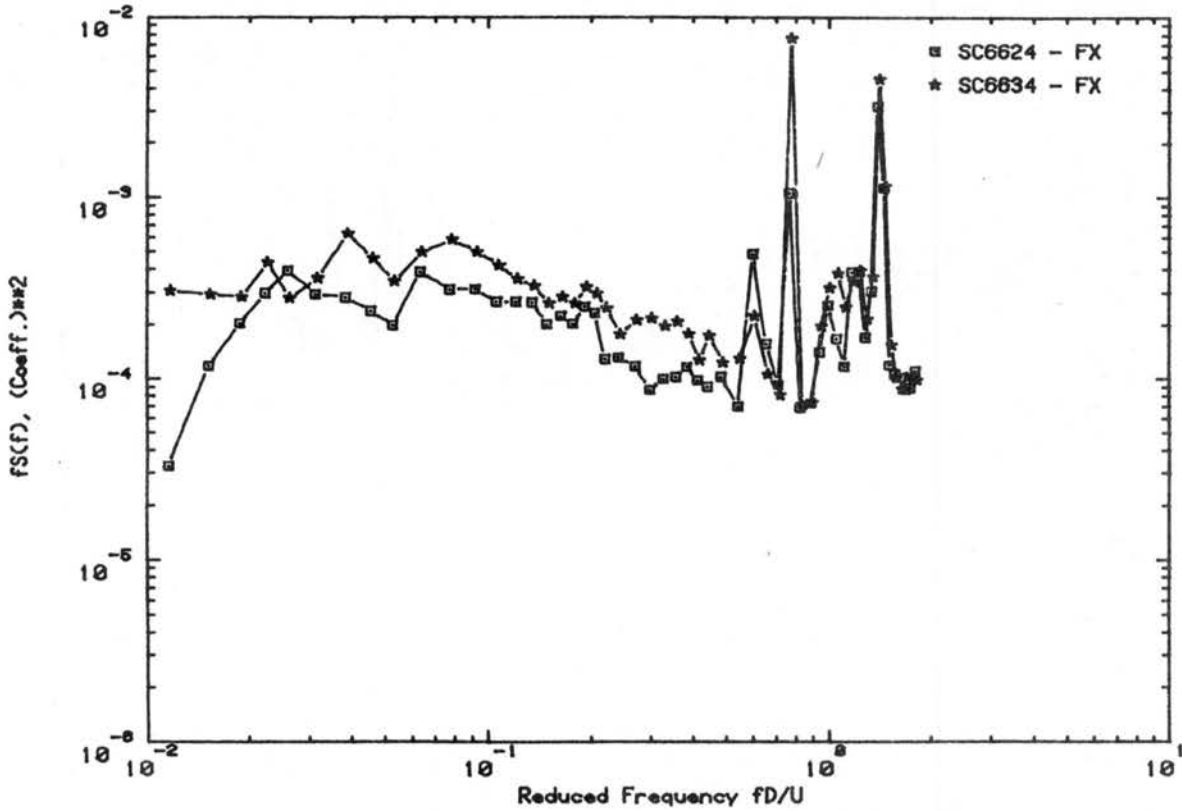


Figure C.14d. Load Spectra for Umbrella Stowed Position, Declination Angle 0° , Hour Angle 0°

RUN NO.662 WIND DIRECTION 40 Deg. VEL. U = 25.3 fps



RUN NO.656 WIND DIRECTION 180 Deg. VEL. U = 45.1 fps

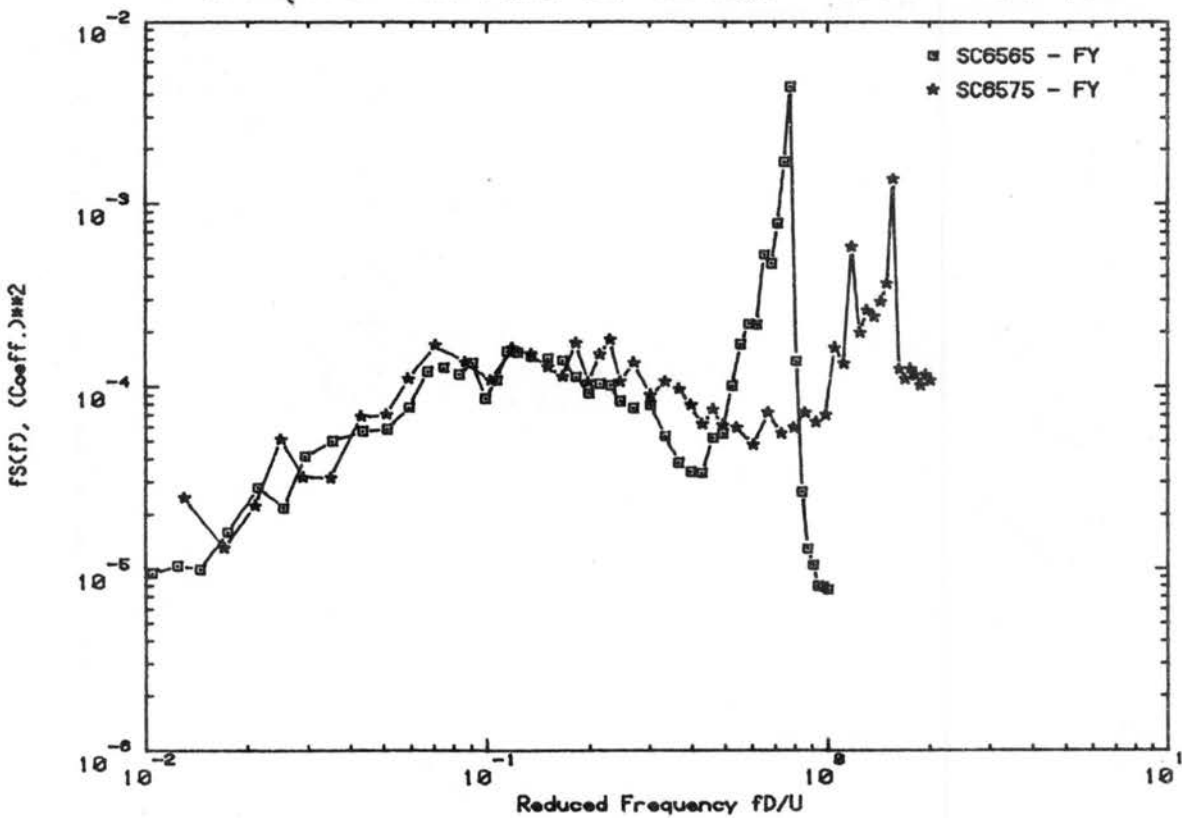


Figure C.14e. Load Spectra for Umbrella Stowed Position, Declination Angle 0°, Hour Angle 0°

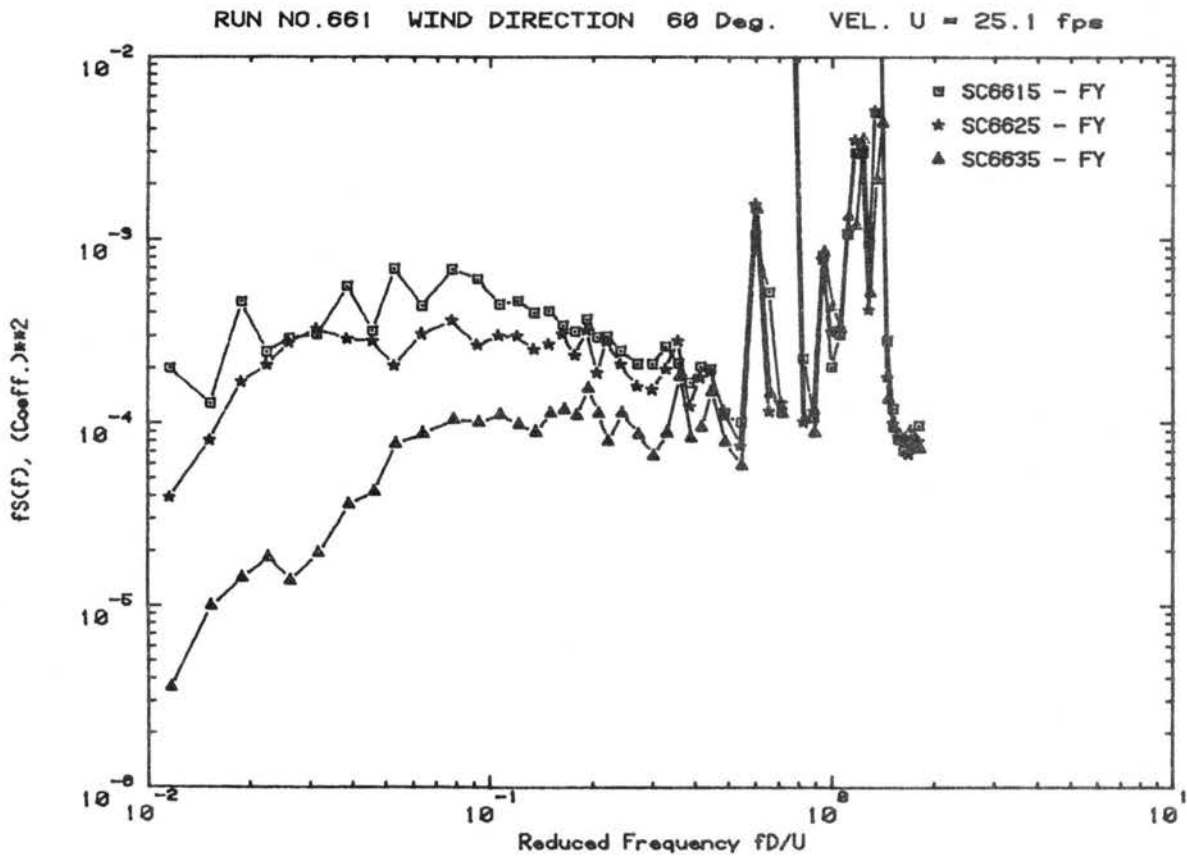
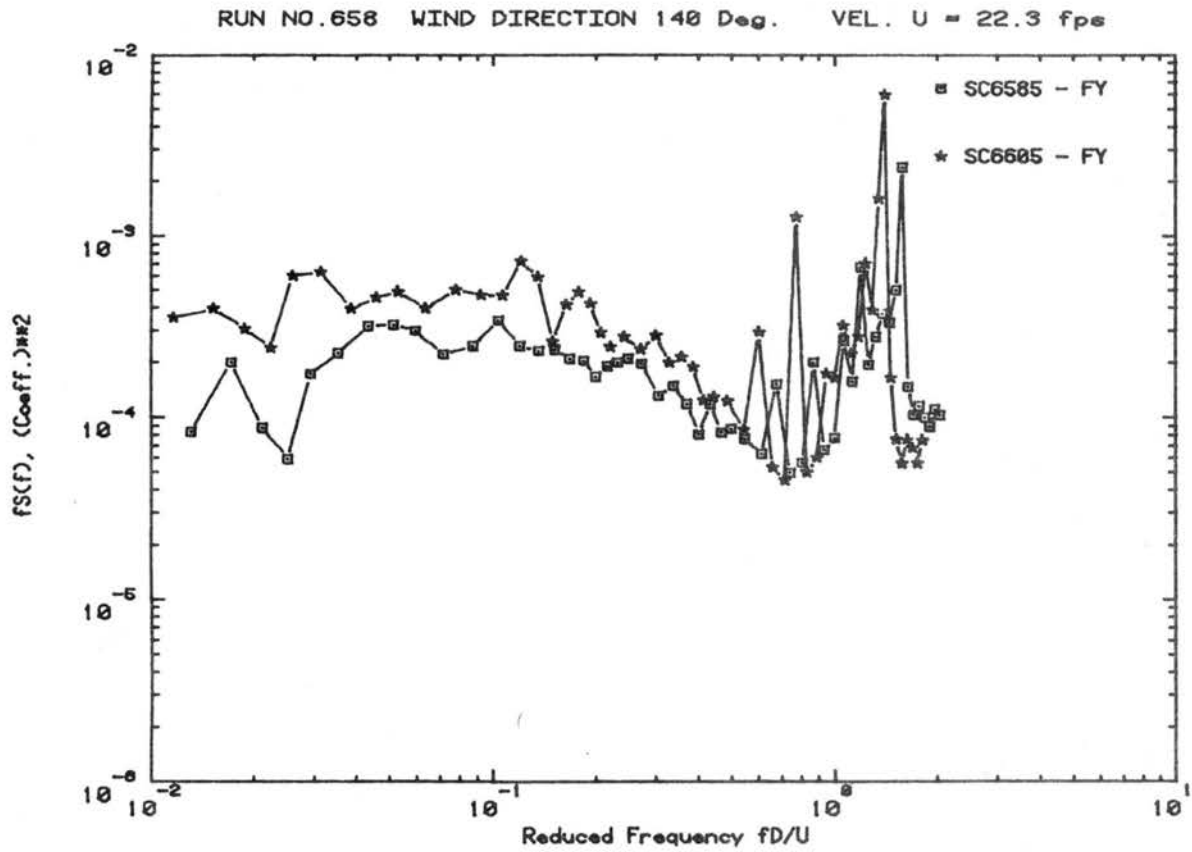
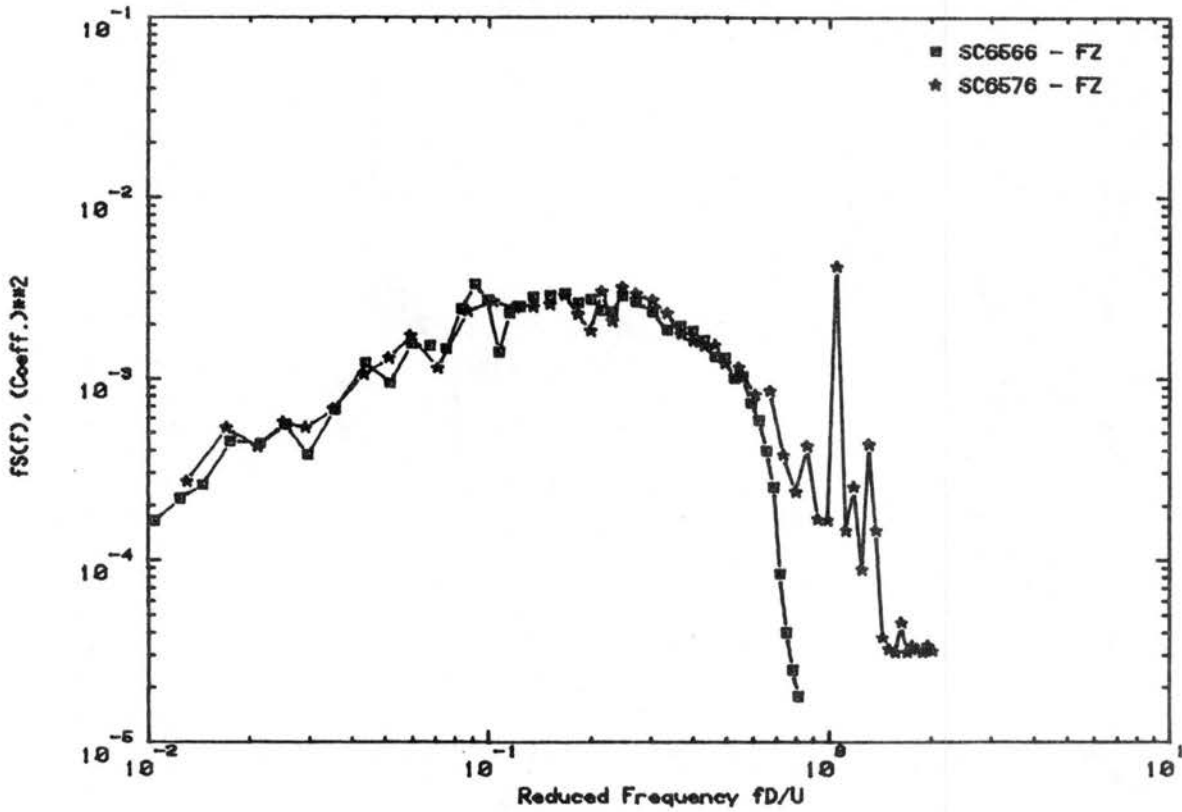


Figure C.14f. Load Spectra for Umbrella Stowed Position, Declination Angle 0° , Hour Angle 0°

RUN NO.656 WIND DIRECTION 180 Deg. VEL. U = 45.1 fps



RUN NO.658 WIND DIRECTION 140 Deg. VEL. U = 22.3 fps

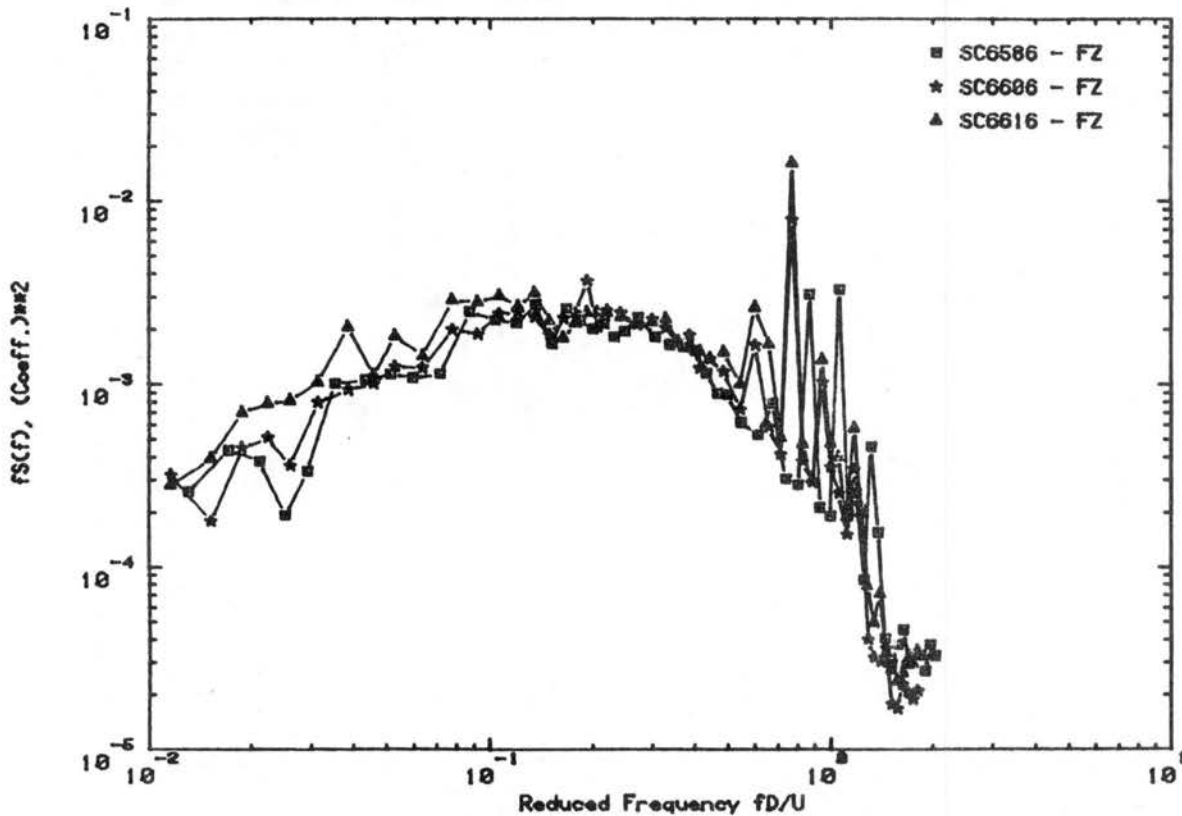


Figure C.14g. Load Spectra for Umbrella Stowed Position, Declination Angle 0°, Hour Angle 0°

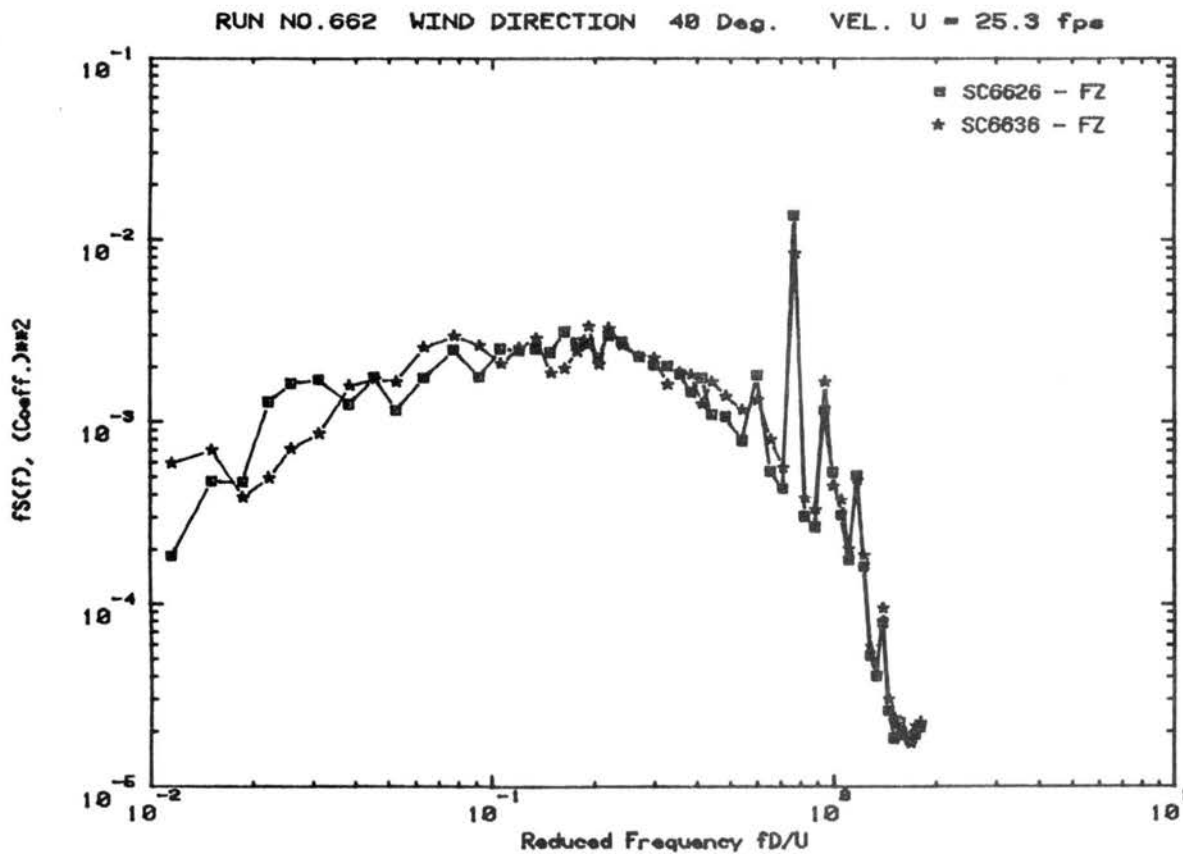


Figure C.14h. Load Spectra for Umbrella Stowed Position, Declination Angle 0° , Hour Angle 0°

APPENDIX D

MODAL ANALYSIS AND RANDOM VIBRATION

	<u>Page</u>
Reduction to SDOF System Using Modal Analysis	D-2
Solution of the Governing Equation Using Random Vibration Theory .	D-4
Nomenclature	D-7
References	D-9

Reduction to SDOF System Using Modal Analysis

A common analytical model of a tall building, suitable for the analysis of dynamic horizontal loading, is to consider it a chain of lumped masses, connected in series by beam elements. Displacements in the x-direction, y-direction, and rotations about the (vertical) z-axis are considered independently. For each of these components, the structural "frame" model will have n degrees of freedom, corresponding to the side-sway (or rotation) of each floor or lumped mass point. The system may then be described by an $n \times n$ stiffness matrix $[k]$, with an "input" n -component load vector $\{P\}$, and an "output" n -component displacement vector $\{x\}$.

In a static system, these are related by the familiar equation

$$\{P\} = [k]\{x\} .$$

When the loading varies with time and height, however, a complete description would be

$$[m]\{\ddot{x}\} + [c]\{\dot{x}\} + [k]\{x\} = \{P\}$$

where $[m]$ is the matrix of lumped masses, $[c]$ is a matrix of damping coefficients, and $\{x\}$ and $\{P\}$ are now functions of time. This represents a system of n simultaneous equations, which would be difficult to solve even if $\{P\}$ could be determined. If a transformation to a system of "generalized coordinates" is applied, these simultaneous equations are simplified to n uncoupled equations. Each equation corresponds to one of the generalized coordinates, ξ_i , which also has an associated natural frequency f_i and mode shape $\{\phi\}_i$. Furthermore, due to the frequency distribution of wind energy, almost all of the excitation occurs in the fundamental mode associated with the lowest

natural frequency. It is then only necessary to consider the first of the generalized coordinate equations, which appears as

$$m^* \ddot{\xi} + c^* \dot{\xi} + k^* \xi = P^* \quad (D.1)$$

where

$$m^* = \{\phi\}^T [m] \{\phi\}$$

$$c^* = \{\phi\}^T [c] \{\phi\}$$

$$k^* = \{\phi\}^T [k] \{\phi\}$$

$$P^* = \{\phi\}^T \{P\} .$$

These are referred to as the generalized mass, damping, stiffness, and load, respectively. This governing equation is that of a conventional single-degree of freedom system. The solution of the system, ξ , is related to the actual system by

$$\{x\} = \xi \{\phi\} . \quad (D.2)$$

It can be shown that the natural frequency of the system is

$$f_o = \frac{1}{2\pi} \sqrt{k^*/m^*} . \quad (D.3)$$

A further key property of tall structures is that the mode shape may be approximated by a straight line, that is $\phi_i = \alpha z_i$ or $\{\phi\} = \alpha \{z\}$. Since the magnitude of a mode shape is arbitrary, α may be taken as unity. The generalized mass then becomes

$$m^* = \{z\}^T [m] \{z\} = \sum_i m_i z_i^2 \quad (D.4)$$

which is approximately the mass moment of inertia, I , about the base.

The generalized load is

$$P^* = \{z\}^T \{P\} = \sum_i P_i z_i \quad (D.5)$$

which is the moment about the base, M . The displacement vector is

$$\{x\} = \xi\{z\}, \text{ or } x(z) = \xi z$$

which shows that ξ is the rotation of the structure (which remains a straight line by assumption) about its base, θ . By analogy to the SDOF system the generalized stiffness k^* is equivalent to a simple rotational stiffness k_θ . Introducing the critical damping ratio,

$$\begin{aligned} \zeta &= \frac{c}{c_{cr}} = \frac{c^*}{c_{cr}^*} = \frac{c^*}{2\sqrt{k^*m^*}} \\ &= 2m^*\omega_0 \end{aligned}$$

where $\omega_0 = 2\pi f_0$ is the natural circular frequency, the governing Equation (D.1) may be rewritten as

$$I\ddot{\theta} + 2I\zeta\omega_0\dot{\theta} + k_\theta\theta = M(t) . \quad (D.6)$$

Solution of the Governing Equation Using Random Vibration Theory

Equation (D.6) is most easily solved in the frequency domain when the loading $M(t)$ is random in time, since an arbitrary function of time can be described by a superposition of sinusoidal functions. For such a harmonic function at frequency f ,

$$M(t) = M_0 \sin(2\pi ft + \psi),$$

the solution is (in magnitude, ignoring phase)

$$\theta(t) = \frac{1}{k_\theta} H(f) \cdot M(t)$$

where the frequency response function $H(f)$ is defined as

$$H(f) = \frac{1}{\sqrt{[1-(f/f_0)^2]^2 + (2\zeta f/f_0)^2}} .$$

In terms of the spring load M , which is equal to

$$= k_\theta\theta,$$

the solution is simply

$$M(t) = H(f) \cdot M(t) .$$

Note that $M(t)$ and $M(t)$ are both moments, and that $H(f)$ is dimensionless. If the driving frequency f is near the structure's natural frequency f_0 , and the damping ratio ζ is low, this function is an amplification factor describing a condition known as resonance. $M(t)$ is properly described as an externally applied base moment, whereas $M(t)$ is an internal or "response" base moment. Note that if $M(t)$ were externally applied to the structure and a static analysis performed, the calculated response (displacement or internal forces) would be the same as the actual response due to the real fluctuating load $M(t)$. Thus $M(t)$ is also referred to as a "static equivalent load."

When the loading $M(t)$ is random in time, its statistical description as a superposition of harmonics is its "power spectral density," denoted $S_M(f)$. The response moment is then also described as a power spectral density, $S_M(f)$. The general result of random vibration theory is the relationship between these two, which is simply

$$S_M(f) = |H(f)|^2 \cdot S_M(f) . \quad (D.7)$$

The relating function $|H(f)|^2$ is just the square of the frequency response function, and is referred to in general as the transfer function:

$$|H(f)|^2 = \frac{1}{[1-(f/f_0)^2]^2 + (2\zeta f/f_0)^2} . \quad (D.8)$$

This particular transfer function is also referred to as the "mechanical admittance."

The principal usefulness of the power spectral density of a function is that its variance may be computed as the area under the spectrum:

$$\sigma_M^2 = \int_0^{\infty} S_M(f) df \quad . \quad (D.9)$$

The integration of Equation (D.9) was performed on the computer using numerical integration. Another accepted procedure in the present context is to use the so-called white noise approximation; then

$$\sigma_M^2 = S_M(f_o) \int_0^{\infty} |H(f)|^2 df \quad .$$

The integration can be performed analytically, with the result

$$\sigma_M^2 = \frac{\pi}{4\zeta} f_o S_M(f_o) \quad . \quad (D.10)$$

The square root of this is the desired rms dynamic response σ_M . Note that any value of natural frequency f_o and damping ratio ζ may be incorporated after the test results, $S_M(f)$, are obtained. The results from the two techniques were compared and gave similar results. For quick estimates of the rms response one can read the coefficient $C_{f_o} S_M(f_o)$ from the load-spectral graphs in Appendix C. To convert this coefficient to $f_o S_M(f_o)$ which can be used in Equation (D.10), the coefficient values have to be multiplied by the nondimensionalizing quantities. This can be done for any reduced natural frequency of the model or prototype.

The response is expected to be normally distributed (Gaussian) statistically, and thus can be completely described by its variance σ^2 and mean value \bar{M} (note that the mean response \bar{M} is equal to the mean load \bar{M}). Since the structural damping is very low, the response is also "narrow band," i.e., it can be loosely described as vibration at a

single frequency f_0 with randomly varying amplitude. Each cycle of vibration has a maximum and negative "peak" value associated with it. It is this series of peaks which are of interest insofar as structural design for strength or stiffness is concerned. It can be shown that these peak values obey a Rayleigh probability distribution, which is easily obtained from σ_M^2 . The expected value, variance, etc. of these peaks could be easily found from the Rayleigh distribution. What is more desirable, however, are statistics describing the largest peak which is likely to occur. Such an analysis is beyond the scope of this review, and the following result is simply stated:

$$\hat{M} = \bar{M} + g_p \sigma \quad (D.11)$$

Here \hat{M} is the expected value of the largest peak M occurring during a duration T of the loading M . The so-called "peak factor" g_p is calculated as follows [D3]

$$g_p = \mu + \frac{.5772\mu}{\mu^2 - 1} \quad (D.12)$$

where
$$\mu = \sqrt{2\ell n\nu T} + \frac{\ell n\sqrt{2\ell n\nu T}}{\sqrt{2\ell n\nu T}}$$

$$v = f_0 \sqrt{8\zeta} \quad .$$

Nomenclature

$[c]$	Damping matrix
c^*	Generalized damping
f_o	Natural cyclic frequency of fundamental mode
g	Peak factor
$ H(f) ^2$	Mechanical admittance (transfer function)
I	Mass moment of inertia of fundamental mode approximated by straight-line shape
$[k]$	Stiffness matrix
k^*	Generalized stiffness
k_θ	Rotational stiffness of fundamental mode approximated by straight-line shape
M	Resultant base moment of externally-applied wind load
\bar{M}	Response (internal, static equivalent) base moment
$[m]$	Mass matrix
m^*	Generalized mass
m_i	Mass lumped at floor i
$\{P\}$	Vector of P_i
P_i	Resultant force of wind load acting at floor i
P^*	Generalized load
$S_{()}(f)$	Power spectral density of ()
$\{x\}$	Vector of floor displacements
$\{z\}$	Vector of z_i
z_i	Height of floor i
ζ	Critical damping ratio
θ	Rotation of fundamental mode approximated by straight-line shape
ξ	Generalized coordinate
$\sigma_{()}$	Standard deviation (fluctuating rms) of ()

σ^2 ()	Variance of ()
{ ϕ }	Mode shape
ψ	Phase angle
ω_0	Natural circular frequency
($\bar{\quad}$)	Temporal mean of ()
($\hat{\quad}$)	Expected peak value of ()

APPENDIX D--REFERENCES

- D1. Clough, Ray W., and J. Penzien, Dynamics of Structures, McGraw-Hill Book Company, New York, 1975.
- D2. Crandall, Stephen H., and William D. Mark, Random Vibration in Mechanical Systems, Academic Press, New York, 1963.
- D3. Davenport, A. G., N. Isyumov, H. Rothman, and H. Tanaka, "Wind-Induced Response of Suspension Bridges - Wind Tunnel Model and Full Scale Observations," Wind Engineering, Proceedings of the Fifth International Conference, Cermak, J. E. (ed.), Fort Collins, Colorado, July 1979, Pergamon Press, Oxford, 1980, Vol. 2, pp. 807-824.